NOVEL APPLICATIONS OF COMPREHENSIVE TWO-DIMENSIONAL GAS CHROMATOGRAPHY TIME-OF-FLIGHT MASS SPECTROMETRY

by

Amy L. Payeur

A dissertation submitted in partial fulfillment
of the requirements for the degree of
Doctor of Philosophy
(Chemistry)
in The University of Michigan
2011

Doctoral Committee:

Professor Robert T. Kennedy, Co-Chair
Professor Richard D. Sacks, Co-Chair (Deceased)
Professor Mark E. Meyerhoff
Emeritus Professor Philip A. Meyers
Professor Michael D. Morris
Associate Professor Kristina I. Håkansson

To Mom and Dad, with love.

Acknowledgements

If nothing else, my graduate school experience has been unique, and has certainly made me not only a stronger scientist but also a much stronger person. It's hard to really thank everyone who had a hand in making my time here everything that it was, but, I am definitely going to try. I'd first like to thank my advisor, Dr. Robert T. Kennedy, for all of his guidance and support. The stronger scientist part is mostly his doing. But I also owe him a thank you for taking me on in my second year and making my transition from the Sacks Lab to the Kennedy Lab as easy as he possibly could. I would also like to thank my committee Dr. Mark Meyerhoff, Dr. Michael Morris and Dr. Kristina Hakansson for all of their help as well. A very special thank you goes to my cognate member Dr. Philip Meyers for not only being a great "geo advisor" but for also being incredibly supportive of me both personally and professionally.

Thank you to the Kennedy Lab members both past and present; many of you have been both fantastic lab mates and wonderful friends. Dr. Kendra Reid Evans, Maura Perry, Gwen Anderson, Dr. Omar Mabrouk, Dr. Claire Chisolm, Dr. Hernan Fuentes and Dr. Anna Clark: thank you for always believing in me and always knowing when I needed a Ben & Jerry's break.

This accomplishment would not have been possible without the encouragement, support and understanding of my friends Dr. John Henssler, Dr. Nick Deprez, Dr. Jon

Mortison, Dr. Cornelius Kristalyn, Dr. Max Bailor, Dr. Caleb Bates, Katrina Lexa, Matt and Ahleah Rohr Daniel, Dr. Chris Avery, Brad and Sarah Grincewicz, Katie Frey, Diedre Murch, Dr. Andrew Higgs, and Dr. Antek Wong-Foy. Knowing that you were all (and always will be) in my corner made each day of graduate school just a little bit easier, I'm not sure what I would have done without each of you. Kristin Bonomo and Stephanie Perry: thank you for being two of my biggest fans not only during my time here at Michigan but back in the day at Union as well.

Thank you to everyone at Leco and Restek for their technical guidance and friendship over the years, especially, Joe Binkley, John Heim, Todd Barton, Chris Immoos, Lucas Smith, Frank Dorman and Jack Cochran.

Thank you to all the Sacks Lab alumni who made my first two years of graduate school absolutely amazing. I have never met a group of people who epitomized the adage "Work Hard, Play Hard" as well as you all. Dr. Joshua Whiting, Dr. Mark Libardoni, Dr. Randy Lambertus, Dr. Cory Fix, Dr. Peter Stevens, Dr. Shaelah Reidy, Dr. Shai Kendler, Dr. Juan Sanchez and Meg Ziegler, thank you, for your continued friendship and support; The Chromies will always hold a *very* special place in my heart. Dr. Megan McGuigan, it always feels like "thank you" is never enough. The role you have played in my life as a mentor, a colleague, and most importantly a friend is absolutely invaluable and I will never be able to truly thank you for everything that you do.

Dr. Richard Sacks, where do I begin? Thank you for your contagious enthusiasm and love of science. Thank you for your encouragement, your understanding and for being an amazing mentor. Although my time with you was way too short, you have left

an impression with me forever and I will always be grateful that I was able to work with you. I think of you every time a thunderstorm rolls through; thanks for checking in, I needed the extra push.

Thank you to my amazing family especially Mom, Dad, Nick, and Mimi, I definitely would not be here if it weren't for your love, your support and your ability to at least pretend to understand why I was still in school all this time ☺. Thank you to my Memere and Pepere, who are not here to physically see this day, but are no doubt looking down, smiling and extremely proud of what their granddaughter has accomplished. Finally, thank you, Dr. William Porter. Words cannot truly express how blessed I feel to have had someone who believes in me the way that you do as my partner through most of this journey; I can't wait for our next trip together.

TABLE OF CONTENTS

LIST OF FIGURES

LIST OF TABLES

LIST OF APPENDICES

Chapter 1

INTRODUCTION

Gas Chromatography Background

Gas Chromatography (GC) is the most widely used analytical technique for the separation of volatile and semi-volatile organic compounds. The popularity of this technique can be attributed to the ease of use, the relatively low cost of instrumentation, the wide variety of detectors available, and the possibility of rapid, high resolution separations. GC has been used for numerous applications including the separation of essential oils[1, 2], environmental studies[3], forensics[4, 5] and in clinical research[6].

The separation produced by a chromatographic system is influenced by many factors. In capillary GC, these include column length, inner diameter (i.d.), stationary phase film thickness, carrier gas type, flow rate, detectors, and inlets. In order to more directly compare the general separation performance from system to system, or column to column, a number of metrics have been developed. One of the most common metrics used to compare systems is efficiency. Efficiency is described by the length of column required to obtain the equivalent separation that would occur under equilibrium conditions for specified values of distribution ratio (K) and phase volume ratio (V_r).[7] This length is called the height equivalent to a theoretical plate (H).

H is best described using the kinetic model which was introduced by Golay in 1958[8] for open tubular columns and takes into consideration the rates of various processes that contribute to band dispersion, Equation 1.1.

$$H = \frac{Bf_1f_2}{\mu_{avg}} + \left(\frac{C_g f_1}{f_2} + C_s\right)\mu_{avg} \tag{1.1}$$

B is the longitudinal diffusion term, f_1 is the Golay-Giddings gas compression correction factor, f_2 is the Martin-James gas compression factor, C_g contains the contributions from the resistance to mass transport in the mobile phase and band broadening due to parabolic laminar flow effects, C_s is the resistance to mass transport in the stationary phase, and μ_{avg} is the average carrier gas velocity.

The gas compression factors f_1 and f_2 are described in Equations 1.2 and 1.3

$$f_1 = \frac{9(P^4-1)(P^2-1)}{8(P^3-1)^2} \tag{1.2}$$

$$f_2 = \frac{3(P^2-1)}{2(P^3-1)} \tag{1.3}$$

where *P* is the ratio of inlet to outlet pressure. The longitudinal diffusion term *B*, derived from Einstein's equation for one-dimensional diffusion, describes peak broadening as a consequence of the residence time of the solute within the column and the nature of the carrier gas.[9] This term is defined in Equation 1.4

$$B = \frac{2D_g}{\mu_{avg}} \tag{1.4}$$

where D_g is the binary diffusion coefficient of the analyte in the carrier gas. The effect of this term becomes significant only at low carrier gas velocities; because it is inversely

proportional to μ_{avg}. B is only a minor contributor to band broadening at high average carrier gas velocities.

Resistance to mass transport, C_s and C_g, are non-equilibrium band broadening caused by the finite time required for a solute molecule to move from one of the phases to the other phase while they are carried through the column by carrier gas flow. The C_g term also includes band broadening caused by Taylor dispersion or parabolic laminar flow (maximum flow at column center, minimal flow at column walls) effects which cause band broadening due to analytes in these regions travelling at different local carrier gas velocities. Equations 1.5 and 1.6 describe the C_g and C_s terms of the Golay equation

$$C_g = \frac{1 + 6k + 11k^2}{24(k+1)^2} \frac{r^2}{D_g} \mu_{avg} \tag{1.5}$$

$$C_s = \frac{2}{3} \frac{k}{(k+1)^2} \frac{{d_f}^2}{D_s} \mu_{avg} \tag{1.6}$$

where k is the capacity factor, r is the inner radius of the column, d_f is the stationary phase thickness and D_s is the binary diffusion coefficient for the analyte and stationary phase. The radius of commercially available columns is usually three orders of magnitude greater than the film thickness so the C_s is often overwhelmed by the C_g term and therefore neglected.

Golay plots (plate height vs. carrier gas velocity) can be used to visualize and evaluate the effects that chromatographic parameters have on separation efficiency. For example, Figure 1.1[9] shows efficiency increasing substantially with decreasing column length at high carrier gas velocities for 0.25 mm i.d. columns, using helium as a carrier gas at 50 °C and with k and D_g values of 5.0 and 0.4 cm^2/s, respectively.

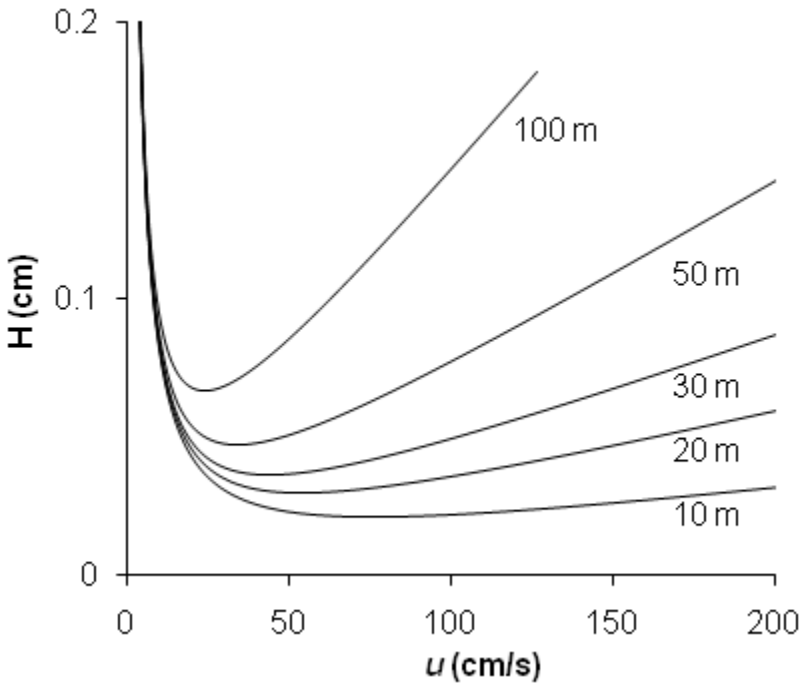

Figure 1.1 Golay plot for 0.25 mm i.d. thin-film columns of various lengths using helium as carrier gas. A binary diffusion coefficient of 0.4 cm^2/s and a retention factor of 5.0 are assumed. [9]

However, column resolving power, another metric to be considered, decreases steadily with decreasing column length. The number of theoretical plates, N, is a measure of the width of sample bands as they elute from the column. N is defined in Equation 1.7

$$N = \frac{L}{H} \tag{1.7}$$

where L is the length of the capillary column. Note that high efficiency does not directly correlate to high resolving power and it is possible for a long, low efficiency column to have better resolving power than a short, high efficiency column.

Another important method for evaluating a GC separation is peak capacity. Peak capacity is a measure of how many completely resolved peaks can fit within the time of the chromatogram at a defined resolution, or the ratio of peak separation to average base peak width, and is given by Equation 1.8

$$n_c = 1 + \frac{\sqrt{N}}{4R_s} \ln\left(\frac{t_{RL}}{t_M}\right) \quad (1.8)$$

where R_s is the user-defined resolution, t_{RL} is the retention time of the last eluting component, and t_M is the time it takes for an unretained analyte to reach the detector, also known as the hold-up time. Based on this equation, a 30 m, 0.25 mm i.d. capillary with 4,000 plates per meter, a t_M of 1 min., a μ of 50 cm/s and a runtime of 30 min would have a peak capacity of 250 peaks. However, Equation 1.8 assumes that the mixture components elute with perfect spacing, thus obtaining useful information for the entire time window of the chromatogram. In real samples, this perfectly spaced elution does not occur; instead, peaks tend to be randomly distributed in the chromatogram so that the probability of peak overlap is high in complex mixtures. It is typical that the peak capacity requirement is greater than the number of components in a mixture if all analytes are going to be resolved. Statistical analysis has shown that the required peak capacity may be nearly 20 times the number of peaks in the chromatogram in order to separate completely about 90 % of the peaks.[10, 11] For example, to resolve 90 out of 100 components a peak capacity of 1910 would be required.[11]

Many current interests in the area of chromatography focus on extremely complex samples such as petrochemicals,[12, 13] fragrances,[14] and metabolomics,[15, 16] that can contain >>1000 species and therefore high peak capacity is essential. In 1991, a

remarkable advancement in peak capacity was made by the late John Phillips with the introduction of comprehensive two-dimensional gas chromatography (GC × GC).[17]

Comprehensive Two-Dimensional Gas Chromatography Background

Over the past two decades, GC × GC has developed into a popular method for the separation of complex mixtures in research laboratories. GC × GC has been used to analyze biological, environmental, food, forensics, pharmaceutical and fragrance samples,[18] and the growing popularity of this technique is indicated by the nearly seven times increase in the number of publications per year since 2000. Figure 1.2 shows a schematic of a typical GC × GC instrument.

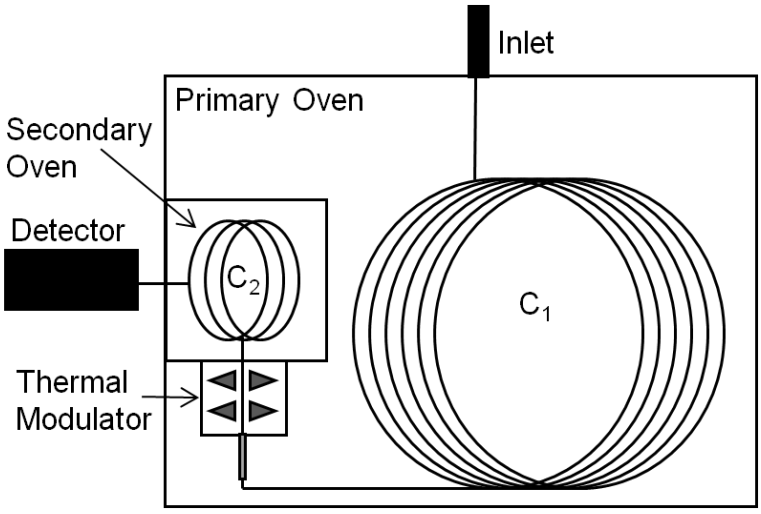

Figure 1.2 GC × GC instrument schematic showing C_1 (column 1) connected in series by a low dead volume connection through the thermal modulator to C_2 (column 2) which continues through a transfer line to the detector. C_1 and C_2 are housed in independently temperature programmed ovens.

The key to this instrument is the placement of two columns in series with a modulator interface between them. The modulator provides the second, relatively short column with smaller subsets of the original matrix eluting from the relatively long, primary column, and the second column generates a series of high-speed separations.[19, 20] The two columns separate analytes based on different molecular properties. The first column is

usually non-polar, separating analytes primarily based on volatility and the second column typically has a polar stationary phase that separates components by polarity. Ideally, the two dimensions in a GC × GC separation would operate statistically independent and the entire two dimensional plane of the chromatogram would be available for peak separation.[21] This is often referred to as an orthogonal separation and is illustrated in Figure 1.3 where (a) demonstrates the separation space available for a one dimensional separation, (b) represents what would be obtained from performing a separation on two columns connected in series with identical stationary phase chemistries and (c) shows the separation space available in two-dimensional chromatography when orthogonal columns are employed.

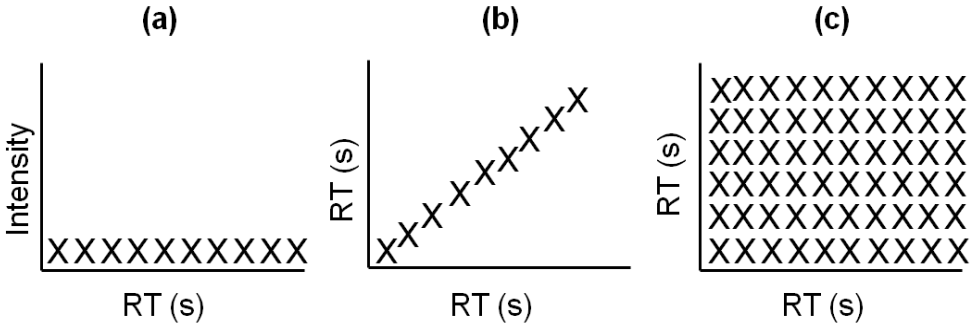

Figure 1.3 Theoretical demonstration of peak capacity achieved with orthogonal first and second dimension columns. Peak capacity possible in one-dimension (a); peak capacity possible with two columns of identical stationary phase chemistries connected in series (b); theoretical peak capacity in and orthogonal GC × GC separation (c).

The modulator is used to trap and focus a portion of a band eluting from the first column and then periodically inject it as a narrower, more concentrated band into the second column. With the dual-stage thermal modulator commercially available through Leco Corporation (St. Joseph, MI), this is accomplished using a series of liquid-nitrogen-cooled nitrogen jets and hot air jets. Valve modulators, resistively heated modulators, cryogenic modulators, and additional jet based modulators have also been used. Each

type of modulator has advantages and disadvantages including temperature limitations, robustness, portability and consumption of cryogens.[22] Although most current GC × GC work is focused on applications, modulators continue to be an area of active development.

Besides peak capacity increase, GC × GC also can improve sensitivity because of the effect of the modulator at the end of the first column. Figure 1.4 shows a conceptual comparison between an unmodulated peak (A) and a modulated peak (B); the area of the unmodulated peak is equal to the sum of the area of the modulated peak.[23]; however, the intensity of the narrow modulated peak slices is 10-50 times the height of the unmodulated peak. This greatly increased peak height, caused by the focusing action of the thermal modulator, significantly increases detectability, thus making this technique well-suited for trace level analytes that would not be detected in one-dimensional GC.

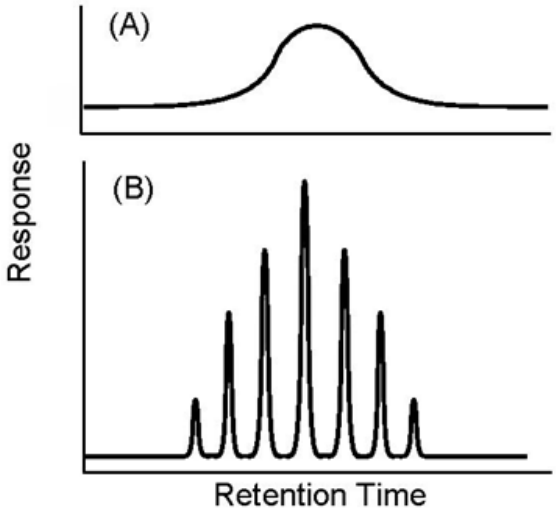

Figure 1.4 Schematic of unmodulated (A) and modulated (B) peaks in GC × GC. Adapted from reference[23]

The output of the GC × GC is a string of very fast separations that are in 2-20 s intervals and continue for the duration of the first-column separation. Typically, several

hundred second-column separations are obtained and merged by software to generate a two-dimensional chromatogram in which detector data are plotted on a two-dimensional retention plane rather than on a simple time axis. This is represented schematically in Figure 1.5 where the detector sees a continuous stream of one-dimensional data that is then split and rotated based on the modulation period before the software merges the slices to create the final contour plot.

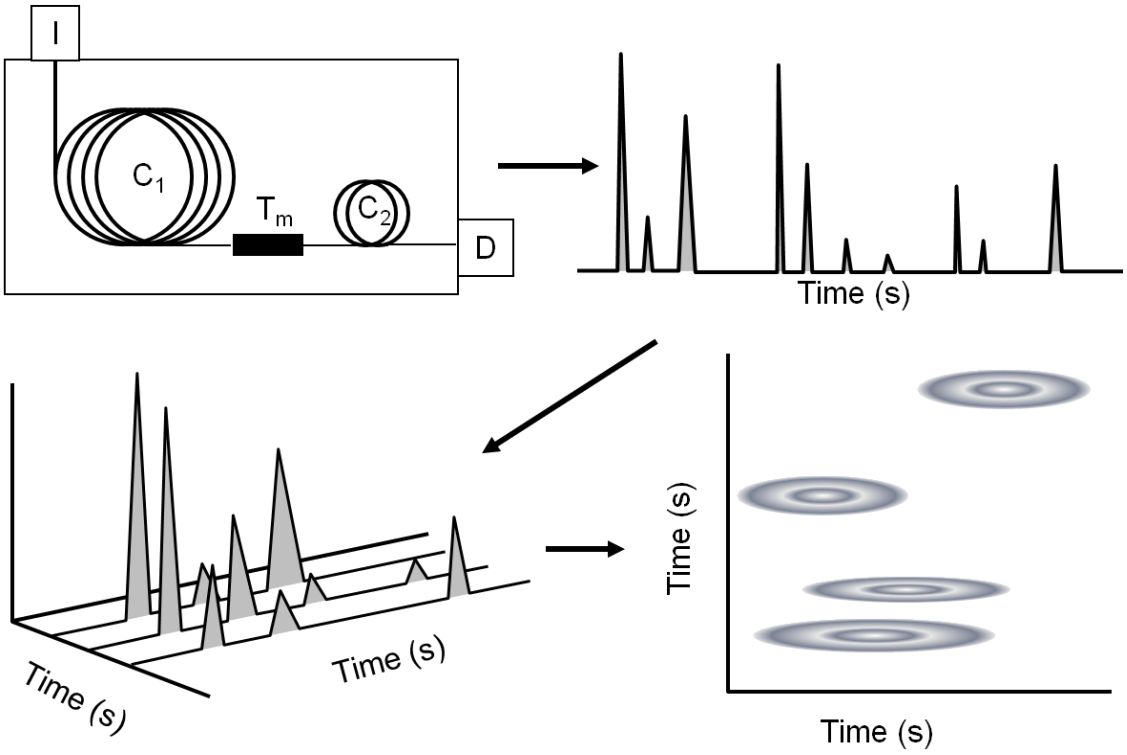

Figure 1.5 Schematic of data processing performed in GC × GC showing chromatograms being chopped and merged to display contour plots based on modulation period.

Detectors with fast response times are required due to the sharp bands (200-500 ms) produced by the fast second column separation.[19] Although various detectors have been developed for high speed GC, such as flame ionization detectors and

quadrupole mass spectrometers,[24] ToFMS can acquire data for a full mass range at rates fast enough for GC × GC while quadrupoles usually need to be run in single ion monitoring mode when coupled with GC × GC. ToFMS can track very narrow peaks, allows for automated peak finding, and the spectra are not concentration dependent because the ionization is pulsed.[20, 24]

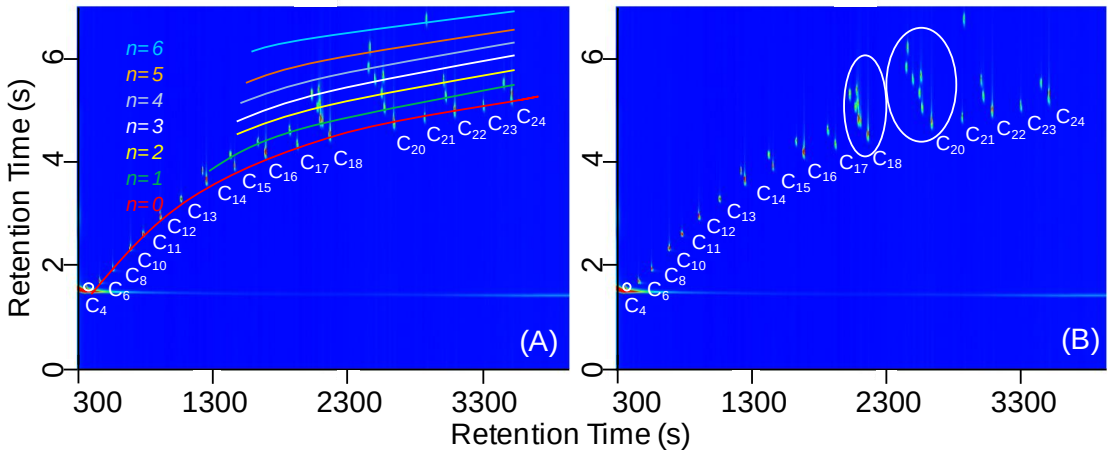

Figure 1.6 GC × GC chromatogram of fatty acid methyl esters emphasizing the elution of homologous series along an arc (A) and clustered elution of compound classes (B). The clustered elution of C_{18} and C_{20} FAMEs is highlighted by the white ovals. n, number of double bonds.

Besides higher resolution, the two-dimensional separation plane of GC × GC allows for structured chromatograms in which compound classes have characteristic patterns. Homologous series of analytes tend to elute in characteristic lines (or curves) and compound classes tend to elute in clusters, both of which can be easily recognized. An example of this structure can be found in Figure 1.6 where the fatty acid methyl esters (FAMEs) with the same number of double bonds elute along the same arcs (A) and the FAMEs with the same number of carbons are clustered together (B). The structured nature of the chromatograms assists in classification and identification of components even in the absence of pure standards.

Peak Capacity in GC × GC

Peak capacity in GC × GC ($n_{cGC \times GC}$) is generally assumed to be equal to the peak capacity of the first dimension column (n_{c1}) times the peak capacity of the second dimension column (n_{c2}), Equation 1.9.

$$n_{c,GC \times GC} = n_{c1} \cdot n_{c2} \quad (1.9)$$

Under this assumption, a first dimension column with a peak capacity of 250 coupled in series to a second dimension column with a peak capacity of 10 would provide a two-dimensional peak capacity of 2500. In reality though, the actual peak capacity of GC × GC is always less than $n_{c1} \cdot n_{c2}$. One reason for this lower peak capacity is because modulation causes some peak broadening in the reconstructed first dimension. Even under conditions where the peak capacities in both dimensions are optimized, peaks in the first dimension can be 23 % wider with modulation than without effectively lowering n_{c1}.[25] Additionally, useful peak capacity in the second dimension is often reduced by the use of columns with film thicknesses and column temperatures that lead to the smallest capacity factors being close to 1.5, a choice that leaves an empty portion of second dimension separation space.[25]

Because the performance of columns in two-dimensional systems is not directly equivalent to the performance of the stand alone columns, making it difficult to directly compare peak capacities, other metrics have been developed to more directly compare one-dimensional and two-dimensional systems. One of the metrics is the concept of peak capacity gain (G_n) that results from the addition of the second dimension to a one-dimensional system. G_n is described simply in Equation 1.10[25]

$$G_n = \frac{n_{c,GC\times GC}}{n_{c1,o}} \tag{1.10}$$

where $n_{c1,o}$ is the peak capacity of the stand alone first dimension column. However, because we know that the actual peak capacity of GC × GC is always less than $n_{c1} \cdot n_{c2}$, a more accurate description of peak capacity gain is found in Equation 1.11[25]

$$G_{n,opt} = \frac{0.13{N_1}^{1/3}}{R_{s,min,1}} \tag{1.11}$$

where N_1 is the first dimension column plate number and $R_{s,min,1}$ is the lowest acceptable resolution in the first dimension. This equation accounts for losses in both dimensions from an optimal GC × GC system and assumes the data analysis of the stand alone first dimension is applied to the second dimension of GC × GC.

A system that is estimated to be optimal[25] can be considered here to calculate the best possible peak capacity gain in GC × GC. In this system the first dimension column is 30 m long with a 250 µm i.d. and a 0.1 mm stationary phase film thickness and the second column is 0.86 m long with the same i.d. and film thickness as the first dimension column. When $R_{s,min,1}$ is 1.5 $G_{n,opt}$ is about 9.3 and when $R_{s,min,1}$ is 1, $G_{n,opt}$ is about 14. Unfortunately, current technology does not allow for GC × GC systems to run perfectly optimized. For example, the current modulator technology injects pulses on the second column that are widths an order of magnitude higher than optimal.[26] When the peak capacity gain from using a current GC × GC system instead of the one-dimensional equivalent (defined as a one-dimensional system that has the same analysis time and the same minimum detectable concentration as the GC × GC system in question) the $G_{n,eq}$

(no longer optimal values, therefore now referred to as peak capacity gain equivalent) values drop to about 3 and 4 for $R_{s,min,1}$ values of 1.5 and 1, respectively.[25]

Despite the shortcomings of current GC × GC technology to fully utilize the potential peak capacity gain over equivalent one-dimensional separations, the technique still has great analytical importance and is unmatched by conventional GC for many, but not all, complex samples. Additional disadvantages that must be weighed when choosing to use GC × GC or GC are costs of commercial instruments (several hundred thousand dollars) and the cryogenics required. Computing power is another necessity because chromatogram files can exceed 2 GB when processed and, if computing power is low, can take hours to process. User experience must also be considered due to the increased complexity and high maintenance requirements of current instrumentation.

Dissertation Overview

The goal of this research project was to utilize the separation and detection power of GC × GC and apply it to novel applications in the areas of geology and metabolomics. All experiments were performed using the commercially available Leco Pegasus 4D which is an Agilent 6890 gas chromatograph modified for comprehensive two-dimensional gas chromatography and coupled to a Pegasus time-of-flight mass spectrometer.

Chapter 2 describes both a metabolite profiling and metabolomics analysis of extracts from INS-1 cells incubated in 3 mM, 7 mM and 17 mM glucose. Chapter 3 discusses the use of GC × GC-ToFMS to analyze the total lipid content of INS-1 cell extracts incubated in 0 mM, 0.5 mM, 10 mM and 20 mM glucose. Chapter 4 describes

the use of pyrolysis-GC × GC to analyze Mediterranean Sea sediments, known as sapropels, with high total organic carbon concentrations. Finally, Chapter 5 summarizes and describes future directions for the work completed in Chapters 2 through 4.

References

(1) Shellie, R.; Mondello, L.; Marriott, P.; Dugo, G. *J. Chromatogr. A* **2002**, *970*, 225-234.
(2) Veriotti, T.; Sacks, R. *Anal. Chem.* **2001**, *73*, 4395-4402.
(3) Grall, A. J.; Zellers, E. T.; Sacks, R. D. *Environ. Sci. Technol.* **2001**, *35*, 163-169.
(4) Merola, G.; Gentili, S.; Tagliaro, F.; Macchia, T. *Analytical and bioanalytical chemistry*, *397*.
(5) Lowe, R. H.; Barnes, A. J.; Lehrmann, E.; Freed, W. J.; Kleinman, J. E.; Hyde, T. M.; Herman, M. M.; Huestis, M. A. *J. Mass Spectrom.* **2006**, *41*, 175-184.
(6) Paik, M.-J.; Ahn, Y.-H.; Lee, P. H.; Kang, H.; Park, C. B.; Choi, S.; Lee, G. *Clin. Chim. Acta* **2010**, *411*, 1532-1535.
(7) Sacks, R. D.; University of Michigan: Ann Arbor, MI, pp 79.
(8) Golay, M. J. E. *Nature* **1958**, *182*, 1146-1147.
(9) Grob, R. L.; Barry, E. F.; Wiley, I. *Modern practice of gas chromatography*; Wiley-Interscience: Hoboken, N.J., 2004.
(10) Giddings, J. C. *Unified separation science*; Wiley: New York, 1991.
(11) Mondello, L.; Lewis, A. C.; Bartle, K. D. *Multidimensional chromatography*; Wiley: West Sussex, England ; New York, 2002.
(12) Adam, F.; Bertoncini, F.; Coupard, V.; Charon, N.; Thiebaut, D.; Espinat, D.; Hennion, M. C. *J. Chromatogr. A* **2008**, *1186*, 236-244.
(13) Farwell, C.; Reddy, C. M.; Peacock, E.; Nelson, R. K.; Washburn, L.; Valentine, D. L. *Environ. Sci. Technol.* **2009**, *43*, 3542-3548.
(14) Cordero, C.; Bicchi, C.; Joulain, D.; Rubiolo, P. *J. Chromatogr. A* **2007**, *1150*, 37-49.
(15) Mohler, R. E.; Tu, B. P.; Dombek, K. M.; Hoggard, J. C.; Young, E. T.; Synovec, R. E. *J. Chromatogr. A* **2008**, *1186*, 401-411.
(16) Kusano, M.; Fukushima, A.; Kobayashi, M.; Hayashi, N.; Jonsson, P.; Moritz, T.; Ebana, K.; Saito, K. *Journal of Chromatography B-Analytical Technologies in the Biomedical and Life Sciences* **2007**, *855*, 71-79.
(17) Liu, A.; Phillips, J. B. *J. Chromatogr. Sci.* **1991**, *29*, 227-231.
(18) Wang, Y.; Qian, C.; Norwood, D.; McCaffrey, J. *J. Liq. Chromatogr. Rel. Technol.* **2010**, *33*, 1082-1115.
(19) McGuigan, M.; Waite, J. H.; Imanaka, H.; Sacks, R. D. *J. Chromatogr. A* **2006**, *1132*, 280-288.
(20) Dimandja, J. M. D. *Anal. Chem.* **2004**, *76*, 167A-174A.
(21) Adahchour, M.; Beens, J.; Brinkman, U. A. T. *J. Chromatogr. A* **2008**, *1186*, 67-108.
(22) Cortes, H.; Winniford, B.; Luong, J.; Pursch, M. *J. Sep. Sci.* **2009**, *32*, 883-904.
(23) Marriott, P.; Shellie, R. *Trac-Trends in Analytical Chemistry* **2002**, *21*, 573-583.
(24) Song, S. M.; Marriott, P.; Wynne, P. *J. Chromatogr. A* **2004**, *1058*, 223-232.
(25) Blumberg, L. M.; David, F.; Klee, M. S.; Sandra, P. *J. Chromatogr. A* **2008**, *1188*, 2-16.
(26) Blumberg, L. M. *J. Sep. Sci.* **2008**, *31*, 3352-3357.

Chapter 2

METABOLITE PROFILING AND METABOLOMIC ANALYSIS OF INS-1 CELLS USING COMPREHENSIVE TWO-DIMENSIONAL GAS CHROMATOGRAPHY TIME-OF-FLIGHT MASS SPECTROMETRY

Introduction

A thorough understanding of systems biology is important to discover biomarkers and disease mechanisms. Systems biology is comprised of genomics, transcriptomics, proteomics and metabolomics, all of which are complimentary to each other. The metabolome can be defined as the quantitative complement of all the low-molecular weight molecules (<3000 m/z) present in cells in a particular physiological or developmental state. Studying the metabolome has provided the understanding that changes in individual enzyme levels can have significant effects on the concentration of a variety of individual metabolites even if there is little effect on metabolic fluxes.[1] The benefits of metabolomics over transcriptomics and proteomics include the fact that the metabolome is further down the line of gene to function and reflects more closely the activities of the cell at a functional level. Changes in the metabolome are "downstream" results of gene expression and thus may be amplified relative to changes in the transcriptome and proteome.[1] Additionally, unlike transcripts or protein identifications, metabolites are not organism specific and therefore the analytical protocol used to measure a specific metabolite is applicable to fungi, prokaryotes, plants and animals.[2]

The field of metabolomics has been broken down into four different strategies; metabolite target analysis, metabolite profiling, metabolomic analysis and metabolic

fingerprinting. Metabolite target analysis is restricted to metabolites of a particular system that would be directly affected by abiotic or biotic perturbation.[2] Metabolite target analysis is usually accomplished with gas chromatography-mass spectrometry (GC-MS), liquid chromatography-mass spectrometry (LC-MS), or high performance liquid chromatography (HPLC).[2] Metabolite profiling analysis is focused on a group of metabolites, such as those associated with a specific pathway, and metobolomics is the comprehensive analysis of the whole metabolome under a given set of conditions.[1] Both metabolite profiling and metabolomics can be completed using comprehensive two-dimensional gas chromatography coupled to mass spectrometry (GC × GC-MS), HPLC-MS, LC-MS, or LC coupled to nuclear magnetic resonance (LC-NMR).[2] Metabolic fingerprinting is the classification of samples on the basis of either their biological relevance or origin and often involves NMR, direct infusion electrospray ionization MS (DIMS), laser desorption ionization MS (LDI-MS), fourier transform infrared spectroscopy (FT-IR), and Raman spectroscopy.[1, 2]

In this work we use GC × GC time-of-flight MS (ToFMS) to perform both a metabolite profiling and a metabolomics analysis of INS-1 cells. INS-1 cells are a clonal cell line often used as a model for the pancreatic β-cell. β-cells are one of the four major cell types found in the islets of Langerhans, which are "islands" of cells found in the pancreas of mammals.[3] β-cells secrete insulin in response to glucose as well as other nutrients, hormones and nervous stimuli.[3] Type 2 diabetes is characterized by the development of early insulin resistance and the failure of β-cells to compensate with hyperinsulinemia.[3] Failure of the β-cell is crucial to development of type 2 diabetes.

Better understanding of normal and dysfunctional metabolism in these cells may be expected to give insight into β-cell failure in type 2 diabetes.

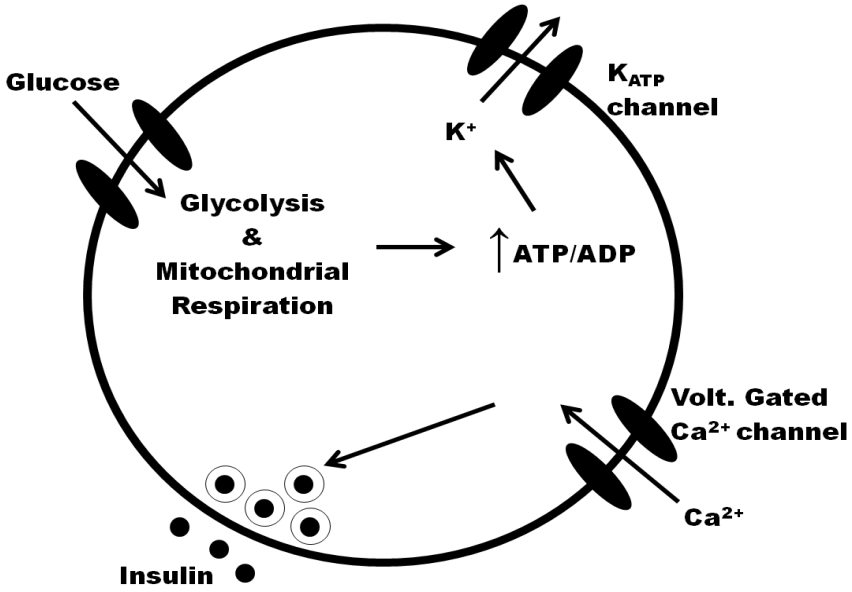

Figure 2.1 Schematic of glucose stimulated insulin secretion (GSIS). Glucose enters the cell through the glucose transporter, triggers glycolysis and mitrochondrial respiration which leads to an increase in the ATP/ADP ratio resulting in closure of the ATP-sensitive K^+-channel (K_{ATP}). The resultant membrane depolarization opens the voltage-dependant Ca^{2+}-channel and allows a flux of calcium into the cell triggering exocytosis of insulin.[4]

Glucose stimulated insulin secretion (GSIS) is metabolically driven as outlined in Figure 2.1. Glucose enters the cell through the glucose transporter and triggers glycolysis and mitochondrial respiration which leads to an increase in the ATP/ADP ratio in the cell and results in closure of the ATP-sensitive K^+-channel (K_{ATP}). The resultant membrane depolarization opens the voltage-dependent Ca^{2+}-channel and allows a flux of calcium into the cell, triggering exocytosis of insulin.[5] Despite the overwhelming data supporting this mechanism for GSIS, there is strong evidence that additional K_{ATP} channel-independent pathways exist, evidence of which is demonstrated in Figure 2.2.[6] In Figure 2.2[6] the response of test cells diverges from that of the control cells approximately 6 minutes after exposure to 250 μM diazoxide and KCl. Diazoxide prevents K_{ATP} channel

operation, therefore the continued release of insulin must be independent of the K_{ATP} channel. A schematic of the K_{ATP} dependent and K_{ATP} channel-independent pathways can be found in Figure 2.3.[7]

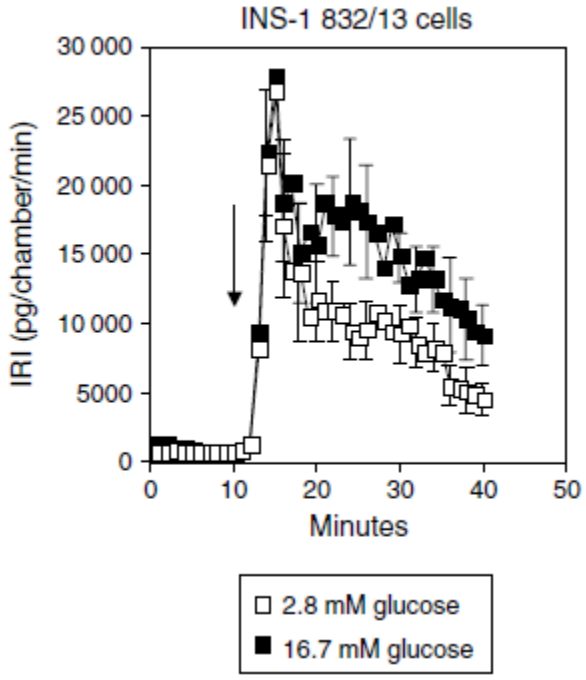

Figure 2.2 Evidence of K_{ATP}-channel independent pathway. The open squares are control cells and the closed squares are test cells. Both the control and the test cells were equilibrated by exposure to Krebs Ringer HEPES buffer (KRHB) containing 2.8 mM glucose for 40 min. AT the ten minute time point both samples were exposed to 250 μM diazoxide and 40 mM KCl at the same time point the test cells were exposed to KRHB containing 16.7 mM glucose. After 6 minutes the insulin secretion of the cells diverged, the control cells slowly decrease and the test cell show an increased rate of release despite the elimination of the KATP-dependant pathway by the diazoxide. (Used with permission from[6])

Although glucose is required for normal insulin secretion, excessive glucose can lead to glucotoxicity and β-cell dysfunction. Once the primary pathogenesis of diabetes is established, hyperglycemia ensues and exerts additional damaging, toxic effects on the β-cell.[8] It has been proposed that continuous overstimulation of the β-cell by glucose could eventually lead to depletion of insulin stores, worsening of hyperglycemia, and deterioration of β-cell function.[8, 9] β-cell lines can be used as a model for glucotoxicity by exposing the cells to media containing high concentrations of glucose for extended

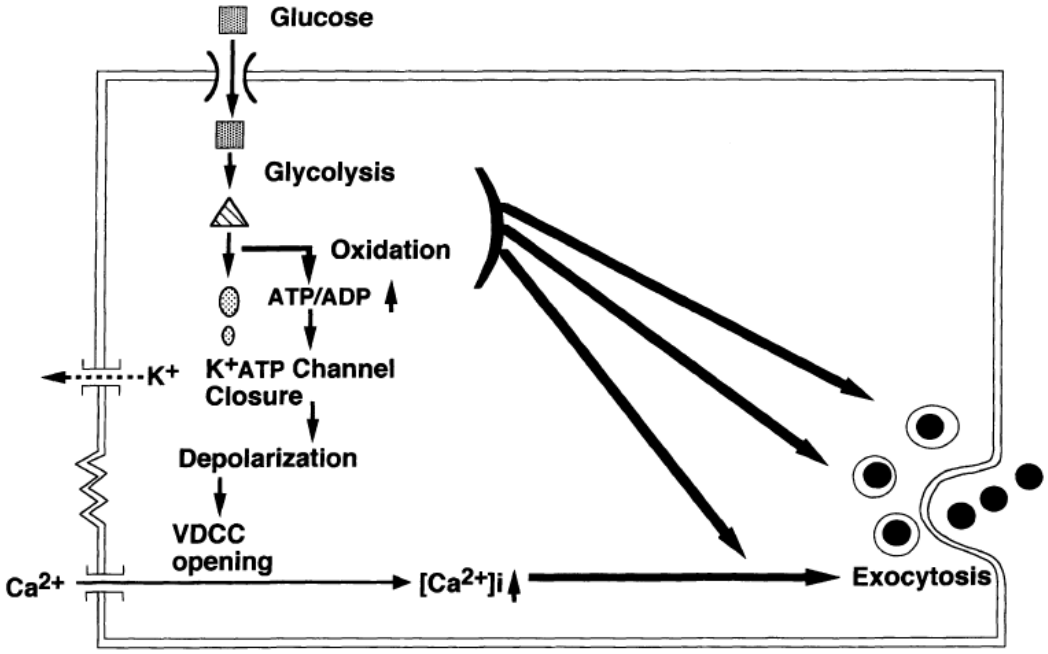

Figure 2.3 K_{ATP} channel-dependent (left) and K_{ATP} channel-independent (arrows on right) glucose signaling pathways in the β-cell are shown. Glucose is transported into the β-cell and is metabolized by a cascade of reactions. The metabolic signals give multiple pathways leading to insulin exocytosis. VDCC, L-type voltage-dependent Ca2+ channel; [Ca2+]i, cytosolic free Ca2+ concentration. (Used with permission from[7])

periods of time.[8, 10] For example, a previous study has shown that cells cultured in 0.8 mM glucose for a prolonged period (multiple passes over several weeks) maintained insulin content and GSIS while identical cells cultured in 11.1 mM glucose had drastically compromised insulin content and GSIS.[8] Specifically, INS-1 cells have been used to show that glucotoxic β-cells have additional, more distal defects in the exocytotic pathway,[8, 10, 11] that glucotoxicity alters calcium handling in cells, and that glucotoxicity alters the expression of several key proteins in exocytosis.[10] Thus, an analysis of the INS-1 metabolome may help identify pathways that are activated during hyperglycemia and glucotoxicity and lead to a better understanding of type 2 diabetes.[11]

In this study, we used GC × GC to determine metabolite changes that occur as a function of increasing glucose from 3 to 7 to 17 mM. We use both metabolite profiling

and undirected metabolomics analysis. The metabolite profiling analysis focuses on the glycolysis and mitochondrial respiration step of GSIS by targeting metabolites amendable to GC in the citric acid cycle and glycolysis as shown in Figure 2.4.

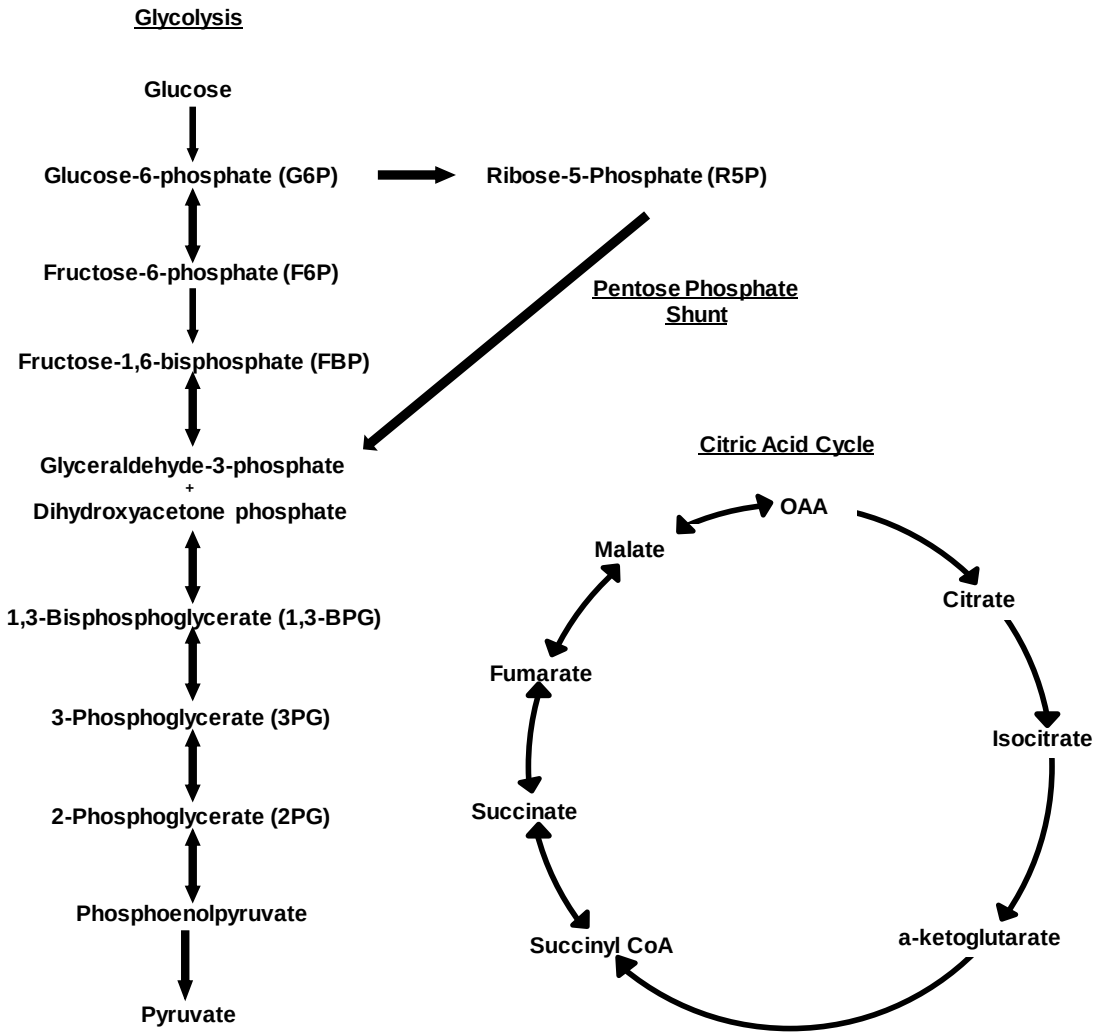

Figure 2.4 Schematics of glycolysis, the pentose phosphate shunt, and the citric acid (TCA) cycle. When glucose enters the cell, glycolysis is initiated and the glucose is metabolized to pyruvate which enters the TCA cycle.[4]

Additionally, amino acids can feed into pathways of glucose oxidation and anaplerosis; thus amino acids were profiled as well.[12] In this work we double the number of target analytes identified when compared to a previous GC/MS study of INS-1 cells stimulated

by glucose and show that our results are in good agreement with what has been observed previously.[13]

While the metabolite profiling experiments allowed us to examine the reproducibility of the method and ensure that it provided results consistent with known metabolic changes, the metabolomics method allowed us to identify changes in additional metabolites under the experimental conditions. Such changes provide clues to metabolic pathways associated with insulin secretion and allowed for the detection of changes at supramaximal (for insulin secretion) glucose concentrations. As discussed earlier, such changes may help to identify pathways associated with glucotoxicity.

GC × GC was used for this work because it is capable of both metabolite profiling and metabolomic analysis. Additionally, the increased detectability and increased peak capacity provide distinct advantages when compared to other methods used for metabolite analysis. Metabolomics using GC × GC is a rapidly emerging area of study; however, prior to this work, it has not been applied to insulin secreting cells. Previous work includes analysis of metabolites in rye grass samples,[14] urine,[15] blood plasma,[16, 17] mouse spleen tissue extracts,[18, 19] rice,[20] and yeast cells.[21, 22]

Experimental

Reagents

All chemicals were purchased from Sigma-Aldrich (St. Louis, MO) unless otherwise noted. Roswell Park Memorial Institute (RPMI) media, fetal bovine serum (FBS), HEPES, and penicillin-streptomycin were purchased from Invitrogen Corp. (Carlsbad, CA). Cell lifters and 10 cm polystyrene non-pyrogenic culture dishes were

purchased from Corning (Lowell, MA). Methoxyamine hydrochloride, pyridine, HPLC grade methanol, citrate, 4 dram screw cap vials, 2 mL autosampler vials and 200 µL inserts were purchased from Fisher Scientific (Fairfield, NJ). Ornithine was from Acros Organics (Morris Plain, NJ). D^6-succinate was from Cambridge Isotopes (Andover, MA).

Samples

INS-1 cells were cultured on 10 cm plates in RPMI-1640 (+l-glutamine) supplemented with 10 % FBS, 1 mM pyruvate, 10 mM HEPES, 50 µM 2-β-mercaptoethanol, and 1 unit penicillin-streptomycin. INS-1 cells were grown to confluence (~4 x 10^7 cells) in 10 cm polystyrene dishes with RPMI culture media. All cells used in a particular experiment were seeded at the same time, taking care to minimize variability by using precise volumes of reagents and seed cells.

Krebs-Ringer-HEPES buffer (KRHB) was prepared to contain 3 mM glucose, 20 mM HEPES, 118 mM NaCl, 5.4 mM KCl, 2.4 mM CaCl, 1.2 mM $MgSO_4$, and 1.2 mM KH_2PO_4, and adjusted to pH 7.4 with HCl. Cells were washed once with 10 mL of KRHB prior to incubation in 10 mL of KRHB for 30 min. The KRHB glucose concentration was then left at 3 mM or raised to 7 or 17 mM for 18 min at 37 °C. Each glucose concentration was prepared in quadruplicate, however, only three plates were available for 3 and 17 mM. After treatment, cells were washed once with 10 mL milli-Q water and snap frozen with liquid nitrogen. Plates were stored at -80 °C until extraction.

Extraction and Derivatization

Extraction was performed by adding 700 µL of ice cold 80:20 methanol water to each plate and scraping for approximately 1 min. Samples were then transferred to

4 dram glass vials and dried on an Eppendorf Vacufuge (Hauppauge, NY) at room temperature for 1.5 h. After drying, samples were capped and stored at -80 °C until derivatization. All samples were derivatized within 24 h of being analyzed by GC × GC.

Derivatization was performed by warming the extracted samples to room temperature, d^6-succinate and ^{13}C-glucose were added such that the final concentration of each would be 30 μM in the final derivatization volume of 130 μL and the samples were placed on the vacufuge for 20 min. Fifty μL of 20 mg/mL methoxyamine hydrochloride in pyridine was added and samples were incubated at 30 °C for 1.5 h. 80 μL of Regisil (BSTFA with 10% TMCS) was then added to each sample followed by incubation at 70 °C for 50 min. Samples were allowed to shake at room temperature for 1.5 h and then transferred to 2 mL autosampler vials with 200 μL inserts.

Comprehensive Two-Dimensional Gas Chromatography Time-of-Flight Mass Spectrometry

GC×GC analysis was performed on a Leco Pegasus III with 4D upgrade (St. Joseph, MI). The primary column was a 30 m Rxi®-1ms (0.25 mm i.d., 0.18 μm film) and the secondary column was a 2 m Rtx®-200 (0.18 mm i.d., 0.2 μm film) both from Restek Corporation (Bellefonte, PA). A 1 μL injection was made with an Agilent 7683 automatic liquid sampler (Palo Alto, CA) in splitless mode and five replicates were completed for each sample. The primary oven was maintained at 70 °C for 0.5 min and then increased at a rate of 3 °C per minute to 250 °C and maintained for 5 min. The secondary oven and the thermal modulator were offset from the primary oven by 5 °C and 30 °C respectively. A modulation period of 7 s was used and the hot pulse time (length of time the hot jet fires to initiate injection on the second dimension) was 0.6 s. A flow rate of 1 mL/min

ultra-high purity helium with an inlet and mass spectral transfer line temperature of 250 ℃ and 300 ℃, respectively, were maintained. A mass range of m/z 45 to 1000 was collected at a rate of 200 spectra/s after a 390 s solvent delay. The ion source was maintained at 200 °C.

Preparation and Analysis of Standards

A stock solution containing ornithine, ribose-5-phosphate (R5P), glucose-6-phosphate (G6P), 3-phosphoglycerate (3PG), pyruvate, lactate, citrate, isocitrate, fumarate, succinate, frucutose-6-phosphate (F6P) and malate was prepared in milli-Q water. Aliquots were transferred to 4 dram vials such that the final concentration would be 30 μM (after derivatization). A commercially available amino acid standard (Sigma-Aldrich, St. Louis, MO) was also diluted and transferred to 4 dram vials; the final concentration was again 30 μM in 130 μL final volume. Standards were evaporated to dryness, derivatized using the same methodology and analyzed under the same chromatographic conditions as the INS-1 cell extracts.

Data Analysis

Leco ChromaTOF version 4.22 was used for instrument control and data processing. Identification of target analytes was completed through mass spectral library searches and comparison to metabolite standard retention times. The National Institutes of Standards and Technology (NIST) mass spectral library (version 2.0) and a library obtained from the Max Planck Institue of Molecular and Plant Physiology (http://www-en.mpimp-golm.mpg.de/02-instUeberInstitut/04-instRessources/webbasedRsrc/metaboliteMSL/index.html) were used. A similarity threshold of 700/1000 between a library mass spectrum and an analyte mass spectrum

was considered a match. This value was determined to be sufficiently high to minimize the number of false positives while also limiting the number of false negatives. Retention time shifts within 1 modulation period, in the first dimension, were allowed and 0.2 seconds, in the second dimension, as this was on the order of the typical second dimension peak widths.[18]

Statistical significance was determined in GraphPad Prism version 3.03 (La Jolla, CA) using a one way ANOVA analysis and a Newman-Keuls post-hoc test. All statistical analysis was performed using the ratio of peak area to d^6-succinate peak area except for glucose which was analyzed using ^{13}C-glucose instead of d^6-succinate. Metabolite mapping was performed using the Metscape[23] plug-in for Cytoscape.[24, 25]

Results

Metabolite Standards

A commercially available amino acid standard containing 30 µM alanine, valine, glycine, serine, methoinine, aspartate, proline, threonine, isoleucine, phenylalanine, glutamine, lysine, tyrosine, cystine, arginine and histidine was derivatized and analyzed via GC × GC to verify detectability and determine retention times of the available amino acids. As Figure 2.5 illustrates, all analytes were detected and identified except histidine and arginine. Cystine was detected but is not shown in Figure 2.5 for clarity. Glycolysis and citric acid cycle metabolites amendable to GC were also analyzed to verify detectability and determine retention times, and a representative chromatogram can be found in Figure 2.6. 2-Phosphoglycerate (2PG), data not shown, was also detected when a sample containing only 2PG and 3PG was run.

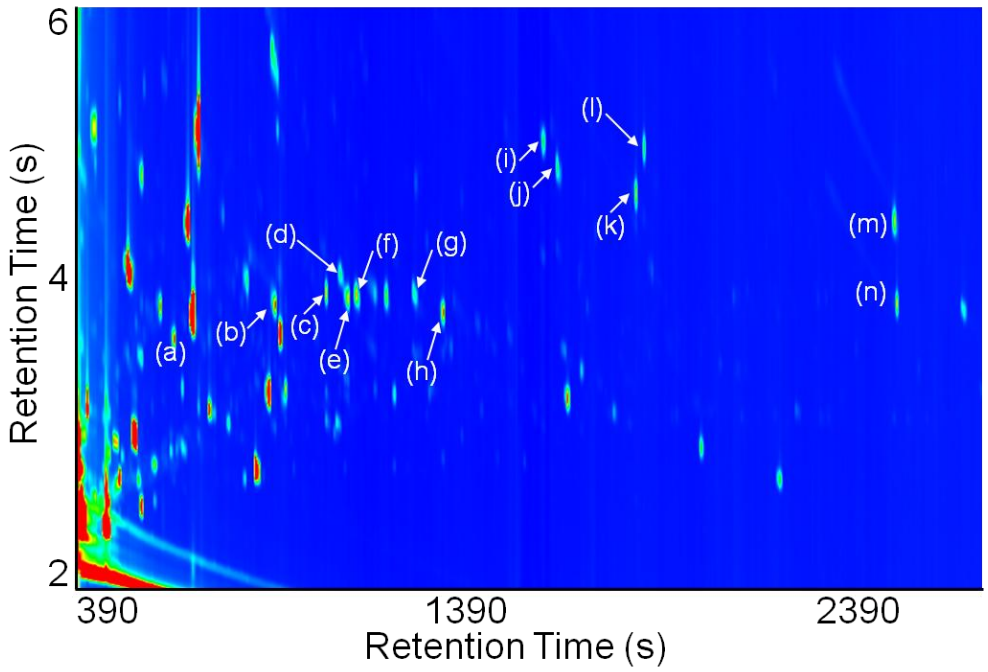

Figure 2.5 Total ion chromatogram of the commercially available amino acid standard. Alanine (a), valine (b), leucine (c), proline (d), isoleucine (e), glycine (f), serine (g), theronine (h), methionine (i), aspartate (j), phenylalanine (k), glutamine (l), tyrosine (m), lysine (n).

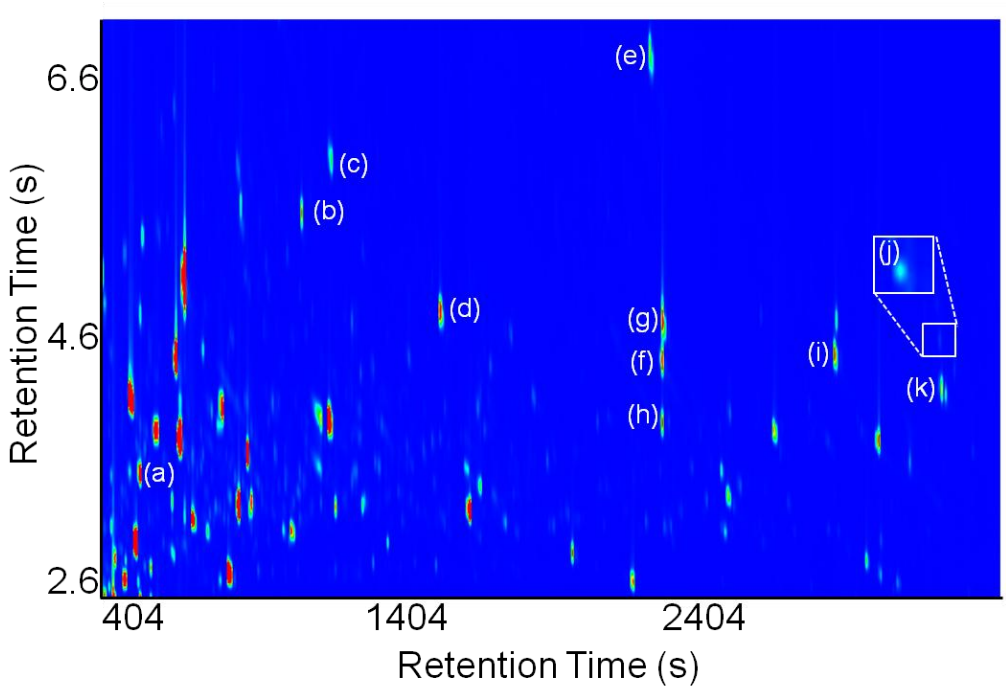

Figure 2.6 Total ion chromatogram of glycolysis and TCA standards. Lactate (a), succinate (b), fumarate (c), malate (d), 3PG (e), citrate (f), isocitrate (g), ornithine (h), R5P (i), F6P (j), G6P (k).

In LC studies of similar metabolites citrate and isocitrate are often reported as one peak, as are G6P and F6P. Using GC × GC we are able to separate these isomers. All detectable standard analytes plus glucose were used as target metabolites during analysis of the INS-1 cell extracts. Calibration curves were created for 15 standard analytes. Linear correlation coefficients of 0.99 or greater were achieved in the range of 1 to 30 µM. A representative calibration curve for proline is shown in Figure 2.7.

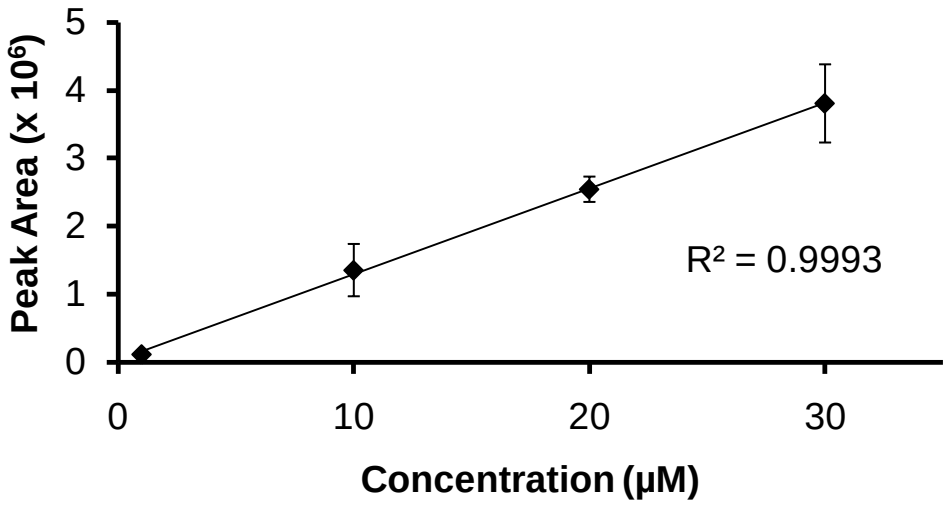

Figure 2.7 Calibration curve for proline. Samples were analyzed in triplicate and error bar is ± standard deviation.

Metabolite Profiling

Figure 2.8 illustrates a glucose-stimulated insulin secretion dose-response curve from INS-1 cells. As can be seen here, cells were stimulated at glucose concentrations that correlate with low (3 mM), moderate (7 mM), and high (17 mM) insulin release. Twenty seven of thirty target metabolites (listed in Table 2.1) were detected in INS-1 cell extracts at all three glucose concentrations. Lysine was not detected at 3 mM glucose. It was also only detected in one 7 mM sample and one 17 mM sample. Isocitrate and cystine were not detected in any of the INS-1 cell extracts. A representative total ion

chromatogram (TIC) can be found in Figure 2.9 (top) with additional ion channels and zoomed in portions (boxes below TIC) demonstrating the location of the twenty seven targets.

The average relative standard deviations (RSDs) for repeat, 1 μL, splitless injections of the same extract, or technical RSDs, were 18, 17 and 14 %. The technical RSD of the 30 μM amino acid standard and glycolysis/tca standard were 12 % and 13 %, respectively. The average RSDs of each successful injection at a given glucose concentration, or biological RSDs, were 27, 24 and 20 % for 3 mM, 7 mM and 17 mM glucose respectively. The technical and biological RSDs for each analyte, at each glucose concentration, can be found in Tables 2.2 and 2.3. Metabolite levels at each glucose concentration were compared using one-way ANOVA.

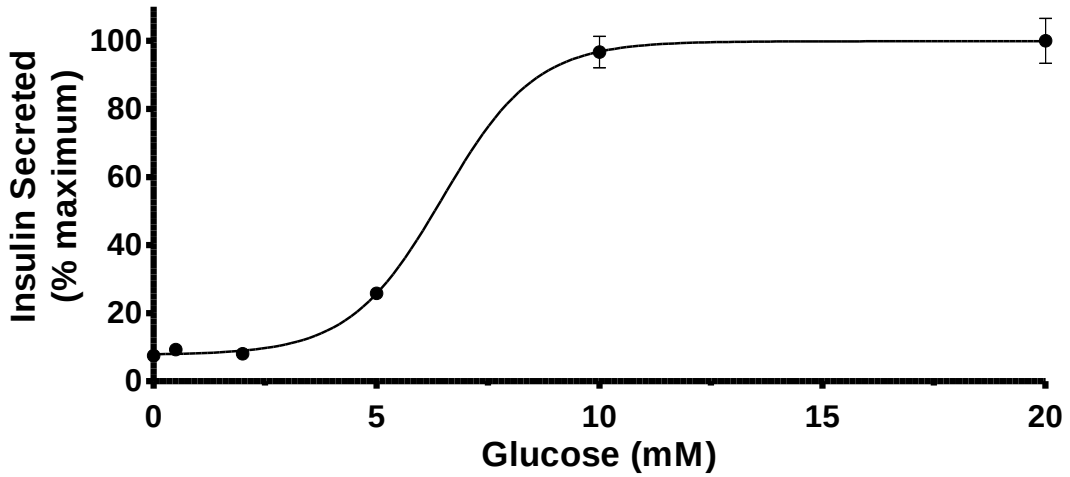

Figure 2.8 Glucose dose-response curve where maximal insulin release occurs at ~10 mM glucose. Data was obtained from 10cm plates of INS-1 grown to ~ 70% confluence (31 MM cells) in RPMI. Media changed to low glucose RPMI (3mM) for ~20 hr prior to experiment. Media changed to KRB (no glucose + 0.2% FAF BSA) and spiked to indicated glucose concentration. Media removed for insulin measurement and metabolism quenched at30 min. Error bars are SEM. n=3. Data and figure courtesy of Matthew Lorenz.

Table 2.1 List of target metabolites.

Ornithine	Alanine
Ribose-5-Phosphate	Valine
Glucose-6-Phosphate	Glycine
3-Phosphoglycerate	Serine
2-Phosphoglycerate	Methionine
Pyruvate	Aspartate
Lactate	Proline
Citrate	Threonine
Isocitrate	Isoleucine
Fumarate	Phenylalanine
Succinate	Glutamine
Fructose-6-Phosphate	Lysine
Malate	Tyrosine
Cystine	

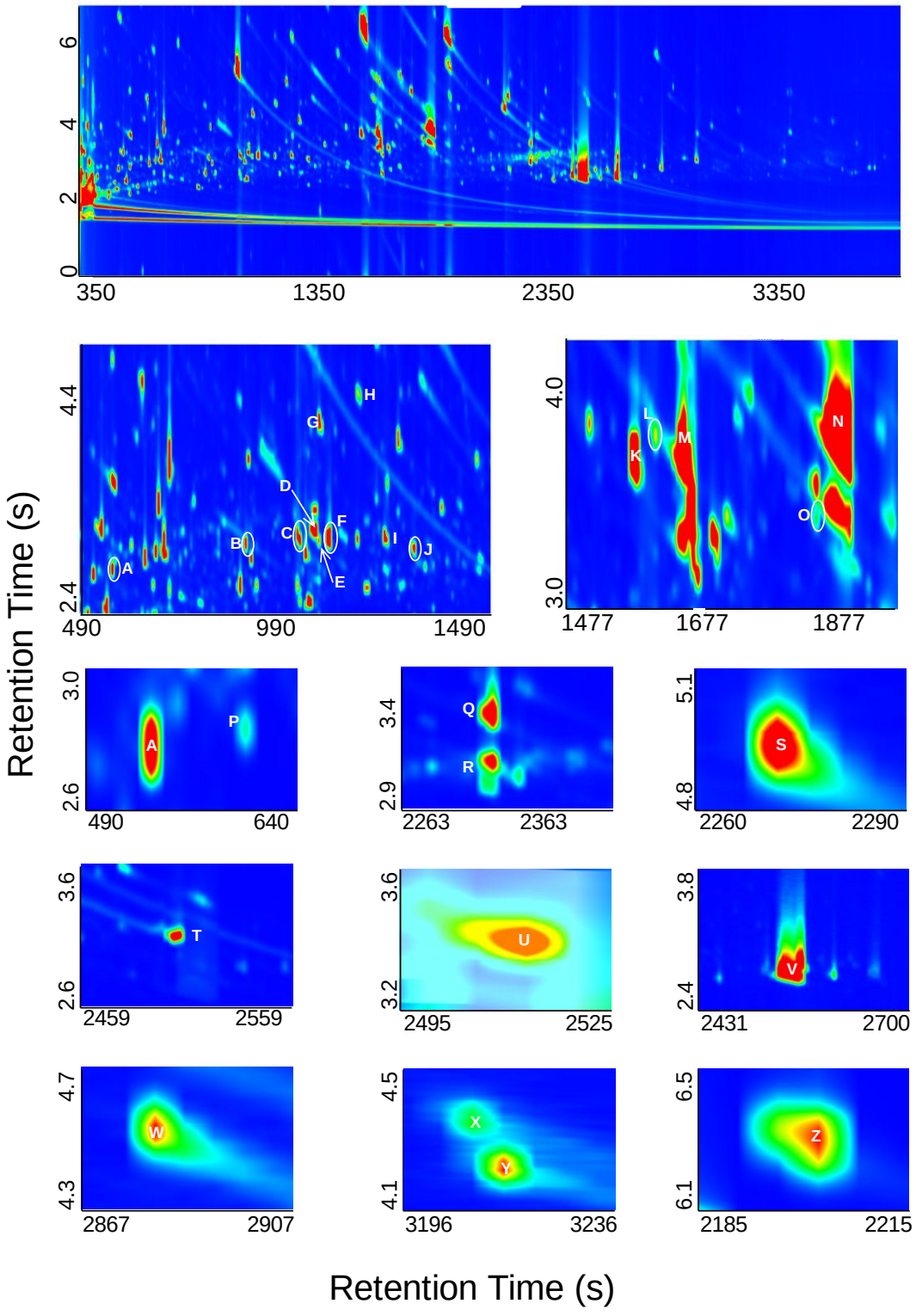

Figure 2.9 Total ion chromatogram of a 17 mM INS-1 cell extract (top). Analytes of interest are highlighted for clarity. Lactate (A), valine (B), leucine (C), proline (D), isoleucine (E), glycine (F), succinate (G), fumarate (H), serine (I), threonine (J), malate (K), methionine (L), aspirate (M), glutamate (N), phenylalanine (O), pyruvate (P), citrate (Q), ornithine (R), 3PG (S), lysine (T), tyrosine (U), glucose (V), R5P (W), F6P (X), G6P (Y), 2PG (Z).

Table 2.2 Technical relative standard deviations for metabolite profiling analysis

	3 mM Glucose	7 mM Glucose	17 mM Glucose
Alanine	11	18	16
Valine	12	11	6.5
Proline	13	18	13
Glycine	16	17	16
Fumarate	11	9.1	11
Threonine	13	16	12
Malate	6.4	10	7.1
Methionine	31	23	20
Aspartate	20	25	16
Phenylalanine	13	27	25
Ornithine	50	42	22
Citrate	11	9.8	20
Tyrosine	18	23	22
R5P	33	8.5	18
F6P	29	13	14
G6P	25	25	12
Succinate	7.4	9.6	4.1
Glutamine	24	11	12
Isoleucine	12	16	14
Leucine	7.8	24	9.9
Lactate	7.45	18	17
Pyruvate	34	12	9.5
Serine	36	25	9.7
Glucose	2.8	9.5	18
3PG	5.2	9.8	10
2PG	12	11	10

Table 2.3 Biological relative standard deviations for metabolite profiling analysis.

	3 mM Glucose	7 mM Glucose	17 mM Glucose
Alanine	12	20	1.9
Valine	4.6	26	18
Proline	13	16	4.9
Glycine	5.4	20	14
Fumarate	13	14	12
Threonine	7.2	36	19
Malate	35	27	14
Methionine	37	24	39
Aspartate	37	7.4	22
Phenylalanine	72	39	38
Ornithine	64	36	46
Citrate	19	26	20
Tyrosine	39	63	43
R5P	37	14	32
F6P	58	22	20
G6P	43	31	24
Succinate	13	12	11
Glutamine	44	13	8.0
Isoleucine	25	20	32
Leucine	17	43	16
Lactate	15	13	5.1
Pyruvate	5.5	27	19
Serine	49	56	18
Glucose	3.2	3.6	25
3PG	13	4.4	8.0
2PG	7.2	11	10

Metabolomic Analysis

Fisher Ratio anlaysis was used to perform a metabolomic analysis of all analytes changing between each glucose concentration, that is, from 3 mM glucose to 7 mM glucose, from 3 mM glucose to 17 mM glucose and from 7 mM glucose to 17 mM glucose. A Fisher Ratio is defined as the class-to-class variation of the detector signal divided by the sum of the within-class variations of the detector signal and is calculated using Equation 3.1[15]

$$Fisher\ Ratio = \frac{{\sigma_{cl}}^2}{{\sigma_{err}}^2} \tag{3.1}$$

where σ_{cl} is the class-to-class variation and σ_{err} is the within-class variation. σ_{cl} and σ_{err} are described in Equations 3.2 and 3.3[15]

$${\sigma_{cl}}^2 = \frac{\sum(\bar{x}_i - \bar{x})^2 n_i}{(h-1)} \tag{3.2}$$

$${\sigma_{err}}^2 = \frac{\sum\left(\sum\left(\bar{x}_{ij} - \bar{x}\right)^2\right) - (\sum(\bar{x}_i - \bar{x})^2 n_i)}{(N-h)} \tag{3.3}$$

Where n_i is the number of measurements in the i^{th} class, $\bar{x}_i$ is the mean of the i^{th} class, $\bar{x}$ is the overall mean, h is the number of classes, $\bar{x}_{ij}$ is the i^{th} measurement of the j^{th} class and N is the total number of sample profiles.[15]

One advantage of using the Fisher Ratio calculation is that the calculation is robust against biological diversity because it differentiates class-to-class variation from within-class variation. Additionally, unlike other statistical methods, it does not just consider a subset, such as the TIC or a single mass channel, of the 4D data generated by

GC × GC-ToFMS. The Fisher Ratio calculation considers all of the data simultaneously and objectively identifies the most significant differences between complex samples.[21]

A significant Fisher Ratio must be determined by the analyst;[26] therefore, to establish a reasonable threshold for this data set, all of the 3 mM glucose data was randomized into two groups and a Fisher Ratio analysis performed the results of which can be found in Figure 2.10(A).

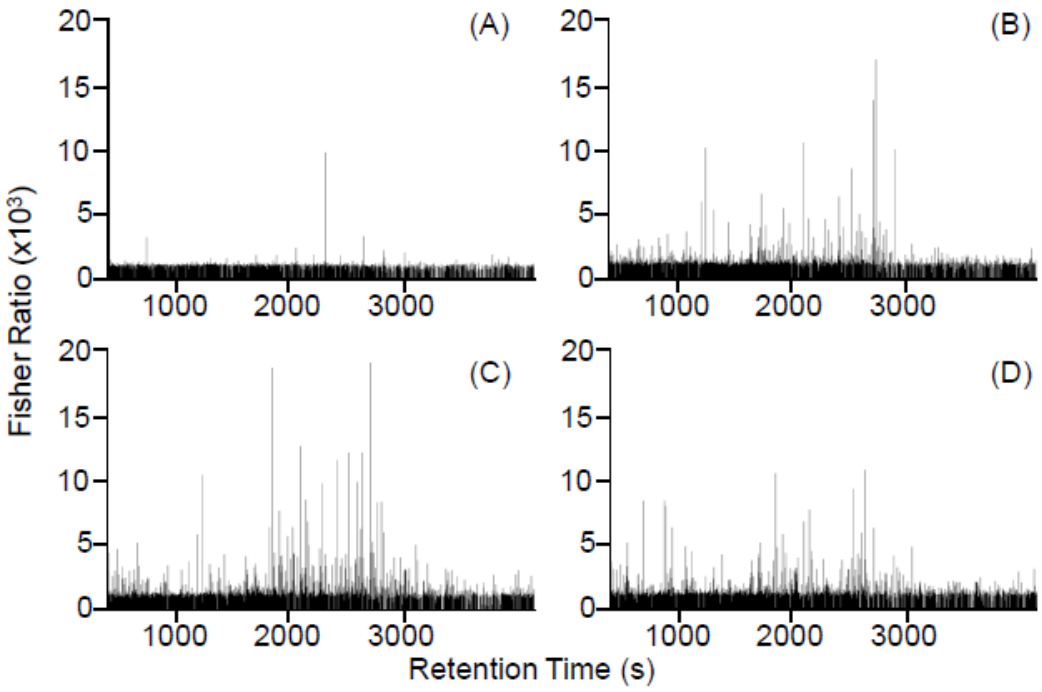

Figure 2.10 Fisher Ratio plots for randomized 3 mM glucose groups (A), 3 mM glucose compared to 7 mM glucose (B), 3 mM glucose compared to 17 mM glucose (C) and 7 mM glucose compared to 17 mM glucose (D). The red line in (A) indicates the 1064 threshold.

Aside from a few artifacts, there is little change between analytes when the two randomized 3 mM groups are compared. A value of 1064 was chosen as the threshold for this work, i.e. any compounds with a Fisher Ratio of greater than 1064 were considered to be changing significantly between the glucose concentrations. This threshold is shown

on the 3 mM versus 3 mM glucose and 3 mM versus 17 mM glucose Fisher Ratio plots in Figure 2.11. As shown on the histograms in Figure 2.12, the threshold of 1064 excludes all but 4 % of the data from the 3 mM versus 3 mM glucose analysis and 34 % from the 3 mM versus 17 mM data, thus providing a minimum number of both false positives and false negatives.

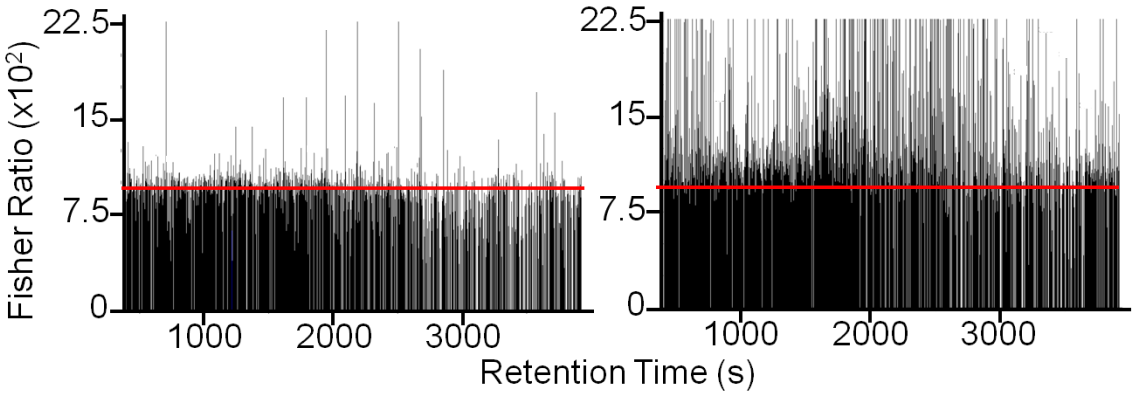

Figure 2.11 Zoomed in Fisher Ratio plots for 3 mM versus 3 mM glucose (left) and 3 mM versus 17 mM glucose (right) with red line indicating the 1064 threshold.

Of the 3128 peaks detected in the 3 mM versus 3 mM glucose data set, 135 (4 %) are above the 1064 threshold which is highlighted in Figures 2.11 and 2.12. However, only 38 of the peaks were identified by the software and 8 of those peaks can be attributed to column bleed or the derivatization agent. Therefore, approximately 1 % of the peaks detected in the 3 mM versus 3 mM data were significantly changing and are potential false negatives at the 1064 threshold. Contributions from column bleed and derivatization reagents were also disregarded. Fisher Ratio plots for the analysis of 3 mM glucose to 7 mM glucose, 3 mM glucose to 17 mM glucose and 7 mM glucose to 17 mM glucose can be found in Figures 2.10(B) through (D). Unlike in 2.10(A), there are 1133 analytes with a Fisher Ratio greater than 1064 in the 3 mM to 17 mM analysis and 882 and 1051

in the 3 mM glucose to 7 mM glucose and 7 mM to 17 mM glucose analyses respectively.

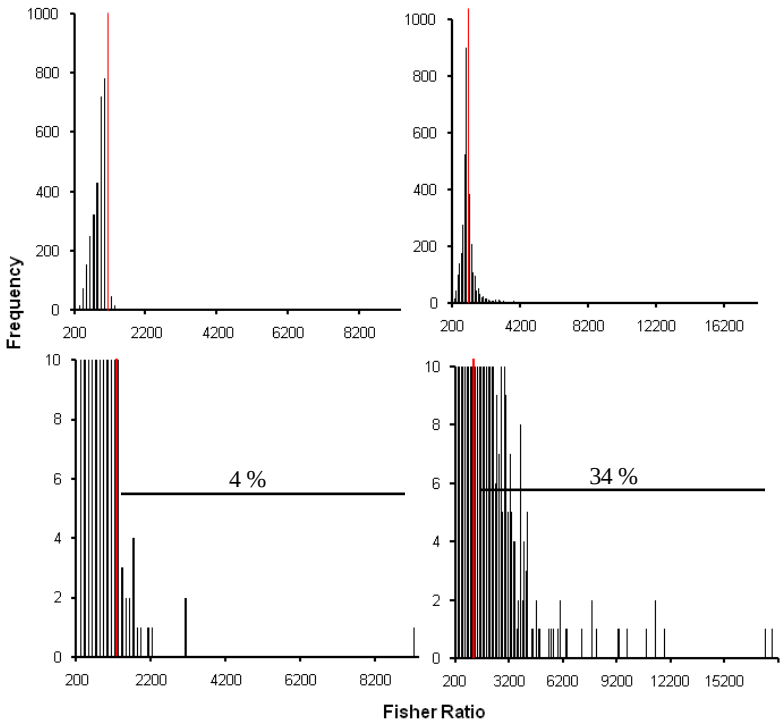

Figure 2.12 Histograms of Fisher Ratios for 3 mM vs 3 mM glucose (top left) and 3 mM vs 17 mM glucose (top right). Rescaled histograms of Fisher Ratios for 3 mM vs 3 mM glucose (bottom left) and 3 mM vs 17 mM glucose (bottom right). Red lines indicate the location of the 1064 Fisher Ratio threshold with only 4 % of the compounds in the 3 mM vs 3 mM glucose data falling above this threshold.

Nine hundred fifty (3 mM to 17 mM), 696 (3 mM to 17 mM) and 873 (7 mM to 17 mM) of the analytes with a Fisher Ratio above 1064 were not identified, i.e. a match between the mass spectrum for the peak and a library mass spectrum of 70 % or greater did not exist. Additionally, if a duplicate was found, the peak with the lower Fisher Ratio was disregarded as well. Kyoto Encyclopedia of Genes and Genomes (KEGG)[27-29] identifications were assigned to all analytes for which a KEGG ID existed and analytes with multiple derivatives were only included once. This process, which is summarized in Figure 2.11, left 73, 80, and 65 analytes of interest in the 3 mM to 7 mM, 3 mM to

17 mM and 7 mM to 17 mM data sets, respectively. The final lists for each data set, including KEGG ID, direction of change, average areas and area differences, can be found in Appendices A through C.

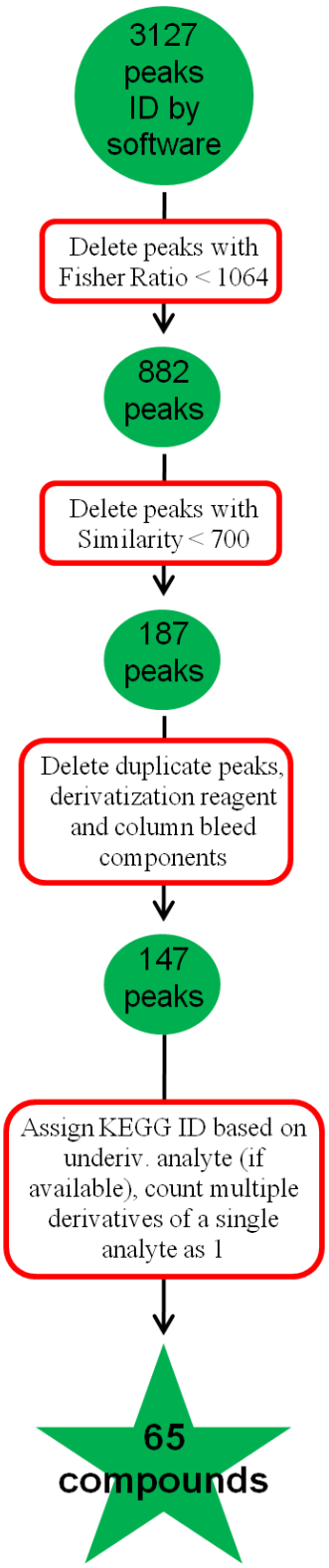

Figure 2.13 Flow chart summarizing the process used for determining analytes of interests in the 7 mM to 17 mM glucose data set after Fisher Ratio analysis. This method was also used for the 3 mM to 7 mM and 3 mM to 17 mM glucose data sets.

To interpret the changes in cellular content of these analytes and to identify metabolic pathways that were affected by glucose, we used the Metscape[23] plug-in for Cytoscape.[24, 25] Cytoscape is an open source software platform for the visualization and analysis of complex data sets such as the metabolomics data acquired in this work. The maps of the metabolic pathways obtained for each of the three data sets are shown in Figures 2.14 through 2.16 where the red dots represent the analytes input by the user (or seeds) and the blue spots represent other metabolites involved in the pathways, the black dots are reactions that the analytes are involved in and the lines connect the related metabolites and reactions to create the map of pathways. The maps each consist of one big network where all of the target analytes are connected, a few small sub networks, and some isolated analytes that are not connected to the pathways involved or for which a pathway does not exist. Each of these components is highlighted in Figure 2.14 for clarity. The analytes were involved in 32 metabolic pathways that can be found in Table 2.4. Additionally, a list of isolated analytes can be found in Table 2.5.

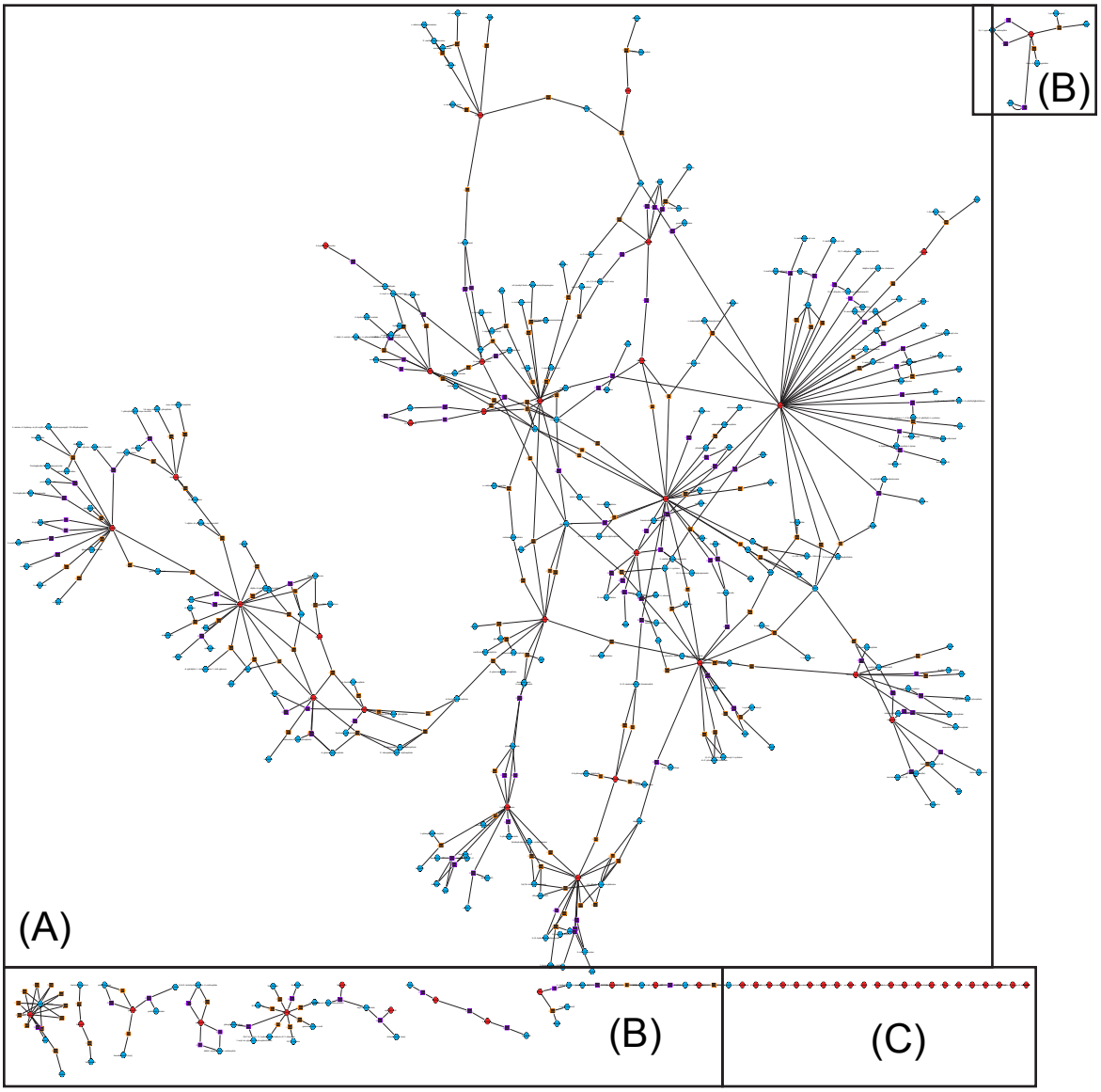

Figure 2.14 Pathway map for 3 mM to 7 mM glucose data set obtained from Metscape.[23] The large main network is shown in (A), sub networks are highlighted in (B) and isolated analytes in (C).

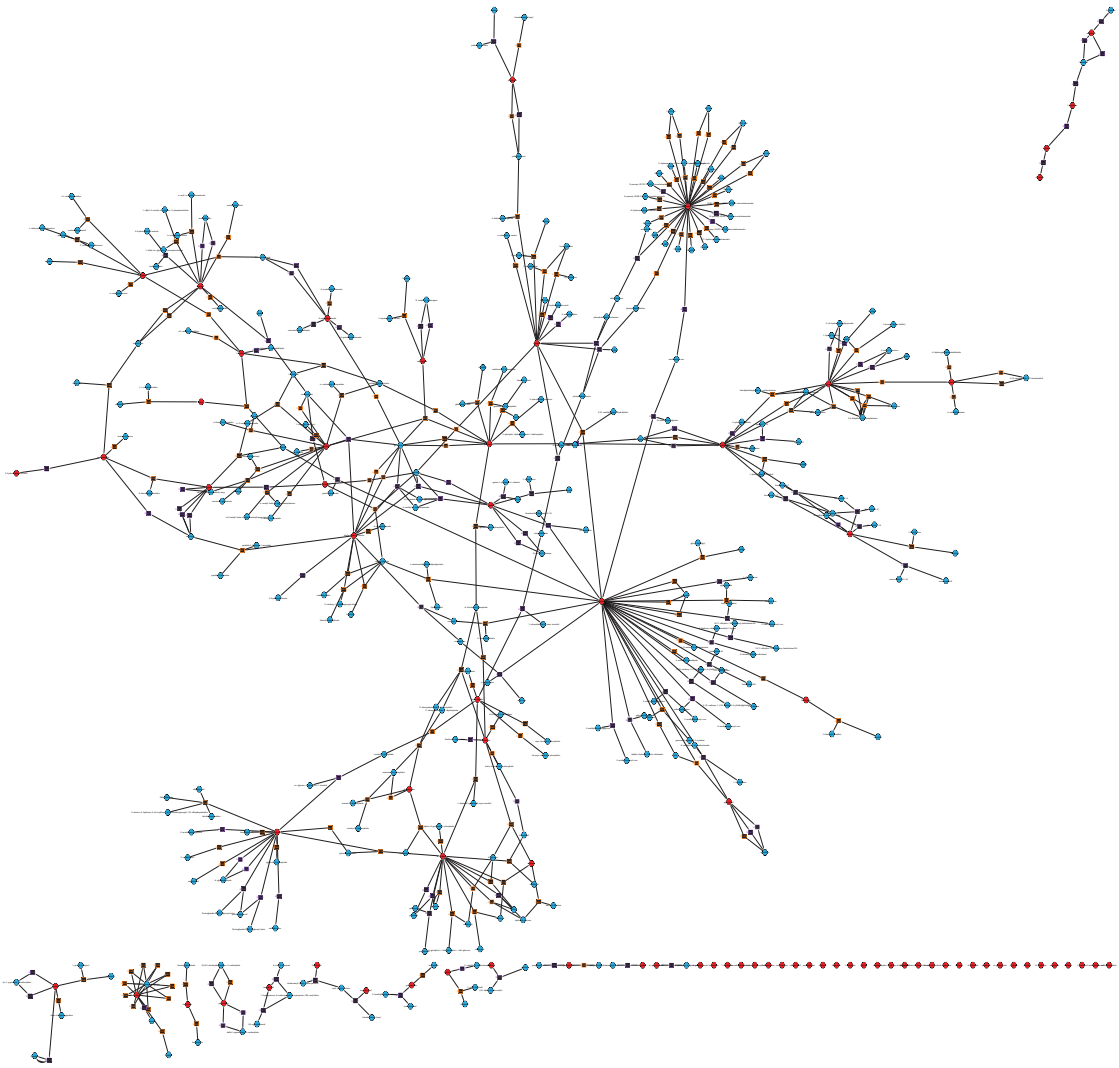

Figure 2.15 Pathway map for 3 mM glucose to 17 mM glucose obtained from Metscape.[23]

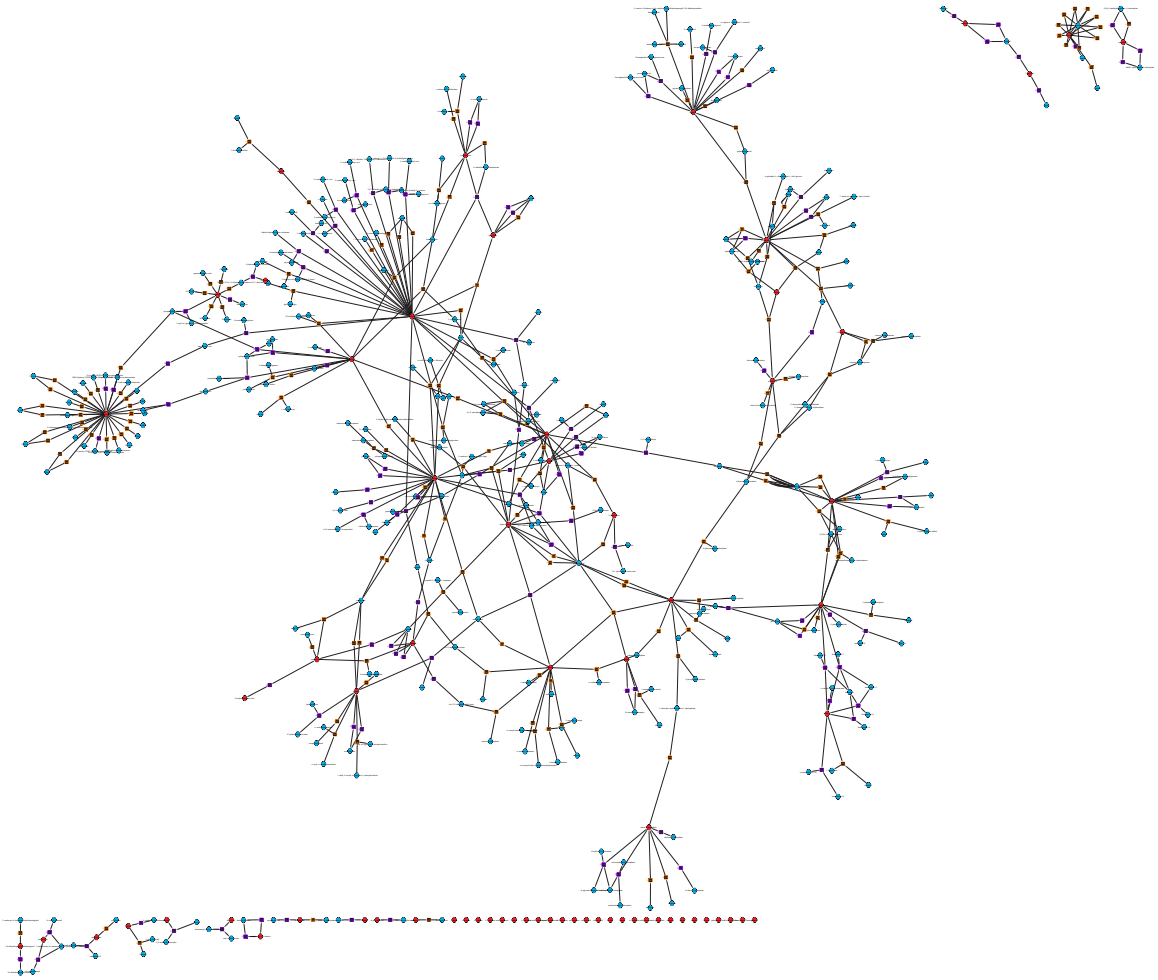

Figure 2.16 Pathway map for 7 mM glucose to 17 mM glucose obtained from Metscape.[23]

Table 2.4 Active metabolic pathways, as indicated by Metscape,[23] for metabolomic analysis.

	3 mM to 7 mM	3 mM to 17 mM	7 mM to 17 Mm
Aminosugars metabolism	x	x	x
Arachidonic acid metabolism	x	x	x
Bile acid biosynthesis	x	x	x
Biopterin metabolism	x	x	x
Butanoate metabolism	x	x	x
De novo fatty acid biosynthesis	x	x	x
Di-unsaturated fatty acid beta-oxidation	-	-	x
Fructose and mannose metabolism	x	x	x
Galactose metabolism	x	x	x
Glycerophospholipid metabolism	x	x	x
Glycine, serine, alanine and threonine metabolism	x	x	x
Glycolysis and Gluconeogenesis	x	x	x
Glycosphingolipid metabolism	x	x	x
Histidine metabolism	x	x	x
Leukotriene metabolism	x	x	x
Linoleate metabolism	x	x	x
Lysine metabolism	x	x	x
Methionine and cysteine metabolism	x	x	x
Omega-6 fatty acid metabolism	x	x	x
Pentose phosphate pathway	x	x	x
Phosphatidylinositol phosphate metabolism	x	x	x
Porphyrin metabolism	x	x	x
Propanoate metabolism	x	x	x
Prostaglandin formation from arachidonate	x	x	x
Purine metabolism	x	x	x
Pyrimidine metabolism	x	x	x
Saturated fatty acids beta-oxidation	x	x	-
TCA cycle	x	x	x
Tyrosine metabolism	x	x	x
Urea cycle and metabolism of arginine, proline, glutamate, aspartate and asparagine	x	x	x
Valine, leucine and isoleucine degradation	x	x	x
Vitamin B3 (nicotinate and nicotinamide) metabolism	x	x	x
Vitamin B5 - CoA biosynthesis from pantothenate	-	-	x

Table 2.5 List of isolated analytes as indicated by Metscape analysis.[23]

Analyte	3 mM to 7 mM	3 mM to 17 mM	7 mM to 17 mM
(r)- malate	x	-	-
2-trans,6-trans-farnesol	x	x	x
5-cholestene	-	x	x
5-oxo-d-proline	x	x	x
6-carboxyheanoate	-	x	x
aminomalonate	-	-	x
aspirin	-	-	x
azulene	x	x	x
butanal	-	x	x
caprylic acid	x	-	x
decanal	-	x	x
d-erythrose	x	x	x
d-fructose-2-phosphate	-	x	-
d-galactonate	x	x	x
d-galacturonate	-	x	-
d-ribonate	-	x	-
diethanolamine	x	-	-
d-ribonate	x	-	-
elaidic acid	x	x	x
ent-kaurene	x	x	x
galacturonic acid	-	-	x
glutarate	x	x	x
hexanoate	-	x	-
hydroxylamine	x	-	-
l-arabinfuranose	x	-	-
l-arabinose	-	x	-
l-lyxose	-	x	x
l-norleucine	-	x	x
l-norvaline	x	-	-
l-octanol	-	x	-
l-rhamnose	x	x	x
malonate	-	x	x
mannitol	x	x	x
myristoleic acid	x	-	-
orthophosphate	x	x	x
orthophosphate	-	x	x
oxalate	x	x	-
pentadecane	x	-	x
suberic acid	x	x	x
tridecane	-	x	-
xylose	-	x	x

Discussion

Metabolite Profiling

Twelve more target analytes than what was detected in a previous GC/MS study were indentified in this work.[13] The novel targets detected are methionine, phenylalanine, tyrosine, F6P, succinate, glutamate, leucine, isoleucine, 2PG, 3PG and lactate, all as trimethylsilyl derivatives. Additionally, in the previous GC/MS study,[13] hydroxyproline was detected but, in this study, proline was detected and identified. Compared to the previous GC/MS report, the biological RSDs reported here are slightly high for 3 mM and 7 mM glucose but the technical RSDs are in good agreement at all glucose concentrations.[13] It is possible that the higher biological irreproducibility at 3 mM and 7 mM glucose is a result of fewer replicates for these glucose concentrations. Due to a series of instrument and human errors only three plates were analyzed for both 3 mM and 7 mM glucose, while all four plates were analyzed at 17 mM glucose.

Consistent with previous results,[13, 30] glucose, G6P, pyruvate, citrate, fumarate, succinate and malate all increased from 3 to 7 to 17 mM glucose (see Figures 2.17 and 2.18). As illustrated in Figure 2.17, unlike the previous study where G6P is only detected at 16.8 mM glucose,[13] G6P is detected at all three glucose concentrations. The lack of a statistical significance in the increase of G6P from 3 to 7 to 17 mM glucose can likely be explained by the large error bars which is was also observed at 16.8 mM in the previous data.[13] Additionally, 2PG decreased from 3 mM glucose to 17 mM glucose. F6P, 3PG, R5P and lactate did not show any statistically significant change with glucose concentration.

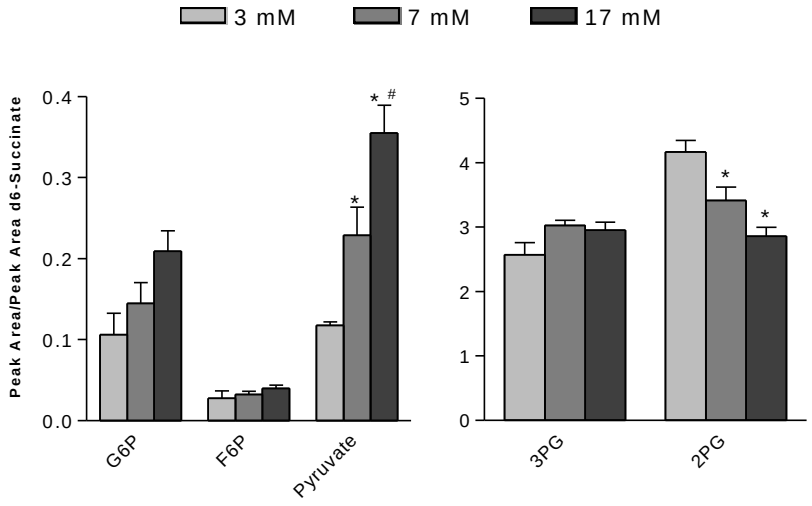

Figure 2.17 Effect of glucose on detectable glycolysis analytes. Statistical significance was tested using one-way ANOVA analysis. (*) is statistically different than 3 mM and (#) is statistically different from 7 mM.

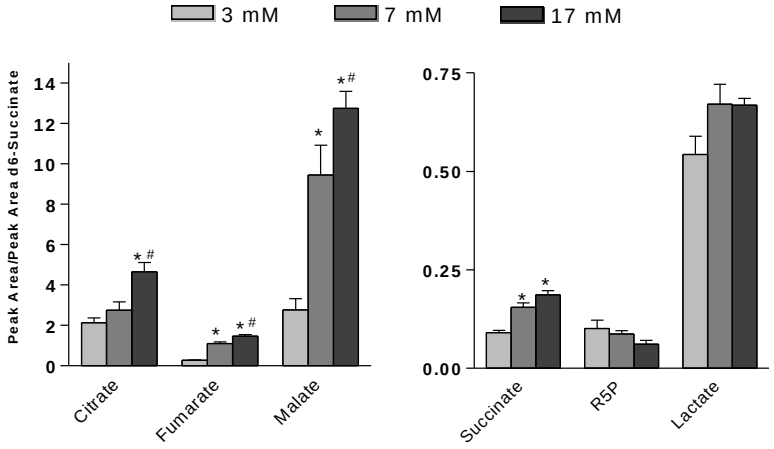

Figure 2.18 Effect of glucose on detectable TCA and pentose phosphate shunt (R5P) analytes. Statistical significance was tested using one-way ANOVA analysis. (*) is statistically different than 3 mM and (#) is statistically different from 7 mM.

The changes to the amino acids detected can be seen in Figure 2.19. Consistent with previous GC/MS work[13] alanine increased and valine, glycine, and threonine did not change significantly. Although ornithine and serine do not show statistically significant differences, both analytes follow trends similar to that shown in previous work[13] with serine increasing and ornithine decreasing. The major differences between this work and

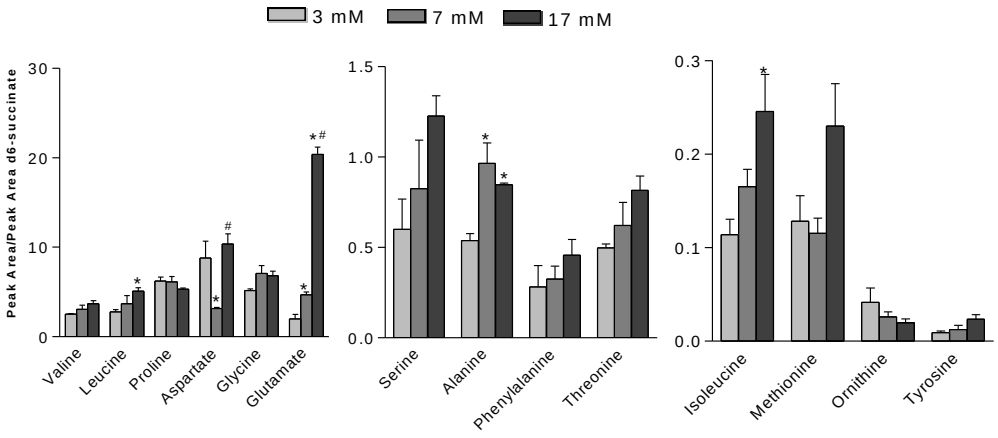

Figure 2.19 Effect of glucose on detectable amino acids. Statistical significance was tested using one-way ANOVA analysis. (*) is statistically different than 3 mM and (#) is statistically different from 7 mM

the previous study[13] are that leucine, proline, phenylalanine, isoleucine, methionine and tyrosine were detected. Additionally, in the previous study[13] aspartate and glutamate decreased whereas in this work aspartate decreased from 3 mM glucose to 7 mM glucose and increased from 7 mM glucose to 17 mM and glutamate increased from 3 mM to 7 mM to 17 mM glucose. These differences may be the result of different derivatization methods, differences in the length of time that the cells were stimulated for or differences in how long the cells were allowed to equilibrate in low glucose before stimulation at higher glucose concentrations.

Metabolomic Analysis

For the studies reported above, we measured metabolites at 3 different glucose concentrations. The step from 3 to 7 to 17 mM glucose increases insulin secretion, so pathways activated may be involved in glucose-stimulated insulin secretion. Further, chronic stimulation with 17 mM glucose may lead to glucotoxicity in INS-1 cells;[8] therefore pathways activated at this highest glucose concentration may be candidates for

involvement in development of glucotoxicity. Based on this consideration, we analyzed the pathways activated using MetScape.[23]

In addition to the distinct visual differences seen in Figures 2.14 through 2.16, the maps also differed in the pathways, seed analytes and number of reactions involved. This information can be found for all three data sets in Appendices D through F. Not surprisingly, three of the metabolic pathways involved for each data set were the citric acid cycle (TCA cycle), the pentose phosphate pathway and glycolysis and gluconeogenesis, which, as discussed previously, are known to be involved in GSIS. These data are in good agreement with the metabolite profiling data such that all of the seed analytes involved in these pathways, as seen in Appendices D through F, that overlap with previous target analytes change in the same direction. That is, malate, fumarate, citrate and pyruvate all increase from low to moderate to high glucose while ribose-5-phosphate decreases with increasing glucose in both the metabolite profiling and metabolomics data analysis. Other activated pathways with potential links to diabetes, GSIS and glucotoxicity are discussed below.

Linoleate, or linoleic acid (LA), metabolism is shown in Figure 2.20.[27-29] LA is an essential, omega-6 fatty acid that must be metabolized to be utilized by the body and is required for the biosynthesis of arachidonic acid (AA). Thus, as LA concentration decreases, AA concentration should increase. The increase in AA observed in this work is plotted in Figure 2.21. If LA concentration were plotted with AA, the trend would be exactly the opposite of that seen for AA. However, unlike AA, LA detection was not reproducible with RSDs of >100% and therefore was not included in Figure 2.21 for clarity. In addition to being linked to AA metabolism, LA metabolism is of interest in this

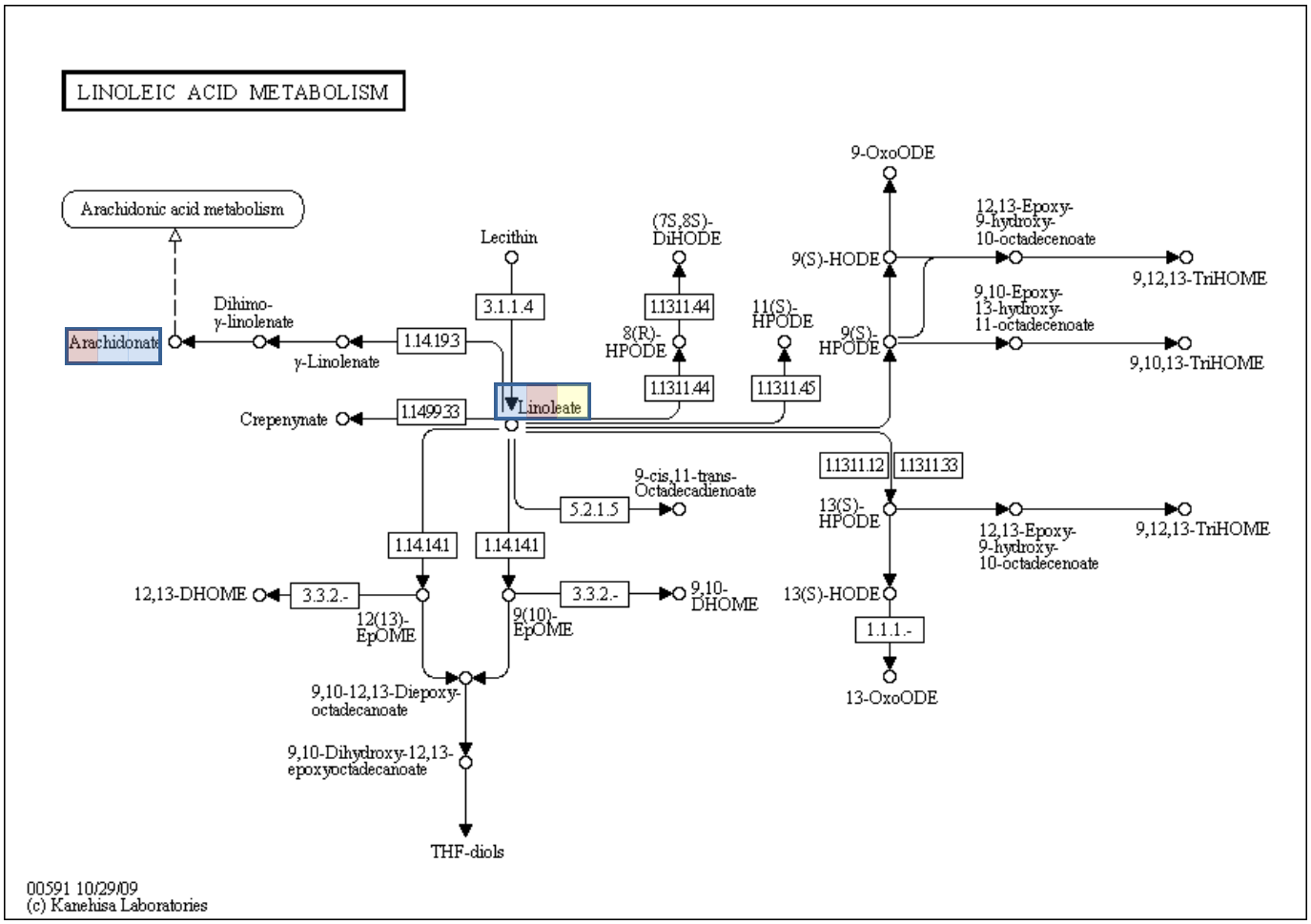

Figure 2.20 Linoleic acid metabolism pathway as obtained by KEGG database.[27-29] Blue boxes indicate analytes detected in metabolomic analysis. Boxes filled from left to right indicating if the analytes increased (blue), decreased (yellow), or did not change (red) from 3 mM glucose to 7 mM glucose, 3 mM glucose to 17 mM glucose and 7 mM glucose to 17 mM glucose.

context because the first step in linoleate metabolism is the conversion of LA to γ-linoleic acid (GLA) by Δ-6-desaturase, this is also the rate limiting step in LA metabolism.[31, 32] In 1955 it was discovered that diabetic animals require more LA than non-diabetic animals,[33] a requirement that was later explained by an impairment of Δ-6-desaturase enzyme activity and thus LA to GLA conversion.[34] It is possible that glucotoxic conditions contribute to the impairment of Δ-6-desaturase enzyme activity and therefore it would be interesting to further investigate this pathway under such conditions.

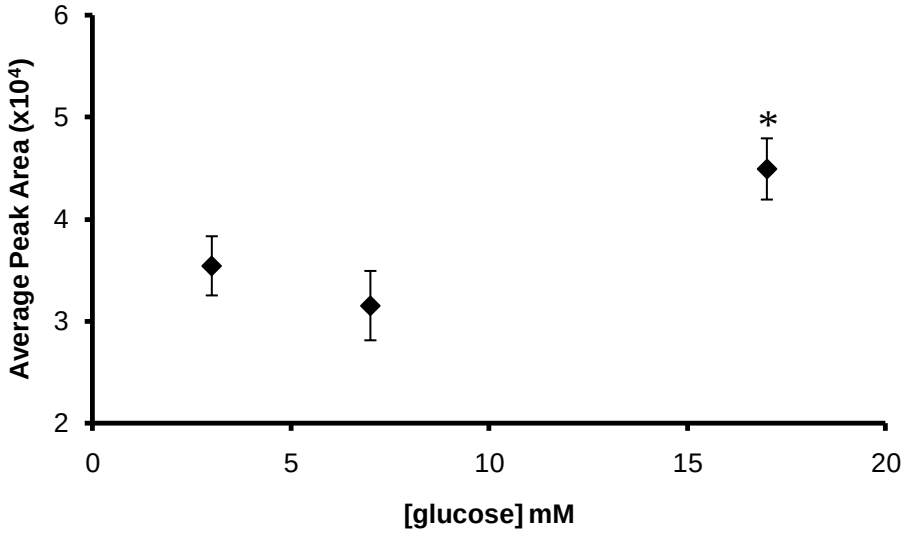

Figure 2.21 Plot of the average peak area of arachidonic acid at 3, 7 and 17 mM glucose indicating the substantial increase of AA at 17 mM glucose. Error bars are SEM and * indicates statistical significance as calculated using a student's t-test.

In our work, we found that AA varied in AA metabolism (Figure 2.22),[27-29] prostaglandins metabolism and leukotriene metabolism for 7 mM to 17 mM and 3 mM to 17 mM but not 3 mM to 7 mM glucose, see Appendices D through F. Additionally, as can be seen in Figure 2.21, AA was significantly elevated at 17 mM glucose relative to the lower glucose concentrations which is consistent with a previous GC study.[35]

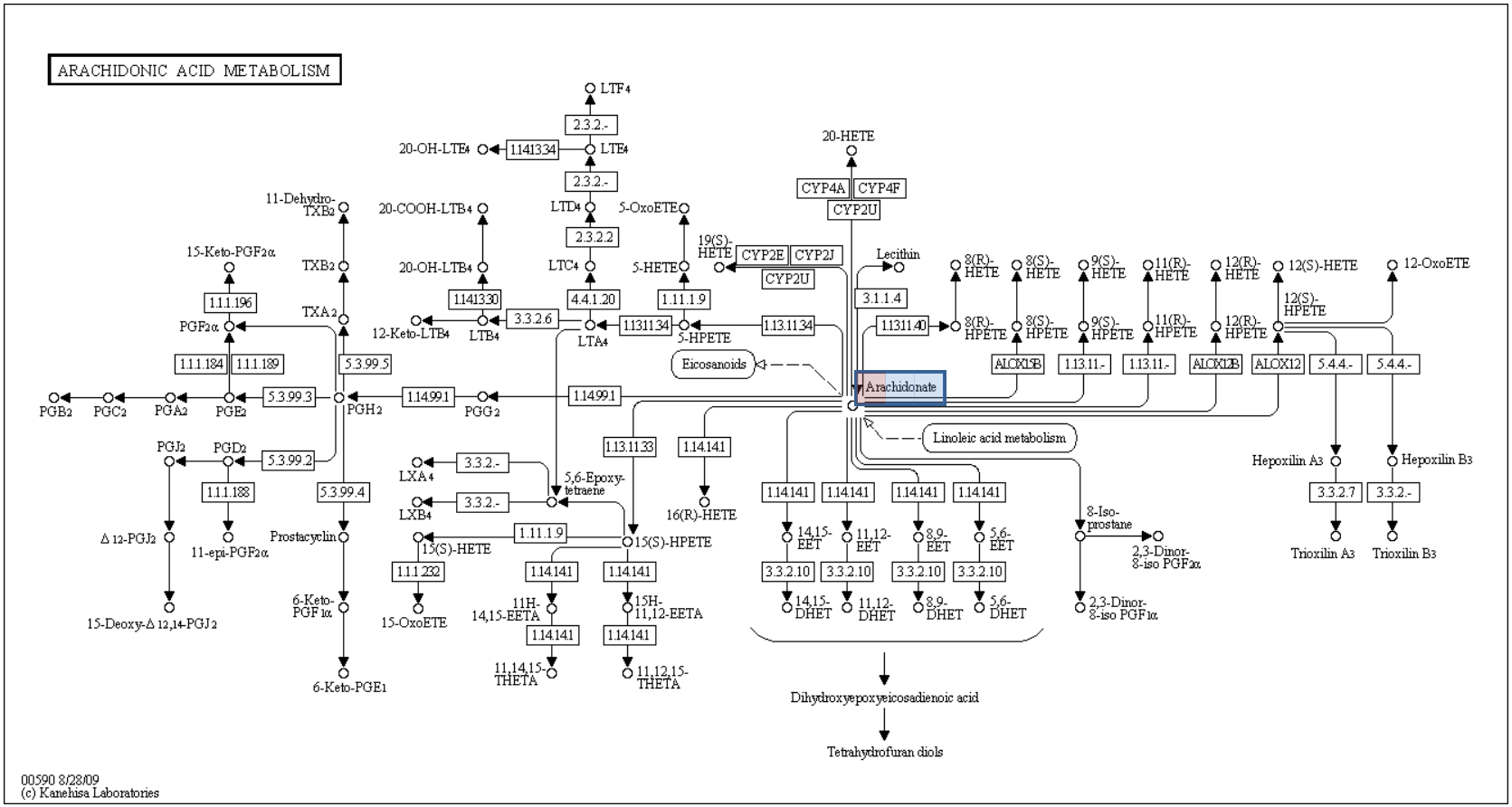

Figure 2.22 Arachidonic acid metabolism pathway as obtained from KEGG database.[27-29] Blue boxes indicate analytes detected by metabolomic analysis. Boxes filled from left to right indicating if the analytes increased (blue), decreased (yellow), or did not change (red) from 3 mM glucose to 7 mM glucose, 3 mM glucose to 17 mM glucose and 7 mM glucose to 17 mM glucose.

In this previous study the authors stimulated islets at 3 mM and 17 mM glucose and analyzed the relative abundance of free AA as well as palmitate, linoleate, oleate and stearate by extraction and methylesterfication followed by GC/MS.[35] Arachidonic acid is an important omega-6 fatty acid that is involved in cellular signaling, the normal function of pancreatic β-cells, GSIS, and can be linked to a number of diseases including obesity.[36-38] Exogenous AA has been shown to enhance insulin secretion from β-cells and a reduction of endogenous AA has been shown to significantly reduce GSIS in human islets.[38] Recent work has also demonstrated that AA (an unsaturated fatty acid) has a positive effect on attenuating the negative effects of palmitic acid (a saturated fatty acid).[38] Palmitic acid can lead to excessive generation of ROS[38], which can contribute to glucotoxicity. Thus, the recent result of AA mediated rescue of cells from palmitic acid mediated dysfunction has led to the discussion of further investigation of its metabolism and metabolites to better understand and potentially treat diabetes.[38]

Although AA acid can have a protective effect, its metabolites can also have a negative effect on insulin secretion. Specifically, cyclooxygenase (COX)-generated and lipoxygenase (LOX)-generated arachidonic acid metabolites which are associated with these potential destructive effects. COX activity leads to prostaglandins and LOX produce leukotrienes.[39] Both prostaglandins and leukotrienes mediate signals of inflammation[39] which is an important pathological process that leads to β-cell dysfunction and death in type 2 diabetes.[40] Additionally, COX activity can be responsible for the production of ROS such as hydrogen peroxide[39] which can further contribute to β-cell dysfunction and glucotoxicity. However, it has been shown that AA metabolism through COX and LOX pathways is not required for AA to have a stimulatory effect on

human islets.[41] Therefore, it is thought that selective inhibition of these enzymes would have a dual protective role; it would minimize β-cell dysfunction and enhance endogenous arachidonic acid levels.[41]

Another involved pathway is butanoate metabolism (see Figure 2.23[27-29]) which, in Appendices D through F, shows from 3 mM to 17 mM glucose, acetoacetate and 3-hydroxybutanoic acid increase, from 7 mM to 17 mM glucose, acetoacetate increases and butanoate decreases, and from 3 mM to 7mM glucose, butanoate decreases. This decrease in butanoate is of interest because in addition to being linked to the citric acid cycle, glycolysis and the synthesis and degradation of ketone bodies as shown in Figure 2.23,[27-29] dietary supplements of butanoate have recently been shown to improve insulin sensitivity in mice.[42] It is suspected that butanoate stimulates mitochondrial function through the induction of peroxisome proliferator-activated receptor (PPAR)-γ coactivator PGC-1α, which is a transcriptome activator.[42] PGC-1α controls energy metabolism by interaction with several transcription factors that direct gene transcription for mitochondrial biogenesis and respiration and a reduction in the function of PGC-1α is related to reduction in fatty acid oxidation, mitochondrial dysfunction and risk for insulin resistance.[42] A number of the metabolites involved in butanoate metabolism, which can be found in Figure 2.23,[27-29] can be detected by the technique used in this work. Therefore it may be interesting to repeat this experiment with a butanoate treatment prior to glucose stimulation. Additionally, if this method could be adapted to islet analysis, it could be used to analyze healthy islets as well as diseased islets before and after dietary butanoate supplementation.

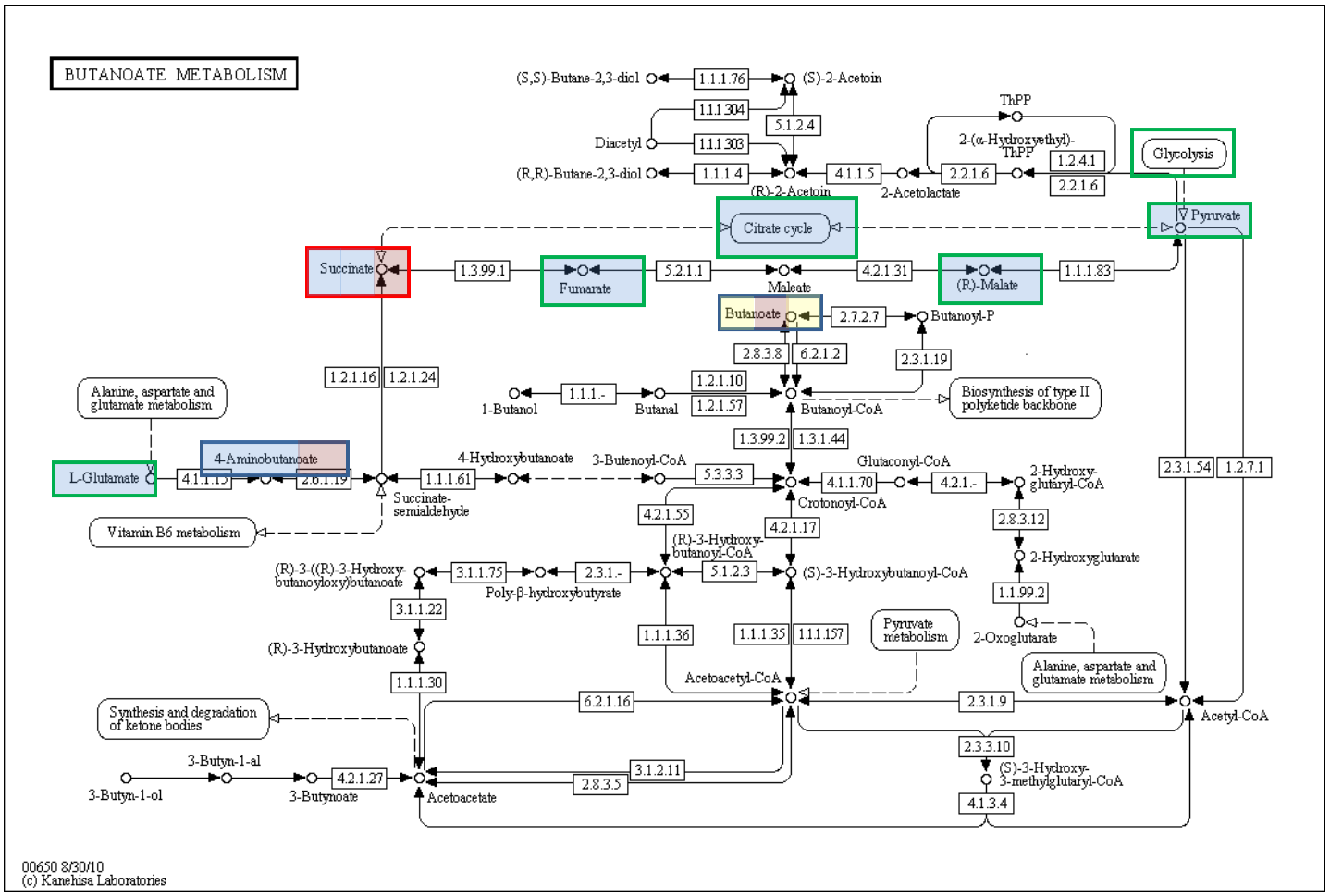

Figure 2.23 Butanoate metabolism pathway obtained from KEGG database.[27-29] Blue boxes indicate analytes detected by metabolomics analysis, red boxes indicate analytes detected by metabolite profiling and green boxes indicate analytes detected in both methods. Boxes filled from left to right indicating if the analytes increased (blue), decreased (yellow), or did not change (red) from 3 mM glucose to 7 mM glucose, 3 mM glucose to 17 mM glucose and 7 mM glucose to 17 mM glucose.

As seen in Appendices D through F, serine is only increasing in glycerophospholipid metabolism at 3 mM to 17 mM and 7 mM to 17 mM glucose. This can likely be explained by the relation to the glycine, serine and threonine metabolism pathway (includes alanine in appendices) that feeds into glycerophospholipid metabolism as seen in Figure 2.24.[27-29] As observed in Appendices D through F, serine is also only involved for glycine, serine and theronine metabolism at 3 mM to 17 mM and 7 mM to 17 mM glucose. The same is true for glycosphingolipid metabolism, shown in Figure 2.25,[27-29] which is also fed serine by the glycine, serine, and threonine metabolism pathway. The precursor of all complex glycosphingolipids is ceramide which is formed by *de novo* synthesis or catabolism of glycosphingolipids and sphingomyelin. The rate of *de novo* synthesis is regulated by the availability of the precursors serine as well as palmitoyl-CoA.[43] It is well established that glycosphingolipids are involved in intercellular communication events and cell differentiation;[43] however, several studies have indicated that glycosphingolipids interfere directly with insulin signaling and pharmacological reduction of glycosphingolipid synthesis has been found to improve insulin resistance in rodents.[43] Thus, evidence is accumulating for a role for glycosphingolipids in insulin resistance.

It is interesting to note that, although the increasing trend in serine concentration is apparent in Figure 2.18, the previously discussed one-way ANOVA analysis did not find a statistical significance between the concentrations at 3, 7 and 17 mM glucose and the Fisher Ratio analysis did. This highlights the advantage of using the Fisher Ratio analysis; the ability to consider all data simultaneously and objectively identify the most significant differences.[21]

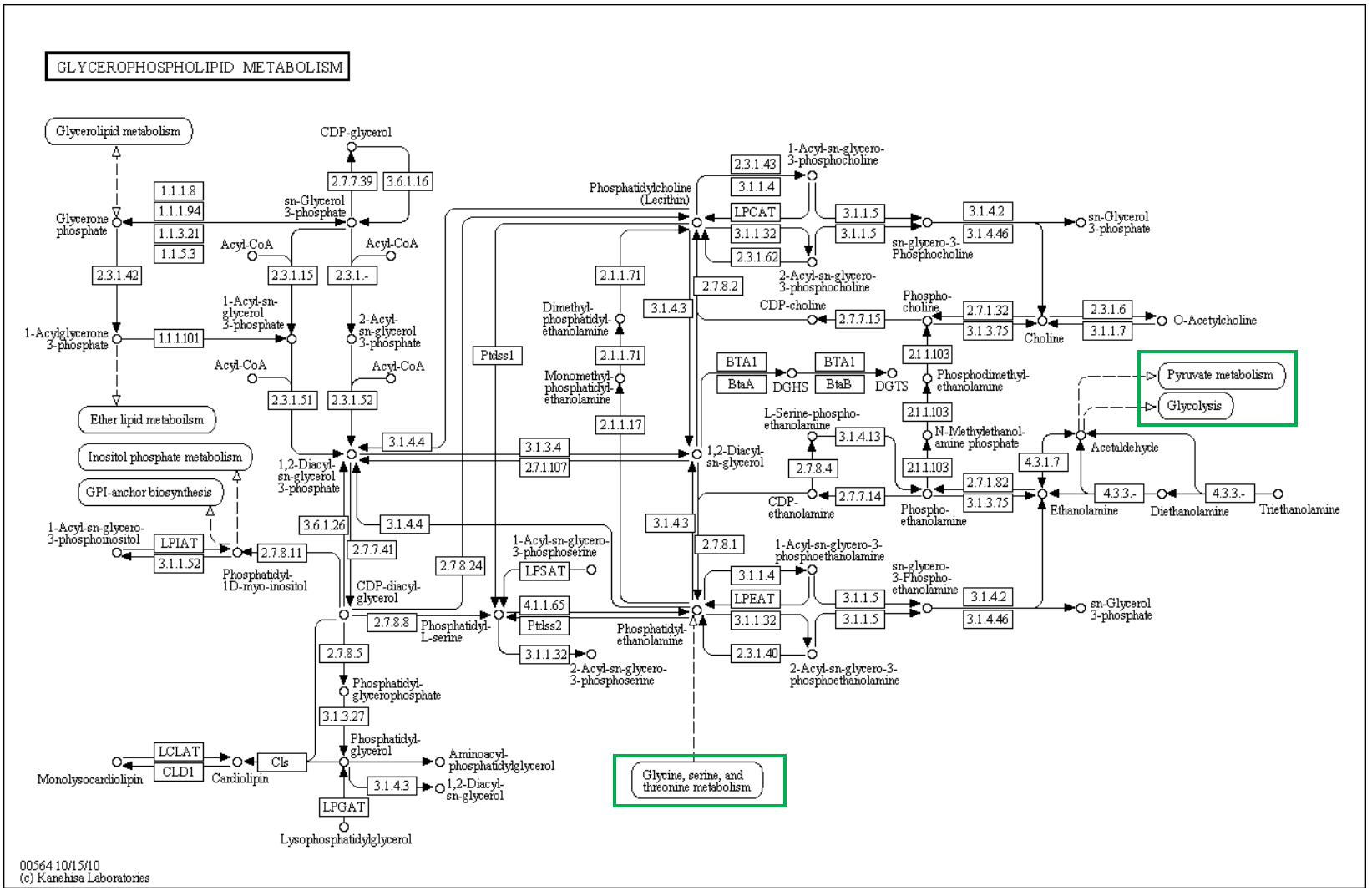

Figure 2.24 Glycerophospholipid metabolism pathway obtained from KEGG database.[27-29] Green boxes indicate pathways containing analytes detected in both the metabolite profiling and metabolomics analysis.

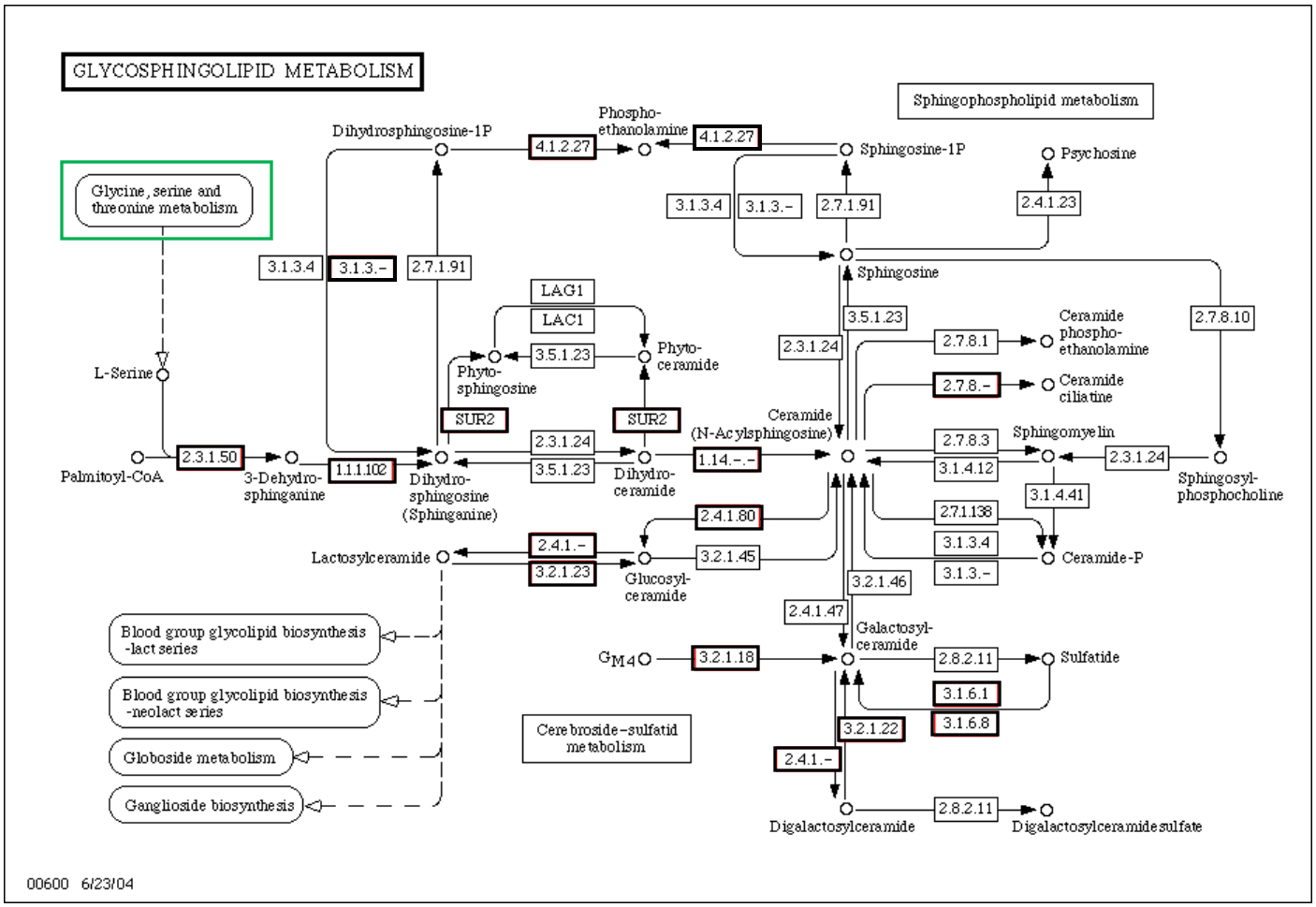

Figure 2.25 Glycosphingolipid metabolism pathway as obtained from KEGG database.[27-29] Green boxes indicate pathways containing analytes detected in both the metabolite profiling and metabolomics analysis.

Vitamin B3 or, nicotinate and nicotinamide, (which are precursors of the coenzymes nicotinamide-adenine dinucleotide (NAD^+) and nicotinamide-adenine dinucleotide phosphate ($NADP^+$)) metabolism and vitamin B5-CoA biosynthesis from pantothenate (the main function of which is to synthesize CoA, an essential coenzyme in a variety of reactions) are two pathways that are also interesting (see Figures 2.26 and 2.27).[27-29] Until recently, neither pathway had been associated with insulin secretion. A previous study looking at NMR-based metabolomic and transcriptomic data from urine, blood, liver, inguinal subcutaneous fat and skeletal muscle collected from db/db diabetic mice reported novel disease effects on nicotinamide metabolites and pantothenate.[44] A second study utilizing HPLC analysis of urine from 14 diabetic and 14 non-diabetic patients as well as metabolic data from adult Sprague-Dawley rats found that nicotinamide overload induced an increase in plasma N^1-methylnicotinamide which is associated with oxidative stress and insulin resistance, thus playing a role in type 2 diabetes.[45] Thus, it would be interesting to further investigate the role of this pathway in GSIS and β-cell dysfunction.

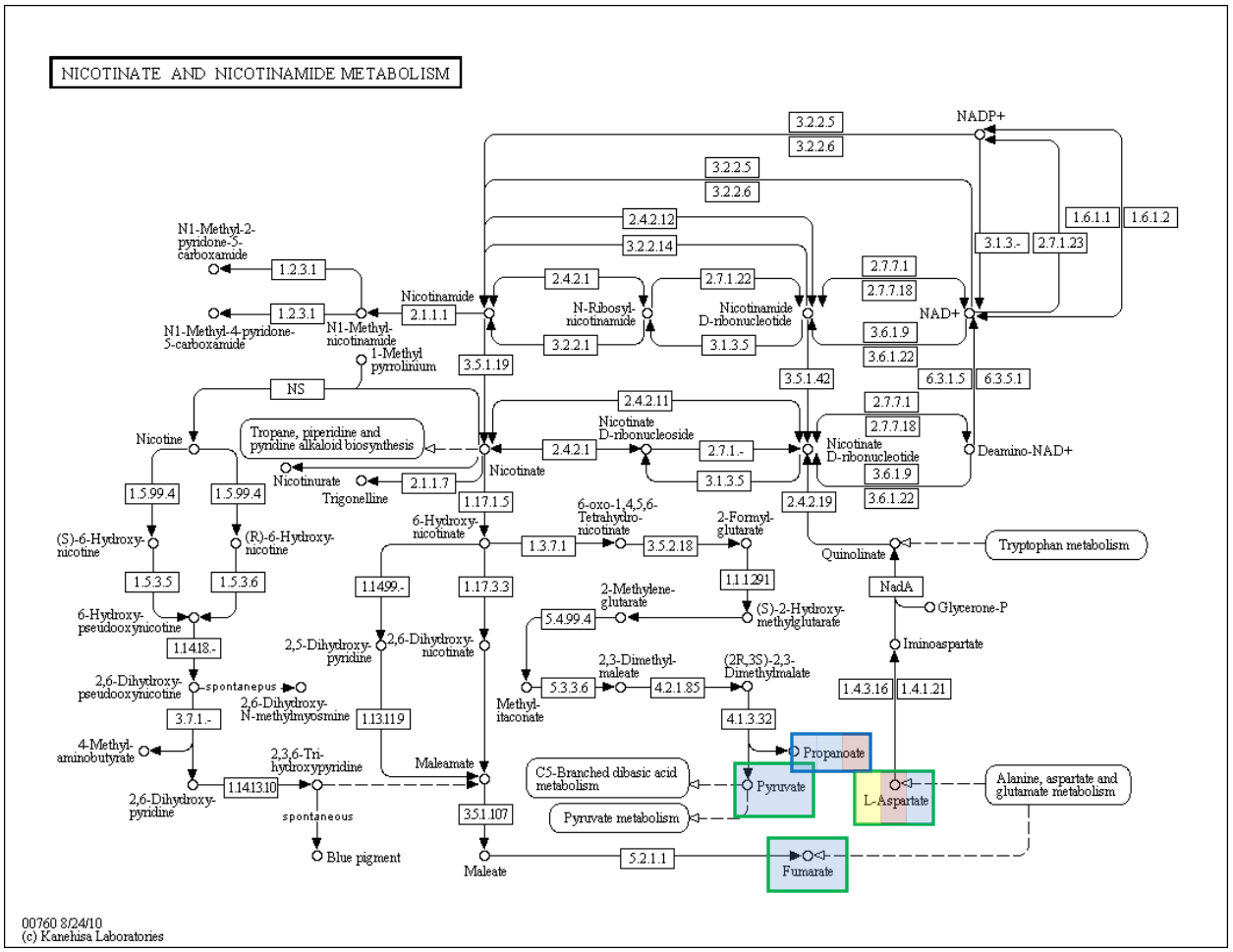

Figure 2.26 Vitamin B3 (nicotinate and nicotinamide) metabolism as obtained from the KEGG database.[27-29] Blue box indicates analytes detected by metbolomic analysis, green boxes indicate analytes detected by both metabolite profiling and metaboloic analysis. Boxes filled from left to right indicating if the analytes increased (blue), decreased (yellow), or did not change (red) from 3 mM glucose to 7 mM glucose, 3 mM glucose to 17 mM glucose and 7 mM glucose to 17 mM glucose.

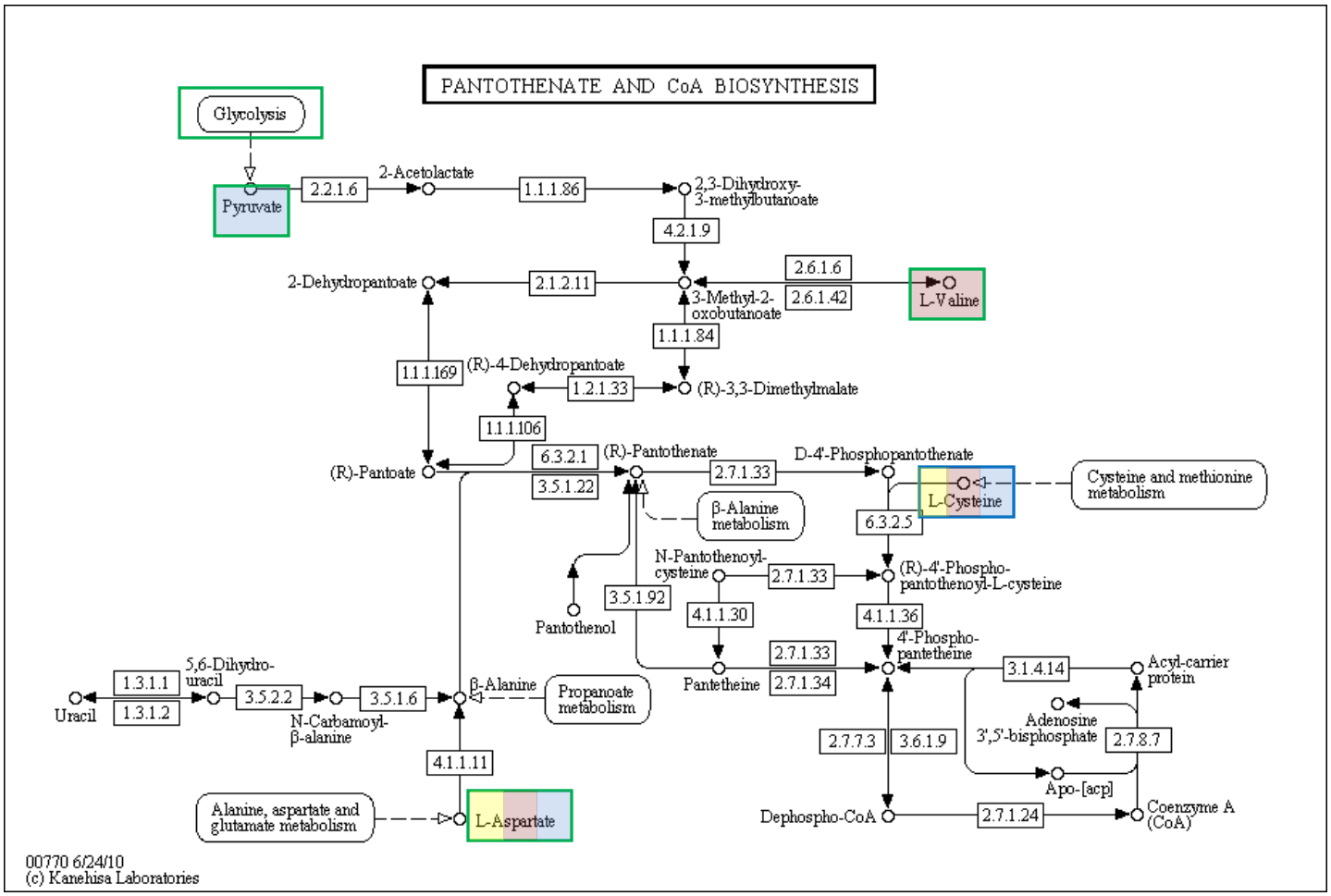

Figure 2.27 Vitamin B5-CoA biosynthesis from pantothenate pathway as obtained from the KEGG database.[27-29] Blue boxes indicate analytes detected by metabolomic analysis, green boxes indicate analytes (and glycolysis which contains analytes detected by) metabolite profiling and metabolomic analysis. Boxes filled from left to right indicating if the analytes increased (blue), decreased (yellow), or did not change (red) from 3 mM glucose to 7 mM glucose, 3 mM glucose to 17 mM glucose and 7 mM glucose to 17 mM glucose.

The urea cycle and metabolism of arginine, proline, glutamate, aspartate and asparagine pathways (see Figure 2.28[27-29]), the main function of which is to excrete the excess nitrogen resulting from metabolic breakdown of amino acids,[46] shows an increase in involved analytes from 3 mM to 7 mM and 3 mM to 17 mM glucose as determined by Metscape and can been seen in Appendices D through F. These increases are particularly dramatic for fumarate, glutamine, glycine, proline and urea which increase 588, 1490, 614, 194 and 985 % respectively from 3 mM glucose to 17 mM glucose. Although no direct link to GSIS, β-cell dysfunction or glucotoxicity has been previously identified, it has been hypothesized that a break down in the urea cycle may lead to the generation of pathogenic nitric oxide which may cause the destruction of β-cells.[47] Given this hypothesis and the involvement of the pathway observed in our study, it appears that urea cycle and metabolism arginine, proline, glutamate, aspartate and asparagine is a pathway worth focusing on in future studies.

Tyrosine metabolism, the main function of which is protein synthesis as well as serving as a precursor to neurotransmitters and hormones, is also an interesting pathway. However, previous to this work, this pathway has not been directly related to insulin release, diabetes or glucotoxicity. The pathway appears to be more involved from 3 mM to 7 mM and 7 mM to 17 mM than 3 mM to 17 mM glucose, perhaps indicating an inhibition of the pathway at high glucose concentrations. This is not surprising given that the tyrosine metabolism pathway, as seen in Figure 2.29,[27-29] is directly related to the citric acid cycle, another pathway which is directly affected by glucose concentration. Specifically, tyrosine can decompose into acetoacetate and fumarate, both of which can then enter the citric acid cycle.

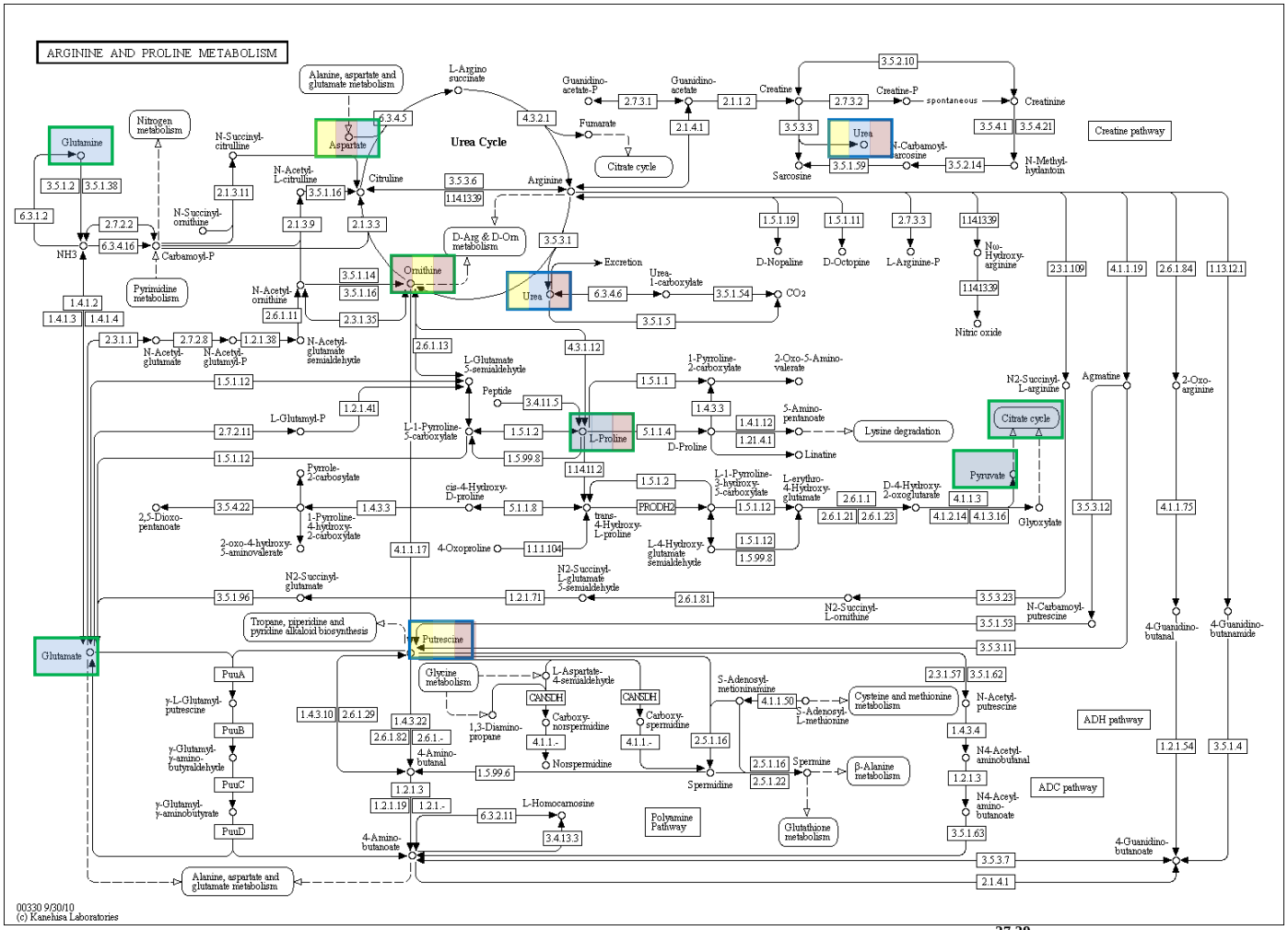

Figure 2.28 The urea cycle and metabolism of arginine and proline as obtained from the KEGG database.[27-29] Blue boxes indicate analytes detected by metabolomics analysis and green boxes indicate analytes detected by metabolite profiling and metabolmics analysis.

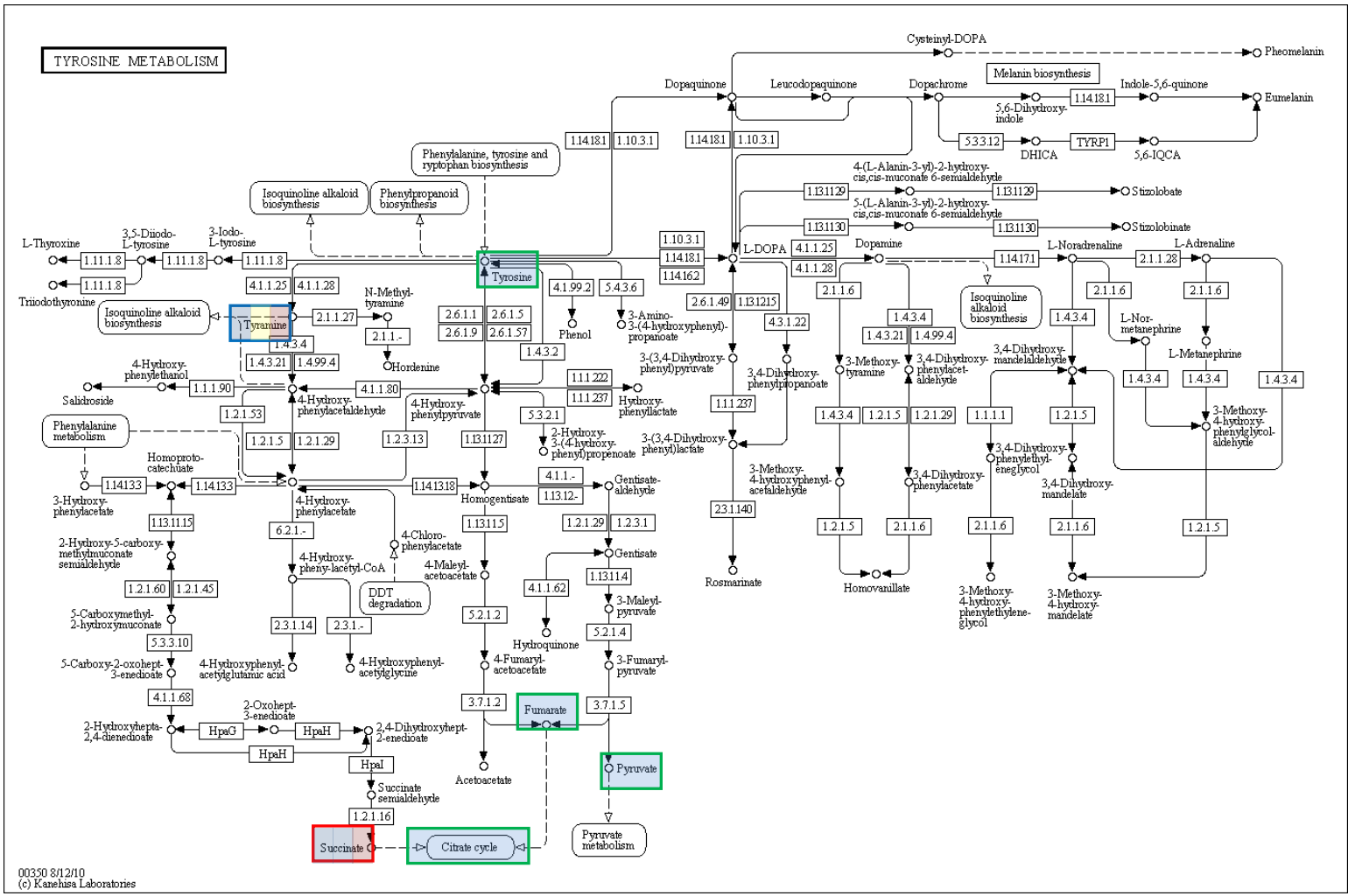

Figure 2.29 Tyrosine metabolism pathway as obtained from KEGG database.[27-29] Blue boxes indicate analytes detected by metabolomics analysis, red boxes indicate analytes detected by metabolite profiling and green boxes indicate analytes detected in both methods.

Conclusion

We have demonstrated the utility of GC × GC-ToFMS for both metabolite profiling and metabolomic analysis of mammalian cells with excellent reproducibility. The number of detectable, target analytes has been nearly doubled compared to previous GC analysis.[13] Additionally non-target analytes and the associated metabolic pathways have been investigated. Comparison of the metabolite profiling and metabolomic analysis shows good agreement between both data sets. Metabolomic analysis has demonstrated 9 activated pathways with potential or previously described relationships to GSIS, β-cell dysfunction and diabetes. Metabolites from these pathways could be included in future target analysis to gain a better understanding of the effects of glucose on INS-1 cell metabolism. Further experiments could be performed to better understand the non-target analytes and the associated metabolic pathways.

References

(1) Goodacre, R.; Vaidyanathan, S.; Dunn, W. B.; Harrigan, G. G.; Kell, D. B. *Trends Biotechnol.* **2004**, *22*, 245-252.

(2) Hollywood, K.; Brison, D. R.; Goodacre, R. *Proteomics* **2006**, *6*, 4716-4723.

(3) Kulkarni, R. N. *The International Journal of Biochemistry & Cell Biology* **2004**, *36*.

(4) Edwards, J. L., University of Michigan, Ann Arbor, 2006.

(5) Fernandez, C.; Fransson, U.; Hallgard, E.; Spegel, P.; Holm, C.; Krogh, M.; Warell, K.; James, P.; Mulder, H. *J. Proteome Res.* **2008**, *7*, 400-411.

(6) Straub, S. G.; Sharp, G. W. G. *Diabetes-Metabolism Research and Reviews* **2002**, *18*, 451-463.

(7) Komatsu, M.; Sato, Y.; Aizawa, T.; Hashizume, K. *Endocr. J.* **2001**, *48*, 275-288.

(8) Poitout, V.; Robertson, R. P. *Endocr. Rev.* **2008**, *29*, 351-366.

(9) Unger, R. H.; Grundy, S. *Diabetologia* **1985**, *28*, 119-121.

(10) Dubois, M.; Vacher, P.; Roger, B.; Huyghe, D.; Vandewalle, B.; Kerr-Conte, J.; Pattou, F.; Moustaid-Moussa, N.; Lang, J. C. *Endocrinology* **2007**, *148*, 1605-1614.

(11) Roche, E.; Farfari, S.; Witters, L. A.; Assimacopoulos-Jeannet, F.; Thumelin, S.; Brun, T.; Corkey, B. E.; Saha, A. K.; Prentki, M. *Diabetes* **1998**, *47*, 1086-1094.

(12) Nolan, C. J.; Prentki, M. *Trends Endocrinol. Metab.* **2008**, *19*, 285-291.

(13) Fernandez, C.; Fransson, U.; Hallgard, E.; Spegel, P.; Holm, C.; Krogh, M.; Warell, K.; James, P.; Mulder, H. *J. Proteome Res.* **2008**, *7*, 400-411.

(14) Hope, J. L.; Prazen, B. J.; Nilsson, E. J.; Lidstrom, M. E.; Synovec, R. E. *Talanta* **2005**, *65*, 380-388.

(15) Pierce, K. M.; Hoggard, J. C.; Hope, J. L.; Rainey, P. M.; Hoofnagle, A. N.; Jack, R. M.; Wright, B. W.; Synovec, R. E. *Analytical Chemistry* **2006**, *78*, 5068-5075.

(16) Huang, X. D.; Regnier, F. E. *Anal. Chem.* **2008**, *80*, 107-114.

(17) Li, X.; Xu, Z.; Lu, X.; Yang, X.; Yin, P.; Kong, H.; Yu, Y.; Xu, G. *Anal. Chim. Acta* **2009**, *633*, 257-262.

(18) Shellie, R. A.; Welthagen, W.; Zrostlikova, J.; Spranger, J.; Ristow, M.; Fiehn, O.; Zimmermann, R. *J. Chromatogr. A* **2005**, *1086*, 83-90.

(19) Welthagen, W.; Shellie, R. A.; Spranger, J.; Ristow, M.; Zimmermann, R.; Fiehn, O. *Metabolomics* **2005**, *1*, 65-73.

(20) Kusano, M.; Fukushima, A.; Kobayashi, M.; Hayashi, N.; Jonsson, P.; Moritz, T.; Ebana, K.; Saito, K. *Journal of Chromatography B-Analytical Technologies in the Biomedical and Life Sciences* **2007**, *855*, 71-79.

(21) Mohler, R. E.; Dombek, K. M.; Hoggard, J. C.; Young, E. T.; Synovec, R. E. *Anal. Chem.* **2006**, *78*, 2700-2709.

(22) Mohler, R. E.; Tu, B. P.; Dombek, K. M.; Hoggard, J. C.; Young, E. T.; Synovec, R. E. *J. Chromatogr. A* **2008**, *1186*, 401-411.

(23) Gao, J.; Tarcea, V. G.; Karnovsky, A.; Mirel, B. R.; Weymouth, T. E.; Beecher, C. W.; Cavalcoli, J. D.; Athey, B. D.; Omenn, G. S.; Burant, C. F.; Jagadish, H. V. *Bioinformatics*, *26*, 971-973.

(24) Cline, M. S.; Smoot, M.; Cerami, E.; Kuchinsky, A.; Landys, N.; Workman, C.; Christmas, R.; Avila-Campilo, I.; Creech, M.; Gross, B.; Hanspers, K.; Isserlin,

R.; Kelley, R.; Killcoyne, S.; Lotia, S.; Maere, S.; Morris, J.; Ono, K.; Pavlovic, V.; Pico, A. R.; Vailaya, A.; Wang, P. L.; Adler, A.; Conklin, B. R.; Hood, L.; Kuiper, M.; Sander, C.; Schmulevich, I.; Schwikowski, B.; Warner, G. J.; Ideker, T.; Bader, G. D. *Nature Protocols* **2007**, *2*, 2366-2382.

(25) Shannon, P.; Markiel, A.; Ozier, O.; Baliga, N. S.; Wang, J. T.; Ramage, D.; Amin, N.; Schwikowski, B.; Ideker, T. *Genome Res.* **2003**, *13*, 2498-2504.

(26) Mohler, R. E.; Dombek, K. M.; Hoggard, J. C.; Pierce, K. M.; Young, E. T.; Synovec, R. E. *Analyst* **2007**, *132*, 756-767.

(27) Kanehisa, M.; Goto, S. *Nucleic Acids Res.* **2000**, *28*, 27-30.

(28) Kanehisa, M.; Goto, S.; Furumichi, M.; Tanabe, M.; Hirakawa, M. *Nucleic Acids Res.* **2010**, *38*, D355-D360.

(29) Kanehisa, M.; Goto, S.; Hattori, M.; Aoki-Kinoshita, K. F.; Itoh, M.; Kawashima, S.; Katayama, T.; Araki, M.; Hirakawa, M. *Nucleic Acids Res.* **2006**, *34*, D354-D357.

(30) Alarcon, C.; Barton, W.; Prentki, M.; Corkey, B. E.; Rhodes, C. J. *Diabetes* **2002**, *51*, 2496-2504.

(31) Horrobin, D. F. *Prog. Lipid Res.* **1992**, *31*, 163-194.

(32) Horrobin, D. F. *Am. J. Clin. Nutr.* **1993**, *57*, S732-S737.

(33) Peifer, J. J.; Holman, R. T. *Arch. Biochem. Biophys.* **1955**, *57*, 520-521.

(34) Mercuri, O.; Peluffo, R. O.; Brenner, R. R. *Biochim. Biophys. Acta* **1966**, *116*, 409-&.

(35) Wolf, B. A.; Pasquale, S. M.; Turk, J. *Biochemistry* **1991**, *30*, 6372-6379.

(36) Wymann, M. P.; Schneiter, R. *Nat Rev Mol Cell Biol* **2008**, *9*, 162-176.

(37) Ramanadham, S.; Hsu, F.-F.; Zhang, S.; Bohrer, A.; Ma, Z.; Turk, J. *BBA-Mol. Cell. Biol. L.* **2000**, *1484*, 251-266.

(38) Keane, D.; Takahashi, H. K.; Dhayal, D.; Morgan, N. G.; Curi, R.; Newsholme, P. *Clin. Sci.* **2010**, *Immediate Publication*.

(39) Meves, H. *Br. J. Pharmacol.* **2008**, *155*, 4-16.

(40) Ma, K.; Nunemaker, C. S.; Wu, R.; Chakrabarti, S. K.; Taylor-Fishwick, D. A.; Nadler, J. L. *J. Clin. Endocrinol. Metab.*, *95*, 887-893.

(41) Persaud, S. J.; Muller, D.; Belin, V. D.; Kitsou-Mylona, I.; Asare-Anane, H.; Papadimitriou, A.; Burns, C. J.; Huang, G. C.; Amiel, S. A.; Jones, P. M. *Diabetes* **2007**, *56*, 197-203.

(42) Gao, Z. G.; Yin, J.; Zhang, J.; Ward, R. E.; Martin, R. J.; Lefevre, M.; Cefalu, W. T.; Ye, J. P. *Diabetes* **2009**, *58*, 1509-1517.

(43) Langeveld, M.; Aerts, J. *Prog. Lipid Res.* **2009**, *48*, 196-205.

(44) Connor, S. C.; Hansen, M. K.; Corner, A.; Smith, R. F.; Ryan, T. E. *Mol. BioSyst.* **2010**, *6*, 909-921.

(45) Zhou, S. S.; Li, D.; Sun, W. P.; Guo, M.; Lun, Y. Z.; Zhou, Y. M.; Xiao, F. C.; Jing, L. X.; Sun, S. X.; Zhang, L. B.; Luo, N.; Bian, F. N.; Zou, W.; Dong, L. B.; Zhao, Z. G.; Li, S. F.; Gong, X. J.; Yu, Z. G.; Sun, C. B.; Zheng, C. L.; Jiang, D. J.; Li, Z. N. *World Journal of Gastroenterology* **2009**, *15*, 5674-5684.

(46) Voet, D.; Voet, J. G. *Biochemistry*, 3 ed.; John Wiley & Sons, Inc.: Hoboken, NJ, 2004.

(47) Bauer, J. A. *Med. Hypotheses* **1998**, *51*, 71-73.

Chapter 3

ANALYSIS OF LIPID COMPOSITION IN INS-1 CELLS VIA COMPREHENSIVE TWO-DIMENSIONAL GAS CHROMATOGRAPHY TIME-OF-FLIGHT MASS SPECTROMETRY

Introduction

Fatty acids play an important role in nutrition, health, and biochemistry. The consumption of fatty acids has been linked to a number of diseases including heart disease, hypertension, diabetes, rheumatoid arthritis and Chrohn's disease.[1-3] Fatty acids also serve as biomarkers; for example, docosahexaenoic acid has been used as an indicator of severe left ventricular dilation in heart failure patients.[4] Fatty acids can also serve as signaling molecules in a variety of ways including activation of receptors such as PPARγ.[5] Furthermore, imbalances in lipid signaling pathways have been shown to contribute to the progression of chronic inflammation, autoimmunity, cancer, hypertension, and metabolic diseases.[6] As a result of the significance of fatty acids, their measurement in biological samples is of interest. Fatty acid analysis is complicated by their wide variety found in biological samples. They occur with a wide range of carbon chain lengths that may be saturated, monounsaturated, and polyunsaturated. Fatty acids may be free or bound as esters in lipids such as triacylglycerols, glycerophospholipids, and sphingolipids.

Fatty acids are commonly analyzed via gas chromatography (GC) after transformation into methyl esters. Other methods such as pyrolysis GC [7] and high performance liquid chromatography (HPLC) have also been applied for fatty acid

measurements.[8] Multidimensional techniques including comprehensively coupled liquid chromatography and gas chromatography (LC × GC)[9,10] and comprehensive two-dimensional gas chromatography (GC × GC) are also gaining popularity.[11, 12]

It has been shown that the use of GC × GC instead of traditional GC to determine fatty acid methyl esters (FAMEs) enhances overall resolution, which is important because these samples often contain compounds with similar structures that are difficult to separate in a one-dimensional analysis.[3, 13] In GC × GC, FAMEs with the same carbon number elute as clusters with predictable patterns. As carbon number increases, first dimension retention time increases so that a homologous series appears along an arc in a traditional contour plot. Esters with the same number of double bonds appear on arcs offset from that for saturated fatty acids. The inherent structure of these chromatograms aids in identification of FAMEs even when a pure standard is not available. Improved resolution and detectability, compared to one-dimensional GC, also make it possible to detect and identify odd chain fatty acids that are usually present in trace amounts.[11, 13]

GC × GC has previously been used to analyze fatty acids in biodiesel, [14, 15] human plasma,[3] algae,[16] and edible fats and oils including subcutaneous pig, cow, sheep, and poultry tissue as well as vegetable, fish, peanut, and olive oils.[11-13, 17] Despite this extensive list of applications for GC × GC analysis of fatty acids, little work has focused on developing or evaluating methods for analysis of fatty acids in cell culture lines by GC × GC. Such analysis is likely to be of value in understanding the role of fatty acids in signaling and disease pathophysiology. In this work, we demonstrate the applicability of GC × GC for determination of total fatty acid content in the INS-1 cell culture line.

INS-1 cells are a β-cell line and useful model for insulin secretion and diabetes studies. In β-cells, fatty acids may serve as signaling molecules or energy sources.[6, 18, 19] Disturbances of fatty acid metabolism have been implicated in diabetes.[6, 18] Therefore, determination of fatty acid content may help elucidate the roles of fatty acids in these cells and their link to insulin secretion and diabetes. Previous methods for determining fatty acids in INS-1 cells include HPLC [8] and GC.[20] With these methods, 11 and 15 fatty acids were identified and quantified, respectively. Using the GC × GC method reported here, we discover an additional 15 fatty acids, most at higher carbon number and degree of saturation than previously reported, in these cells. These results establish a method for aiding studies of the role of fatty acids in β-cells. These also demonstrate the utility of GC × GC for the determination of FAMEs in cell culture lines, suggesting a potential role for studying signaling in other cell lines as well.

Experimental

Chemicals

All chemicals were purchased from Sigma-Aldrich (St.Louis, MO) unless otherwise noted. Roswell Park Memorial Institute (RPMI) media, fetal bovine serum (FBS), HEPES, and penicillin-streptomycin were purchased from Invitrogen Corp (Carlsbad, CA). Cells lifters and 10 cm polystyrene non-pyrogenic culture dishes were purchased from Corning (Lowell, MA). Fifteen mL polypropene sterile centrifuge tubes, HPLC grade methanol, ACS certified sulfuric acid and potassium hydroxide were obtained from Fisher Scientific (Fairfield, NJ). Hexane was from Acros Organics (Morris Plain, NJ) and the 37 component FAME mix was from Supelco (Bellefonte, PA).

Samples

INS-1 cells were cultured on 10 cm plates in RPMI-1640 (+l-glutamine) supplemented with 10 % FBS, 1 mM pyruvate, 10 mM HEPES, 50 μM 2-β-mercaptoethanol, and 1 unit penicillin-streptomycin. INS-1 cells were grown to confluence (~4 x 10^7 cells) in 10 cm polystyrene dishes with RPMI culture media. All cells used in a particular experiment were seeded at the same time taking care to minimize variability by using precise volumes of reagents and seed cells.

Krebs-Ringer-HEPES buffer (KRHB) was prepared to contain 20 mM HEPES, 118 mM NaCl, 5.4 mM KCl, 2.4 mM CaCl, 1.2 mM $MgSO_4$, and 1.2 mM KH_2PO_4 and adjusted to pH 7.4 with HCl. Cells were washed once with 10 mL of KRHB prior to treatment in 10 mL of KRHB containing 0, 0.5, 10, or 20 mM glucose for 1 h at 37 °C. Each concentration was prepared in triplicate. After treatment, cells were washed once with 10 mL milli-Q water and snap frozen with liquid nitrogen. Plates were stored at -80 °C until extraction.

Fatty Acid Methyl Ester Synthesis

Fatty acid methyl esters were synthesized from the total lipid content as described by O'Fallon et al.[21] The only modification was that samples were not homogenized in a coffee grinder. Briefly, 5.3 mL of methanol was measured and an aliquot added to the cell plate. The plate was scraped and transferred to a 15 mL centrifuge tube. This procedure was repeated with the remainder of the methanol. Seven hundred μL of 10 M potassium hydroxide was added followed by incubation in a 55 °C water bath for 1.5 h with vigorous shaking every 20 min. The samples were cooled to below room

temperature with a cool water bath followed by the addition of 580 μL of 12 M sulfuric acid and an additional 1.5 h of incubation at 55 °C with shaking every 20 min. The tubes were cooled again to below room temperature with a cool water bath and 3 mL of hexane was added to each. The samples were vortexed for 5 min followed by centrifugation at 1600 *g* for 5 min. The hexane layer was transferred to a capped 4 dram vial and stored at -20 °C until analysis.

Comprehensive Two-Dimensional Gas Chromatography Time-of-Flight Mass Spectrometry

GC × GC analysis was performed on a Leco Pegasus III with 4D upgrade (St. Joseph, MI). The primary column was a 30 m Rxi®-1ms (0.25 mm i.d., 0.18 μm film), and the secondary column was a 2 m Rtx®-17silms (0.1 mm i.d., 0.1 μm film) both from Restek Corporation (Bellefonte, PA). A 1 μL injection was made with an Agilent 7683 automatic liquid sampler (Palo Alto, CA) in splitless mode, and four replicates were completed for each sample. For temperature programming, the primary oven was maintained at 40 °C for two minutes and then increased at a rate of 30 °C per minute to 160 °C, the rate was then slowed to 2 °C per minute until 260 °C was reached and maintained for 0.5 minutes. The secondary oven and the thermal modulator were offset from the primary oven by 5 °C and 30 °C respectively. A modulation period, or second dimension injection frequency, of 7 s was used. The hot pulse time (length of time the hot jet fires to initiate injection on the second dimension) was 0.8 s. A flow rate of 2 mL/min ultra high purity helium with an inlet and mass spectral transfer line temperature of 250 °C were maintained. A mass range of m/z 45 to 650 was collected at a rate of 200 spectra/s after a 400 s solvent delay. The ion source was maintained at 200 °C.

The Supelco 37 component FAME mix was analyzed at 0.25, 0.75 and 2.5 mg/ml, in triplicate, under identical conditions to the cell extracts for validation of the method linearity. Additionally, the mix was analyzed neat with the following chromatographic differences. A 150:1 split ratio was used in addition to a 1 mL/min flow rate. The final temperature was 270 °C and was maintained for 5 minutes. The mass spectral solvent delay was 300 s.

Data Analysis

Leco ChromaTOF version 4.22 was used for instrument control and data processing. The National Institutes of Standards and Technology (NIST) mass spectral library (version 2.0) was used to aid in peak identification. Statistical significance was determined in GraphPad Prism version 3.03 (La Jolla, CA) using a one way ANOVA analysis and a Newman-Keuls post-hoc test.

Results and Discussion

Analysis of 37 Component FAME Standard

In initial experiments, a standard mixture of 37 FAMEs was analyzed to ensure that the column set and conditions used would provide adequate resolution. As shown in Figure 3.1, good resolution and ordered retention is achieved with these conditions. Clustered elution of FAMEs with the same carbon number but a varying degree of saturation is readily observed in the C_{18} and C_{20} range of the standard, for example. The elution of FAMEs with the same degree of saturation along a horizontal axis is highlighted by the colored lines. The added benefit of being able to resolve FAMEs with the same degree of saturation but different ω numbers can be seen in Figure 3.1 where

both α-linolenic acid (C18:3 ω3) and γ-linolenic acid (C18:3 ω6) as well as cis-11,14,17-eicosatrienoic acid (C20:3 ω3) and cis-8,11,14-eicosatrienoic acid (C20:3 ω6) are fully resolved. The additional advantage of resolution and detection of odd numbered FAMEs, as previously described,[3, 11] is also demonstrated in Figure 3.1 where C_{11}, C_{15}, C_{17}, C_{21} and C_{23} compounds are all easily detected and identified.

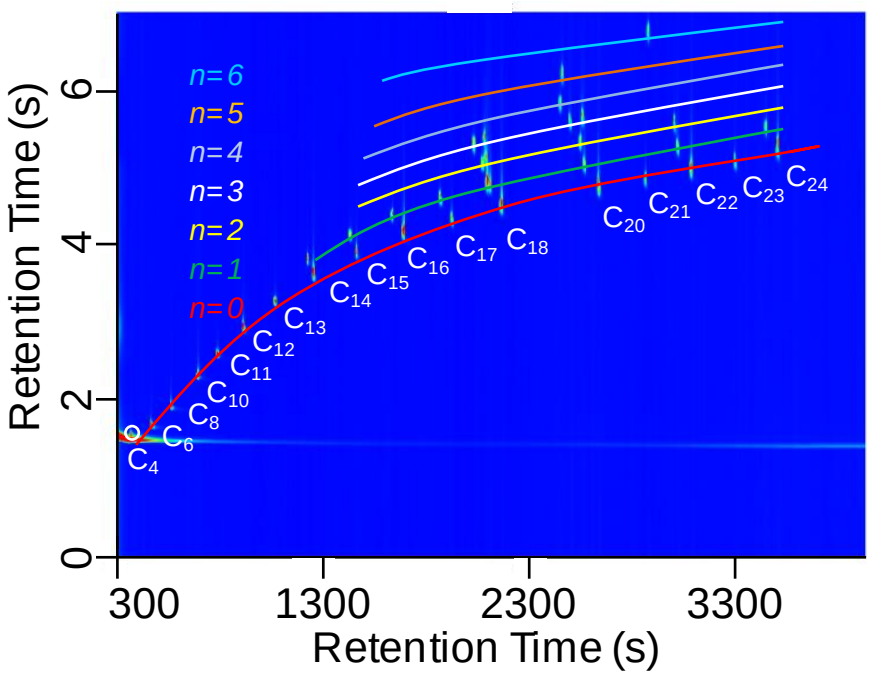

Figure 3.1 GC × GC chromatogram of neat 37 component FAMEs mix where n is the number of double bonds

These results validate the column set and chromatographic conditions for FAMEs used in this work. Changes from the initial methods were made in the flow rate, split ratio, and final temperature, as described in the experimental section, for faster analysis of actual samples containing fewer and less concentrated FAMEs than the commercially available standard.

Analysis of INS-1 Cell extracts

Extracts of INS-1 cells incubated in 10 mM glucose were analyzed via GC × GC after transformation of the total fatty acid concentration to methyl esters. A representative chromatogram is shown in Figure 3.2.

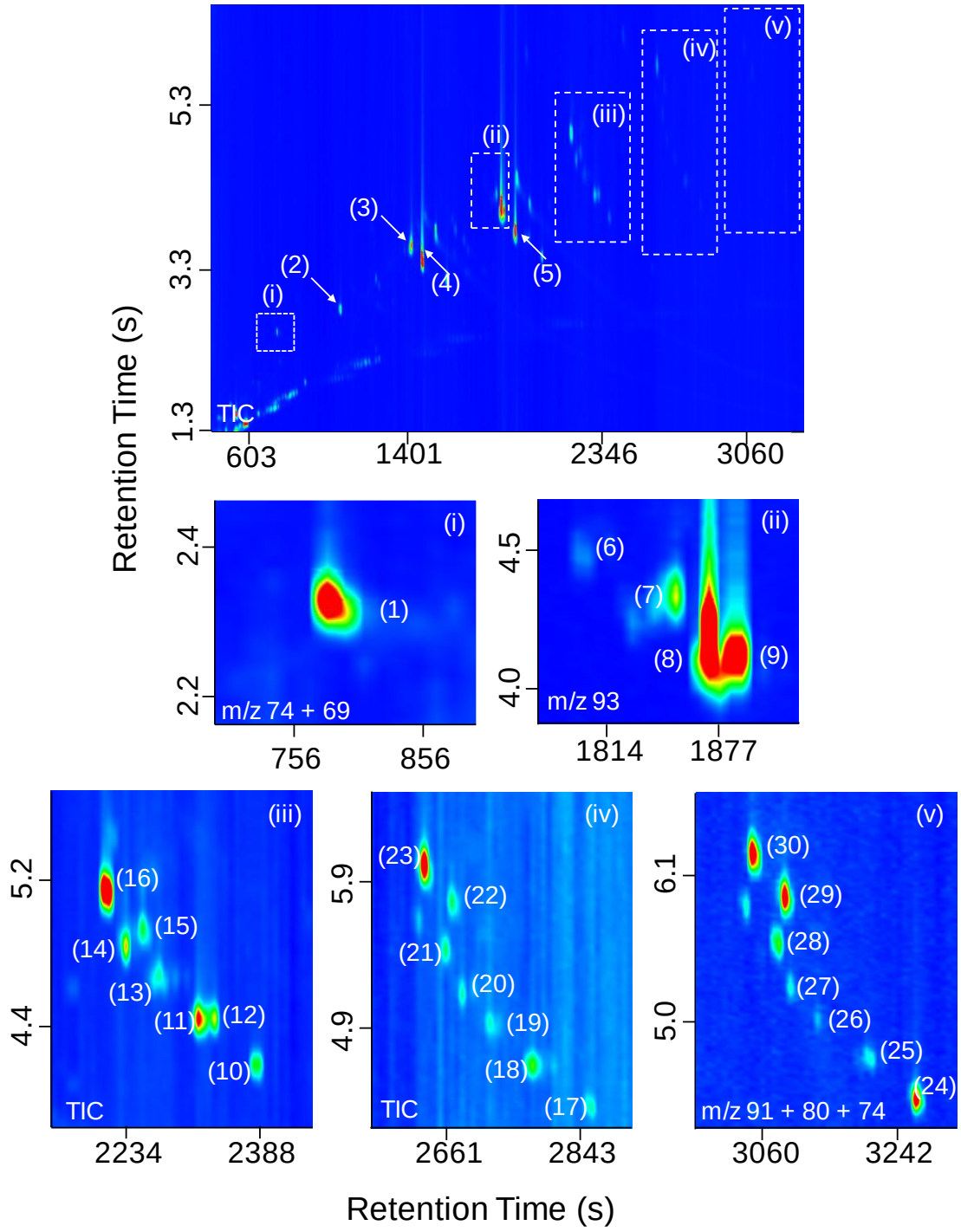

Figure 3.2 GC×GC total ion chromatogram (TIC) of a representative INS-1 cell extract (top). Peaks identified include lauric acid (1), myristic acid (2), palmitoleic acid (3), palmitic acid (4), stearic acid (5), linolenic acid (6), linoliec acid(7), oleic acid (8), elaidic acid (9), arachidic acid (10), cis-11-eicosenoic acid (11), cis-13-eicosenoic acid (12), eicosadienoic acid (13), cis-11,14,17-eicosatrienoic acid (14), cis-8,11,14-eicosatrienoic acid (15), arachidonic acid (16), behenic acid (17), erucic acid (18), brassic acid (19), eicosatetraenoic acid (20), eicosapentaenoic acid (21), clupanodonic acid (22), docosahexaenoic acid (23), lignoceric acid (24), nervonic acid (25), tetracosadienoic acid (26), tetracosatrienoic acid (27), tetracosatetraenoic acid (28), tetracosapentaenoic acid (29), tetracosahexaenoic acid (30). Boxes (i) through (v) are zoomed in portions of the corresponding broken boxes in the top chromatogram at either TIC, m/z 74 + 69, m/z 93, or m/z 91 + 80 + 74, as indicated

Peaks for myristic acid (C14:0), palmitic acid (C16:0), palmitoleic acid (C16:1). and stearic acid (C18:0) dominate the chromatogram; however, signals for other analytes are made apparent by expanding the scale or plotting select mass channels (Figure 3.2i through v). The advantages of using GC × GC are highlighted in Figures 3.2ii through 3.2v. In these portions, the resolution of oleic and elaidic acids, the resolution of cis-11-eicosonic acid and cis-13-eicosonic acid, and the resolution of ω3 and ω6 eicosatrienoic acid, which would not be resolved in one-dimension, can be seen.

In these samples, 30 FAMEs were identified with 12 to 24 carbons and 0 to 6 double bonds. Importantly, 15 fatty acids, of higher carbon number and number of double bonds, not previously identified by GC analysis of lipids in INS-1 cells,[20] are detected and identified. Of the 30 FAMEs identified, 11 were not available as standards. Identification of these 11 analytes was performed by utilizing the chromatogram structure, NIST 02 mass spectral database matches and manual inspection of the mass spectra. The new lipids identified in the INS-1 cells are: lauric acid, linolenic acid, eicosadienoic acid, eicosatrienoic acid, erucic acid, brassic acid, eicosatetraenoic acid, eicosapentaenoic acid, clupanodonic acid, nervonic acid, tetracosenoic acid, tetracosatrienoic acid, and tetracosatetraenoic acid, tetracosapentaenoic acid, tetracosahexaenoic acid.

To evaluate the potential of the method for quantitative analysis, calibration curves were created for 14 FAMEs. Linear correlation coefficients of 0.99 or greater were achieved in the concentration range of 0.25 to 2.5 mg/ml. A representative curve for myristic acid is shown in Figure 3.3.

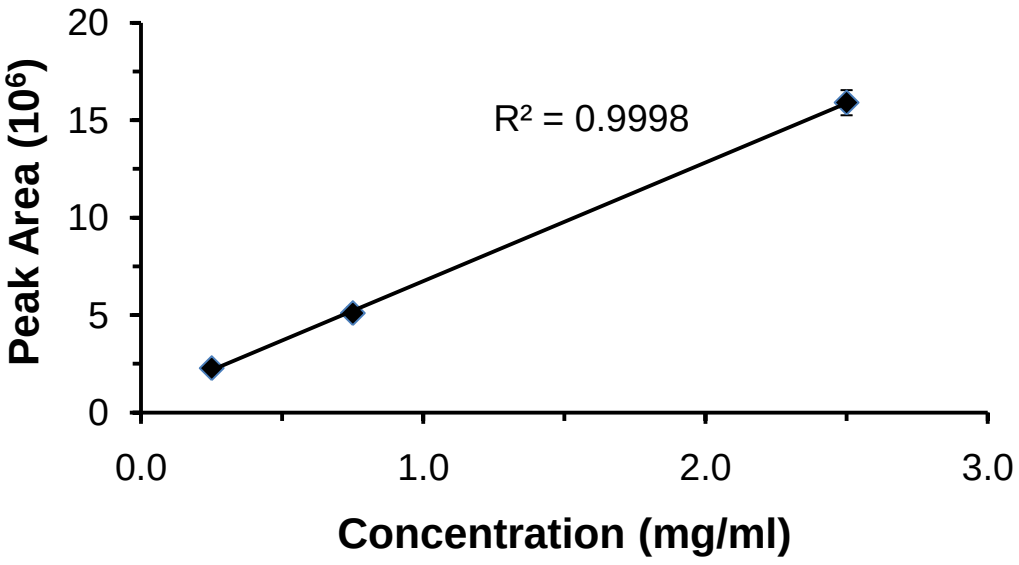

Figure 3.3 Calibration curve for myristic acid. Samples were analyzed in triplicate and error bar is ± 1 SEM

The average RSD for replicate injections of the same sample was 8.4% with a range of 3.14 to 23.21%, see Table 3.1. Replicate analysis of biological samples yielded average RSDs of 12.4% with a range of 4.58 to 36.1% for all analytes except for palmitic acid (0.5 and 10 mM glucose), elaidic acid (0.5 mM glucose), arachidic acid (10 mM glucose), and erucic acid (0 and 0.5 mM glucose), (Table 3.2). The reason for this variability is not well understood. Overall, reproducibility may be improved by use of an internal standard. Possible internal standards include odd chain fatty acids or using a sample prepared with deuterated methanol as an internal standard for each analyte.[22] In summary, the linearity, detection limit, and reproducibility suggest that the method can be used for semi-quantitative analysis for most analytes. Use of internal standards would be expected to improve the quantification ability of the method.

Table 3.1 Average technical variability presented as relative standard deviations (RSDs) at 0 mM, 0.5 mM, 10 mM and 20 mM glucose. Three plates per concentration, four replicates per plate

Fatty Acid	0 mM	0.5 mM	10 mM	20 mM	Average
C12:0	4.7	3.1	9.2	6.6	5.9
C14:0	4.6	3.6	7.1	8.6	5.
C16:0	9.2	4.6	6.4	11	7.9
C16:1	7.2	5.5	12	8.8	8.3
C18:0	7.7	5.4	5.4	5.7	6.1
C18:1 (ω9, cis)	5.6	3.7	6.6	10	6.4
C18:1 (ω9, trans)	14	5.9	10	13	11
C18:2	6.9	5.8	5.6	8.3	6.6
C18:3	5.2	7.1	4.1	7.7	6.0
C20:0	6.3	5.6	5.6	7.0	6.1
C20:1 (cis-11)	12	9.2	7.6	8.0	9.23
C20:1 (cis-13)	6.8	6.1	5.6	7.2	6.4
C20:2	7.9	8.7	7.6	6.8	7.8
C20:3 (ω3)	9.2	7.5	6.5	8.2	7.8
C20:3 (ω6)	5.8	5.1	6.4	8.9	6.6
C20:4	6.7	5.1	5.5	6.7	6.0
C22:0	5.6	5.8	7.1	6.2	6.2
C22:1	11	6.4	11	7.2	9.0
C22:2	20	20	9.8	7.4	14
C22:3	4.3	6.9	7.7	6.9	6.4
C22:4	5.4	10	9.1	12	9.1
C22:5	5.9	7.9	7.9	7.6	7.3
C22:6	6.6	11	14	6.1	9.2
C24:0	9.7	9.1	9.2	9.1	9.3
C24:1	10	5.7	7.3	23	12
C24:2	20	13	14	14	15
C24:3	20	12	17	15	16
C24:4	8.7	3.5	6.4	15	8.4
C24:5	9.5	5.1	11	8.0	8.4
C24:6	6.9	6.5	8.2	12	8.3

Table 3.2 Biological variability presented as relative standard deviations (RSDs) at 0 mM, 0.5 mM, 10 mM and 20 mM glucose. Three plates per concentration, four replicates per plate

Fatty Acid	0 mM	0.5 mM	10 mM	20 mM	Average
C12:0	12	9.5	12	12	11
C14:0	12	6.5	7.3	15	10
C16:0	16	4.8	8.8	18	12
C16:1	8.2	52	44	14	30
C18:0	12	5.7	7.2	17	10
C18:1 (ω9, cis)	8.2	4.6	6.7	12	7.9
C18:1 (ω9, trans)	21	42	13	24	25
C18:2	7.9	7.5	57	13	22
C18:3	7.1	9.5	7.1	16	9.9
C20:0	6.3	12	7.6	19	11
C20:1 (cis-11)	12	16	7.8	19	14
C20:1 (cis-13)	8.0	5.5	6.4	17	9.3
C20:2	10	11	9.6	14	11
C20:3 (ω3)	9.5	5.8	9.6	13	9.5
C20:3 (ω6)	5.5	9.7	8.4	17	10
C20:4	8.7	6.0	7.2	13	8.9
C22:0	5.5	12	15	19	13
C22:1	66	53	17	36	43
C22:2	20	24	26	15	21
C22:3	4.9	6.8	10	18	10
C22:4	5.4	11	10	16	11
C22:5	5.8	8.3	8.7	13	8.9
C22:6	6.4	12	17	14	12
C24:0	8.2	9.5	20	23	15
C24:1	6.1	6.3	14	16	11
C24:2	21	13	17	24	19
C24:3	16	9.8	18	22	17
C24:4	6.6	5.6	6.5	27	11
C24:5	5.8	4.8	12	18	9.9
C24:6	11	6.1	10	19	11

Glucose Stimulated Changes in Fatty Acids

Glucose evokes a number of metabolic changes in β-cells that are linked to cell function. Most importantly, glucose stimulates insulin secretion through metabolism. Although some of the metabolic changes associated with glucose that evoke insulin secretion are known (e.g., an increase the ATP/ADP ratio), it is believed that as yet

unidentified changes also contribute to insulin secretion. Glucose may also be an important signal for adaptation (such as cell growth or increased insulin synthesis). Excessive glucose is known to result in glucotoxicity and impaired β-cell function, which likely plays a role in type 2 diabetes. In view of the important role of glucose for β-cell metabolism, we evaluated the acute effect of incubation in different concentrations of glucose on fatty acid content of INS-1 cells. Glucose concentrations of 0, 0.5, 10, and 20 mM were tested in triplicate and extracts from each were analyzed in quadruplicate.

Table 3.3 summarizes the fatty acid content as a function of extracellular glucose concentration. Several fatty acids showed increases with glucose until the highest concentration where a decrease was observed resulting in an inverted U-shaped dose-response curve (see Figure 3.4). Another group of fatty acids that included lauric, myristic, linolenic, cis-13-eicosenoic, eicosadienoic, cis-11,14,17-eicosatrinoic, cis-8,11,14-eicosatrienoic, arachidonic, eicosapentaenoic, clupanodonic, docosaexaenoic, tetracosadienoic, tetracosatetraenoic, tetracosapentaenoic, and tetracosahexanoic acids experienced no significant change in peak area at 0, 0.5, and 10 mM glucose but showed a significant decrease at 20 mM glucose (see Table 3.3 and Figure 3.4).

Table 3.3 Determination of fatty acids in INS-1 cells incubated for 60 min at different glucose concentrations. Average peak area and ± 1 SEM at 0 mM, 0.5 mM, 10 mM and 20 mM glucose. a = significantly different from 0 mM glucose, b = significantly different from 0.5 mM glucose, c = significantly different from 10 mM glucose. Significance was determined with one way ANOVA test and Newman-Keuls post-hoc test. Three plates per concentration, four replicates per plate.

FAME	Peak Area 0 mM glucose	Peak Area 0.5 mM glucose	Peak Area 10 mM glucose	Peak Area 20 mM glucose
C12:0	1.1E ± 0.04	0.99 ± 0.04	0.99 ± 0.04	0.79 ± 0.03 [a,b,c]
C14:0	20 ± 0.8	20 ± 0.5	22 ± 0.5	17 ± 0.7 [a,b,c]
C16:0	220 ± 1	240 ± 5	250 ± 6	210 ± 11 [c]
C16:1	7.8 ± 0.2	4.6 ± 1.0 [a]	5.7 ± 0.7 [a]	6.6 ± 0.3
C18:0	95 ± 4	110 ± 3 [a]	110 ± 2 [a]	88 ± 4 [b,c]
C18:1 (ω9, cis)	20 ± 0.6	20 ± 0.4	20 ± 0.04	18 ± 0.6 [a,c]
C18:1 (ω9, trans)	8.0 ± 0.6	6.5 ±1	9.6 ± 0.4 [a]	7.4 ± 0.5 [c]
C18:2	3.4 ± 0.1	3.3 ± 0.1	2.5 ± 0.4	2.6 ± 0.1
C18:3	0.16 ± 0.004	0.15 ± 0.006	0.17 ± 0.003	0.13 ± 0.006 [a,b,c]
C20:0	2.6 ± 0.06	2.8 ± 0.01	3.0 ± 0.07 [c]	2.3 ± 0.01 [a,b,c]
C20:1 (cis-11)	1.7 ± 0.07	1.8 ± 0.1	1.9 ± 0.04	1.5 ± 0.08 [b,c]
C20:1 (cis-13)	1.1 ± 0.03	1.1 ± 0.03	1.2 ± 0.02	0.93 ± 0.05 [a,b,c]
C20:2	0.9 ± 0.03	0.93 ± 0.04	0.97 ± 0.03	0.76 ± 0.03 [a,b,c]
C20:3 (ω3)	1.7 ± 0.06	1.7 ± 0.04	1.7 ± 0.05	1.3 ± 0.05 [a,b,c]
C20:3 (ω6)	1.2 ± 0.02	1.2 ± 0.05	1.3 ± 0.03	1.1 ± 0.05 [a,b,c]
C20:4	7.4 ± 0.2	7.1 ± 0.2	7.5 ± 0.2	6.0 ± 0.2 [a,b,c]
C22:0	0.80 ± 0.02	0.97 ± 0.05 [a]	1.0 ± 0.04 [a]	0.775 ± 0.04 [b,c]
C22:1	0.30 ± 0.07	0.24 ± 0.05	0.43 ± 0.02 [a,b]	0.22 ± 0.02 [c]
C22:2	0.35 ± 0.02	0.38 ± 0.04	0.35 ± 0.03	0.32 ± 0.01
C22:3	0.31 ± 0.05	0.32 ± 0.09	0.33 ± 0.1	0.25 ± 0.01
C22:4	0.50 ± 0.01	0.48 ± 0.02	0.51 ± 0.02	0.40 ± 0.02 [a,b,c]
C22:5	1.1 ± 0.02	1.1 ± 0.04	1.1 ± 0.03	0.91 ± 0.03 [a,b,c]
C22:6	5.4 ± 0.1	5.3 ± 0.2	5.4 ± 0.3	4.5 ± 0.2 [a,b,c]
C24:0	0.40 ± 0.01	0.47 ± 0.02	0.47 ± 0.03	0.35 ± 0.02 [b,c]
C24:1	0.091 ± 0.002	0.11 ± 0.003 [a]	0.11 ± 0.004 [a]	0.097 ± 0.004
C24:2	0.073 ± 0.005	0.088 ± 0.005	0.082 ± 0.004	0.063 ± 0.004 [b,c]
C24:3	0.048 ± 0.003	0.051 ± 0.002	0.47 ± 0.002	0.040 ± 0.003
C24:4	0.13 ± 0.003	0.14 ± 0.003	0.14 ± 0.003	0.10 ± 0.008 [a,b,c]
C24:5	0.70 ± 0.01	0.69 ± 0.01	0.70 ± 0.02	0.59 ± 0.03 [a,b,c]
C24:6	0.7 7 ± 0.03	0.79 ± 0.02	0.81 ± 0.02	0.63 ± 0.03 [a,b,c]

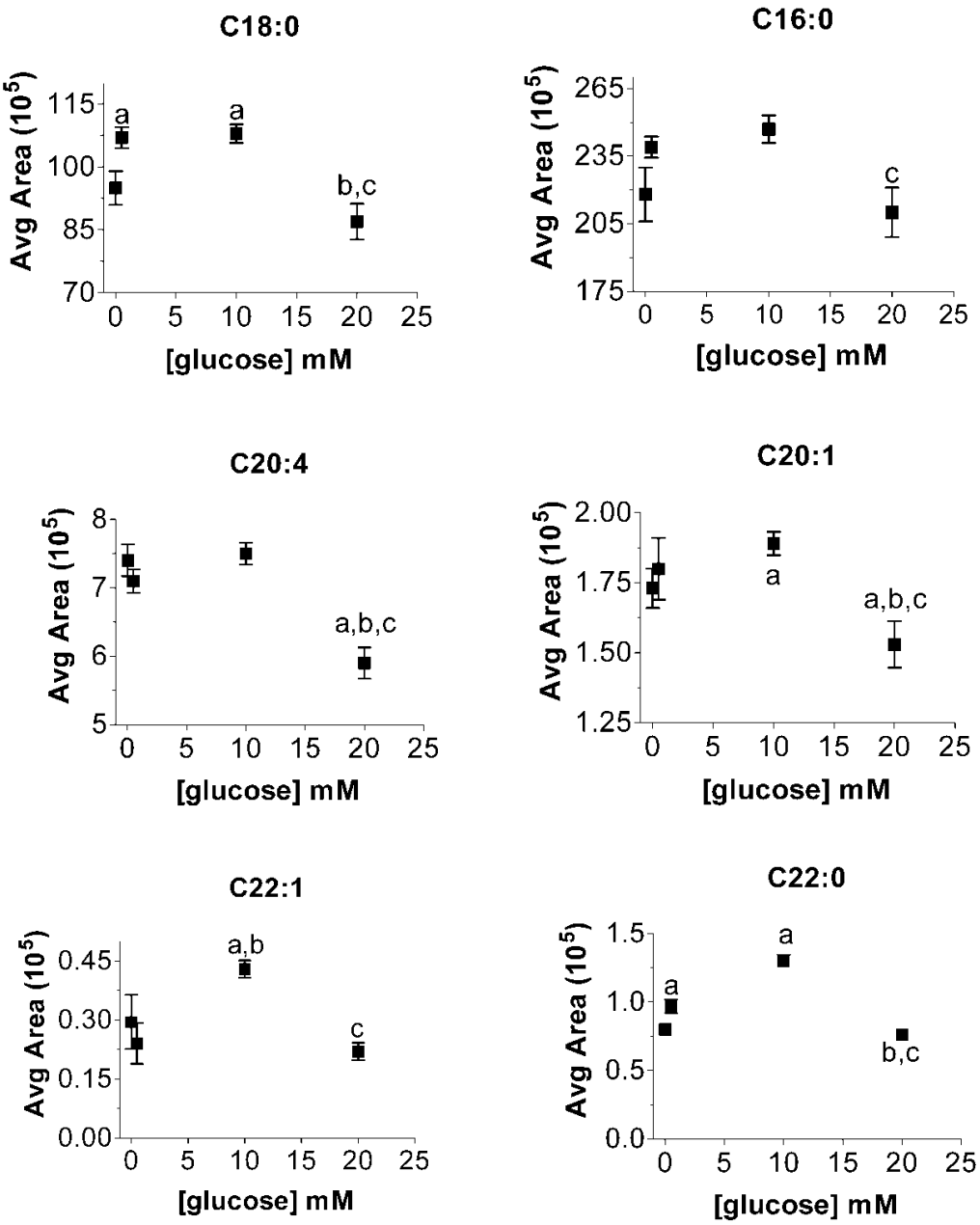

Figure 3.4 Average area of palmitic acid (C16:0), stearic acid (C18:0), eicosenoic acid (C20:1), arachidonic acid (C20:4), behenic acid (C22:0) and erucic acid (C22:1) at 0 mM, 0.5 mM, 10 mM, and 20 mM glucose. Error bars are ± 1 SEM, a = significantly different from 0 mM glucose, b = significantly different from 0.5 mM glucose, c = significantly different from 10 mM glucose. Significance was determined with one way ANOVA test and Newman-Keuls post hoc test

The significance of these changes to cell physiology cannot be discerned without further experimentation; however, these changes do illustrate the potential of the method to provide detailed analysis of the fatty acid profile. Arachidonic acid is of particular interest as it has previously been directly linked to the function of pancreatic β-cells, is involved in glucose-stimulated insulin release, and can be linked to a number of diseases including obesity.[6, 23] Although direct links are less obvious for other fatty acids, it has been established that fatty acids promote insulin secretion and that not all fatty acids have the same insulinotropic potency.[24, 25] Previous work has shown that insulinotropic potency is directly related to fatty acid chain length and degree of saturation with, for example, stearic acid (C18:0) having more of an effect on insulin secretion than palmitic acid (C16:0) and oleic acid (C18:1).[25] As glucose induces changes in metabolism as well as insulin secretion, such changes may be involved in both these processes. Further, excessive glucose can be toxic to INS-1 cells, so the changes that occur at 20 mM glucose may be of interest for understanding the mechanisms of glucotoxicity.

Many fatty acids showed little change as a function of glucose concentration. Because we measured total fatty acids, these stable results do not preclude possible redistribution between different pools, e.g. free and esterfied fatty acids. For example, a previous study has shown substantial changes in myristic acid, palmitic acid, palmitoleic acid, stearic acid, oleic acid, and vaccenic acid in the phospholipid fraction of INS-1 cell extracts,[20] and only minor changes in free fatty acids or other lipid classes.

Our results do not completely agree with a previous study that measured 11 fatty acids (total fatty acid content) in pancreatic islets of Langerhans (microorgans containing β-cells) as in the presence of 0, 5.6, 8.3 and 16 mM glucose via HPLC.[8] In agreement

with this previous study, we observed an increase in stearic acid with glucose concentration and no statistically significant difference for linoleic acid. At moderate glucose concentrations, arachidonic and docosahexaenoic acid concentrations are not statistically different in both the work presented here and the previous islet study.[8] However, at high glucose, we observe a decrease in arachidonic and docosahexaenoic acids that was not previously observed in islets.[8] Additionally, an increase in lauric acid (C12:0), myristic acid (C14:0), palmitic acid (C16:0), and palmitoleic acid (C16:1) concentrations when compared to the absence of glucose were reported in the previous work [8] with islets but not in the INS-1cell data presented here. The changes observed previously[8] in lauric acid and myristic acid are only seen at 16 mM glucose, thus, in view of the inverted U-shaped curve observed in our work, it is possible that these changes are missed in our experiment. The difference in palmitic and palmitoleic acid results may be explained by the high variability observed for these analytes. Another important point is that although islets and INS-1 cells are metabolically similar; they also have substantial differences that could easily affect the lipid profile and content.

Conclusions

We have demonstrated that GC × GC is a viable tool for lipid analysis not only in fats and oils but also cultured cells. The utility of this technique is highlighted by the identification of 15 fatty acid methyl esters not identified in previous analyses of these cells.[8, 20] The potential of the method was also shown for monitoring lipid changes following perturbations, such as glucose concentration. This result hinged on the excellent reproducibility achieved for most of the fatty acids. Further analysis using an internal standard and/or separating lipid classes prior to FAMEs analysis could reveal

valuable information about INS-1 cell metabolism. Additionally, applying the methodology developed in this work to different cell lines may help further elucidate the role of fatty acids in human health and disease states.

References

(1) Simopoulos, A. P. *The American Journal of Clinical Nutrition* **1999**, *70*.
(2) Seppänen-Laakso, T.; Laakso, I.; Hiltunen, R. *Anal. Chim. Acta* **2002**, *465*, 39-62.
(3) Quinto Tranchida, P.; Costa, R.; Donato, P.; Sciarrone, D.; Ragonese, C.; Dugo, P.; Dugo, G.; Mondello, L. *J. Sep. Sci.* **2008**, *31*, 3347-3351.
(4) Rupp, H.; Rupp, T.; Alter, P.; Maisch, B. *Br. Heart J.* **2010**, *96*, 595-598.
(5) Rokling-Andersen, M.; Rustan, A.; Wensaas, A.; Kaalhus, O.; Wergedahl, H.; Rost, T. *Br. J. Nutr.* **2009**, *102*, 995-1006.
(6) Wymann, M. P.; Schneiter, R. *Nat Rev Mol Cell Biol* **2008**, *9*, 162-176.
(7) Fabbri, D.; Baravelli, V.; Chiavari, G.; Prati, S. *J. Chromatogr. A* **2005**, *1100*, 218-222.
(8) Martins, E. F.; Miyasaka, C. K.; Newsholme, P.; Curi, R.; Carpinelli, A. R. *Diabetes Metab.* **2004**, *30*, 21-27.
(9) Janssen, H.-G.; Boers, W.; Steenbergen, H.; Horsten, R.; Flöter, E. *J. Chromatogr. A* **2003**, *1000*, 385-400.
(10) Koning, S. d.; Janssen, H.-G.; Deursen, M. v.; Brinkman, U. A. T. *J. Sep. Sci.* **2004**, *27*, 397-409.
(11) Adahchour, M.; Beens, J.; Brinkman, U. A. T. *J. Chromatogr. A* **2008**, *1186*, 67-108.
(12) Chin, S.-T.; Che Man, Y. B.; Tan, C. P.; Hashim, D. M. *J. Am. Oil Chem. Soc.* **2009**, *86*, 949-958.
(13) Dalluge, J.; Beens, J.; Brinkman, U. A. T. *J. Chromatogr. A* **2003**, *1000*, 69-108.
(14) Tiyapongpattana, W.; Wilairat, P.; Marriott, P. J. *J. Sep. Sci.* **2008**, *31*, 2640-2649.
(15) Adam, F.; Bertoncini, F.; Coupard, V.; Charon, N.; Thiebaut, D.; Espinat, D.; Hennion, M. *J. Chromatogr. A* **2008**, *1186*, 236-244.
(16) Akoto, L.; Stellaard, F.; Irth, H.; Vreuls, R.; Pel, R. *J. Chromatogr. A* **2008**, *1186*, 254-261.
(17) Mondello, L.; Casilli, A.; Tranchida, P. Q.; Dugo, P.; Dugo, G. *J. Chromatogr. A* **2003**, *1019*, 187-196.
(18) Yaney, G. C.; Corkey, B. E. *Diabetologia* **2003**, *46*, 1297.
(19) Nolan, C. J.; Madiraju, M. S. R.; Delghingaro-Augusto, V.; Peyot, M.-L.; Prentki, M. *Diabetes* **2006**, *55*, S16-S23.
(20) MacDonald, M. J.; Dobrzyn, A.; Ntambi, J.; Stoker, S. W. *Arch. Biochem. Biophys.* **2008**, *470*, 153-162.
(21) O'Fallon, J. V.; Busboom, J. R.; Nelson, M. L.; Gaskins, C. T. *J. Anim. Sci.* **2007**, *85*, 279-280.
(22) Li, J.; Yue, Y.; Hu, X.; Zhong, H. *Anal. Chem.* **2009**, *81*, 5080.
(23) Ramanadham, S.; Hsu, F.-F.; Zhang, S.; Bohrer, A.; Ma, Z.; Turk, J. *BBA-Mol. Cell. Biol. L.* **2000**, *1484*, 251-266.
(24) McGarry, J. D. *Diabetes* **2002**, *51*, 7-18.
(25) Stein, D. T.; Stevenson, B. E.; Chester, M. W.; Basit, M.; Daniels, M. B.; Turley, S. D.; McGarry, J. D. *J. Clin. Invest.* **1997**, *100*, 398-403.

Chapter 4

PILOT STUDY OF WHOLE SEDIMENT PYROLYSIS COMPREHENSIVE TWO-DIMENSIONAL GAS CHROMATOGRAPHY TIME-OF-FLIGHT MASS SPECTROMETERY (GC × GC-TOFMS) ON A MEDITERRANEAN SAPROPEL SEQUENCE

Introduction

A common feature within post-Messinian (5 million years and younger) Mediterranean Sea sediment is dark colored, organic rich layers, known as sapropels, intercalated within surrounding light colored, organic poor layers (marls). Concentrations of total organic carbon (TOC) that can exceed 30 wt% in the sapropels imply both elevated production and enhanced preservation of marine organic matter (OM), neither of which occurs under modern conditions in this oligotrophic sea.[1, 2] The exact mechanism for sapropel formation, however, remains under debate and of interest. The periods of time when sapropels were formed correspond to precessional minima (times when the northern hemisphere was tilted towards the sun during the summer, opposite to the current tilt). During the most recent precessional minimum (9-6 thousand years ago), the Mediterranean region was wetter, the Great Plains were drier, and the rainy season of the Asian monsoons was more intense. These and other climate changes might be precursors of what to expect from global warming, which is predicted to cause climate instability and significantly affect how people live today.

Paleoclimatic and paleoceanographic information stored in the OM compositions of sapropels and adjacent sediments potentially includes evidence of changes in the origin

of the organic matter, its mode and rate of marine productivity, and degree of preservation. As examples, organic geochemical studies have employed Rock-Eval pyrolysis to determine that the bulk of the OM in the sapropels is algal in origin.[1, 3, 4] $\delta^{15}N$ values and C/N ratios have been used to establish that microbial nitrogen fixation was important to increased production of marine OM in the sapropels[5-7], and to conclude that nitrogen-rich components of OM were selectively recycled in low-oxygen conditions in the water column.[1, 3, 6] Recognizing that the extractable molecular components rarely represent more than a few percent of the total OM, a previous study utilized Curie-point pyrolysis to liberate molecular components from kerogen isolated from three middle Pliocene sapropels and to verify that enhanced preservation of marine OM was indeed important to their formation.[4]

Gas chromatography is a common tool for the analysis of sapropel extracts. However, the separation of most components is often far from satisfactory as several components tend to coelute and cause large 'humps' or un-unresolved complex mixtures (UCM). The components within the UCMs can only be generalized into a class of molecule but not identified. Comprehensive two-dimensional gas chromatographic (GC × GC) analysis is able to better separate and identify the OM in geological samples. This improvement has been demonstrated previously with the analysis of black shale, oil spill environments, diesel fuel, and petroleum.[8-15] In Figure 4.1, a direct comparison between a one-dimensional analysis yielding two distinct UCMs and a GC × GC analysis of a black shale sample is shown.[15] Unlike in the GC analysis where only *n*-alkanes were identified, in the GC × GC chromatogram *n*-alkanes, mono-, bi-, tri-, tetra- steranes,

pentacyclic hopanes, irregular isoprenoids, monomethylalkanes, and monoethylalkanes were identified.

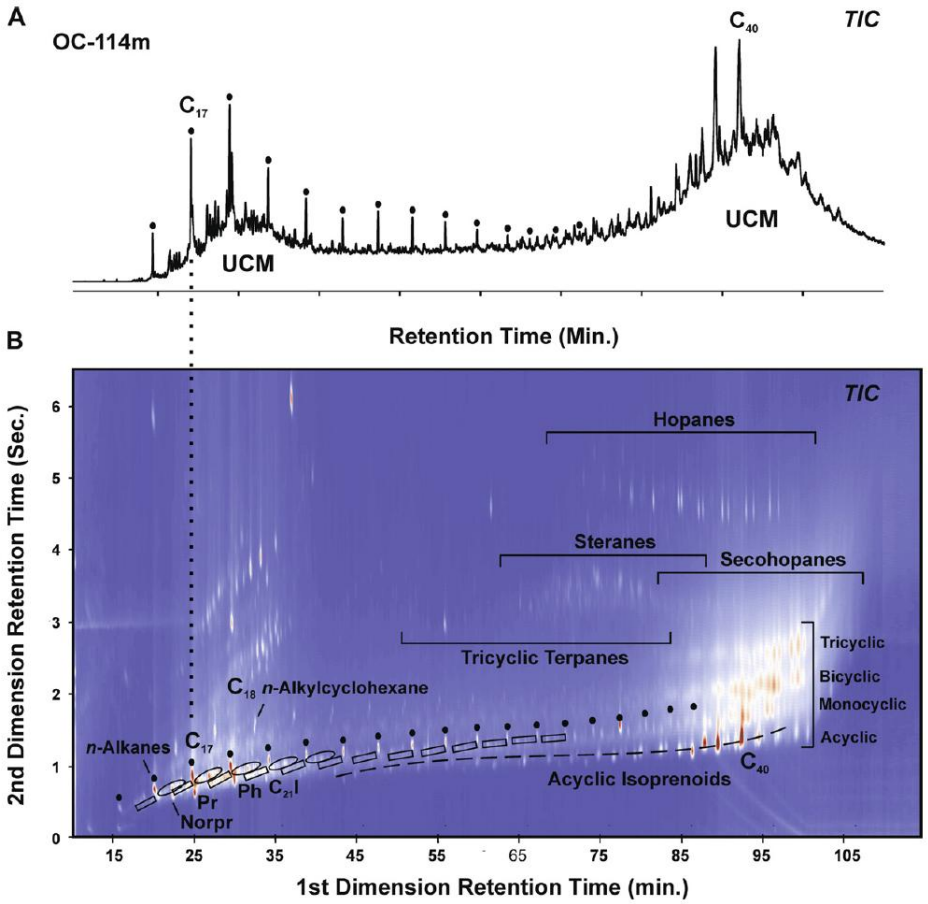

Figure 4.1(A) GC−MS TIC chromatogram of black shale containing two UCMs. (B) GC × GC−MS total ion chromatogram of the same sample with the labeled *n*-alkanes (black circles), mono-, bi-, tri-, tetra- (steranes), and pentacyclic (hopanes). Dotted line indicates irregular isoprenoids. Boxes encapsulate monomethylalkanes. Open ovals enclose monoethylalkanes. (Used with permission)[15]

As mentioned previously, extractable molecular components rarely represent more than a few percent of the total OM. Conversely, in pyrolysis, organic material can be analyzed regardless of solubility. Therefore, the use of pyrolysis, instead of liquid extractions, increases the amount of organic matter available for analysis, as demonstrated in Figure 4.2[16] which compares the GC × GC analysis of a limestone

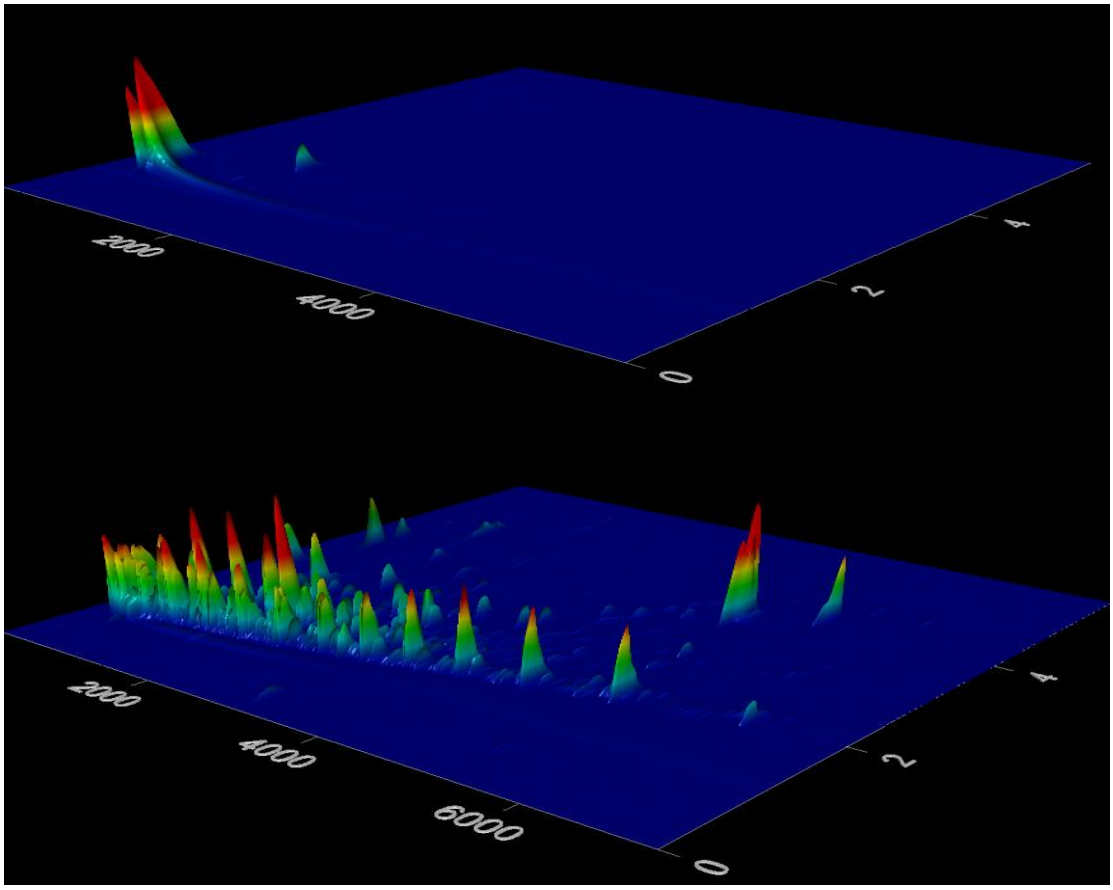

Figure 4.2 GC × GC chromatogram of an EPA method limestone extraction (top) and pyrolysis GC× GC chromatrogram of an identical limestone samples (bottom). In the extract chromatgoram three peaks are present, two are solvent and the third is unidentified. More than 20 peaks were detected in the pyrolysis chromatogram. (Chromatograms courtesy of Dr. Megan McGuigan)

solvent extract with the pyrolysis of limestone. One previous geochemical application of whole sediment Py-GC × GC has been done.[17] In that study, microwave Py-GC × GC with a flame ionization detector was used to study a petroleum source rock. Based on the success of this previous work[17], a similar analytical approach is used to identify differences between sapropels and neighboring OM-poor strata because even samples with little OM would contain adequate analyte material if the whole sediment were analyzed. The increased detectability and peak capacity of GC × GC combined with

pyrolysis was expected to lead to detection of novel organic matter biomarker molecules helping to further elucidate the understanding of sapropel formation.

Experimental

Samples

A sapropel sequence from the Tyrrhenian Basin of the Mediterranean Sea, see Figure 4.3 for location map, was used. The Late Pliocene to Holocene sedimentary record of this semi-isolated sea contains multiple layers of OM-rich sapropels that contrast markedly against the OM-poor homogeneous marls that comprise most of the sediments.[18, 19] We obtained samples from Ocean Drilling Program (ODP) Site 974, which is located at a water depth of 3453 m near the center of the Tyrrhenian Basin. Sediments at this location consist of bioturbated pelagic to hemipelagic nannofossil-rich clays and nannofossil oozes intercaleted sapropel layers.[20] The evidence for bioturbation implies that the bottom waters of this basin contained adequate dissolved oxygen to support infauna for at least some parts of its depositional history.

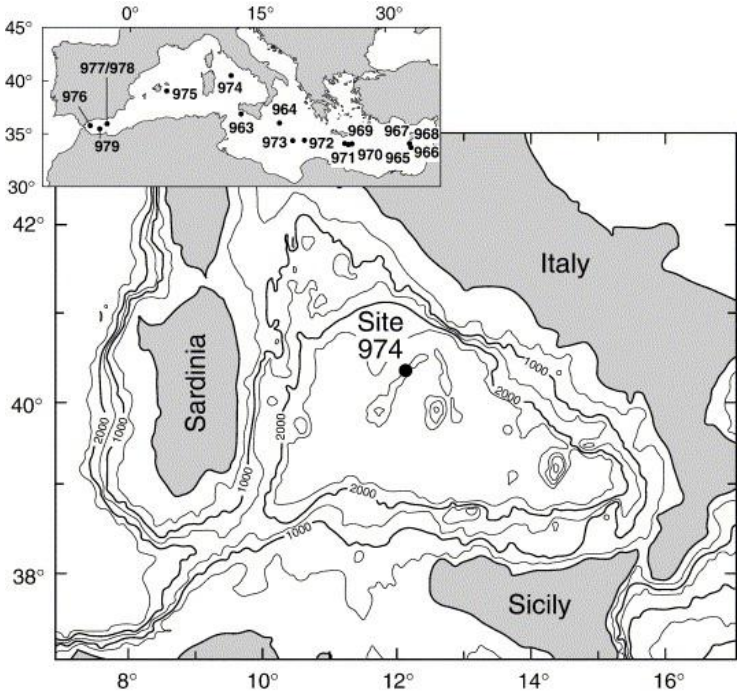

Figure 4.3 Location of ODP Site 974 in the Tyrrhenian Basin of the Mediterranean Sea. Depth contours are in meters below sea level.

Our samples were obtained from a sediment sequence shown in Figure 4.4 and includes the sapropel layer that was deposited during insolation cycle 94, which has a mid-point that corresponds to 997 ka.[21] This sequence was previously sampled at 1 cm intervals for a study of its bulk OM elemental and isotopic properties.[6] A subset of the samples from this earlier study was selected for our pyrolysis studies. The six samples originate from an 18 cm interval that includes the TOC-poor background marl above and below the sapropel and different positions within the TOC-rich layer (Table 4.1). The elevated TOC mass accumulation rates and less negative $\delta^{13}C$ values of the sapropel samples indicate that they record an interval of elevated marine productivity in the Tyrrhenian Sea. The dramatically low $\delta^{15}N$ values suggest the existence of nitrogen fixation during deposition, and high C/N values likely represent preferential degradation

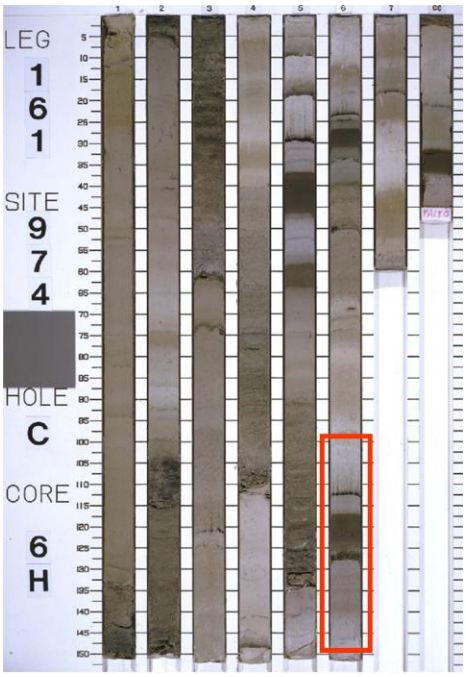

Figure 4.4 Photo of core used for pyrolysis GC × GC analysis. The segment used in this work is highlighted in red. (Photo obtained from the Ocean Drilling Program Data Librarian and used with permission)

of nitrogen-rich forms of OM relative to nitrogen-poor forms. All of these bulk OM parameters are common features of Mediterranean sapropels.[1, 3, 5, 6]

Table 4.1 Samples of ODP Site 974 (Tyrrhenian Basin) insolation cycle 94 sapropel sequence used for pyrolysis GC×GC-ToFMS analyses.

Hole-Core-Section, Interval	Depth (mbsf)	Depth (mcd)	Age (ka)	TOC (%)	C_{org}MAR (mg/cm^2/ky)	$d^{13}C_{org}$ ($^o/_{oo}$)	$d^{15}N_{tot}$ ($^o/_{oo}$)	C/N (atomic)	n-alkane $ACL_{9\text{-}21}$	alk-1-ene $ACL_{9\text{-}20}$	MK $ACL_{9\text{-}19}$
974C-6H-6, 95-97 cm	50.75	56.23	991.5	0.1	6.4	-24.9	5.4	7.4	15.5	14.0*	16.7[t]
974C-6H-6, 112-113 cm	50.92	56.40	995.4	0.16	10.2	-25.1	3.8	8.9	15.2	16.1**	15.6
974C-6H-6, 117-118 cm	50.97	56.45	996.5	2.51	160.4	-23.0	-0.5	17.9	15.5	15.3	15.9
974C-6H-6, 119-120 cm	50.99	56.47	997.0	3.85	326.5	-22.2	-3.2	18.6	15.7	15.2	16.3
974C-6H-6, 123-124 cm	51.03	56.51	997.7	2.33	197.6	-23.2	-0.5	21.7	15.7	14.4	15.6
974C-6H-6, 125-126 cm	51.05	56.53	998.0	0.76	64.5	-23.4	1.9	18.4	12.4	15.4	15.5

Bulk sediment elemental and isotopic data from Meyers and Bernasconi (2005)

ACL = $S(iX_i)/S(X_i)$ where X = peak area and i = range
*$ACL_{10\text{-}20}$ **$ACL_{11\text{-}20}$

[t]$ACL_{15\text{-}17}$

Pyrolysis comprehensive two-dimensional gas chromatography time-of-flight mass spectrometry (Pyr-GC × GC-ToFMS)

GC × GC-ToFMS studies were performed on whole-sediment samples with the Leco Pegasus III with 4D upgrade and a pyrolysis inlet (Pyroprobe 2000, CDS Analytical, Oxford, PA). Each sample (ca. 2 mg) was placed in a quartz tube between plugs of quartz wool. The tube was inserted into a coil probe and pyrolyzed at 600 °C (15 s) under a constant flow of H_2. This pyrolysis temperature was determined to be optimal for pyrolysis of our whole sediment samples using the empirical procedure of McGuigan et al.[22] Briefly, GC × GC chromatograms were obtained for fresh portions of the 119-120 cm interval sample at pyrolysis temperatures of 200, 400, 600, 800 and 1000 ˚C. These chromatograms were then compared to those obtained from one 2 mg sample of the same interval that was pyrolyzed and analyzed at each temperature in increasing order (200 to 1000 °C). Between analyses, the quartz tube was removed immediately after pyrolysis and stored in a sealed vial until the previous chromatogram was complete, and the interface was purged to avoid carry-over. The 600 °C pyrolysis temperature that we empirically determined to be optimal for our whole-sediment analyses is very close to the Curie point pyrolysis temperature (610 °C) used in a previous study[4] of sapropel kerogens but somewhat below the microwave pyrolysis temperature (650 °C) used in a whole-sample study of a petroleum source rock.[17]

Pyrolysis products were transferred into the GC injection port through a heated interface. It is important to note that the valve releasing the pyrolysis products into the GC inlet was manually controlled, which introduced slight differences in GC retention times from sample to sample. An RTX-1 column (Restek Corporation, Bellefonte,PA)

was used in the first dimension (30 m, 0.25 mm i.d., 0.1 µm film) and an RTX-Wax column (Restek Corporation, Bellefonte, PA) in the second dimension (2 m, 0.10 mm i.d., 0.1 µm film). The temperature of the first dimension column oven was initially 40 ºC (5 min hold) and was increased by 4 ºC min^{-1} to 200 ºC (20 min hold). The second dimension column was housed in an oven that had a 5 ºC offset from the main oven, and the modulator had a 30 ºC offset. The ToFMS was operated at 70 eV with a mass range of m/z 35-350 with spectra collected at 100 Hz. The modulation period used was 4 seconds. Instrument control and data processing were performed using ChromaTOF software version 4.22 (Leco Corporation). Data were processed with a signal/noise (S/N) ratio of 75 and 25, a baseline offset of 0.5, and automatic smoothing. Peak identification was done by automated comparison with the National Institute of Standards and Technology (NIST) 02 spectral library, augmented with literature references.[4, 8, 9, 23]

Results and discussion

Column Selection and Chromatographic Conditions

An RTX-Wax column was chosen for the second dimension because it is orthogonal to the non-polar RTX-1 used in the primary dimension and was readily available at the time of the experiment. As can be seen in Figure 4.5A, temperature limits of the polar column caused some chromatographic issues. The upper limit of 250 ˚C (~C_{22}) for the RTX-Wax column forced an isothermal hold at the end of the chromatographic run in order to elute as many higher boiling components as possible. This constraint causes an increase in second dimension retention times due to the high capacity factor (*k*) of these components. In addition, this limitation could possibly have led to analytes not completing elution during the modulation cycle in which they were

injected and eluting instead in the next modulation cycle, also known as chromatographic wrap-around. However, as the components are resolved in our chromatograms, this behavior was not problematic and simply needs to be recognized as a potential issue in future studies. In fact, one could argue that allowing for some wrap-around is an effective use of the chromatographic space rather than leaving two seconds empty in the second dimension.

Peak tailing in the first dimension is also very apparent in peaks such as benzene and toluene (Figure 4.5A). This behavior is likely due to large amounts of these components being present in some samples and thus overloading the first dimension and not experiencing an isothermal separation in the second dimension. As the temperature of the second dimension changes, the temperature that the tail of the peak is experiencing changes, thus decreasing the *k* value and causing the peak to tail downwards rather than elute as a single wide peak.

Results of whole sediment pyrolysis comprehensive two-dimensional gas chromatography time-of-flight mass spectrometry (Py-GC × GC-ToFMS) analyses

Representative GC × GC total ion chromatograms of an OM-rich (TOC 3.85 %) interval (119-120 cm) and an OM-poor (TOC 0.1 %) interval (95-97 cm) are shown in Figures 4.5A and 4.6A, respectively. Differences exist between the pyrolysates of the bulk OM present in the sapropel layer and in the sediment 22 cm above it and are most obvious when comparing the expanded specific mass chromatograms shown in Figures 4.5B through 4.5I and 4.6B through 4.6I. We discuss some of the details of the results of our whole sediment pyrolytic analyses below.

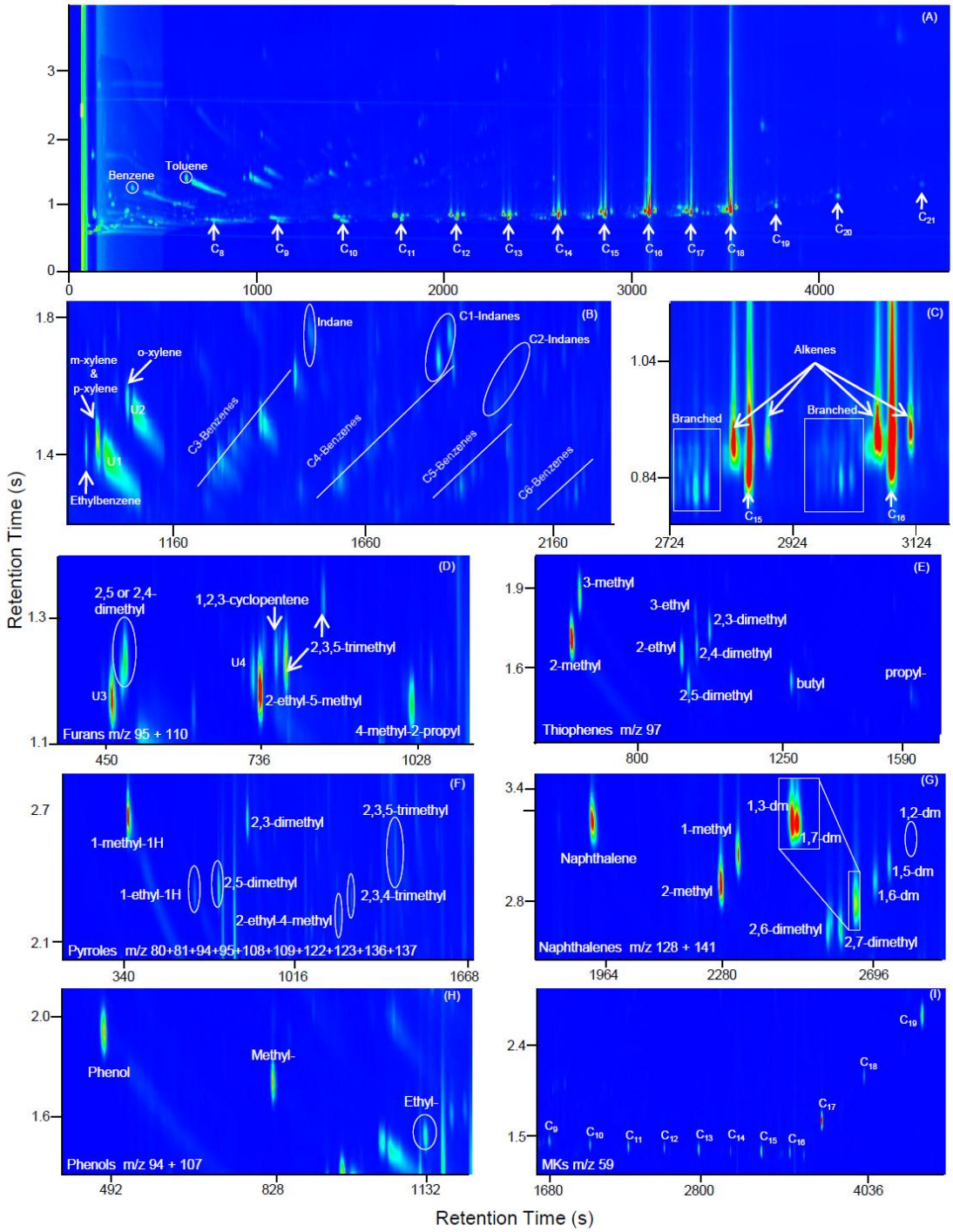

Figure 4.5 GC × GC total ion chromatogram (TIC) of sapropel interval 119-120 cm (A). Expanded regions of interval 119-120 cm: benzene region (B), representative alkene region (C), furan region (D), thiophene region (E), pyrroles (F), naphthalenes (G), phenol region (H), and methyl ketones (MKs) (I). All traces are TIC unless otherwise indicated.

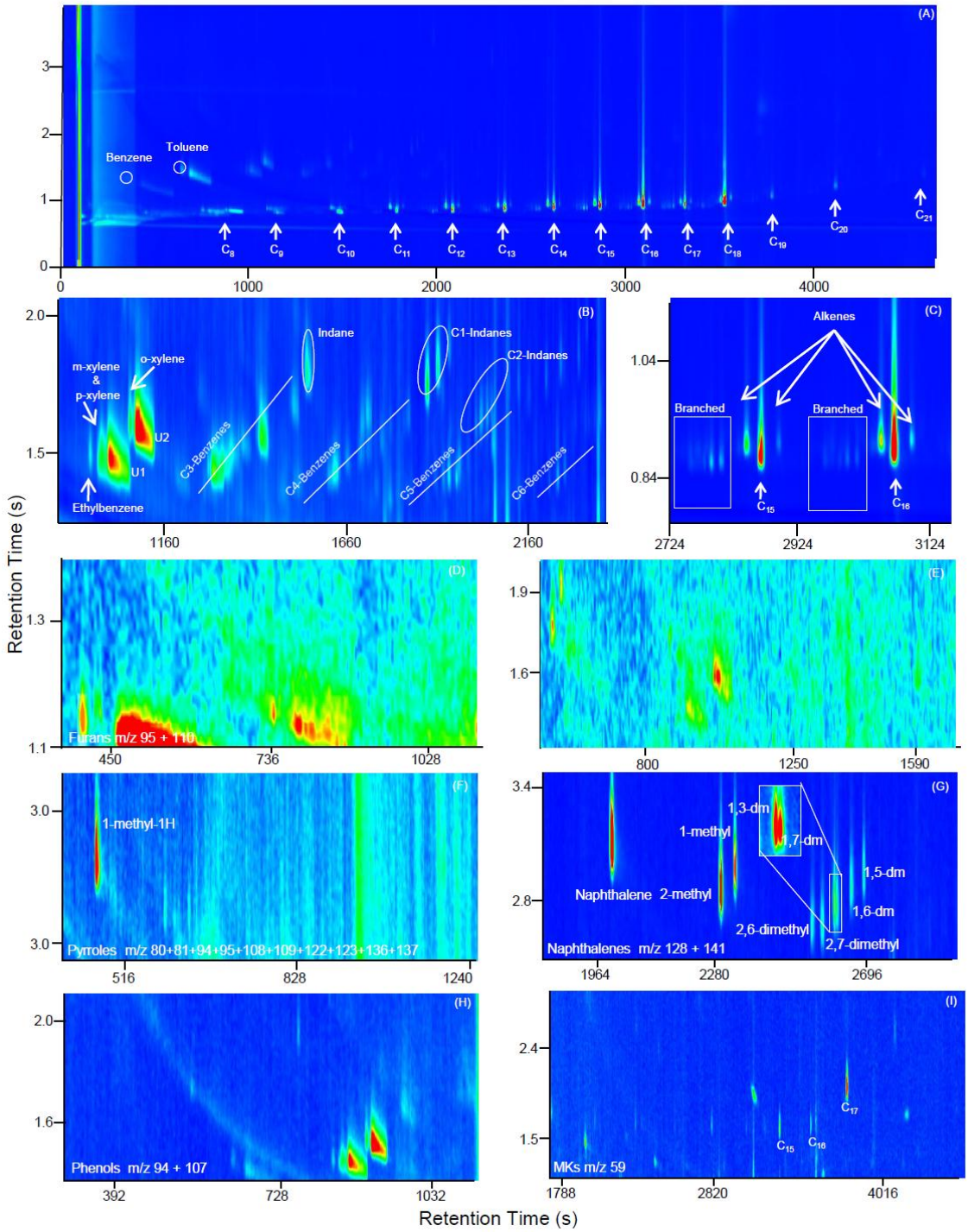

Figure 4.6 GC × GC total ion chromatogram (TIC) of non-sapropel interval 112-113 cm. Expanded regions of interval 112-113 cm: benzene region (B), representative alkene region (C), furan region (D), thiophene region (E), pyrroles (F), naphthalenes (G), phenol region (H), and methyl ketones (MKs) (I). All traces are TIC unless otherwise indicated.

Alkanes and alkenes

Straight chain alkanes were identified in all the two-dimensional chromatograms, as represented by Figures 4.5A and 4.6A. They range from C_8 to C_{21}, similar to the range observed previously[4] in a pyrolytic study of three Pliocene sapropels. The average chain length $(ACL)_{9\text{-}21}$[4] of our Tyrrhenian Basin sapropel pyrolysates are 15.5, 15.7, and 15.7 for intervals 117-118 cm, 119-120 cm, and 123-124 cm, respectively (Table 4.1). The $ACL_{9\text{-}21}$ values of the marl samples, which are 15.5, 15.2, and 12.4 for intervals 95-97 cm, 112-113 cm, and 125-126 cm, see Table 4.1, are similar to those found in the sapropels, although slightly lower on average. In contrast to our results, Menzel et al. observed that sapropel ACL values were larger than those of TOC-poor marls in the pyrolysates of Pliocene sequences from the eastern Mediterranean.[4] We believe that this difference in results is likely to represent real differences between the sapropel depositional conditions in the Pleistocene Tyrrhenian Basin and the Pliocene eastern Mediterranean Sea. Although we cannot give a specific explanation of the nature of the depositional differences, we speculate that slower ventilation of the deep Mediterranean during the Pliocene than in the middle Pleistocene[24] may have limited oxidation of marine OM in the Pliocene sapropels and contributed to the contrasts in the ACL patterns via somewhat better preservation of their OM.

Eluting just prior to the *n*-alkanes, *n*-alk-1-monoenes with the same chain lengths occur, as shown in Figures 4.5C and 4.6C, while *n*-alk-monoenes with a non-terminal double bond elute after the corresponding *n*-alkanes. $ACL_{9\text{-}20}$ values of the alk-1-enes are 14.0, 16.1, 15.3, 15.2, 14.4 and 15.4 for intervals 95-97 cm, 112-113 cm, 119-120 cm, 123-124 cm, and 125-126 cm, respectively. It should be noted however that the ACL

values for Intervals 95-97 cm and 112-113 cm are over the carbon ranges of 10-20 and 11-20, respectively, due to a lack of detectable C_9 and C_{10} alk-1-enes in these samples. In addition, C_{13} and C_{15} alk-1-enes were identified only in interval 117-118 cm after the sample was processed at a signal/noise ratio of 25.

The short chain *n*-alkanes and *n*-alk-1-enes in the pyrolysates have been postulated to derive from the algaenan in the cell walls of several classes of the marine algae that contributed OM to Pliocene sapropels.[4] The greater abundance of even-chain *n*-alkanes and *n*-alkenes than their odd-chain analogs in both the sapropels and the marls (Figs. 4.5 and 4.6) is similar to previous results[4] and may well derive from pyrolysis of algal organic matter. Further, the relatively small ACL values in pyrolysates of the Pleistocene Site 974 sequence may indeed suggest that both the sapropels and the marls contain large proportions of algal-derived OM, an interpretation that is supported by greater contributions of *n*-alkanes and *n*-alk-1-enes in the sapropel samples relative to the marls (Table 4.2). However, our use of the RTX-Wax column limited our analysis to *n*-alkanes < C_{22}, so we were not able to assess contributions of land-plant waxes to this sapropel sequence.

Two isomers of alk-2-enes were detected in most of the samples (Table 4.3). One isomer is clear in both Figures 4.5C and 4.6C, eluting just after the alkane peak in the first dimension. The second one, however, is more difficult to identify because it essentially coelutes with alkanes at these retention times. However, when looking specifically at the C_{10} through C_{13} regions in Figure 4.5, one can easily identify four peaks, three across the top (alk-1-ene, alk-2-ene, alk-2-ene) and one below the center

Table 4.2 Alkanes (x) and branched alkanes (α) identified in the respective intervals. ND = not detected. At least one isomer of branched alkanes was identified where indicated by (α).

	95-97 cm TOC 0.10 %		112-113 cm TOC 0.16 %		117-118 cm TOC 2.51 %		119-120 cm TOC 3.85 %		123-124 cm TOC 2.33 %		125-126 cm TOC 0.76 %	
	Alkane	**Branched**	**Alkane**	**Branched**	**Alkane**	**Branched**	**Alkane**	**Branched**	**Alkane**	**Branched**	**Alkane**	**Branched**
C_8	X	ND	X	ND	X	α	X	α	X	ND	X	ND
C_9	X	ND	X	ND	X	α	X	ND	X	ND	X	ND
C_{10}	X	ND	X	ND	X	α	X	α	X	ND	X	ND
C_{11}	X	α	X	ND	X	α	X	α	X	α	X	ND
C_{12}	X	α	X	ND	X	α	X	α	X	α	X	α
C_{13}	X	α	X	ND	X	α	X	α	X	α	X	α
C_{14}	X	α	X	ND	X	α	X	α	X	α	X	α
C_{15}	X	α	X	α	X	α	X	α	X	α	X	α
C_{16}	X	α	X	ND	X	α	X	α	X	α	X	α
C_{17}	X	α	X	ND	X	α	X	α	X	α	X	α
C_{18}	X	α	X	ND	X	α	X	α	X	α	X	ND
C_{19}	X	ND	X	ND	X	ND	X	α	X	ND	X	ND
C_{20}	X	ND	X	ND	X	ND	X	ND	X	ND	X	ND
C_{21}	X	ND	X	ND	ND	ND	X	ND	ND	ND	ND	ND

Table 4.3 Alk-1-enes and alk-2-enes identified in respective intervals. ~~X~~ indicates a visible peak but the absence of a software peak marker. ND = not detected

	95-97 cm TOC 0.10 %		112-113 cm TOC 0.16 %		117-118 cm TOC 2.51 %		119-120 cm TOC 3.85 %		123-124 cm TOC 2.33 %		125-126 cm TOC 0.76 %	
	Alk-1-ene	**Alk-2-ene**	**Alk-1-ene**	**Alk-2-ene**	**Alk-1-ene**	**Alk-2-ene**	**Alk-1-ene**	**Alk-2-ene**	**Alk-1-ene**	**Alk-2-ene**	**Alk-1-ene**	**Alk-2-ene**
C_9	ND	ND	ND	ND	X	ND	X	X	X	X	X	ND
C_{10}	X	ND	ND	~~X~~	X	X	X	~~XX~~	X	XX	X	XX
C_{11}	X	~~X~~	X	X	X	XX	X	~~XX~~	X	XX	X	XX
C_{12}	X	~~X~~	X	X	X	XX	X	XX	X	XX	X	XX
C_{13}	X	~~X~~	X	~~X~~	X*	~~X~~X	X	~~X~~X	X	XX	X	XX
C_{14}	X	X	X	~~X~~X	X	xx	X	XX	X	XX	X	XX
C_{15}	X	X	X	~~X~~	X*	~~X~~X	X	XX	X	XX	X	XX
C_{16}	X	X	X	~~X~~	X	XX	X	XX	X	XX	X	XX
C_{17}	X	X	X	~~X~~	X	XX	X	XX	X	XX	X	XX
C_{18}	X	X	X	~~X~~	X	~~X~~X	X	XX	X	XX	X	XX
C_{19}	X	ND	X	ND	X	~~X~~	X	~~X~~	X	ND	X	X
C_{20}	X	ND	X	ND	X	ND	X	ND	X	ND	X	ND

* Needed to be reprocessed with a S/N = 25 in order to get peak markers

peak, the alkane. In a number of instances, as indicated by the data in Table 4.3, the peaks were visible but were not identified by the software.

Furans and thiophenes

Sapropel intervals 117-118 cm, 119-120 cm, and 123-124 cm yielded 2,5 or 2,4-dimethyl (not in 123-124 cm), 2-ethyl-5-methyl, 2,3,5-trimethyl, and 4-methyl-2-propyl furans (Table 4.4). Figure 4.5E also has two unknown peaks (U3 and U4) as well as a peak identified by the software as 1,2,3-cyclopentene. Although it is not clear what U4 is, U3 is very likely an isomer of dimethlyfuran that was not identified as a peak by the software, possibly because of a low S/N ratio. The 1,2,3-cyclopentene peak is likely a rearrangement product as no real precursors for this peak are known. It has been proposed that furans are produced by pyrolysis of carbohydrates and that their presence indicates better preservation of labile OM in sapropels than in TOC-poor marls.[25] The absence of a large variety of these compounds in our marl sequence (Figure 4.6D and Table 4.4) is consistent with previous interpretation.[25]

Methyl, ethyl, dimethyl, butyl, and propyl thiophenes were identified in all of the pyrolysis samples, with the exception of intervals 95-97 cm and 125-126 cm (Table 4.4). These compounds appear as the m/z 97 traces in Figures 4.5E and 4.6E and, like the furans, are thought to be carbohydrate pyrolysis products.[25] However, they are formed by incorporation of S^{2-} into their carbohydrate precursors and therefore reflect existence of euxinic conditions at the sea floor or within the upper sediment during sapropel deposition.[26] Such conditions are likely to improve organic matter preservation by a combination of stabilization of reactive forms of organic matter via sulfurization and absence of molecular oxygen that would otherwise allow infaunal grazing on the OM.

Table 4.4 Furans, thipohenes, and pyrroles, identified in respective intervals. ND = not detected, X = detected. TOC is in percent.

	95-97 cm TOC 0.10	112-113 cm TOC 0.16	117-118 cm TOC 2.51	119-120 cm TOC 3.85	123-124 cm TOC 2.33	125-126 cm TOC 0.76
Furans						
2,5 or 2,4-dimethyl	ND	ND	X	X	ND	ND
2-ethyl-5-methyl	ND	ND	X	X	X	ND
2,3,5-trimethyl	ND	ND	X	X	X	ND
4-methyl-2-propyl	ND	ND	X	X	X	ND
Thiophenes						
2-methyl	ND	X	X	X	X	ND
3-methyl	ND	X	X	X	X	ND
2-ethyl	ND	X	X	X	X	ND
3-ethyl	ND	X	X	X	X	ND
2,5-dimethyl	ND	X	X	X	X	ND
2,4-dimethyl	ND	X	X	X	X	ND
2,3-dimethyl	ND	X	X	X	X	ND
butyl	ND	X	X	X	X	ND
propyl	ND	X	X	X	ND	ND
Pyrroles						
1-methyl-1H	X	ND	X	X	ND	ND
1-ethyl-1H	ND	ND	ND	X	X	ND
2,5-dimethyl	ND	ND	X	X	X	ND
2,3-dimethyl	ND	ND	ND	X	X	ND
2-ethyl-4-methyl	ND	ND	X	X	X	ND
2,3,4-trimethyl	ND	ND	X	X	X	ND
2,3,5-trimethyl	ND	ND	X	X	X	ND

The existence of both furans and thiophenes in the pyrolysis products is evidence of improved organic matter preservation.

Pyrroles

A suite of pyrroles, consisting of 1-methyl, 2 and 3-ethyl, 2,5-dimethyl, 2,4-dimethyl, 2,3-dimethyl, 2,3,4-trimethyl, and 2,3,5-trimethyl was found in the three sapropel samples but not in the marl samples (see Figures 4.5F and 4.6F and Table 4.4). Previous results similarly report pyrroles in the pyrolysates of Pliocene sapropel samples

from three locations in the eastern Mediterranean and not in the surrounding marl.[4] It has been proposed that these alkyl pyrroles are likely derived from tetrapyrrole pigments such as chlorophyll.[25] The relatively labile nature of tetrapyrrole pigments argues against their delivery from continental sources.[4] Instead, the common presence of these chlorophyll derivatives in both the Pleistocene (1 Mya) and Pliocene (3 Mya) sapropels from four different locations suggests that heightened production and improved preservation of marine OM were typically linked during times of sapropel deposition.

Alkyl aromatics

Alkyl aromatics in pyrolysates can have many precursors from the mix of material that can constitute kerogen.[27] We found benzene, toluene, indane, methyl and dimethylindanes, naphthalenes, and methylated and alkylated benzenes in all of the pyrolysates of the Hole 974C sequence (Tables 4.5 & 4.6). Toluene has been reported as a pyrolysis product of humic acids.[26] It is likely present in both the sapropel and marl samples because humic acids from both terrigenous and marine sources produce toluene when pyrolyzed.[26]

Table 4.5 Naphthalenes and phenols identified in respective intervals. ND = not detected, X = detected

	95-97 cm TOC 0.10 %	112-113 cm TOC 0.16 %	117-118 cm TOC 2.51 %	119-120 cm TOC 3.85 %	123-124 cm TOC 2.33 %	125-126 cm TOC 0.76 %
Naphthalenes						
naphthalene	X	X	X	X	X	X
2-methyl	X	X	X	X	X	X
1-methyl	X	X	X	X	X	X
2,6-dimethyl	X	X	X	X	X	X
2,7-dimethyl	X	X	X	X	X	X
1,3-dimethyl	X	X	X	X	X	X
1,7-dimethyl	X	X	X	X	X	X
1,6-dimethyl	X	X	X	X	X	X
1,5-dimethyl	X	X	X	X	X	X
1,2-dimethyl	ND	ND	ND	X	X	X
Phenols						
phenol	ND	ND	X	X	X	ND
methyl	ND	ND	X	X	X	ND
ethyl	ND	ND	X	ND	X	ND

Table 4.6 Benzene and indane isomers identified in respective intervals. ND = not detected, X = detected. TOC is in percent.

	95-97 cm TOC 0.10	112-113 cm TOC 0.16	117-118 cm TOC 2.51	119-120 cm TOC 3.85	123-124 cm TOC 2.33	125-126 cm TOC 0.76
Benzene	X	X	X	X	X	X
Toluene	X	X	X	X	X	X
Ethyl benzene	X	X	X	X	X	X
m-xylene + p-xylene	X	X	X	X	X	X
o-xylene	X	X	X	X	X	X
Sub. Benzenes						
isopropyl	ND	ND	ND	X	X	ND
propyl	X	X	X	X	X	X
1-ethyl-3-methyl	X	ND	X	X	X	X
1-ethyl-4-methyl	ND	X	X	X	X	ND
1,3,5-trimethyl	X	ND	X	X	X	X
1-ethyl-2-methyl	ND	X	X	X	X	X
1,2,4-trimethyl	X	X	X	X	X	X
1,2,3-trimethyl	ND	X	X	X	X	X
butyl	X	X	X	X	X	X
1-methyl-2-propyl	X	X	X	X	X	X
1-ethyl-2,4-dimethyl-	X	ND	X	X	X	X
2-ethyl-1,4-dimethyl-	X	ND	ND	X	X	ND
1,2,4,5-tetramethyl	ND	X	X	X	X	X
1,2,3,4-tetramethyl	ND	ND	X	X	X	X
pentyl	X	X	X	X	X	X
1-methyl-4-(2-methylpropyl)-	X	X	X	X	X	X
hexylbenzene	X	X	X	X	X	X
Indanes						
Indane	X	X	X	X	X	X
methyl	X	ND	X	X	X	ND
dimtheyl	X	X	X	X	X	ND
dimethyl	X	ND	X	X	ND	ND

Methyl and dimethyl naphthalenes were also found in the six pyrolysates (Table 4.5). A typical distribution is highlighted at m/z 128 +141 in Figures 4.5G and 4.6G. The presence of naphthalenes may be evidence of Type II kerogen and is likely formed in marine settings with a major source consisting of autochthonous OM from phytoplankton with smaller contributions of allochthonous higher plant matter.[28] Indane,

methylindane, and dimethylindane were identified in both the sapropel and the marl samples, as shown in Figures 4.5B and 4.6B.

Ethylbenzene, meta, para and ortho-xylene were also identified in all of the samples, see Figures 4.5B and 4.6B. Interestingly, as can be seen in Figure 4.5B and slightly less so in 4.6B, in all instances there were additional peaks immediately following the main xylene peaks in the first dimension, U1 and U2. Although these peaks appear to be quite intense, particularly in Figure 4.5B, they either do not contain peak markers or are identified as xylenes. It is thought that peaks U1 and U2 are merely peak tails of the xylene components, however, it is not understood why a gap exists between the peak and the tail in a number of chromatograms.

The alkylated benzene region is presented in Figures 4.5B and 4.6B. Trimethyl, tetramethyl, pentamethyl, and hexamethyl benzenes are highlighted in both figures. The trimethyl and tetramethyl benzenes are more prevalent than the pentyl and hexyl methyl benzenes as indicated by the trimethyl and tetramethyl benzenes having an average peak area an order of magnitude greater than that of the pentyl and hexyl benzenes (data not shown). The dominance of trimethyl and tetramethyl benzenes in sapropel layers agrees with previous reports.[4, 27] The pattern is consistent with the Rock-Eval identification of Type II or Type II S kerogen in Pleistocene sapropels at Site 974 reported previously.[3] Also, as shown previously,[27] the absolute amount of alkyl benzenes obtained as flash pyrolysis products is greater from Type II and Type II S kerogen than from Type I and Type III kerogen. Moreover, the prevalence of tetramethyl benzenes (specifically 1, 2, 3, 4- and 1, 2, 3, 5-tetramethyl benzene) is a pyrolysis biomarker for kerogen-bound carotenoids, particularly isorenieratene, that are derived from green sulfur bacteria, which

are nitrogen-fixing obligate anaerobes.[27] 1,2,3,4-tetramethyl benzene is found in the three sapropel samples we pyrolyzed and in the closely underlying marl sample, but not in the overlying marl samples (Table 4.6). The presence of this postulated derivative of isorenieratene indicates that the cycle 94 sapropel layer was created under euxinic conditions in the photic zone of the Tyrrhenian Sea, as concluded by multiple investigators for sapropel layers elsewhere in the Mediterranean basin.

Phenols

Phenol, methyl phenol, and ethyl phenol were identified in the sapropel intervals 117-118 cm, 119-120 cm and 123-124 cm, see Figure 4.5H. In Figure 4.6H (non-sapropel interval 95-97 cm), it can be seen that the phenols are missing, which was also the case for the intervals 112-113 cm and 125-126 cm. The peaks that are visible in Figure 4.6H are the xylenes and the associated tails discussed previously and labeled in Figure 4.6B.

Methyl Ketones

Methyl ketones C_9 through C_{19} were identified in all of the pyrolysates (Table 4.7) with the exception of interval 95-97 cm. It should be noted, however, that although the peaks are identified in interval 112-113 cm the S/N was notably lower for this sample compared to the others (S/N ~40 compared to S/N >75). Interval 112-113 cm had to be reprocessed in ChromaTOF with S/N threshold of 25 in order to obtain identification of the methyl ketones.

Methyl ketones have been reported in a number of marine sedimentary settings [4, 29, 30] yet their origin remains enigmatic. Because their molecular distributions are usually dominated by odd-chain-length components, they have been postulated to be the products

Table 4.7 Methyl ketones identified in respective sapropel samples. ND = not detected, X indicates that a peak was identified by the software

	95-97 cm TOC 0.10 %	112-113 cm TOC 0.16 %	117-118 cm TOC 2.51 %	119-120 cm TOC 3.85 %	123-124 cm TOC 2.33 %	125-126 cm TOC 0.76 %
C_9	ND	x	x	x	x	x
C_{10}	ND	x	x	x	x	x
C_{11}	ND	x	x	x	x	x
C_{12}	ND	x	x	x	x	x
C_{13}	ND	x	x	x	x	x
C_{14}	ND	x	x	x	x	x
C_{15}	x	x	x	x	x	x
C_{16}	x	x	x	x	x	x
C_{17}	x	x	x	x	x	x
C_{18}	ND	x	x	x	x	x
C_{19}	ND	x	x	x	x	x

either of microbial oxidation of odd-chain-length *n*-alkanes[29] or of microbial decarboxylation of even-chain-length *n*-alkanoic acids.[30] Because of their common presence in the pyrolysates of the Site 974 samples, we conclude that these molecular fragments likely represent the straight carbon chains of biolipids that have survived since these sediments were deposited 1 Mya. The $ACL_{9\text{-}19}$ values of both the sapropels (15.9 mean) are slightly larger than those of the marls (15.5), which neither value is significantly different from the ACL values of the *n*-alkanes or the *n*-alkenes (Table 4.1).

Potential Benefits of Py-GC × GC-ToFMS

The often mentioned benefits of GC × GC are increased peak capacity, increased detectability, and structured chromatograms. The benefit of peak capacity is the most obvious in extremely complex samples such as diesel oil[11] where thousands of peaks can be identified and most would not be resolved without the extra chromatographic space provided. This extra space is also beneficial in the less complex samples described here, however. For example, in a number of cases the alk-2-ene peak that would have co-eluted

with the corresponding alkane peaks is easily identified as a separate analyte even without the use of mass spectral deconvolution. In addition, analytes eluting later in the second dimension, such as the naphthalenes, do not co-elute with the substituted benzenes or the alkane/alkenes with similar first dimension retention times.

Structured chromatograms were beneficial in the identification of peaks in the sapropel samples. The structure obtained from GC × GC can be seen clearly in Figures 4.5 and 4.6 where similar compounds such as the C_3 through C_6-benzenes elute as a group along the x-axis and the isomers of each carbon number elute as separate groups along the y-axis. The increased detectability is demonstrated by the methyl ketones and the alkenes, where peaks were only identified by the software after reprocessing with a S/N threshold of 25. The reprocessing capability indicates that these peaks are only present in trace amounts and may have gone undetected in one-dimensional gas chromatographic analysis. It is estimated that a 30-fold increase in sensitivity can be expected in GC × GC[31] and with further optimization it is likely that this technique could be used to successfully identify previously undetected analytes in sapropels and other geological samples.

A benefit of pyrolysis is that it releases organic fragments that have been incorporated into macromolecular organic matter and possibly also the mineral matrix of sediments. This benefit is, of course, tempered by the likelihood that the molecular constitution of the original material has been altered first by diagenesis and again by pyrolysis. Nonetheless, useful information about the origin and alteration of the organic constituents can be inferred from the pyrolysis products.

Conclusions

Our evaluation of GC × GC-ToFMS analysis of the molecular fragments released by pyrolysis of whole sediment samples of a middle Pleistocene sapropel sequence shows that this analytical approach can yield important information about the delivery and preservation of OM during sapropel deposition. In agreement with previous work and indicative of a wetter climate and a stratified and more productive water column, we found evidence of elevated marine productivity during the deposition of the sapropel layer as suggested by the presence of alkyl pyrroles in the sapropel pyrolysates but not in those of the marls. These compounds are considered the pyrolysis products of tetrapyrrole pigments like chlorophyll, which are unlikely to survive transport from land sources and are thus produced locally in the surface ocean. Improved preservation of marine OM under conditions of diminished oceanic circulation is indicated by higher abundances of shorter chain aliphatic hydrocarbons, pyrroles, furans, and alkyl aromatics in the sapropel pyrolysates than in the marls. The presence of phenols possibly derived from lignin in the sapropel pyrolysates but not in those of the marls may indicate overall improved preservation of OM in general. The more common presence of thiophenes in the pyrolysates of the sapropel samples than in those of the marls records the existence of euxinic conditions at or near the sea floor during sapropel deposition. Tetramethyl benzenes, likely derived from isorenieratene, are present in the sapropel samples but not in the marls, recording euxinic conditions within the photic zone during the period of sapropel formation.

Although a broad spectrum of products was released by pyrolysis of the OM in the whole sediment samples and a large number of the components were successfully

separated and identified using GC × GC, the original goal of detecting and identifying novel organic matter biomarkers was not fulfilled. However, paleoclimatic and paleoceanographic information was obtained for this sapropel sequence without the need for time and solvent intensive liquid extractions. This work demonstrates the first example of whole sediment pyrolysis GC × GC analysis of a sapropel sequence as well as the potential for continued use of this technique when studying other whole sediment samples.

Based on our evaluation of the GC × GC-ToFMS pyrolysis analysis of the whole sediment samples, we suggest that future similar analyses include several refinements to produce the best results. The optimal pyrolysis conditions should be identified using the experimental protocol described previously.[22] We established that 15 s at 600 ˚C were the optimal conditions for our sapropel sequence samples, but a different time at a higher or lower temperature might be more suitable for other types of whole sediment samples.

Operation of the transfer valve from the pyrolysis inlet into the first dimension GC column could be automated to obtain identical transfer times. We operated this valve manually, which introduced slight differences in GC retention times and complicated identifications of pyrolysates. Stationary phases of both the first dimension and second dimension columns should be selected to optimize analysis of the sample type and the analytes of interest. We were obligated to use an RTX-Wax for our second dimension column because of shared uses of the Pegasus system. This phase limited oven temperatures to 250 ˚C and hence constrained our analysis to pyrolysis fragments no larger than 22 carbon atoms. A higher temperature capability for the second column would have been more suitable for our sapropel sequence.

References

(1) Bouloubassi, I.; Rullkotter, J.; Meyers, P. A. *Mar. Geol.* **1999**, *153*, 177-197.
(2) Rinna, J.; Warning, B.; Meyers, P. A.; Brumsack, H. J.; Rullkotter, J. *Geochim. Cosmochim. Acta* **2002**, *66*, 1969-1986.
(3) Meyers, P. A.; Doose, H. *Proceedings, Ocean Drilling Program, Scientific Results* **1999**, *161*, 383-390.
(4) Menzel, D.; van Bergen, P. F.; Veld, H.; Brinkhuis, H.; Damste, J. S. S. *Org. Geochem.* **2005**, *36*, 1037-1053.
(5) Milder, J. C.; Montoya, J. P.; Altabet, M. A. *Proceedings, Ocean Drilling Program, Scientific Results* **1999**, *161*, 401-411.
(6) Meyers, P. A.; Bernasconi, S. M. *Mar. Geol.* **2005**, *220*, 41-58.
(7) Higgins, M. B.; Robinson, R. S.; Carter, S. J.; Pearson, A. *Earth. Planet. Sci. Lett.*, *290*, 102-107.
(8) Frysinger, G. S.; Gaines, R. B. *J. Sep. Sci.* **2001**, *24*, 87-96.
(9) Gaines, R. B.; Frysinger, G. S.; Hendrick-Smith, M. S.; Stuart, J. D. *Environ. Sci. Technol.* **1999**, *33*, 2106-2112.
(10) Nelson, R. K.; Kile, B. M.; Plata, D. L.; Sylva, S. P.; Xu, L.; Reddy, C. M.; Gaines, R. B.; Frysinger, G. S.; Reichenbach, S. E. *Environmental Forensics* **2006**, *7*, 33-44.
(11) Wang, F. C. Y.; Robbins, W. K.; Greaney, M. A. *J. Sep. Sci.* **2004**, *27*, 468-472.
(12) Ávila, B. M. F.; Aguiar, A.; Gomes, A. O.; Azevedo, D. A. *Org. Geochem.*, *41*, 863-866.
(13) Pomerantz, A. E.; Ventura, G. T.; McKenna, A. M.; Canas, J. A.; Auman, J.; Koerner, K.; Curry, D.; Nelson, R. K.; Reddy, C. M.; Rodgers, R. P.; Marshall, A. G.; Peters, K. E.; Mullins, O. C. *Org. Geochem.*, *41*, 812-821.
(14) Ventura, G. T.; Raghuraman, B.; Nelson, R. K.; Mullins, O. C.; Reddy, C. M. *Org. Geochem.*, *41*, 1026-1035.
(15) Ventura, G. T.; Kenig, F.; Reddy, C. M.; Frysinger, G. S.; Nelson, R. K.; Van Mooy, B.; Gaines, R. B. *Org. Geochem.* **2008**, *39*, 846-867.
(16) McGuigan, M. Dissertatioin, University of Michigan, Ann Arbor, MI, 2005.
(17) Wang, F. C. Y.; Walters, C. C. *Anal. Chem.* **2007**, *79*, 5642-5650.
(18) Cramp, A.; O'Sullivan, G. *Mar. Geol.* **1999**, *153*, 11-28.
(19) Emeis, K. C.; Sakamoto, T.; Wehausen, R.; Brumsack, H. J. *Palaeogeography Palaeoclimatology Palaeoecology* **2000**, *158*, 371-395.
(20) Comas, M. C.; Zahn, R.; Klaus, A.; Aubourg, C.; Belanger, P. E.; Bernasconi, S. M.; Cornell, W.; de Kaenel, E. P.; de Larouziere, F. D.; Doglioni, C.; Doose, H.; Fukusawa, H.; Hobart, M.; Iaccarino, S. M.; Ippach, P.; Marsaglia, K.; Meyers, P.; Murat, A.; O'Sullivan, G. M.; Platt, J. P.; Prasad, M.; Siesser, W. G.; Skilbeck, C. G.; Soto, J. I.; Tandon, K.; Torii, M.; Tribble, J. S.; Wilkens, R. H.; Riegel, R. N. *Annotation: Individual papers are cited separately* **1996**, *161*, 1023.
(21) Laskar, J.; Joutel, F.; Boudin, F. *Astron. Astrophys.* **1993**, *270*, 522-533.
(22) McGuigan, M.; Waite, J. H.; Imanaka, H.; Sacks, R. D. *J. Chromatogr. A* **2006**, *1132*, 280-288.
(23) Budzinski, H.; Raymond, N.; Nadalig, T.; Gilewicz, M.; Garrigues, P.; Bertrand, J. C.; Caumette, P. *Org. Geochem.* **1998**, *28*, 337-348.

(24) Gallego-Torres, D.; Martinez-Ruiz, F.; Meyers, P. A.; Paytan, A.; Jimenez-Espejo, F. J.; Ortega-Huertas, M. *Biogeosciences* **2010**, *In Press*.
(25) Sinninghe Damste, J. S.; Kok, M. D.; Koster, J.; Schouten, S. *Earth. Planet. Sci. Lett.* **1998**, *164*, 7-13.
(26) Dick, C.; Ediger, V.; Fabbri, D.; Gaines, A. F.; Love, G. D.; McGinn, A.; McRae, C.; Murray, I. P.; Nicol, B. J.; Snape, C. E. *Fuel* **2002**, *81*, 431-448.
(27) Hartgers, W. A.; Damste, J. S. S.; Deleeuw, J. W. *Geochim. Cosmochim. Acta* **1994**, *58*, 1759-1775.
(28) Killops, S.; Killops, V. *Introduction to Organic Geochemistry*, 2nd ed.; Blackwell Publishing: Malden, MA, 2005.
(29) Simoneit, R. T.; Mazurek, M. A.; Brenner, S.; Crisp, P. T.; Kaplan, I. R. *Deep-Sea Research* **1979**, *26*, 879-892.
(30) Volkman, J. K.; Farrington, J. W.; Gagosian, R. B.; Wakeham, S. G. *Lipid composition of coastal marine sediments from the Peru upwelling region.*; Wiley: New York, 1983.
(31) Marriott, P.; Shellie, R. *Trac-Trends in Analytical Chemistry* **2002**, *21*, 573-583.

Chapter 5

SUMMARY AND FUTURE WORK

Summary

A metabolite profiling and a metabolomics method utilizing comprehensive two-dimensional gas chromatography time-of-flight mass spectrometry (GC × GC-ToFMS) was developed and applied to INS-1 cells, an insulin-secreting cell line commonly used as a model in diabetes studies. Twenty seven target metabolites were identified at low, moderate and high glucose concentrations with an average technical relative standard deviation (RSD) of 18, 17 and 14 % and biological RSDs of 27, 24 and 20 % for 3 mM, 7 mM and 17 mM glucose respectively. Thirty two metabolic pathways were identified in the metabolomic analysis, nine of which are discussed in relation to a previous or a potential relevance to glucose stimulated insulin release, β-cell dysfunction or diabetes. This work demonstrates the utility of this technique for both targeted and global metabolic analysis as well as identifies potential target analytes and pathways for future experiments.

A GC × GC-ToFMS method was also developed for the determination of total fatty acids in cultured mammalian cells. Like the previous metabolomic profiling and metabolomic study, this method was applied to INS-1 cells. In this method, lipids were extracted and transformed to fatty acid methyl esters for analysis. GC × GC analysis revealed the presence of 30 identifiable fatty acids in the extract. This result doubles the number of fatty acids previously identified in these cells.[1, 2] The method yielded linear

calibrations and an average relative standard deviation of 8.4 % for replicate injections of samples and 12.4 % for replicate analysis of different samples. The method was used to demonstrate changes in fatty acid content as a function of glucose concentration on the cells. The results demonstrated the utility of this method for analysis of fatty acids in mammalian cell cultures.

Evaluation of the use of GC × GC-ToFMS to analyze the pyrolysis products of six whole sediment samples obtained from above, within, and below a 1 million year old organic matter (OM) rich Mediterranean sapropel layer was performed. Analysis of whole sediment samples can avoid analytical bias that might result from isolation of OM components from the sediment matrix. Although the temperature limit of the second GC column used constrained the analyses to pyrolysis products containing <22 carbon atoms, differences were found between the OM-rich sapropel samples and the OM-poor background marls. The presence of alkyl pyrroles, which are probably derived from chlorophyll, in pyrolysates of the sapropels but not in those of the marls indicates higher marine productivity and greater OM preservation accompanied deposition of the sapropels. Detection of tetramethyl benzenes that are considered to be pyrolysates derived from isorenieratene in the sapropel samples is evidence that nitrogen-fixing green sulfur bacteria contributed to the high productivity. Greater abundances of shorter chain aliphatic hydrocarbons, pyrroles, furans, and alkyl aromatics in the pyrolysates of sapropel samples relative to the marls confirm better preservation of marine OM in the sapropels. In addition, the presence of larger amounts of thiophenes in the sapropels than in the marls is consistent with the existence of euxinic conditions during sapropel

deposition. The combination of whole-sediment pyrolysis and GC × GC-ToFMS is promising, but requires careful selection of pyrolysis temperature and column selection.

Future Work

Metabolite Profiling and Metabolomics Analysis

The results presented in Chapter 2, specifically the metabolomics analysis, could lead to the inception of a number of different experiments to further probe the effect of glucose on the INS-1 cell line. Given that arachidonic acid (AA) and AA metabolism are involved in a number of the pathways discussed, it would be reasonable to make AA and its metabolite analytes of interest. The experiment performed in Chapter 2 could be repeated with AA instead of glucose in order to probe the effects of this analyte on INS-1 cell metabolism. Alternatively, a variety of experiments could be performed to test the theory that AA has a positive effect on insulin secretion in β-cells. For example, after treatment with high glucose, some of the cells could be treated with AA. Alternatively, cells could be treated with palmitic acid followed by AA. In both cases, metabolite profiling and metabolomic analysis similar to that performed in Chapter 2 could be used for analysis.

INS-1 cells could also be selectively treated with specific COX and LOX inhibitors prior to glucose treatment, and a similar analysis performed. The COX and LOX inhibitors needed could be determined by performing a PCR analysis of the cells to determine which COX and LOX enzymes are expressed in the INS-1 cell line used. It has been shown previously that the enzymes expressed in human and rat islets vary slightly. Therefore, it is reasonable to assume that there is also variation in the enzymes expressed

in the INS-1 cell line.[3] Finally, through all of the experiments suggested above, prostaglandin E(2) (PGE(2)) could be a target metabolite. It has been shown previously that this analyte is detectable using GC/MS and a derivatization method similar to the one used in Chapter 2.[4]

Another pathway that would be interesting to investigate further is the butanoate metabolism pathway. Given previous results that dietary butanote improve insulin sensitivity in mice,[5] it would be interesting to simultaneously treat INS-1 cells with butanoate and glucose followed by an analysis similar to that described in Chapter 2. If the method developed in Chapter 2 could be adopted for islets studies, as is discussed below, it would also be interesting to perform a study identical to that presented in Chapter 2 using islets from mice that had and had not received dietary butanoate.

Propanoate metabolism is also a potential pathway for future interest. INS-1 cells could be incubated in propanoate prior to extraction followed by metabolite profiling and metabolomics analysis. Changes in the current set of target metabolites would be expected given that propanoate can enter the citric acid cycle via succinyl CoA. Additionally, treatment with methyl-succinate, which can cross into the mitochondria to be converted to succinyl CoA, may also be interesting. An interesting follow up experiment for either of these secretagogues would be to block the conversion of succinyl CoA, by knocking down methymalonyl CoA mutase, and repeating the initial experiment.

Analysis of Lipids

The advantages of utilizing GC × GC for lipid analysis can be further exploited for the separation of lipid classes. Lipids can be separated into cholesterol ethers, triglycerides, free fatty acids, and phospholipids through the use of thin-layer chromatography on silica gel plates.[2] Although this would require an alternative method of fatty acid methyl ester synthesis, it would also allow for analysis of redistribution between lipid classes. Additionally, the phospholipids can be further separated into phosphatidylcholines, phosphatidylethanolamines, phosphatidylinositol, and phosphatidylserines[2] allowing for even more detailed analysis of the fatty acid redistribution.

Quantifaction of FAMEs could be improved by using stable isotope labeling. Similar to previous work,[6] FAMEs synthesis, as described in Chapter 3, could be completed on plates of INS-1 cells using both methanol and deuterated methanol. A single plate at a given concentration would be synthesized with the deuterated methanol allowing it to serve as in internal standard for all of the other samples. An aliquot of the deuterated extract could then be combined with an aliquot of an unlabelled extract to create a sample that has an isotope labeled standard for every analyte. Samples could then be analyzed by GC × GC as previously described and quantification would be based on peak area ratios. Preliminary work in this area has been completed and a sample chromatogram is shown in Figure 5.1. The overall chromatography is quite similar to

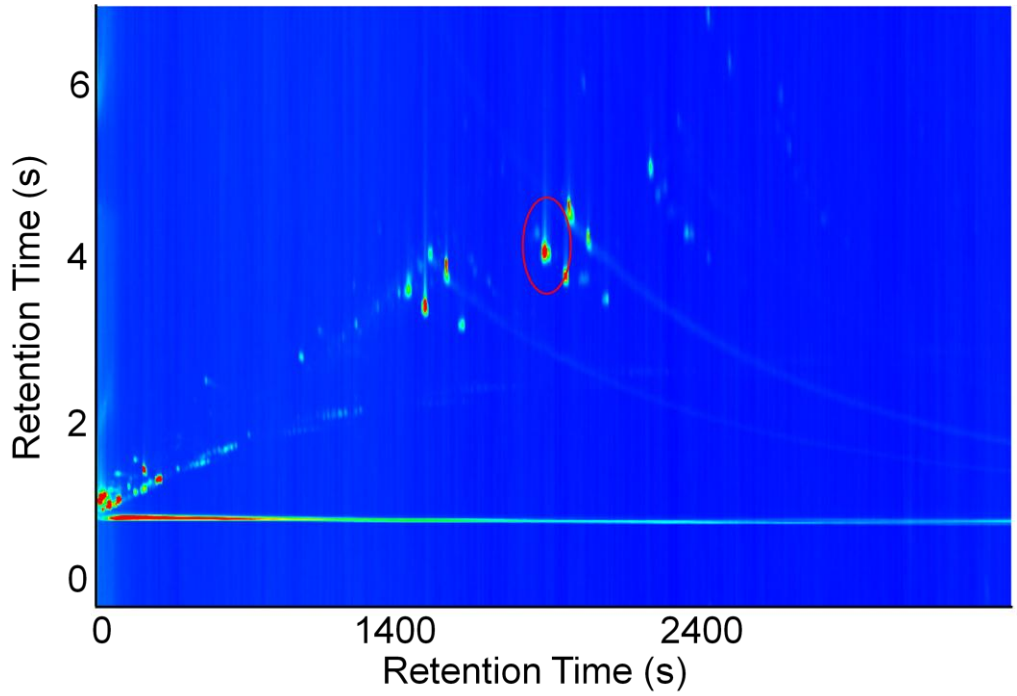

Figure 5.1 Fatty acid methyl esters in INS-1 cells combined with an isotopically labeled standard. Coelution so the C18:1 isomers is highlighted by the red circle.

what was shown previously is Chapter 3, with a few exceptions. The first is that the resolution obtained for the C18:1 isomers is completely lost with the addition of the labeled standard and the overloading causes relative standard deviations to be three times higher than those reported in Chapter 3. Additionally, if a split ratio or a dilution of the isotope labeled standard are used to try and resolve the co-elution issue, the less concentrated analytes of interest are lost. Thus, further optimization of this methodology is required.

Pancreatic β-cells

In the work presented in Chapters 2 and 3, INS-1 cells, clonal β-cells, were used for the analysis of β-cells at varying concentrations of glucose. This is a common practice in metabolomics research due to the ease of obtaining significant quantities of INS-1 cells compared to isolating islets from animals. However, some questions have been raised in

the literature about the homogeneity of clonal β-cells as well as the possibility of the metabolism being devoted primarily to cellular replication (a low frequency occurrence in postmitotic primary β-cells).[7] Thus, repetition of the experiments presented here with pancreatic islets isolated from mice would be beneficial in obtaining an improved knowledge of β-cell metabolism. The increased detectability provided by GC × GC will likely ease the number of islets required to obtain detectable amounts of metabolites. Therefore, with appropriate modification of the extraction procedures to account for isolated islets not being fixed to the cell plates, the metabolite profiling, metabolomic and fatty acid methyl ester analyses presented here could reasonably be repeated using isolated mice islets instead of clonal, INS-1, β-cells.

Sapropel Studies

The pilot study of pyrolysis GC × GC analysis of Mediterranean sapropels, presented in Chapter 4, further demonstrates the significant potential of this technique in the geochemical community. Optimization of the methods could be achieved by analyzing split ratio, column selection, and sample size. Additionally, implementation of an alternative modulation method may greatly benefit the analysis of higher molecular weight analytes. Through personal communication with the authors of a previous geochemical study[8], we were made aware of limitations of the dual stage thermal modulator used in this work. For analytes in the C30 to C40 range, the liquid nitrogen cooled nitrogen cold jets are too cold and the compounds are not sufficiently released onto the second column.

To perform modulation better suited for the higher boiling compounds present in sapropel samples, the solenoid valves that pulse the cold jets could be by-passed, and

instead a continuous cold jet flow could be run at a couple liters per minute (divided between the two jets). When the hot jets switch on, the cold flow would be blown away similar to other modulators used for GC × GC. Alternatively, the experiment could be run in two parts. First, samples would be analyzed focusing on low-boiling components using an optimized version of the chromatography presented in Chapter 4 and the current modulator conditions. A second set of identical samples could then be run focusing on the high-boiling point compounds. In this instance, the liquid nitrogen would be omitted from the modulation process, and room temperature compressed nitrogen would be used for the "cold" jet.

Environmental Implications

The recent oil spill in the Gulf of Mexico, caused by the explosion of the Deepwater Horizon drilling rig on April 20, 2010, is the largest oil spill in US history, to date. It has been estimated that 4.4 million (± 20 %) barrels of oil, the equivalent of 7.0×10^5 m^3, were released into the Gulf of Mexico.[9] The environmental implications of such a spill are severe and will continue to be observed well into the future. Analysis of contaminated sediments (both terrestrial and sea) will certainly be of interest both environmentally and geochemically for years to come. Previous GC × GC studies have evaluated the weathering of oil in previous spill locations and found the geochemical information obtained could be used to better understand biodegradation and phototransformation in the field and improve estimates of hydrocarbon concentrations in the water column.[10] Thus, the methods described previously could lead to improved assessments of wildlife exposures to hydrocarbons after oil spills.[10]

The pyrolysis GC × GC method presented in Chapter 4 could be adapted for the analysis of sediment from various underwater locations in the Gulf of Mexico. This method could further help improve the understanding of oil weathering after large scale spills. Additionally, because extraction is not necessary for pyrolysis analysis, the use of pyrolysis GC × GC could significantly increase sample throughput. With higher sample throughput a greater number of geographical locations could be targeted and analyzed without additional time requirements, further increasing the information available about the weathering and environmental effects of the Gulf Coast oil spill.

Overall Chromatographic Improvement

The recent advancement in the Leco ChromaTOF software (v. 4.30) and the Pegasus modulator, which allows for what is known as variable modulation, may also prove to be beneficial in the analysis of complex samples such as those presented in Chapters 2 and 4. Variable modulation is demonstrated in Figure 5.2, a sample chromatogram obtained from Leco Separation Science. The modulation period in Figure 5.2 is increased from 3 to 4 to 5 seconds as the analysis is completed. This technique can be a significant time saver as the second dimension separation time can be tailored for portions of the chromatogram rather than just the component that elutes last from the second dimension. An increase of resolution in the first dimension is obtained by decreasing the modulation period in regions of the chromatogram that do not contain analytes which are highly retained in the second dimension.[11] Additionally, variable modulation allows for the hot pulse time to be varied throughout the chromatographic analysis.

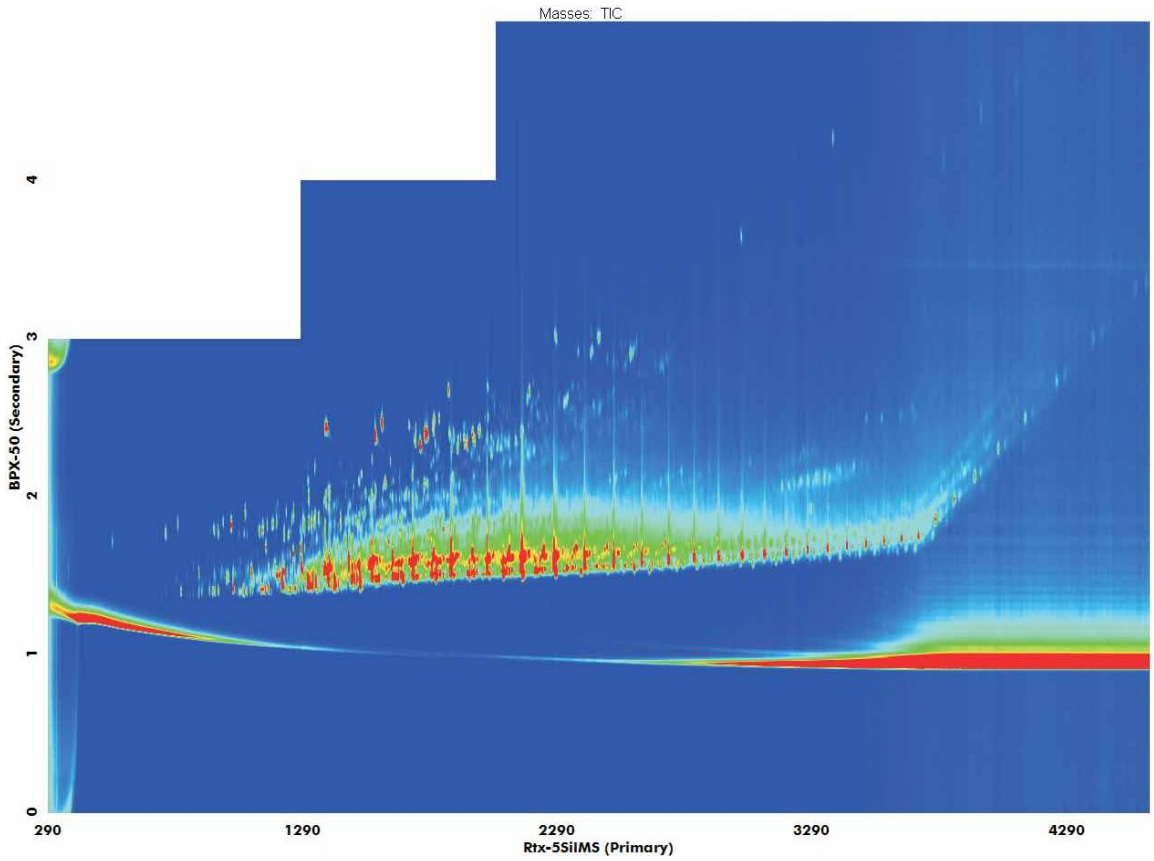

Figure 5.2 GC × GC chromatogram using variable modulation. Notched appearance of the upper left portion of the chromatogram indicates where the modulation period was increased from 3 to 4 to 5 seconds. (Chromatogram obtained from Leco Separation Science and used with permission)[11]

Prior to variable modulation, the hot pulse time was selected to provide the best overall second dimension peak shape across the chromatogram. The ability to decrease the hot pulse duration allows for increased trapping efficiency in the modulator in regions with more volatile analytes. Conversely, desorption efficiency of less volatile analytes is increased by utilizing hot pulses of increased duration.[11] These new features will allow for improved chromatography in complex samples and thus have the potential to aid in the separation and detection of novel and or significant analytes that were previously identifiable even in GC × GC.

References

(1) Martins, E. F.; Miyasaka, C. K.; Newsholme, P.; Curi, R.; Carpinelli, A. R. *Diabetes Metab.* **2004**, *30*, 21-27.

(2) MacDonald, M. J.; Dobrzyn, A.; Ntambi, J.; Stoker, S. W. *Arch. Biochem. Biophys.* **2008**, *470*, 153-162.

(3) Persaud, S. J.; Muller, D.; Belin, V. D.; Kitsou-Mylona, I.; Asare-Anane, H.; Papadimitriou, A.; Burns, C. J.; Huang, G. C.; Amiel, S. A.; Jones, P. M. *Diabetes* **2007**, *56*, 197-203.

(4) Fischer, C. *Biomed. Mass Spectrom.* **1984**, *11*, 114-117.

(5) Gao, Z. G.; Yin, J.; Zhang, J.; Ward, R. E.; Martin, R. J.; Lefevre, M.; Cefalu, W. T.; Ye, J. P. *Diabetes* **2009**, *58*, 1509-1517.

(6) Li, J.; Yue, Y.; Hu, X.; Zhong, H. *Anal. Chem.* **2009**, *81*, 5080.

(7) Fernandez, C.; Fransson, U.; Hallgard, E.; Spegel, P.; Holm, C.; Krogh, M.; Warell, K.; James, P.; Mulder, H. *J. Proteome Res.* **2008**, *7*, 400-411.

(8) Ventura, G. T.; Kenig, F.; Reddy, C. M.; Frysinger, G. S.; Nelson, R. K.; Van Mooy, B.; Gaines, R. B. *Org. Geochem.* **2008**, *39*, 846-867.

(9) Crone, T. J.; Tolstoy, M. *Science* **2010**, science.1195840.

(10) Arey, J. S.; Nelson, R. K.; Reddy, C. M. *Environ. Sci. Technol.* **2007**, *41*, 5738-5746.

(11) Leco In *Leco Applications Notes*; Leco Corporation: St. Joseph, MI, 2010.

Appendix A

List of Peaks Identified as changing by Fisher Ratio Analysis from 3 mM glucose to 7 mM glucose with KEGG identifications, direction of change, Fisher Ratios and Peak Areas

Software Identification	Fisher Ratio	Direction of Change	KEGG ID	Peak Area		
				7 mM - 3 mM	3 mM	7 mM
1,4-Butanediamine, N,N,N',N'-tetrakis(trimethylsilyl)-	1422.7	↓	C00134	-3.89E+05	2.72E+06	2.33E+06
MANNITOL TMS	15842	↑	C00392	1.60E+05	3.61E+04	1.96E+05
2-Butenedioic acid (E)-, bis(trimethylsilyl) ester	9400.7	↑	C00122	8.12E+05	2.43E+05	1.05E+06
Glutamine, tris(trimethylsilyl)-	5047.9	↑	C00064	1.40E+07	3.08E+06	1.71E+07
Malic acid, tris(trimethylsilyl) ester	3852.4	↑	C00149	1.84E+06	5.26E+05	2.37E+06
Butanoic acid, 4-[bis(trimethylsilyl)amino]-, trimethylsilyl ester	3628.6	↓	C00246	-5.03E+06	7.14E+06	2.11E+06
D-Ribofuranose, 1,2,3,5-tetrakis-O-(trimethylsilyl)-	3462.3	↑	C16639	9.07E+05	1.54E+06	2.45E+06
Erythro-Pentonic acid, 2-deoxy-3,4,5-tris-O-(trimethylsilyl)-, trimethylsilyl ester	3361.4	↑	C03826	3.32E+04	2.82E+04	6.14E+04
PHOSPHORIC ACID,O,O,O-TMS	3356.5	↓	C00009	-1.30E+07	1.61E+07	3.09E+06
2-Piperidinecarboxylic acid, tert-butyldimethylsilyl ester, (DL)-	3000.8	↑	C00408	2.97E+06	5.47E+05	3.52E+06
GALACTOSE MEOX1 TMS	2868	↑	C00124	4.15E+05	4.45E+03	4.20E+05
9-Tetradecenoic acid, trimethylsilyl ester	2542	↓	C08322	-5.03E+04	1.00E+05	4.99E+04
L-Aspartic acid, N-(trimethylsilyl)-, bis(trimethylsilyl) ester	2244.2	↓	C00049	-2.57E+06	9.05E+06	6.48E+06
Galactonic acid, 2,3,4,5,6-pentakis-O-(trimethylsilyl)-, trimethylsilyl ester	2030.3	↓	C00880	-1.37E+05	2.00E+05	6.34E+04
Pentanedioic acid, 2-(methoxyimino)-, bis(trimethylsilyl) ester	1998.1	↑	C00489	4.32E+04	1.61E+04	5.93E+04
Ribonic acid, 2,3,4,5-tetrakis-O-(trimethylsilyl)-, trimethylsilyl ester	1925.7	↑	C01685	1.78E+03	4.93E+03	6.70E+03
GLYCINE,N,N,O-TMS	1862	↑	C00037	2.06E+06	3.60E+06	5.66E+06
Benzoic acid trimethylsilyl ester	1792.1	↓	C00180	-7.09E+05	2.09E+06	1.38E+06
Palmitic Acid	1779	↓	C00249	-8.80E+05	4.21E+06	3.33E+06
Pyroglutamic acid	1748.8	↑	C02237	1.31E+05	2.95E+05	4.26E+05
Propanoic acid, 2-(methoxyimino)-, trimethylsilyl ester	1674.2	↑	C00163	1.53E+05	1.35E+05	2.88E+05
ALANINE,N,O-TMS	1640.9	↓	C00041	-2.43E+04	3.45E+04	1.02E+04
Trimethylsilyl ether of glycerol	1528.2	↑	C00116	3.57E+04	3.15E+03	3.89E+04
FRUCTOSE MEOX1 5TMS	1511.1	↓	C00095	-1.22E+05	1.43E+05	2.13E+04
Tetradecanoic acid, trimethylsilyl ester	1482.4	↓	C06424	-5.47E+04	1.85E+05	1.31E+05

RHAMNOSE MEOX2 4TMS	1472.5	↑	C00507	1.45E+04	3.10E+04	4.55E+04
XYLULOSE MEOX 4TMS	1422.9	↑	C00312	3.22E+03	3.38E+03	6.60E+03
Uridine, 2',3',5'-tris-O-(trimethylsilyl)-	1409.2	↓	C00299	-4.17E+04	9.51E+04	5.34E+04
4-AMINOBUTYRIC ACID 3TMS	1398.3	↑	C00334	1.26E+03	3.60E+04	3.73E+04
trans, trans-Farnesol, trimethylsilyl ether	1384.6	↑	C01126	1.97E+04	2.91E+04	4.88E+04
Myo-Inositol, 1,2,3,4,5,6-hexakis-O-(trimethylsilyl)-	1371.2	↓	C00137	-5.39E+05	3.21E+06	2.67E+06
Dodecanoic acid, ethyl ester	1367.2	↓	C02679	-6.28E+03	1.05E+04	4.26E+03
L-Norvaline, N-(trimethylsilyl)-, trimethylsilyl ester	1345.4	↓	C01826	-2.67E+05	3.21E+05	5.40E+04
Urea, N,N'-bis(trimethylsilyl)-	1340.8	↓	C00086	-5.05E+05	1.27E+06	7.70E+05
SUCROSE TMS	1336.5	↓	C00089	-1.54E+04	2.88E+04	1.34E+04
Tyrosine, O-trimethylsilyl-, trimethylsilyl ester	1302.2	↑	C00082	1.47E+05	7.58E+05	9.05E+05
Acetic acid, bis[(trimethylsilyl)oxyl]-, trimethylsilyl ester	1281.7	↑	C00033	8.42E+04	4.78E+04	1.32E+05
Trimethylsiloxy(trimethylsilyl)proline	1262.2	↑	C00148	2.50E+04	2.78E+04	5.28E+04
Arabinofuranose, 1,2,3,5-tetrakis-O-(trimethylsilyl)-	1261.2	↓	C06115	-1.79E+04	1.77E+05	1.59E+05
Alanine, phenyl-, trimethylsilyl ester, dl-	1248.6	↓	C00079	-3.08E+05	6.39E+05	3.31E+05
Propanoic acid, 2-[(trimethylsilyl)oxy]-, trimethylsilyl ester	1207.2	↓	C00022	-6.56E+03	1.88E+04	1.22E+04
Octanoic acid, trimethylsilyl ester	1204.2	↓	C06423	-1.09E+04	6.15E+04	5.06E+04
Sebacic acid, bis(trimethylsilyl) ester	1203	↑	C08277	3.50E+03	2.64E+03	6.14E+03
L-Cysteine, N,S-bis(trimethylsilyl)-, trimethylsilyl ester	1179.4	↓	C00097	-2.24E+04	2.32E+05	2.09E+05
ERYTHROSE MEOX1 3TMS	1177.7	↓	C01796	-3.15E+04	7.38E+04	4.24E+04
Kaur-15-ene, (5à,9à,10á)-	1174.5	↓	C06090	-4.36E+04	1.78E+05	1.35E+05
CITRIC ACID TMS	1164.7	↑	C00158	3.98E+06	0.00E+00	3.98E+06
Pentadecane	1156.2	↓	C08388	-2.50E+04	4.74E+04	2.24E+04
HYDROXYBUTANOIC ACID,O,O-TMS	1155.8	↑	C00989	9.95E+03	2.64E+04	3.64E+04
Tris(trimethylsilyl)hydroxylamine	1154.6	↑	C00192	1.21E+04	4.37E+04	5.59E+04
D-Ribose, 2,3,4-tris-O-(trimethylsilyl)-, O-methyloxime, 5-[bis(trimethylsilyl) phosphate]	1123	↓	C00117	-2.65E+04	1.07E+05	8.04E+04
Azulene, 1,2,3,4,5,6,7,8-octahydro-1,4-dimethyl-7-(1-methylethylidene)-, (1S-cis)-	1121.6	↑	C13392	5.72E+03	1.31E+04	1.88E+04
GLUCOSE MEOX2 5TMS	1118.9	↑	C00031	2.13E+06	1.68E+06	3.81E+06

DIETHANOLAMINE,N,O,O-TMS	1116.5	↓	C06772	-7.25E+03	2.99E+04	2.26E+04
ACONITIC ACID 3TMS	1115.4	↑	C00417	5.69E+03	9.07E+03	1.48E+04
ISOLEUCINE,N,O-TMS	1115.1	↑	C00407	1.76E+05	7.65E+05	9.41E+05
D-Glucuronic acid, 2,3,4,5-tetrakis-O-(trimethylsilyl)-, trimethylsilyl ester	1113.9	↑	C16245	3.57E+03	1.37E+04	1.73E+04
N,O,O-Tris(trimethylsilyl)-L-threonine	1108.4	↑	C00188	3.24E+03	1.71E+04	2.04E+04
Phenylethanolamine triTMS	1108	↓	C02735	-1.23E+04	3.51E+04	2.28E+04
9,12-Octadecadienoic acid (Z,Z)-, trimethylsilyl ester	1089.6	↑	C01595	1.07E+05	1.02E+05	2.09E+05
l-Valine, trimethylsilyl ester	1077	↓	C00183	-4.48E+04	8.25E+04	3.77E+04
TYRAMINE,N,O-TMS	1071	↑	C00483	1.47E+04	5.34E+04	6.82E+04

Appendix B

List of Peaks Identified as changing by Fisher Ratio Analysis from 3 mM glucose to 17 mM glucose with KEGG identifications, direction of change, Fisher Ratios and Peak Areas

Software Identification	Fisher Ratio	Direction of Change	KEGG ID	Peak Area		
				17 mM - 3 mM	3 mM	17 mM
2-Butenedioic acid (E)-, bis(trimethylsilyl) ester	9683	↑	C00122	1.43E+06	2.43E+05	1.67E+06
XYLOSE MEOX2 4TMS	7943.6	↑	C01394	3.70E+04	2.07E+04	5.78E+04
GALACTOSE MEOX1 TMS	5809.5	↓	C00124	-1.48E+06	1.52E+06	4.57E+04
2-Propenoic acid, 2-[(trimethylsilyl)oxy]-, anhydride with bis(trimethylsilyl) hydrogen phosphate	4148.8	↑	C00511	1.11E+04	3.45E+02	1.15E+04
MANNITOL TMS	4120.1	↑	C00392	2.92E+05	7.75E+03	3.00E+05
D-Ribofuranose, 1,2,3,5-tetrakis-O-(trimethylsilyl)-	3996.4	↑	C16639	1.09E+06	1.54E+06	2.63E+06
Glutamine, tris(trimethylsilyl)-	3920.7	↑	C00064	5.41E+06	3.63E+05	5.77E+06
Malic acid, tris(trimethylsilyl) ester	3807.2	↑	C00149	1.72E+05	6.31E+04	2.35E+05
Tyrosine, O-trimethylsilyl-, trimethylsilyl ester	3702.4	↑	C00082	1.12E+06	7.58E+05	1.88E+06
Erythro-Pentonic acid, 2-deoxy-3,4,5-tris-O-(trimethylsilyl)-, trimethylsilyl ester	3648.4	↑	C03826	5.24E+04	2.65E+04	7.89E+04
trans-9-Octadecenoic acid, trimethylsilyl ester	3575.8	↓	C01712	-2.01E+05	6.83E+05	4.82E+05
ISOLEUCINE,N,O-TMS	3464.8	↑	C16434	9.94E+05	7.65E+05	1.76E+06
L-Aspartic acid, N-(trimethylsilyl)-, bis(trimethylsilyl) ester	3338.2	↓	C00049	-3.71E+06	8.13E+06	4.42E+06
SERINE,N,O,O-TMS	3308.7	↑	C00065	1.09E+06	1.23E+06	2.32E+06
XYLITOL 5TMS	3239.6	↑	C00379	1.48E+04	1.24E+03	1.60E+04
trans, trans-Farnesol, trimethylsilyl ether	3198.3	↑	C01126	2.84E+04	2.91E+04	5.75E+04
N,O,O-Tris(trimethylsilyl)-L-threonine	3023.3	↑	C00188	2.70E+05	4.97E+05	7.67E+05
LEUCINE, N,O-TMS	2855.1	↑	C00123	2.75E+06	2.95E+06	5.69E+06
SUCROSE TMS	2841.2	↓	C00089	-1.66E+04	2.62E+04	9.63E+03
Propanoic acid, 2-oxo-3-(trimethylsilyl)-, trimethylsilyl ester	2807.1	↑	C00163	-3.89E+04	1.07E+05	6.79E+04
2-Piperidinecarboxylic acid, tert-butyldimethylsilyl ester, (DL)-	2763.4	↑	C00408	2.76E+05	1.43E+05	4.19E+05
3-OXOGLUTARIC ACID MEOX1 TMS	2611.7	↑	C00026	4.02E+05	1.05E+06	1.45E+06
Pyroglutamic acid	2609.5	↑	C02237	9.19E+04	1.41E+04	1.06E+05
XYLULOSE MEOX 4TMS	2579.4	↑	C00312	2.23E+06	3.12E+06	5.35E+06

Palmitic Acid	2464.2	↓	C00249	9.32E+03	3.47E+03	1.28E+04
Tetradecanoic acid, trimethylsilyl ester	2298.7	↓	C06424	-7.76E+05	4.21E+06	3.43E+06
ALANINE,N,O-TMS	2174.8	↑	C00041	-6.34E+04	1.85E+05	1.22E+05
HYDROXYBUTANOIC ACID,O,O-TMS	2156.1	↑	C01089	2.29E+05	6.29E+04	2.92E+05
Uridine, 2',3',5'-tris-O-(trimethylsilyl)-	2155.5	↓	C00299	1.09E+05	1.44E+04	1.24E+05
RHAMNOSE MEOX2 4TMS	2129.8	↑	C00507	-5.35E+04	9.51E+04	4.16E+04
Butanal, 2,3,4-tris[(trimethylsilyl)oxy]-, (R*,R*)-	2117.7	↑	C01412	2.93E+04	3.10E+04	6.03E+04
L-Valine, N-(trimethylsilyl)-, trimethylsilyl ester	2041.7	↑	C00183	2.68E+04	2.21E+04	4.89E+04
Ribonic acid, 2,3,4,5-tetrakis-O-(trimethylsilyl)-, trimethylsilyl ester	1975	↑	C01685	1.62E+06	2.60E+06	4.22E+06
ERYTHROSE MEOX2 TMS	1950.9	↑	C01796	5.22E+03	4.93E+03	1.01E+04
á-DL-Arabinopyranose, 1,2,3,4-tetrakis-O-(trimethylsilyl)-	1911.8	↑	C00259	3.24E+06	3.55E+03	3.25E+06
D-Xylose, tetrakis(trimethylsilyl)-	1897.4	↑	C00181	1.77E+05	2.63E+05	4.39E+05
Benzoic acid trimethylsilyl ester	1886.9	↓	C00180	9.18E+04	7.98E+04	1.72E+05
Pentanedioic acid, 2-(methoxyimino)-, bis(trimethylsilyl) ester	1814.6	↓	C00489	-8.12E+05	2.09E+06	1.27E+06
OXALIC ACID TMS	1739.9	↑	C00209	-1.29E+03	5.88E+03	4.59E+03
Acetic acid, bis[(trimethylsilyl)oxyl]-, trimethylsilyl ester	1722.5	↓	C00033	3.08E+06	3.60E+05	3.44E+06
LAURIC ACID TMS	1694.1	↓	C02679	-2.09E+04	4.78E+04	2.69E+04
Galactonic acid, 2,3,4,5,6-pentakis-O-(trimethylsilyl)-, trimethylsilyl ester	1653.1	↑	C00880	-2.84E+04	9.08E+04	6.24E+04
4-AMINOBUTYRIC ACID 3TMS	1638.9	↓	C00334	7.21E+03	3.71E+03	1.09E+04
Lyxose, tetra-(trimethylsilyl)-ether	1618	↑	C01508	-2.24E+04	4.06E+04	1.83E+04
Myo-Inositol, 1,2,3,4,5,6-hexakis-O-(trimethylsilyl)-	1610.7	↓	C00137	8.70E+04	7.95E+04	1.67E+05
D-Fructose, 1,3,4,5,6-pentakis-O-(trimethylsilyl)-	1570.7	↑	C00095	-2.07E+05	3.21E+06	3.00E+06
Alanine, phenyl-, trimethylsilyl ester, dl-	1536.2	↑	C00079	6.64E+03	1.12E+04	1.78E+04
Arachidonic acid, trimethylsilyl ester	1475.4	↑	C00219	9.46E+03	3.54E+04	4.49E+04
Azelaic acid, bis(trimethylsilyl) ester	1447.2	↑	C08261	9.46E+03	3.54E+04	4.49E+04
O,O,O'-Tris-trimethylsilylmalonate	1427.3	↑	C00383	1.93E+04	5.44E+04	7.37E+04
Glyoxylic acid, di-TMS	1424.2	↑	C00048	5.28E+03	5.16E+03	1.04E+04
Azulene, 1,2,3,4,5,6,7,8-octahydro-1,4-dimethyl-7-(1-methylethylidene)-, (1S-cis)-	1408.3	↑	C13392	5.81E+04	8.55E+04	1.44E+05

1-Octanol, 2,2-dimethyl-	1407.4	↓	C00756	1.84E+04	1.51E+03	1.99E+04
Trimethylsiloxy(trimethylsilyl)proline	1400.5	↑	C00148	-2.09E+05	9.35E+05	7.27E+05
Octadecanoic acid, trimethylsilyl ester	1400.1	↑	C01530	5.06E+04	2.60E+04	7.66E+04
Arabinofuranose, 1,2,3,5-tetrakis-O-(trimethylsilyl)-	1395.8	↓	C06115	2.88E+03	2.70E+03	5.58E+03
ORNITHINE,N,N,N',O-TMS	1363.4	↓	C00077	-2.19E+04	1.77E+05	1.55E+05
Gluconic acid, 2-methoxime, tetra(trimethylsilyl)-, trimethylsilyl ester	1301.7	↓	C00257	-1.14E+05	3.02E+05	1.89E+05
UREA 2TMS	1286.6	↑	C00086	7.46E+05	75710.785	821237.285
ç-Elemene	1273.3	↓	C17094	-2.67E+04	31646.636	4927.352
ASPARAGINE,N,N,O-TMS	1265.3	↑	C00152	4.03E+03	8265.44	12295.035
Octanedioic acid, bis(trimethylsilyl) ester	1265	↑	C08278	9.54E+03	3.59E+04	4.55E+04
MALTOSE MEOX2 TMS	1247.3	↑	C00208	2.29E+03	8.24E+03	1.05E+04
Kaur-15-ene, (5à,9à,10á)-	1241	↑	C06090	6.31E+03	1.77E+04	2.40E+04
Hexanoic acid, trimethylsilyl ester	1212.1	↓	C01585	-7.32E+04	2.40E+05	1.66E+05
Tridecane	1175.7	↑	C13834	-8.26E+03	2.78E+04	1.95E+04
Glycine, N-formyl-, trimethylsilyl ester	1165	↑	C00037	4.49E+06	7.31E+05	5.22E+06
Galacturonic acid, pentakis(trimethylsilyl)-	1160	↑	C00333	1.43E+03	1.35E+04	1.50E+04
Decanal, O-methyloxime	1158.6	↑	C12307	6.35E+03	1.64E+04	2.27E+04
GLYCEROL 3TMS	1150.5	↑	C00116	1.05E+04	3.38E+04	4.42E+04
ERYTHROSE MEOX1 3TMS	1148	↓	C01796	-5.47E+04	3.30E+05	2.75E+05
3à-(Trimethylsiloxy)cholest-5-ene	1139	↑	C05416	3.81E+04	5.17E+04	8.99E+04
á-D-Fructofuranose, 2,3,4,6-tetrakis-O-(trimethylsilyl)-, bis(trimethylsilyl) phosphate	1138.8	↑	C03267	2.02E+04	4.73E+04	6.75E+04
Pentadecane	1138	↓	C08388	-8.36E+04	1.38E+05	5.43E+04
NORLEUCINE,O-TMS	1137.7	↑	C01933	4.85E+04	1.66E+05	2.15E+05
TYRAMINE,N,O-TMS	1133.7	↓	C00483	-1.17E+04	1.63E+05	1.52E+05
Acetoacetic acid, bis(trimethylsilyl)- deriv.	1095.6	↑	C00164	3.40E+03	6.73E+03	1.01E+04
Heptanedioic acid, bis(trimethylsilyl) ester	1090.5	↑	C02656	3.64E+03	3.65E+04	4.02E+04
D-Glucuronic acid, 2,3,4,5-tetrakis-O-(trimethylsilyl)-, trimethylsilyl ester	1089.2	↑	C16245	8.99E+03	9.59E+03	1.86E+04

Appendix C

List of Peaks Identified as changing by Fisher Ratio Analysis from 7 mM glucose to 17 mM glucose with KEGG identifications, direction of change, Fisher Ratios and Peak Areas

Software Identification	Fisher Ratio	Direction of Change	KEGG ID	Peak Area		
				7 mM - 3 mM	3 mM	7 mM
Uridine, 2',3',5'-tris-O-(trimethylsilyl)-	1339	↓	C00299	-1.70E+04	5.54E+04	3.84E+04
XYLOSE MEOX2 4TMS	6406.5	↑	C01394	3.43E+04	2.35E+04	5.78E+04
Butanoic acid, 4-[bis(trimethylsilyl)amino]-, trimethylsilyl ester	4722.9	↓	C00246	-7.91E+05	1.62E+06	8.29E+05
ERYTHROSE MEOX2 TMS	4232.4	↑	C01796	3.38E+06	1.65E+03	3.38E+06
Glutamine, tris(trimethylsilyl)-	4006.3	↓	C00064	-1.15E+07	1.61E+07	4.59E+06
L-Aspartic acid, N-(trimethylsilyl)-, bis(trimethylsilyl) ester	3664.2	↓	C00049	-3.14E+06	5.78E+06	2.64E+06
GALACTOSE MEOX1 TMS	3521.4	↓	C00124	-4.03E+06	8.11E+06	4.08E+06
Gluconic acid, ç-lactone, 5-methoximine, tri(trimethylsilyl)-	3515.9	↑	C00198	2.43E+03	6.22E+03	8.65E+03
Propanoic acid, 2-[(trimethylsilyl)oxy]-, trimethylsilyl ester	3069.2	↑	C00163	1.86E+06	3.35E+06	5.21E+06
LEUCINE, N,O-TMS	2992.7	↑	C00123	2.36E+06	3.33E+06	5.69E+06
SERINE,N,O,O-TMS	2961	↑	C00065	9.65E+05	1.23E+06	2.20E+06
N,O,O-Tris(trimethylsilyl)-L-threonine	2806.9	↑	C00188	2.32E+05	5.35E+05	7.67E+05
ALANINE,N,O-TMS	2508.1	↓	C00041	-9.79E+04	1.59E+05	6.07E+04
2-Butenedioic acid (E)-, bis(trimethylsilyl) ester	2337.8	↑	C00122	6.19E+05	1.05E+06	1.67E+06
Tyrosine, O-trimethylsilyl-, trimethylsilyl ester	2308.2	↑	C00082	9.72E+05	9.05E+05	1.88E+06
ISOLEUCINE,N,O-TMS	2217.8	↑	C16434	8.18E+05	9.41E+05	1.76E+06
MANNOSE MEOX TMS	2137.4	↓	C00159	-1.96E+04	2.84E+04	8.84E+03
PHOSPHORIC ACID,O,O,O-TMS	2064	↑	C00009	4.18E+06	1.16E+06	5.34E+06
Galactonic acid, 2,3,4,5,6-pentakis-O-(trimethylsilyl)-, trimethylsilyl ester	2036.4	↓	C00880	-1.86E+05	2.08E+05	2.15E+04
MANNITOL TMS	1981	↑	C00392	1.71E+05	1.96E+05	3.66E+05
GLYCINE,N,N,O-TMS	1952.6	↓	C00037	-7.43E+04	1.70E+05	9.61E+04
Arachidonic acid, trimethylsilyl ester	1928	↑	C00219	1.34E+04	3.15E+04	4.49E+04
SUCROSE TMS	1853.5	↓	C00089	-3.74E+03	1.34E+04	9.63E+03
Glyoxylic acid, di-TMS	1837.5	↑	C00048	7.38E+04	6.98E+04	1.44E+05
HYDROXYBUTANOIC ACID,O,O-TMS	1771.6	↑	C01089	9.12E+04	3.79E+04	1.29E+05

Azelaic acid, bis(trimethylsilyl) ester	1743	↑	C08261	1.89E+04	5.48E+04	7.37E+04
Azulene, 1,2,3,4,5,6,7,8-octahydro-1,4-dimethyl-7-(1-methylethylidene)-, (1S-cis)-	1733.8	↓	C13392	-7.88E+03	1.39E+04	6.00E+03
Lyxose, tetra-(trimethylsilyl)-ether	1677.6	↑	C01508	1.21E+05	8.13E+04	2.02E+05
9,12-Octadecadienoic acid (Z,Z)-, trimethylsilyl ester	1636.7	↓	C01595	-5.73E+04	2.39E+05	1.81E+05
Galacturonic acid, pentakis(trimethylsilyl)-	1612	↑	C08348	1.95E+04	9.43E+03	2.89E+04
Dodecanoic acid, ethyl ester	1605.3	↑	C02679	7.52E+03	4.26E+03	1.18E+04
Pentanedioic acid, 2-(methoxyimino)-, bis(trimethylsilyl) ester	1604.7	↓	C00489	-2.88E+02	4.63E+03	4.34E+03
Pyroglutamic acid	1525.1	↑	C02237	4.04E+05	1.25E+05	5.29E+05
XYLULOSE MEOX 4TMS	1508.7	↑	C00312	6.19E+03	6.60E+03	1.28E+04
L-Valine, N-(trimethylsilyl)-, trimethylsilyl ester	1506.6	↑	C00183	1.77E+04	2.50E+04	4.27E+04
PYROGLUTAMIC ACID 2TMS	1492.6	↓	C01879	-9.84E+05	1.23E+06	2.46E+05
3-OXOGLUTARIC ACID MEOX1 TMS	1485.4	↑	C00026	5.10E+04	5.93E+04	1.10E+05
trans, trans-Farnesol, trimethylsilyl ether	1478.1	↑	C01126	8.11E+03	4.94E+04	5.75E+04
D-Ribose, 2,3,4-tris-O-(trimethylsilyl)-, O-methyloxime, 5-[bis(trimethylsilyl) phosphate]	1442.4	↓	C00117	-1.25E+04	8.04E+04	6.79E+04
á-DL-Arabinopyranose, 1,2,3,4-tetrakis-O-(trimethylsilyl)-	1441.3	↑	C00259	1.12E+05	3.27E+05	4.39E+05
Acetic acid, bis[(trimethylsilyl)oxyl]-, trimethylsilyl ester	1431	↓	C00033	-5.98E+03	4.09E+04	3.49E+04
Alanine, phenyl-, trimethylsilyl ester, dl-	1411	↑	C00079	2.78E+05	3.31E+05	6.09E+05
Trimethylsilyl acetylsalicylate	1313.7	↓	C01405	-4.16E+05	4.32E+05	1.64E+04
GLYCEROL 3TMS	1274.2	↑	C00116	1.41E+04	3.02E+04	4.42E+04
OXALIC ACID TMS	1259.3	↓	C00209	-5.30E+03	8.39E+03	3.09E+03
Propanedioic acid, bis(trimethylsilyl) ester	1256.5	↑	C00383	4.74E+04	3.88E+04	8.62E+04
Heptanedioic acid, bis(trimethylsilyl) ester	1245	↑	C02656	9.35E+03	3.08E+04	4.02E+04
METHIONINE,N,O-TMS	1241.5	↑	C00073	1.51E+05	1.18E+05	2.69E+05
MALTOSE MEOX2 TMS	1221.4	↑	C00208	2.94E+03	7.59E+03	1.05E+04
PIPECOLIC ACID,O-TMS	1218.9	↓	C00408	-2.27E+05	5.74E+05	3.47E+05
2-Propenoic acid, 3-(4-methoxyphenyl)-, 2-ethylhexyl ester	1212.7	↓	C00511	-7.09E+05	8.77E+05	1.68E+05
Octanoic acid, trimethylsilyl ester	1212.4	↑	C06423	8.38E+03	5.06E+04	5.90E+04
ETHYLENEGLYCOL,O,O-TMS	1207.5	↑	C05576	1.55E+04	2.03E+04	3.58E+04

Kaur-15-ene, (5à,9à,10á)-	1202.5	↑	C06090	7.04E+02	4.27E+03	4.98E+03
ASPARAGINE,N,N,O-TMS	1198.9	↓	C00152	-6.54E+03	2.18E+04	1.53E+04
Butanal, 2,3,4-tris[(trimethylsilyl)oxy]-, (R*,R*)-	1171.1	↑	C01412	9.69E+03	3.92E+04	4.89E+04
RHAMNOSE MEOX2 4TMS	1160.2	↑	C00507	1.48E+04	4.55E+04	6.03E+04
Propanoic acid, 3-[(trimethylsilyl)oxy]-, trimethylsilyl ester	1158.7	↑	C00022	6.52E+04	1.97E+05	2.62E+05
D-Fructose, 1,3,4,5,6-pentakis-O-(trimethylsilyl)-	1154.5	↑	C00095	9.35E+03	1.07E+04	2.00E+04
Aminomalonic acid, tris(trimethylsilyl)-	1151	↑	C00872	2.29E+05	4.59E+05	6.88E+05
Acetoacetic acid, bis(trimethylsilyl)- deriv.	1144.2	↑	C00164	3.47E+03	6.66E+03	1.01E+04
Gluconic acid, 2-methoxime, tetra(trimethylsilyl)-, trimethylsilyl ester	1138.4	↑	C00257	3.60E+03	4.55E+03	8.14E+03
Decanal, O-methyloxime	1132.3	↑	C12307	8.20E+03	1.15E+04	1.97E+04
Malic acid, tris(trimethylsilyl) ester	1131.5	↑	C00497	2.45E+05	1.21E+06	1.45E+06
NORLEUCINE,O-TMS	1111.1	↓	C01933	-2.70E+03	2.12E+05	2.09E+05
Octadecanoic acid, methyl ester	1106.6	↑	C01530	1.02E+03	1.52E+04	1.62E+04
11-Eicosenoic acid, trimethylsilyl ester	1103.2	↑	C16526	3.18E+02	1.45E+04	1.48E+04
3à-(Trimethylsiloxy)cholest-5-ene	1098.8	↑	C05416	1.13E+03	9.94E+04	1.01E+05
Nonanoic acid, trimethylsilyl ester	1086.2	↑	C01601	1.99E+04	6.21E+04	8.20E+04
L-Cysteine, N,S-bis(trimethylsilyl)-, trimethylsilyl ester	1083.2	↑	C00097	1.27E+05	2.09E+05	3.36E+05
l-Valine, trimethylsilyl ester	1074.6	↓	C00183	-4.34E+04	4.43E+05	4.00E+05
Phenylethanolamine triTMS	1068.2	↑	C02735	8.81E+03	2.28E+04	3.16E+04
Octanedioic acid, bis(trimethylsilyl) ester	1067.4	↑	C08278	9.59E+03	3.59E+04	4.55E+04

Appendix D

List of Pathways Identified by Metscape Analysis from 3 mM Glucose to 7 mM Glucose with Reactions, Seeds Involved, Direction of Change and Peak Areas

Reaction	Pathway	Seed	Direction of Change	Average Peak Area		
				7 mM - 3 mM	3 mM	7 mM
R00768	Aminosugars metabolism	glutamine	↑	1.40E+07	3.08E+06	1.71E+07
RE2754	Arachidonic acid metabolism	glycerol				
RE2563	Arachidonic acid metabolism	glycerol	↑	3.57E+04	3.15E+03	3.89E+04
RE2649	Bile acid biosynthesis	propanoate	↑	1.53E+05	1.35E+05	2.88E+05
RE2638	Bile acid biosynthesis	glycine	↑	2.06E+06	3.60E+06	5.66E+06
R03718	Bile acid biosynthesis	glycine				
RE2650	Biopterin metabolism	phenylalanine	↓	-3.08E+05	639263.172	330825.176
R01176	Butanoate metabolism	butanoate	↓	-5.03E+06	7.14E+06	2.11E+06
RE1514	Di-unsaturated fatty acid beta-oxidation	linoleate	↑	1.07E+05	102259.013	208765.898
RE1576	De novo fatty acid biosynthesis	myristic acid	↓	-5.47E+04	1.85E+05	1.31E+05
RN0034	De novo fatty acid biosynthesis	palmitate	↓	-8.80E+05	4.21E+06	3.33E+06
R01706	De novo fatty acid biosynthesis	palmitate				
RE1575	De novo fatty acid biosynthesis	lauric acid	↓	-6.28E+03	1.05E+04	4.26E+03
R00867	Fructose and mannose metabolism	d-fructose	↓	-1.22E+05	1.43E+05	2.13E+04
R00875	Fructose and mannose metabolism	d-fructose				
R00866	Fructose and mannose metabolism	d-fructose				
RE2783	Fructose and mannose metabolism	d-fructose				
RE1342	Fructose and mannose metabolism	d-glucose	↑	2.13E+06	1684859.34	3814592.53
R03634	Galactose metabolism	d-galactose	↑	4.15E+05	4.45E+03	4.20E+05
R01101	Galactose metabolism	d-galactose				
R05549	Galactose metabolism	d-galactose				
R01104	Galactose metabolism	d-galactose				
R01105	Galactose metabolism	d-galactose				
R01100	Galactose metabolism	d-galactose				
R01329	Galactose metabolism	d-galactose				

R01093	Galactose metabolism	d-galactose				
R01095	Galactose metabolism	d-galactose				
R02926	Galactose metabolism	d-galactose				
R01092	Galactose metabolism	d-galactose				
R01103	Galactose metabolism	sucrose & d-galactose	↓	-1.54E+04	2.88E+04	1.34E+04
R01678	Galactose metabolism	d-galactose				
R01036	Glycerophospholipid metabolism	glycerol	↑	3.57E+04	3.15E+03	3.89E+04
R03616	Glycerophospholipid metabolism	glycerol				
R00847	Glycerophospholipid metabolism	glycerol				
RE3507	Glycerophospholipid metabolism	glycerol				
R01352	Glycerophospholipid metabolism	glycerol				
R01041	Glycerophospholipid metabolism	glycerol				
R01350	Glycerophospholipid metabolism	glycerol				
R01351	Glycerophospholipid metabolism	glycerol				
R04452	Glycerophospholipid metabolism	acetate	↑	2.65E+04	14385.659	40885.513
R03038	Glycine, serine, alanine and threonine metabolism	Alanine	↓	-2.43E+04	3.45E+04	1.02E+04
R00369	Glycine, serine, alanine and threonine metabolism	Alanine				
RE1473	Glycine, serine, alanine and threonine metabolism	Alanine				
RE2642	Glycine, serine, alanine and threonine metabolism	Alanine				
R00945	Glycine, serine, alanine and threonine metabolism	Glycine	↑	2.06E+06	3.60E+06	5.66E+06
R00371	Glycine, serine, alanine and threonine metabolism	Glycine				
R00366	Glycine, serine, alanine and threonine metabolism	Glycine				
R06171	Glycine, serine, alanine and threonine metabolism	Glycine				
R01221	Glycine, serine, alanine and threonine metabolism	Glycine				
RE2429	Glycine, serine, alanine and threonine metabolism	Glycine				
R00367	Glycine, serine, alanine and threonine metabolism	Glycine				
R00610	Glycine, serine, alanine and threonine metabolism	Glycine				

RE2427	Glycine, serine, alanine and threonine metabolism	Glycine				
R00751	Glycine, serine, alanine and threonine metabolism	Glycine				
R00565	Glycine, serine, alanine and threonine metabolism	Glycine				
R03425	Glycine, serine, alanine and threonine metabolism	Glycine				
RE2031	Glycine, serine, alanine and threonine metabolism	Glycine				
RE2428	Glycine, serine, alanine and threonine metabolism	Glycine				
R03654	Glycine, serine, alanine and threonine metabolism	Glycine				
R00611	Glycine, serine, alanine and threonine metabolism	Glycine				
RE2117	Glycine, serine, alanine and threonine metabolism	Glycine				
RE2111	Glycine, serine, alanine and threonine metabolism	Glycine				
R00220	Glycine, serine, alanine and threonine metabolism	pyruvate	↑	9.73E+04	143141.61	240399.287
R00704	Glycine, serine, alanine and threonine metabolism	pyruvate				
R03663	Glycine, serine, alanine and threonine metabolism	threonine	↑	3.24E+03	17137.327	20378.485
R00710	Glycolysis and Gluconeogenesis	acetate	↑	2.65E+04	14385.659	40885.513
R00227	Glycolysis and Gluconeogenesis	acetate				
R00235	Glycolysis and Gluconeogenesis	acetate				
R00317	Glycolysis and Gluconeogenesis	acetate				
R00316	Glycolysis and Gluconeogenesis	acetate				
R00216	Glycolysis and Gluconeogenesis	malate & pyruvate	↑	1.84E+06	5.26E+05	2.37E+06
R00214	Glycolysis and Gluconeogenesis	malate				
R00200	Glycolysis and Gluconeogenesis	pyruvate	↑	9.73E+04	143141.61	240399.287
R00344	Glycolysis and Gluconeogenesis	pyruvate				
R00006	Glycolysis and Gluconeogenesis	pyruvate				
R00703	Glycolysis and Gluconeogenesis	pyruvate				
R01699	Glycolysis and Gluconeogenesis	pyruvate				
R00210	Glycolysis and Gluconeogenesis	pyruvate				
R00196	Glycolysis and Gluconeogenesis	pyruvate				

R00711	Glycolysis and Gluconeogenesis	pyruvate & acetate				
R00209	Glycolysis and Gluconeogenesis	pyruvate				
R00014	Glycolysis and Gluconeogenesis	pyruvate				
RE2717	Glycosphingolipid metabolism	d-galactose	↑	4.15E+05	4.45E+03	4.20E+05
RE3632	Histidine metabolism	Glycine	↑	2.06E+06	3.60E+06	5.66E+06
RE1821	Leukotriene metabolism	Glycine	↑	2.06E+06	3.60E+06	5.66E+06
RE0596	Leukotriene metabolism	Glycine				
R07056	Linoleate metabolism	linoleate	↑	1.07E+05	102259.013	208765.898
R07057	Linoleate metabolism	linoleate				
R07064	Linoleate metabolism	linoleate				
RE3409	Linoleate metabolism	linoleate				
R07055	Linoleate metabolism	linoleate				
R03626	Linoleate metabolism	linoleate				
R07063	Linoleate metabolism	linoleate				
R03284	Lysine metabolism	Glycine	↑	2.06E+06	3.60E+06	5.66E+06
R02204	Lysine metabolism	Pipecolate	↑	2.13E+05	3.03E+05	5.16E+05
R02203	Lysine metabolism	Pipecolate				
R02201	Lysine metabolism	Pipecolate				
R02205	Lysine metabolism	Pipecolate				
R00652	Methionine and cysteine metabolism	Glycine	↑	2.06E+06	3.60E+06	5.66E+06
RE2811	Methionine and cysteine metabolism	cysteine	↓	-2.24E+04	231698.474	209254.529
R00896	Methionine and cysteine metabolism	cysteine				
R00782	Methionine and cysteine metabolism	cysteine & pyruvate	↑	9.73E+04	143141.61	240399.287
R00891	Methionine and cysteine metabolism	cysteine				
RE2223	Methionine and cysteine metabolism	cysteine				
R01001	Methionine and cysteine metabolism	cysteine				

R00892	Methionine and cysteine metabolism	cysteine				
R03650	Methionine and cysteine metabolism	cysteine				
R00893	Methionine and cysteine metabolism	cysteine				
R03105	Methionine and cysteine metabolism	pyruvate				
R01049	Pentose phosphate pathway	ribose-5-phosphate	↓	-2.65E+04	106873.904	80412.779
R01057	Pentose phosphate pathway	ribose-5-phosphate				
R01641	Pentose phosphate pathway	ribose-5-phosphate				
R01054	Pentose phosphate pathway	ribose-5-phosphate				
R06590	Pentose phosphate pathway	ribose-5-phosphate				
R01056	Pentose phosphate pathway	ribose-5-phosphate				
R01051	Pentose phosphate pathway	ribose-5-phosphate				
RE0124	Pentose phosphate pathway	d-gluconic acid				
R03331	Phosphatidylinositol phosphate metabolism	glycerol	↑	3.57E+04	3.15E+03	3.89E+04
R01186	Phosphatidylinositol phosphate metabolism	myo-inositol	↓	-5.39E+05	3.21E+06	2.67E+06
R01187	Phosphatidylinositol phosphate metabolism	myo-inositol				
RE3273	Phosphatidylinositol phosphate metabolism	myo-inositol				
R01185	Phosphatidylinositol phosphate metabolism	myo-inositol				
R01194	Phosphatidylinositol phosphate metabolism	myo-inositol				
R01184	Phosphatidylinositol phosphate metabolism	myo-inositol				
R00831	Porphyrin metabolism	Glycine	↑	2.06E+06	3.60E+06	5.66E+06
R00830	Porphyrin metabolism	Glycine				
R01354	Propanoate metabolism	propanoate	↑	1.53E+05	1.35E+05	2.88E+05
RE2067	Prostaglandin formation from arachidonate	glycerol	↑	3.57E+04	3.15E+03	3.89E+04
RE2068	Prostaglandin formation from arachidonate	glycerol				
R02422	Purine metabolism	urea	↓	-5.05E+05	1.27E+06	7.70E+05
R01083	Purine metabolism	fumarate	↑	8.12E+05	2.43E+05	1.05E+06
R01135	Purine metabolism	aspartate	↓	-2.57E+06	9.05E+06	6.48E+06
R01072	Purine metabolism	glutamine	↑	1.40E+07	3.08E+06	1.71E+07

R01231	Purine metabolism	glutamine				
R01397	Pyrimidine metabolism	aspartate	↓	-2.57E+06	9.05E+06	6.48E+06
R00575	Pyrimidine metabolism	glutamine	↑	1.40E+07	3.08E+06	1.71E+07
R00963	Pyrimidine metabolism	uridine	↓	-4.17E+04	9.51E+04	5.34E+04
R00967	Pyrimidine metabolism	uridine				
R01876	Pyrimidine metabolism	uridine				
R02327	Pyrimidine metabolism	uridine				
R00968	Pyrimidine metabolism	uridine				
R02097	Pyrimidine metabolism	uridine				
R00970	Pyrimidine metabolism	uridine				
R01549	Pyrimidine metabolism	uridine				
R01880	Pyrimidine metabolism	uridine				
R02332	Pyrimidine metabolism	uridine				
R01878	Pyrimidine metabolism	uridine				
R00964	Pyrimidine metabolism	uridine				
R01274	Saturated fatty acids beta-oxidation	palmitate	↓	-8.80E+05	4.21E+06	3.33E+06
R00408	TCA cycle	fumarate	↑	8.12E+05	2.43E+05	1.05E+06
R00342	TCA cycle	malate	↑	1.84E+06	5.26E+05	2.37E+06
R02164	TCA cycle	fumarate				
R00412	TCA cycle	fumarate				
R01082	TCA cycle	malate & fumarate				
R00362	TCA cycle	citrate	↑	3.98E+06	0	3975268.33
R01325	TCA cycle	citrate &cis-aconitate	↑	5.69E+03	9069.32	14762.068
R00351	TCA cycle	citrate				
R01324	TCA cycle	citrate				
R00352	TCA cycle	citrate				

R01900	TCA cycle	cis-aconitate				
RE1915	Tyrosine metabolism	cysteine	↓	-2.24E+04	231698.474	209254.529
R01364	Tyrosine metabolism	fumarate	↑	8.12E+05	2.43E+05	1.05E+06
R01795	Tyrosine metabolism	phenylalanine & tyrosine				
R00694	Tyrosine metabolism	phenylalanine	↓	-3.08E+05	639263.172	330825.176
RE1465	Tyrosine metabolism	phenylalanine & tyrosine				
R00689	Tyrosine metabolism	phenylalanine				
R00698	Tyrosine metabolism	phenylalanine				
R00692	Tyrosine metabolism	phenylalanine				
R03660	Tyrosine metabolism	phenylalanine				
R00699	Tyrosine metabolism	phenylalanine				
RE1919	Tyrosine metabolism	pyruvate	↑	9.73E+04	143141.61	240399.287
R02383	Tyrosine metabolism	tyramine	↑	1.47E+04	53443.233	68159.058
R02382	Tyrosine metabolism	tyramine				
RE2124	Tyrosine metabolism	tyramine				
RE2781	Tyrosine metabolism	tyramine				
R00729	Tyrosine metabolism	tyrosine	↑	1.47E+05	758488.51	905112.62
RE0026	Tyrosine metabolism	tyrosine				
R02078	Tyrosine metabolism	tyrosine				
R01815	Tyrosine metabolism	tyrosine				
RE0941	Tyrosine metabolism	tyrosine				
R02918	Tyrosine metabolism	tyrosine				
R00736	Tyrosine metabolism	tyrosine & tyramine				
R03539	Tyrosine metabolism	tyrosine				

RE3062	Tyrosine metabolism	tyrosine				
R00734	Tyrosine metabolism	tyrosine				
R00731	Tyrosine metabolism	tyrosine				
R01920	Urea cycle and metabolism of arginine, proline, glutamate, aspartate and asparagine	putrescine	↓	-3.89E+05	2.72E+06	2.33E+06
RE1537	Urea cycle and metabolism of arginine, proline, glutamate, aspartate and asparagine	putrescine				
R01151	Urea cycle and metabolism of arginine, proline, glutamate, aspartate and asparagine	putrescine				
R01154	Urea cycle and metabolism of arginine, proline, glutamate, aspartate and asparagine	putrescine				
R00670	Urea cycle and metabolism of arginine, proline, glutamate, aspartate and asparagine	putrescine				
R01157	Urea cycle and metabolism of arginine, proline, glutamate, aspartate and asparagine	putrescine				
R00258	Urea cycle and metabolism of arginine, proline, glutamate, aspartate and asparagine	alanine	↓	-2.43E+04	3.45E+04	1.02E+04
R00551	Urea cycle and metabolism of arginine, proline, glutamate, aspartate and asparagine	urea	↓	-5.05E+05	1.27E+06	7.70E+05
R01086	Urea cycle and metabolism of arginine, proline, glutamate, aspartate and asparagine	fumarate	↑	8.12E+05	2.43E+05	1.05E+06
R03647	Urea cycle and metabolism of arginine, proline, glutamate, aspartate and asparagine	aspartate				
R00357	Urea cycle and metabolism of arginine, proline, glutamate, aspartate and asparagine	aspartate				
R00488	Urea cycle and metabolism of arginine, proline, glutamate, aspartate and asparagine	aspartate				
R00355	Urea cycle and metabolism of arginine, proline, glutamate, aspartate and asparagine	aspartate				
R01954	Urea cycle and metabolism of arginine, proline, glutamate, aspartate and asparagine	aspartate				
R00578	Urea cycle and metabolism of arginine, proline, glutamate, aspartate and asparagine	aspartate	↓	-2.57E+06	9.05E+06	6.48E+06
		& glutamine	↑	1.40E+07	3.08E+06	1.71E+07
R00489	Urea cycle and metabolism of arginine, proline, glutamate, aspartate and asparagine	aspartate				

R03421	Urea cycle and metabolism of arginine, proline, glutamate, aspartate and asparagine	aspartate				
R00526	Urea cycle and metabolism of arginine, proline, glutamate, aspartate and asparagine	aspartate				
R05577	Urea cycle and metabolism of arginine, proline, glutamate, aspartate and asparagine	aspartate				
R02549	Urea cycle and metabolism of arginine, proline, glutamate, aspartate and asparagine	4-aminobutanoate	↑	1.26E+03	3.60E+04	3.73E+04
R01987	Urea cycle and metabolism of arginine, proline, glutamate, aspartate and asparagine	4-aminobutanoate				
R00261	Urea cycle and metabolism of arginine, proline, glutamate, aspartate and asparagine	4-aminobutanoate				
R01648	Urea cycle and metabolism of arginine, proline, glutamate, aspartate and asparagine	4-aminobutanoate				
R01986	Urea cycle and metabolism of arginine, proline, glutamate, aspartate and asparagine	4-aminobutanoate				
R01989	Urea cycle and metabolism of arginine, proline, glutamate, aspartate and asparagine	4-aminobutanoate				
R00256	Urea cycle and metabolism of arginine, proline, glutamate, aspartate and asparagine	glutamine				
R03652	Urea cycle and metabolism of arginine, proline, glutamate, aspartate and asparagine	glutamine				
R00253	Urea cycle and metabolism of arginine, proline, glutamate, aspartate and asparagine	glutamine				
R00497	Urea cycle and metabolism of arginine, proline, glutamate, aspartate and asparagine	glycine	↑	2.06E+06	3.60E+06	5.66E+06
R04951	Urea cycle and metabolism of arginine, proline, glutamate, aspartate and asparagine	glycine				
R00135	Urea cycle and metabolism of arginine, proline, glutamate, aspartate and asparagine	proline	↑	2.50E+04	27803.7	52777.33
R01248	Urea cycle and metabolism of arginine, proline, glutamate, aspartate and asparagine	proline				
R01251	Urea cycle and metabolism of arginine, proline, glutamate, aspartate and asparagine	proline				
R01252	Urea cycle and metabolism of arginine, proline, glutamate, aspartate and asparagine	proline				
R03661	Urea cycle and metabolism of arginine, proline, glutamate,	proline				

	aspartate and asparagine					
R01644	Urea cycle and metabolism of arginine, proline, glutamate, aspartate and asparagine	4-hydroxybutanoate	↑	9.95E+03	26409.364	36359.44
R00894	Urea cycle and metabolism of arginine, proline, glutamate, aspartate and asparagine	cysteine	↓	-2.24E+04	231698.474	209254.529
R02743	Urea cycle and metabolism of arginine, proline, glutamate, aspartate and asparagine	cysteine				
R00899	Urea cycle and metabolism of arginine, proline, glutamate, aspartate and asparagine	cysteine				
R00257	Vitamin B3 (nicotinate and nicotinamide) metabolism	glutamine	↑	1.40E+07	3.08E+06	1.71E+07
R02197	Valine, leucine and isoleucine degradation	isoleucine	↑	1.76E+05	765275.077	941063.876
R03656	Valine, leucine and isoleucine degradation	isoleucine				
R02199	Valine, leucine and isoleucine degradation	isoleucine				
R02198	Valine, leucine and isoleucine degradation	isoleucine				
R03665	Valine, leucine and isoleucine degradation	valine	↓	-4.48E+04	82483.602	37692.497
R01214	Valine, leucine and isoleucine degradation	valine				
R04230	Vitamin B5 - CoA biosynthesis from pantothenate	cysteine	↓	-2.24E+04	231698.474	209254.529
R04233	Vitamin B5 - CoA biosynthesis from pantothenate	cysteine				

Appendix E

List of Pathways Identified by Metscape Analysis from 3 mM glucose to 17 mM Glucose with Reactions, Seeds Involved, Direction of Change and Peak Areas

Reaction	Pathway	Seed	Direction of Change	Average Peak Area		
				17 mM - 3 mM	3 mM	17 mM
R00768	Aminosugars metabolism	glutamine	↑	5.41E+06	3.63E+05	5.77E+06
RE3647	Arachidonic acid metabolism	arachidonate	↑	9.46E+03	3.54E+04	4.49E+04
R07052	Arachidonic acid metabolism	arachidonate				
RE3650	Arachidonic acid metabolism	arachidonate				
R07046	Arachidonic acid metabolism	arachidonate				
RE3286	Arachidonic acid metabolism	arachidonate				
R07050	Arachidonic acid metabolism	arachidonate				
R07041	Arachidonic acid metabolism	arachidonate				
R01317	Arachidonic acid metabolism	arachidonate				
RE3649	Arachidonic acid metabolism	arachidonate				
R01596	Arachidonic acid metabolism	arachidonate				
RE3651	Arachidonic acid metabolism	arachidonate				
RE3648	Arachidonic acid metabolism	arachidonate				
RE3653	Arachidonic acid metabolism	arachidonate				
RE3288	Arachidonic acid metabolism	arachidonate				
RE3287	Arachidonic acid metabolism	arachidonate				
RE3289	Arachidonic acid metabolism	arachidonate				
RE3646	Arachidonic acid metabolism	arachidonate				
R07054	Arachidonic acid metabolism	arachidonate				
R01593	Arachidonic acid metabolism	arachidonate				
R07051	Arachidonic acid metabolism	arachidonate				
RE3042	Arachidonic acid metabolism	arachidonate				
R07048	Arachidonic acid metabolism	arachidonate				
RE3654	Arachidonic acid metabolism	arachidonate				
RE2563	Arachidonic acid metabolism	glycerol	↑	1.05E+04	33784.016	44244.974

RE2754	Arachidonic acid metabolism	glycerol				
RE2649	Bile acid biosynthesis	glycine	↑	4.49E+06	730562.804	5222233.54
RE2638	Bile acid biosynthesis	glycine				
R03718	Bile acid biosynthesis	glycine				
RE2649	Bile acid biosynthesis	propanoate	↑	1.42E+05	1.21E+05	2.62E+05
RE2650	Biopterin metabolism	tyrosine	↑	1.12E+06	7.58E+05	1.88E+06
R01357	Butanoate metabolism	acetoacetate	↑	3.40E+03	6727.541	10130.481
R00410	Butanoate metabolism	acetoacetate				
R01361	Butanoate metabolism	3-hydroxybutanoic acid	↑	1.09E+05	1.44E+04	1.24E+05
RE1575	De novo fatty acid biosynthesis	lauric acid	↓	-2.84E+04	9.08E+04	6.24E+04
RE0344	De novo fatty acid biosynthesis	stearate	↑	2.88E+03	2.70E+03	5.58E+03
RE1576	De novo fatty acid biosynthesis	myristic acid	↓	-6.34E+04	1.85E+05	1.22E+05
RN0034	De novo fatty acid biosynthesis	palmitate	↓	-7.76E+05	4.21E+06	3.43E+06
R01706	De novo fatty acid biosynthesis	palmitate				
R01326	Fructose and mannose metabolism	mannose				
R00875	Fructose and mannose metabolism	d-fructose	↑	6.64E+03	1.12E+04	1.78E+04
R00866	Fructose and mannose metabolism	d-fructose				
R00867	Fructose and mannose metabolism	d-fructose				
RE2783	Fructose and mannose metabolism	d-fructose				
R03634	Galactose metabolism	d-galactose	↓	-1.48E+06	1.52E+06	4.57E+04
R01105	Galactose metabolism	d-galactose				
R01100	Galactose metabolism	d-galactose				
R01103	Galactose metabolism	d-galactose & sucrose	↓	-1.66E+04	2.62E+04	9.63E+03
R01678	Galactose metabolism	d-galactose				
R01101	Galactose metabolism	d-galactose				
R05549	Galactose metabolism	d-galactose				

R01104	Galactose metabolism	d-galactose				
R01329	Galactose metabolism	d-galactose				
R01093	Galactose metabolism	d-galactose				
R01095	Galactose metabolism	d-galactose				
R02926	Galactose metabolism	d-galactose				
R01092	Galactose metabolism	d-galactose				
R04452	Glycerophospholipid metabolism	acetate	↓	-2.09E+04	4.78E+04	2.69E+04
RE3299	Glycerophospholipid metabolism	serine	↑	1.09E+06	1.23E+06	2.32E+06
RE3298	Glycerophospholipid metabolism	serine				
RE3301	Glycerophospholipid metabolism	serine				
R00847	Glycerophospholipid metabolism	glycerol	↑	1.05E+04	33784.016	44244.974
R01036	Glycerophospholipid metabolism	glycerol				
R01041	Glycerophospholipid metabolism	glycerol				
R01350	Glycerophospholipid metabolism	glycerol				
R01351	Glycerophospholipid metabolism	glycerol				
R01352	Glycerophospholipid metabolism	glycerol				
R03616	Glycerophospholipid metabolism	glycerol				
RE3507	Glycerophospholipid metabolism	glycerol				
R00945	Glycine, serine, alanine and threonine metabolism	glycine & serine				
R00366	Glycine, serine, alanine and threonine metabolism	glycine & glyoxylate				
R00751	Glycine, serine, alanine and threonine metabolism	glycine & threonine				
R00582	Glycine, serine, alanine and threonine metabolism	serine	↑	1.09E+06	1.23E+06	2.32E+06
R00220	Glycine, serine, alanine and threonine metabolism	serine				
R00585	Glycine, serine, alanine and threonine metabolism	serine				
R03662	Glycine, serine, alanine and threonine metabolism	serine				

R00717	Glycine, serine, alanine and threonine metabolism	glyoxylate	↑	5.81E+04	8.55E+04	1.44E+05
R00475	Glycine, serine, alanine and threonine metabolism	glyoxylate				
R00465	Glycine, serine, alanine and threonine metabolism	glyoxylate				
R03038	Glycine, serine, alanine and threonine metabolism	alanine	↑	2.29E+05	6.29E+04	2.92E+05
RE1473	Glycine, serine, alanine and threonine metabolism	alanine				
RE2642	Glycine, serine, alanine and threonine metabolism	alanine				
R00369	Glycine, serine, alanine and threonine metabolism	alanine				
RE2031	Glycine, serine, alanine and threonine metabolism	alanine				
R03663	Glycine, serine, alanine and threonine metabolism	threonine	↑	2.70E+05	4.97E+05	7.67E+05
R00367	Glycine, serine, alanine and threonine metabolism	glycine	↑	4.49E+06	730562.804	5222233.54
R00371	Glycine, serine, alanine and threonine metabolism	glycine				
R00565	Glycine, serine, alanine and threonine metabolism	glycine				
R00610	Glycine, serine, alanine and threonine metabolism	glycine				
R00611	Glycine, serine, alanine and threonine metabolism	glycine				
R01221	Glycine, serine, alanine and threonine metabolism	glycine				
R03425	Glycine, serine, alanine and threonine metabolism	glycine				
R03654	Glycine, serine, alanine and threonine metabolism	glycine				
R06171	Glycine, serine, alanine and threonine metabolism	glycine				
RE2111	Glycine, serine, alanine and threonine metabolism	glycine				
RE2117	Glycine, serine, alanine and threonine metabolism	glycine				
RE2427	Glycine, serine, alanine and threonine metabolism	glycine				
RE2428	Glycine, serine, alanine and threonine metabolism	glycine				
RE2429	Glycine, serine, alanine and threonine metabolism	glycine				
R00711	Glycolysis and Gluconeogenesis	acetate	↓	-2.09E+04	4.78E+04	2.69E+04
R00316	Glycolysis and Gluconeogenesis	acetate				
R00227	Glycolysis and Gluconeogenesis	acetate				
R00710	Glycolysis and Gluconeogenesis	acetate				
R00235	Glycolysis and Gluconeogenesis	acetate				

R00317	Glycolysis and Gluconeogenesis	acetate				
R00214	Glycolysis and Gluconeogenesis	malate	↑	1.72E+05	6.31E+04	2.35E+05
R00216	Glycolysis and Gluconeogenesis	malate				
RE2717	Glycosphingolipid metabolism	d-galactose	↓	-1.48E+06	1.52E+06	4.57E+04
R01281	Glycosphingolipid metabolism	serine	↑	1.09E+06	1.23E+06	2.32E+06
RE3632	Histidine metabolism	glycine	↑	4.49E+06	730562.804	5222233.54
RE0596	Leukotriene metabolism	glycine	↑	4.49E+06	730562.804	5222233.54
RE1821	Leukotriene metabolism	glycine				
R01595	Leukotriene metabolism	arachidonate	↑	9.46E+03	3.54E+04	4.49E+04
RE3417	Linoleate metabolism	azelaic acid	↑	1.93E+04	5.44E+04	7.37E+04
RE3420	Linoleate metabolism	azelaic acid				
R03284	Lysine metabolism	glycine	↑	4.49E+06	730562.804	5222233.54
R02204	Lysine metabolism	pipecolate	↑	4.02E+05	1.05E+06	1.45E+06
R02203	Lysine metabolism	pipecolate				
R02201	Lysine metabolism	pipecolate				
R02205	Lysine metabolism	pipecolate				
R00652	Methionine and cysteine metabolism	glycine				
R01289	Methionine and cysteine metabolism	serine	↑	1.09E+06	1.23E+06	2.32E+06
R00891	Methionine and cysteine metabolism	serine				
R00590	Methionine and cysteine metabolism	serine				
R01290	Methionine and cysteine metabolism	serine				
RE0324	Omega-6 fatty acid metabolism	arachidonate	↑	9.46E+03	3.54E+04	4.49E+04
RE0124	Pentose phosphate pathway	d-gluconic acid	↑	4.65E+03	3496.041	8144.155
R01187	Phosphatidylinositol phosphate metabolism	m yo-inositol	↓	-2.07E+05	3.21E+06	3.00E+06
R01186	Phosphatidylinositol phosphate metabolism	m yo-inositol				
RE3273	Phosphatidylinositol phosphate metabolism	m yo-inositol				
R01185	Phosphatidylinositol phosphate metabolism	m yo-inositol				
R01184	Phosphatidylinositol phosphate metabolism	m yo-inositol				

R01194	Phosphatidylinositol phosphate metabolism	m yo-inositol				
R03331	Phosphatidylinositol phosphate metabolism	glycerol	↑	1.05E+04	33784.016	44244.974
R01354	Propanoate metabolism	propanoate	↑	1.42E+05	1.21E+05	2.62E+05
RE1978	Prostaglandin formation from arachidonate	arachidonate	↑	9.46E+03	3.54E+04	4.49E+04
RE3455	Prostaglandin formation from arachidonate	arachidonate				
R01590	Prostaglandin formation from arachidonate	arachidonate				
RE3452	Prostaglandin formation from arachidonate	arachidonate				
RE3458	Prostaglandin formation from arachidonate	arachidonate				
RE3449	Prostaglandin formation from arachidonate	arachidonate				
RE2068	Prostaglandin formation from arachidonate	glycerol	↑	1.05E+04	33784.016	44244.974
RE2067	Prostaglandin formation from arachidonate	glycerol				
R01072	Purine metabolism	glutamine	↑	5.41E+06	3.63E+05	5.77E+06
R01231	Purine metabolism	glutamine				
R01135	Purine metabolism	asparate	↓	-3.71E+06	8.13E+06	4.42E+06
R01083	Purine metabolism	fumarate	↑	1.43E+06	2.43E+05	1.67E+06
R02422	Purine metabolism	urea	↑	7.46E+05	75710.785	821237.285
R01876	Pyrimidine metabolism	uridine	↓	-5.35E+04	9.51E+04	4.16E+04
R02327	Pyrimidine metabolism	uridine				
R02097	Pyrimidine metabolism	uridine				
R00970	Pyrimidine metabolism	uridine				
R01549	Pyrimidine metabolism	uridine				
R01880	Pyrimidine metabolism	uridine				
R02332	Pyrimidine metabolism	uridine				
R00964	Pyrimidine metabolism	uridine				
R00963	Pyrimidine metabolism	uridine				
R00967	Pyrimidine metabolism	uridine				
R00968	Pyrimidine metabolism	uridine				
R01878	Pyrimidine metabolism	uridine				

R00575	Pyrimidine metabolism	glutamine	↑	5.41E+06	3.63E+05	5.77E+06
R01397	Pyrimidine metabolism	asparate	↓	-3.71E+06	8.13E+06	4.42E+06
R01274	Saturated fatty acids beta-oxidation	palmitate	↓	-7.76E+05	4.21E+06	3.43E+06
R00342	TCA cycle	malate	↑	1.72E+05	6.31E+04	2.35E+05
R00362	TCA cycle	acetate	↓	-2.09E+04	4.78E+04	2.69E+04
R00412	TCA cycle	fumarate	↑	1.43E+06	2.43E+05	1.67E+06
R01082	TCA cycle	fumarate				
R00408	TCA cycle	fumarate				
R02164	TCA cycle	fumarate				
R00268	TCA cycle	a-ketoglutarate	↑	9.19E+04	14112.359	106009.21
RE0361	TCA cycle	a-ketoglutarate				
R00621	TCA cycle	a-ketoglutarate				
R00709	TCA cycle	a-ketoglutarate				
R01795	Tyrosine metabolism	tyrosine	↑	1.12E+06	7.58E+05	1.88E+06
RE3062	Tyrosine metabolism	tyrosine				
RE0026	Tyrosine metabolism	tyrosine				
R00734	Tyrosine metabolism	tyrosine				
R02078	Tyrosine metabolism	tyrosine				
RE1465	Tyrosine metabolism	tyrosine				
R00736	Tyrosine metabolism	tyrosine				
RE0941	Tyrosine metabolism	tyrosine				
R01815	Tyrosine metabolism	tyrosine				
R00729	Tyrosine metabolism	tyrosine				
R02918	Tyrosine metabolism	tyrosine				
R03539	Tyrosine metabolism	tyrosine				
R00731	Tyrosine metabolism	tyrosine				
R01364	Tyrosine metabolism	fumarate	↑	1.43E+06	2.43E+05	1.67E+06
R00692	Tyrosine metabolism	phenylalanine	↑	4.06E+05	3.10E+05	7.17E+05

R03660	Tyrosine metabolism	phenylalanine				
R00689	Tyrosine metabolism	phenylalanine				
R00694	Tyrosine metabolism	phenylalanine				
R00698	Tyrosine metabolism	phenylalanine				
R00699	Tyrosine metabolism	phenylalanine				
R02382	Tyrosine metabolism	tyramine	↓	-2.67E+04	31646.636	4927.352
R02383	Tyrosine metabolism	tyramine				
RE2124	Tyrosine metabolism	tyramine				
RE2781	Tyrosine metabolism	tyramine				
R00261	Urea cycle and metabolism of arginine, proline, glutamate, aspartate and asparagine	4-aminobutanoate	↑	36077.002	37757.204	73834.206
R01648	Urea cycle and metabolism of arginine, proline, glutamate, aspartate and asparagine	4-aminobutanoate				
R01986	Urea cycle and metabolism of arginine, proline, glutamate, aspartate and asparagine	4-aminobutanoate				
R02549	Urea cycle and metabolism of arginine, proline, glutamate, aspartate and asparagine	4-aminobutanoate				
R01987	Urea cycle and metabolism of arginine, proline, glutamate, aspartate and asparagine	4-aminobutanoate				
R00243	Urea cycle and metabolism of arginine, proline, glutamate, aspartate and asparagine	a-ketoglutarate	↑	91896.851	14112.359	106009.21
R01248	Urea cycle and metabolism of arginine, proline, glutamate, aspartate and asparagine	a-ketoglutarate				
R00248	Urea cycle and metabolism of arginine, proline, glutamate, aspartate and asparagine	a-ketoglutarate				
R00270	Urea cycle and metabolism of arginine, proline, glutamate, aspartate and asparagine	a-ketoglutarate				
R00258	Urea cycle and metabolism of arginine, proline, glutamate, aspartate and asparagine	a-ketoglutarate				
R03534	Urea cycle and metabolism of arginine, proline, glutamate, aspartate and asparagine	a-ketoglutarate				
R00578	Urea cycle and metabolism of arginine, proline, glutamate, aspartate and asparagine	asparate & glutamine	↓	-3.71E+06	8.13E+06	4.42E+06

R03421	Urea cycle and metabolism of arginine, proline, glutamate, aspartate and asparagine	asparate				
R00526	Urea cycle and metabolism of arginine, proline, glutamate, aspartate and asparagine	asparate				
R05577	Urea cycle and metabolism of arginine, proline, glutamate, aspartate and asparagine	asparate				
R03647	Urea cycle and metabolism of arginine, proline, glutamate, aspartate and asparagine	asparate				
R00357	Urea cycle and metabolism of arginine, proline, glutamate, aspartate and asparagine	asparate				
R00488	Urea cycle and metabolism of arginine, proline, glutamate, aspartate and asparagine	asparate				
R00355	Urea cycle and metabolism of arginine, proline, glutamate, aspartate and asparagine	asparate				
R01954	Urea cycle and metabolism of arginine, proline, glutamate, aspartate and asparagine	asparate				
R01251	Urea cycle and metabolism of arginine, proline, glutamate, aspartate and asparagine	asparate				
R00489	Urea cycle and metabolism of arginine, proline, glutamate, aspartate and asparagine	asparate				
R00253	Urea cycle and metabolism of arginine, proline, glutamate, aspartate and asparagine	glutamine	↑	5.41E+06	3.63E+05	5.77E+06
R00256	Urea cycle and metabolism of arginine, proline, glutamate, aspartate and asparagine	glutamine				
R03652	Urea cycle and metabolism of arginine, proline, glutamate, aspartate and asparagine	glutamine				
R00667	Urea cycle and metabolism of arginine, proline, glutamate, aspartate and asparagine	ornithine	↓	-113645.303	302159.156	188513.853
R00669	Urea cycle and metabolism of arginine, proline, glutamate, aspartate and asparagine	ornithine				
R01398	Urea cycle and metabolism of arginine, proline, glutamate, aspartate and asparagine	ornithine				
R00135	Urea cycle and metabolism of arginine, proline, glutamate, aspartate and asparagine	proline	↑	50577.225	26032.511	76609.736
R03661	Urea cycle and metabolism of arginine, proline, glutamate, aspartate and asparagine	proline				
R01252	Urea cycle and metabolism of arginine, proline, glutamate, aspartate and	proline				

	asparagine					
RE1537	Urea cycle and metabolism of arginine, proline, glutamate, aspartate and asparagine	putrescine				
R01920	Urea cycle and metabolism of arginine, proline, glutamate, aspartate and asparagine	putrescine				
R01989	Urea cycle and metabolism of arginine, proline, glutamate, aspartate and asparagine	putrescine & 4-aminobutanoate				
R01151	Urea cycle and metabolism of arginine, proline, glutamate, aspartate and asparagine	putrescine				
R01154	Urea cycle and metabolism of arginine, proline, glutamate, aspartate and asparagine	putrescine				
R01157	Urea cycle and metabolism of arginine, proline, glutamate, aspartate and asparagine	putrescine				
R00670	Urea cycle and metabolism of arginine, proline, glutamate, aspartate and asparagine	putrescine				
R01086	Urea cycle and metabolism of arginine, proline, glutamate, aspartate and asparagine	fumarate	↑	1.43E+06	2.43E+05	1.67E+06
R00497	Urea cycle and metabolism of arginine, proline, glutamate, aspartate and asparagine	glycine	↑	4.49E+06	730562.804	5222233.54
R04951	Urea cycle and metabolism of arginine, proline, glutamate, aspartate and asparagine	glycine				
R00551	Urea cycle and metabolism of arginine, proline, glutamate, aspartate and asparagine	urea	↑	7.46E+05	75710.785	821237.285
R03648	Urea cycle and metabolism of arginine, proline, glutamate, aspartate and asparagine	asparagine	↑	4.03E+03	8265.44	12295.035
RE2032	Urea cycle and metabolism of arginine, proline, glutamate, aspartate and asparagine	asparagine				
RE2644	Urea cycle and metabolism of arginine, proline, glutamate, aspartate and asparagine	asparagine				
R03657	Valine, leucine and isoleucine degradation	leucine	↑	2.75E+06	2.95E+06	5.69E+06
R01090	Valine, leucine and isoleucine degradation	leucine				
R03665	Valine, leucine and isoleucine degradation	valine	↑	1.62E+06	2.60E+06	4.22E+06
R01214	Valine, leucine and isoleucine degradation	valine				

R01360	Valine, leucine and isoleucine degradation	acetoacetate	↑	3.40E+03	6727.541	10130.481
R00257	Vitamin B3 (nicotinate and nicotinamide) metabolism	glutamine	↑	5.41E+06	3.63E+05	5.77E+06

Appendix F

List of Pathways Identified by Metscape Analysis from 7 mM glucose to 17 mM Glucose with Reactions, Seeds Involved, Direction of Change and Peak Areas

Reaction	Pathway	seed	Direction of Change	Average Peak Area		
				17 mM - 7 mM	7 mM	17 mM
R00768	Aminosugars metabolism	glutamine	↓	-1.15E+07	1.61E+07	4.59E+06
R07041	Arachidonic acid metabolism	arachidonate	↑	1.34E+04	3.15E+04	4.49E+04
R01593	Arachidonic acid metabolism	arachidonate				
RE3651	Arachidonic acid metabolism	arachidonate				
R07046	Arachidonic acid metabolism	arachidonate				
R07051	Arachidonic acid metabolism	arachidonate				
RE3287	Arachidonic acid metabolism	arachidonate				
R01317	Arachidonic acid metabolism	arachidonate				
RE3650	Arachidonic acid metabolism	arachidonate				
RE3288	Arachidonic acid metabolism	arachidonate				
R07048	Arachidonic acid metabolism	arachidonate				
R07050	Arachidonic acid metabolism	arachidonate				
RE3646	Arachidonic acid metabolism	arachidonate				
RE3042	Arachidonic acid metabolism	arachidonate				
RE3649	Arachidonic acid metabolism	arachidonate				
RE3286	Arachidonic acid metabolism	arachidonate				
RE3654	Arachidonic acid metabolism	arachidonate				
RE3647	Arachidonic acid metabolism	arachidonate				
RE3653	Arachidonic acid metabolism	arachidonate				
R01596	Arachidonic acid metabolism	arachidonate				
RE3648	Arachidonic acid metabolism	arachidonate				
RE3289	Arachidonic acid metabolism	arachidonate				
R07054	Arachidonic acid metabolism	arachidonate				
R07052	Arachidonic acid metabolism	arachidonate				
RE2563	Arachidonic acid metabolism	glycerol	↑	1.41E+04	30179.373	44244.974

RE2754	Arachidonic acid metabolism	glycerol				
RE2638	Bile acid biosynthesis	glycine	↓	-7.43E+04	1.70E+05	9.61E+04
R03718	Bile acid biosynthesis	glycine				
RE2649	Bile acid biosynthesis	propanoate	↑	1.86E+06	3.35E+06	5.21E+06
RE2650	Biopterin metabolism	tyrosine	↑	9.72E+05	9.05E+05	1.88E+06
R01357	Butanoate metabolism	acetoacetate	↑	3.47E+03	6655.777	10130.481
R00410	Butanoate metabolism	acetoacetate				
R01361	Butanoate metabolism	acetoacetate				
R01176	Butanoate metabolism	butanoate	↓	-7.91E+05	1.62E+06	8.29E+05
	De novo fatty acid biosynthesis	stearate	↑	1.02E+03	15157.211	16176.875
RE1575	De novo fatty acid biosynthesis	lauric acid	↑	7.52E+03	4.26E+03	1.18E+04
RE1514	Di-unsaturated fatty acid beta-oxidation	linoleate	↓	-5.73E+04	2.39E+05	1.81E+05
R00866	Fructose and mannose metabolism	d-fructose	↑	9.35E+03	10660.345	20009.769
R00875	Fructose and mannose metabolism	d-fructose				
RE2783	Fructose and mannose metabolism	d-fructose				
R00867	Fructose and mannose metabolism	d-fructose				
R01326	Fructose and mannose metabolism	d-mannose	↓	-1.96E+04	2.84E+04	8.84E+03
R01105	Galactose metabolism	d-galactose	↓	-4.03E+06	8.11E+06	4.08E+06
R01101	Galactose metabolism	d-galactose				
R01678	Galactose metabolism	d-galactose				
R01095	Galactose metabolism	d-galactose				
R01329	Galactose metabolism	d-galactose				
		& d-mannose	↓	-1.96E+04	2.84E+04	8.84E+03
R02926	Galactose metabolism	d-galactose				
R03634	Galactose metabolism	d-galactose				
R05549	Galactose metabolism	d-galactose				
R01092	Galactose metabolism	d-galactose				
R01104	Galactose metabolism	d-galactose				

R01093	Galactose metabolism	d-galactose				
R01103	Galactose metabolism	d-galactose				
		& sucrose	↓	-3.74E+03	1.34E+04	9.63E+03
R01100	Galactose metabolism	d-galactose				
RE3301	Glycerophospholipid metabolism	serine	↑	9.65E+05	1.23E+06	2.20E+06
RE3298	Glycerophospholipid metabolism	serine				
RE3299	Glycerophospholipid metabolism	serine				
R01351	Glycerophospholipid metabolism	glycerol	↑	1.41E+04	30179.373	44244.974
R01352	Glycerophospholipid metabolism	glycerol				
R01350	Glycerophospholipid metabolism	glycerol				
RE3507	Glycerophospholipid metabolism	glycerol				
R01041	Glycerophospholipid metabolism	glycerol				
R03616	Glycerophospholipid metabolism	glycerol				
R00847	Glycerophospholipid metabolism	glycerol				
R01036	Glycerophospholipid metabolism	glycerol				
R04452	Glycerophospholipid metabolism	acetate	↓	-5.98E+03	4.09E+04	3.49E+04
R03038	Glycine, serine, alanine and threonine metabolism	alanine	↓	-9.79E+04	1.59E+05	6.07E+04
RE2642	Glycine, serine, alanine and threonine metabolism	alanine				
RE1473	Glycine, serine, alanine and threonine metabolism	alanine				
RE2031	Glycine, serine, alanine and threonine metabolism	alanine				
R00369	Glycine, serine, alanine and threonine metabolism	alanine				
RE2429	Glycine, serine, alanine and threonine metabolism	glycine	↓	-7.43E+04	1.70E+05	9.61E+04
R03654	Glycine, serine, alanine and threonine metabolism	glycine				
R00366	Glycine, serine, alanine and threonine metabolism	glycine				
		& glyoxylate				
RE2111	Glycine, serine, alanine and threonine metabolism	glycine				
R06171	Glycine, serine, alanine and threonine metabolism	glycine				
RE2117	Glycine, serine, alanine and threonine metabolism	glycine				

R00367	Glycine, serine, alanine and threonine metabolism	glycine				
RE2427	Glycine, serine, alanine and threonine metabolism	glycine				
R00945	Glycine, serine, alanine and threonine metabolism	glycine				
		& serine				
RE2428	Glycine, serine, alanine and threonine metabolism	glycine				
R00751	Glycine, serine, alanine and threonine metabolism	glycine				
		& threonine	↑	2.32E+05	5.35E+05	7.67E+05
R00610	Glycine, serine, alanine and threonine metabolism	glycine				
R01221	Glycine, serine, alanine and threonine metabolism	glycine				
R00565	Glycine, serine, alanine and threonine metabolism	glycine				
R00611	Glycine, serine, alanine and threonine metabolism	glycine				
R03425	Glycine, serine, alanine and threonine metabolism	glycine				
R00371	Glycine, serine, alanine and threonine metabolism	glycine				
R00465	Glycine, serine, alanine and threonine metabolism	glyoxylate	↑	7.38E+04	6.98E+04	1.44E+05
R00475	Glycine, serine, alanine and threonine metabolism	glyoxylate				
R00717	Glycine, serine, alanine and threonine metabolism	glyoxylate				
RO2821	Glycine, serine, alanine and threonine metabolism	methionine	↑	1.51E+05	118295.916	269211.712
R00704	Glycine, serine, alanine and threonine metabolism	pyruvate	↑	185057.809	240399.287	425457.096
R03662	Glycine, serine, alanine and threonine metabolism	serine	↑	9.65E+05	1.23E+06	2.20E+06
R00582	Glycine, serine, alanine and threonine metabolism	serine				
R00585	Glycine, serine, alanine and threonine metabolism	serine				
R00220	Glycine, serine, alanine and threonine metabolism	serine				
R03663	Glycine, serine, alanine and threonine metabolism	threonine				
R00317	Glycolysis and Gluconeogenesis	acetate	↓	-5.98E+03	4.09E+04	3.49E+04
R00711	Glycolysis and Gluconeogenesis	acetate				
R00316	Glycolysis and Gluconeogenesis	acetate				
R00235	Glycolysis and Gluconeogenesis	acetate				
R00710	Glycolysis and Gluconeogenesis	acetate				

R00227	Glycolysis and Gluconeogenesis	acetate				
R00196	Glycolysis and Gluconeogenesis	pyruvate	↑	185057.809	240399.287	425457.096
R00006	Glycolysis and Gluconeogenesis	pyruvate				
R00014	Glycolysis and Gluconeogenesis	pyruvate				
R00200	Glycolysis and Gluconeogenesis	pyruvate				
R00209	Glycolysis and Gluconeogenesis	pyruvate				
R00210	Glycolysis and Gluconeogenesis	pyruvate				
R00214	Glycolysis and Gluconeogenesis	pyruvate				
R00216	Glycolysis and Gluconeogenesis	pyruvate				
R00344	Glycolysis and Gluconeogenesis	pyruvate				
R00703	Glycolysis and Gluconeogenesis	pyruvate				
R01699	Glycolysis and Gluconeogenesis	pyruvate				
RE2717	Glycosphingolipid metabolism	d-galactose	↓	-4.03E+06	8.11E+06	4.08E+06
R01281	Glycosphingolipid metabolism	serine	↑	9.65E+05	1.23E+06	2.20E+06
RE3632	Histidine metabolism	glycine	↓	-7.43E+04	1.70E+05	9.61E+04
R01595	Leukotriene metabolism	arachidonate	↑	1.34E+04	3.15E+04	4.49E+04
RE0596	Leukotriene metabolism	glycine	↓	-7.43E+04	1.70E+05	9.61E+04
RE1821	Leukotriene metabolism	glycine				
RE3417	Linoleate metabolism	azelaic acid	↑	1.89E+04	5.48E+04	7.37E+04
RE3420	Linoleate metabolism	azelaic acid				
R07063	Linoleate metabolism	linoleate	↓	-5.73E+04	2.39E+05	1.81E+05
RE3409	Linoleate metabolism	linoleate				
R07056	Linoleate metabolism	linoleate				
R07057	Linoleate metabolism	linoleate				
R07055	Linoleate metabolism	linoleate				
R03626	Linoleate metabolism	linoleate				
R07064	Linoleate metabolism	linoleate				
RE3411	Linoleate metabolism	nonanoate	↑	1.99E+04	62086.16	82035.258

R02201	Lysine metabolism	pipecolate	↓	-226936.216	574259.195	347322.979
R02205	Lysine metabolism	pipecolate				
R02203	Lysine metabolism	pipecolate				
R02204	Lysine metabolism	pipecolate				
R03284	Lysine metabolism	glycine	↓	-7.43E+04	1.70E+05	9.61E+04
R00652	Methionine and cysteine metabolism	glycine	↓	-7.43E+04	1.70E+05	9.61E+04
		& methionine	↑	1.51E+05	118295.916	269211.712
R00892	Methionine and cysteine metabolism	cysteine	↑	1.27E+05	209254.529	336439.947
RE2811	Methionine and cysteine metabolism	cysteine				
R01001	Methionine and cysteine metabolism	cysteine				
RE2223	Methionine and cysteine metabolism	cysteine				
R00893	Methionine and cysteine metabolism	cysteine				
R00782	Methionine and cysteine metabolism	cysteine				
R03650	Methionine and cysteine metabolism	cysteine				
R00896	Methionine and cysteine metabolism	cysteine				
R00946	Methionine and cysteine metabolism	methionine				
RE2030	Methionine and cysteine metabolism	methionine				
R00648	Methionine and cysteine metabolism	methionine				
R00177	Methionine and cysteine metabolism	methionine				
R03659	Methionine and cysteine metabolism	methionine				
RE2640	Methionine and cysteine metabolism	methionine				
R03105	Methionine and cysteine metabolism	pyruvate	↑	185057.809	240399.287	425457.096
R00590	Methionine and cysteine metabolism	serine	↑	9.65E+05	1.23E+06	2.20E+06
R01290	Methionine and cysteine metabolism	serine				
R00891	Methionine and cysteine metabolism	serine				
		& cysteine				
R01289	Methionine and cysteine metabolism	serine				
RE0324	Omega-6 fatty acid metabolism	arachidonate	↑	1.34E+04	3.15E+04	4.49E+04

RE0124	Pentose phosphate pathway	d-gluconic acid	↑	3.60E+03	4546.984	8144.155
R01641	Pentose phosphate pathway	ribose-5-phospate	↓	-1.25E+04	8.04E+04	6.79E+04
R06590	Pentose phosphate pathway	ribose-5-phospate				
R01057	Pentose phosphate pathway	ribose-5-phospate				
R01051	Pentose phosphate pathway	ribose-5-phospate				
R01054	Pentose phosphate pathway	ribose-5-phospate				
R01056	Pentose phosphate pathway	ribose-5-phospate				
R01049	Pentose phosphate pathway	ribose-5-phospate				
R01520	Pentose phosphate pathway	d-glucono-1,5-lactone	↑	2.43E+03	6.22E+03	8.65E+03
R01521	Pentose phosphate pathway	d-glucono-1,5-lactone				
R01194	Phosphatidylinositol phosphate metabolism	d-galactose	↓	-4.03E+06	8.11E+06	4.08E+06
R03331	Phosphatidylinositol phosphate metabolism	glycerol	↑	1.41E+04	30179.373	44244.974
R00830	Porphyrin metabolism	glycine	↓	-7.43E+04	1.70E+05	9.61E+04
R00831	Porphyrin metabolism	glycine				
R01354	Propanoate metabolism	propanoate	↑	1.86E+06	3.35E+06	5.21E+06
R01590	Prostaglandin formation from arachidonate	arachidonate	↑	1.34E+04	3.15E+04	4.49E+04
RE3449	Prostaglandin formation from arachidonate	arachidonate				
RE3452	Prostaglandin formation from arachidonate	arachidonate				
RE3455	Prostaglandin formation from arachidonate	arachidonate				
RE1978	Prostaglandin formation from arachidonate	arachidonate				
RE3458	Prostaglandin formation from arachidonate	arachidonate				
RE2067	Prostaglandin formation from arachidonate	glycerol	↑	1.41E+04	30179.373	44244.974
RE2068	Prostaglandin formation from arachidonate	glycerol				
R01231	Purine metabolism	glutamine	↓	-1.15E+07	1.61E+07	4.59E+06
R01072	Purine metabolism	glutamine				
R01083	Purine metabolism	fumarate	↑	6.19E+05	1.05E+06	1.67E+06
R01135	Purine metabolism	aspartate	↓	-3.14E+06	5.78E+06	2.64E+06

R00575	Pyrimidine metabolism	glutamine	↓	-1.15E+07	1.61E+07	4.59E+06
R01397	Pyrimidine metabolism	aspartate	↓	-3.14E+06	5.78E+06	2.64E+06
R02327	Pyrimidine metabolism	uridine	↓	-1.70E+04	5.54E+04	3.84E+04
R01880	Pyrimidine metabolism	uridine				
R00963	Pyrimidine metabolism	uridine				
R00967	Pyrimidine metabolism	uridine				
R01878	Pyrimidine metabolism	uridine				
R00970	Pyrimidine metabolism	uridine				
R01549	Pyrimidine metabolism	uridine				
R01876	Pyrimidine metabolism	uridine				
R00964	Pyrimidine metabolism	uridine				
R02097	Pyrimidine metabolism	uridine				
R00968	Pyrimidine metabolism	uridine				
R02332	Pyrimidine metabolism	uridine				
R02164	TCA cycle	fumarate	↑	6.19E+05	1.05E+06	1.67E+06
R01082	TCA cycle	fumarate & malate				
R00408	TCA cycle	fumarate				
R00412	TCA cycle	fumarate				
R00268	TCA cycle	a-ketoglutarate	↑	5.10E+04	5.93E+04	1.10E+05
R00709	TCA cycle	a-ketoglutarate				
RE0361	TCA cycle	a-ketoglutarate				
R00621	TCA cycle	a-ketoglutarate				
R00362	TCA cycle	acetate	↓	-5.98E+03	4.09E+04	3.49E+04
R01364	Tyrosine metabolism	glutamine	↓	-1.15E+07	1.61E+07	4.59E+06
RE0941	Tyrosine metabolism	glutamine				
R02918	Tyrosine metabolism	glutamine				
RE3062	Tyrosine metabolism	glutamine				

R00731	Tyrosine metabolism	glutamine				
R01815	Tyrosine metabolism	glutamine				
R00734	Tyrosine metabolism	glutamine				
R02078	Tyrosine metabolism	glutamine				
RE0026	Tyrosine metabolism	glutamine				
R00729	Tyrosine metabolism	glutamine				
R03539	Tyrosine metabolism	glutamine				
R03660	Tyrosine metabolism	phenylalanine	↑	2.78E+05	3.31E+05	6.09E+05
R00694	Tyrosine metabolism	phenylalanine				
R00698	Tyrosine metabolism	phenylalanine				
R00699	Tyrosine metabolism	phenylalanine				
R00692	Tyrosine metabolism	phenylalanine				
RE1465	Tyrosine metabolism	phenylalanine				
R00689	Tyrosine metabolism	phenylalanine				
R01795	Tyrosine metabolism	phenylalanine				
R00736	Tyrosine metabolism	tyrosine	↑	9.72E+05	9.05E+05	1.88E+06
R04880	Tyrosine metabolism	3,4-dihydroxyphenoletheneglycol	↑	1.55E+04	20282.07	35816.138
R04881	Tyrosine metabolism	3,4-dihydroxyphenoletheneglycol				
RE1915	Tyrosine metabolism	cysteine	↑	1.27E+05	209254.529	336439.947
RE1919	Tyrosine metabolism	pyruvate	↑	185057.809	240399.287	425457.096
R02743	Urea cycle and metabolism of arginine, proline, glutamate, aspartate and asparagine	5-oxoproline	↑	4.04E+05	1.25E+05	5.29E+05
R03749	Urea cycle and metabolism of arginine, proline, glutamate, aspartate and asparagine	5-oxoproline				
R00251	Urea cycle and metabolism of arginine, proline, glutamate, aspartate and asparagine	5-oxoproline				
R03534	Urea cycle and metabolism of arginine, proline, glutamate, aspartate and asparagine	a-ketoglutarate	↑	5.10E+04	5.93E+04	1.10E+05

R00243	Urea cycle and metabolism of arginine, proline, glutamate, aspartate and asparagine	a-ketoglutarate				
R00355	Urea cycle and metabolism of arginine, proline, glutamate, aspartate and asparagine	a-ketoglutarate & aspartate				
R00270	Urea cycle and metabolism of arginine, proline, glutamate, aspartate and asparagine	a-ketoglutarate				
R00258	Urea cycle and metabolism of arginine, proline, glutamate, aspartate and asparagine	a-ketoglutarate & alanine	↓	-9.79E+04	1.59E+05	6.07E+04
R00248	Urea cycle and metabolism of arginine, proline, glutamate, aspartate and asparagine	a-ketoglutarate				
R05577	Urea cycle and metabolism of arginine, proline, glutamate, aspartate and asparagine	aspartate	↓	-3.14E+06	5.78E+06	2.64E+06
R00488	Urea cycle and metabolism of arginine, proline, glutamate, aspartate and asparagine	aspartate				
R01954	Urea cycle and metabolism of arginine, proline, glutamate, aspartate and asparagine	aspartate				
R00526	Urea cycle and metabolism of arginine, proline, glutamate, aspartate and asparagine	aspartate				
R03421	Urea cycle and metabolism of arginine, proline, glutamate, aspartate and asparagine	aspartate				
R00489	Urea cycle and metabolism of arginine, proline, glutamate, aspartate and asparagine	aspartate				
R03647	Urea cycle and metabolism of arginine, proline, glutamate, aspartate and asparagine	aspartate				
R00578	Urea cycle and metabolism of arginine, proline, glutamate, aspartate and asparagine	aspartate & glutamine				
R00357	Urea cycle and metabolism of arginine, proline, glutamate, aspartate and asparagine	aspartate				
R01086	Urea cycle and metabolism of arginine, proline, glutamate, aspartate and asparagine	fumarate	↑	6.19E+05	1.05E+06	1.67E+06
R00253	Urea cycle and metabolism of arginine, proline, glutamate, aspartate and asparagine	glutamine	↓	-1.15E+07	1.61E+07	4.59E+06
R00256	Urea cycle and metabolism of arginine, proline, glutamate,	glutamine				

	aspartate and asparagine					
R03652	Urea cycle and metabolism of arginine, proline, glutamate, aspartate and asparagine	glutamine				
R00497	Urea cycle and metabolism of arginine, proline, glutamate, aspartate and asparagine	glycine	↓	-7.43E+04	1.70E+05	9.61E+04
R04951	Urea cycle and metabolism of arginine, proline, glutamate, aspartate and asparagine	glycine				
R00894	Urea cycle and metabolism of arginine, proline, glutamate, aspartate and asparagine	cysteine	↑	1.27E+05	209254.529	336439.947
R00899	Urea cycle and metabolism of arginine, proline, glutamate, aspartate and asparagine	cysteine				
R03648	Urea cycle and metabolism of arginine, proline, glutamate, aspartate and asparagine	asparagine	↓	-6537.452	21844.953	15307.501
RE2032	Urea cycle and metabolism of arginine, proline, glutamate, aspartate and asparagine	asparagine				
RE2644	Urea cycle and metabolism of arginine, proline, glutamate, aspartate and asparagine	asparagine				
R03657	Valine, leucine and isoleucine degradation	leucine	↑	2.36E+06	3.33E+06	5.69E+06
R01090	Valine, leucine and isoleucine degradation	leucine				
R01214	Valine, leucine and isoleucine degradation	valine	↑	1.77E+04	2.50E+04	4.27E+04
R03665	Valine, leucine and isoleucine degradation	valine				
R01360	Valine, leucine and isoleucine degradation	acetoacetate	↑	3.47E+03	6655.777	10130.481
R00257	Vitamin B3 (nicotinate and nicotinamide) metabolism	glutamine	↓	-1.15E+07	1.61E+07	4.59E+06
R04233	Vitamin B5 - CoA biosynthesis from pantothenate	cysteine	↑	1.27E+05	209254.529	336439.947
R04230	Vitamin B5 - CoA biosynthesis from pantothenate	cysteine				

Appendix G

Location of Raw and Processed Data Files for Chapters 2 & 3

All raw data files for Chapters 2 and 3 are backed up on the lab hard drive in appropriately marked folders and remain on the Pegasus Computer. Additionally, all of the raw data files for Chapter 2 as well as archived versions of the data processing methods and references can be found on the hard drive provided for Bob. Archived information can be restored directly into ChromatTOF and used to process data without having to rewrite the methods if desired.

Processed Data Files

For additional ChromaTOF user information see the manual which can be accessed as a PDF by opening ChromaTOF as directed below and clicking help followed by ChromaTOF help.

Chapter 2

All processed chromatograms used for the metabolite profiling analysis are located on the Pegasus Workstation (Drive E) computer. To start the software, double click the gray Pegasus icon and click "login" (no password needed). On the left hand side, click "Acquired Samples." All of the processed chromatograms are in the folder labeled "3 to 7 to 17." An example sample name is as follows: 7mM A (5mVIIa):3 where 7 is the concentration of glucose, A is the plate identification, 5 is the page number in notebook mVII (m distinguishes the "metabolomics" notebooks from the "sapropel" notebooks) and a identifies the replicate on that page. The number after the colon is

added automatically by the software to distinguish samples with the same name. In this case, that would occur, for example, if the autosampler were to misfire and the run to be restarted with the same name.

Data was processed with both a 0.1 and 0.2 second peak width for the second dimension. Shown below is the method for the 0.2 second peak width and the box that should be changed to 0.1 for the 0.1 second method is highlighted in orange.

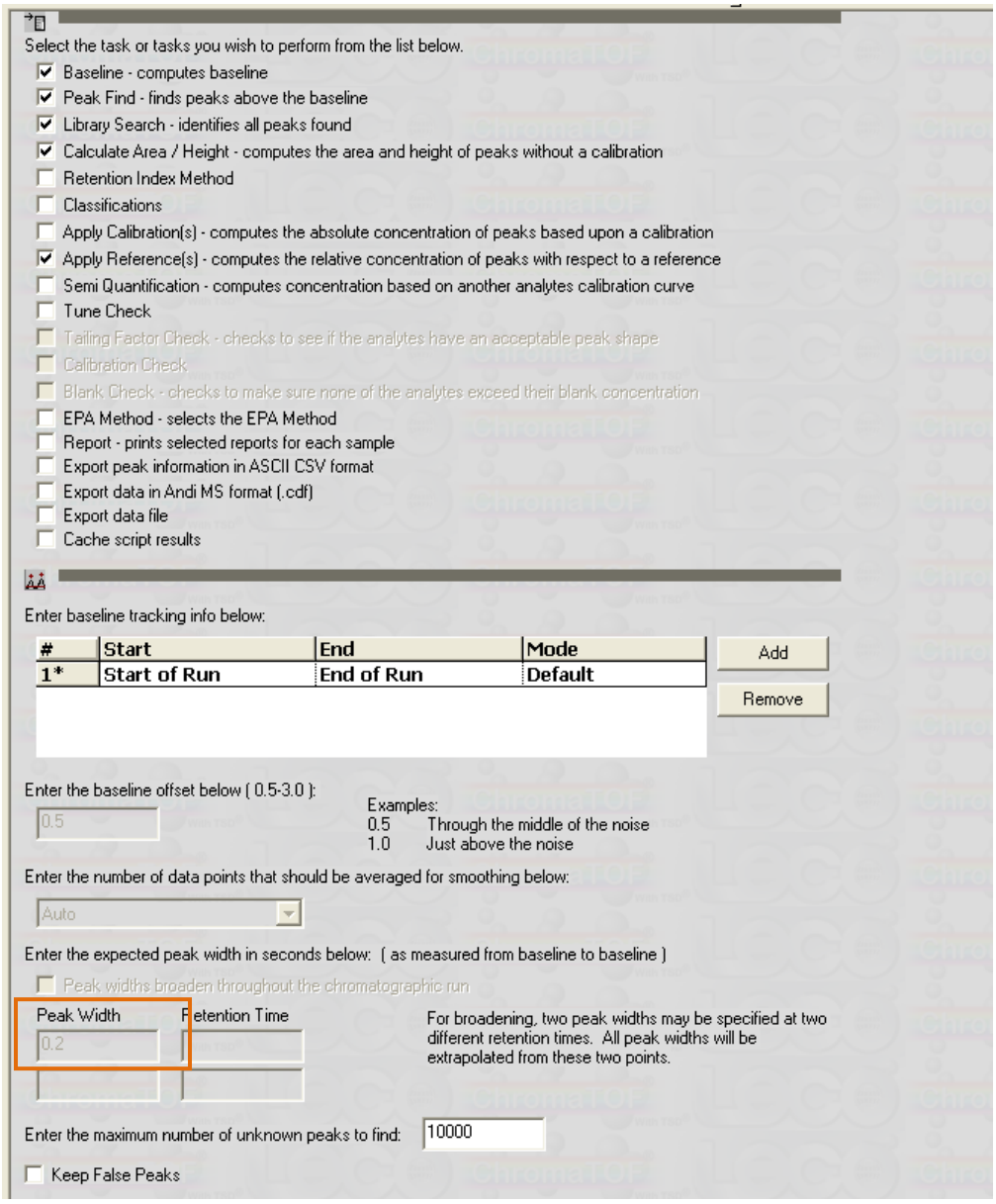

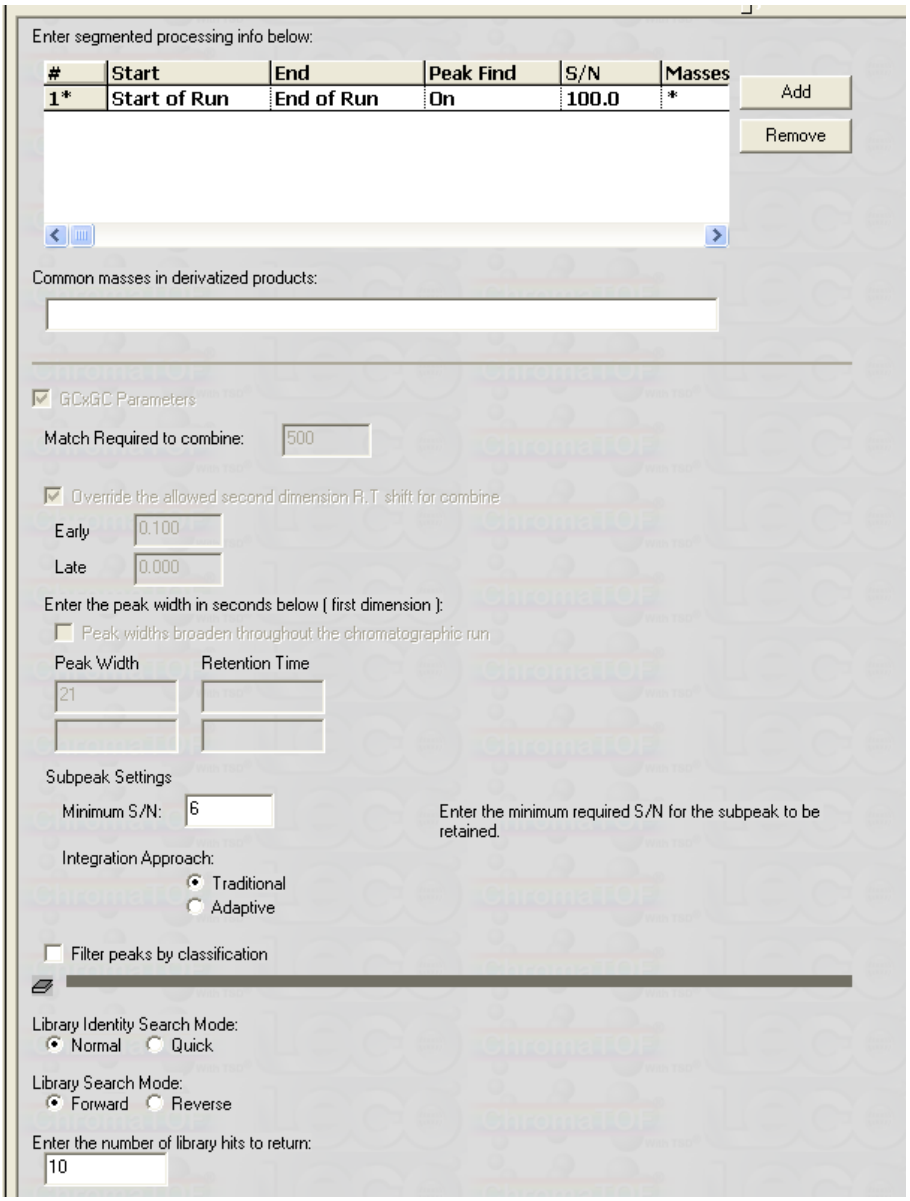
Enter segmented processing info below:
Start End Peak Find S/N Masses
1* Start of Run End of Run On 100.0 *
Add
Remove
Common masses in derivatized products:
GCxGC Parameters
Match Required to combine: 500
Override the allowed second dimension R.T shift for combine
Early 0.100
Late 0.000
Enter the peak width in seconds below (first dimension):
Peak widths broaden throughout the chromatographic run
Peak Width
Retention Time
21
Subpeak Settings
Minimum S/N: 6
Enter the minimum required S/N for the subpeak to be retained.
Integration Approach:
Traditional
Adaptive
Filter peaks by classification
Library Identity Search Mode:
Normal Quick
Library Search Mode:
Forward Reverse
Enter the number of library hits to return:
10

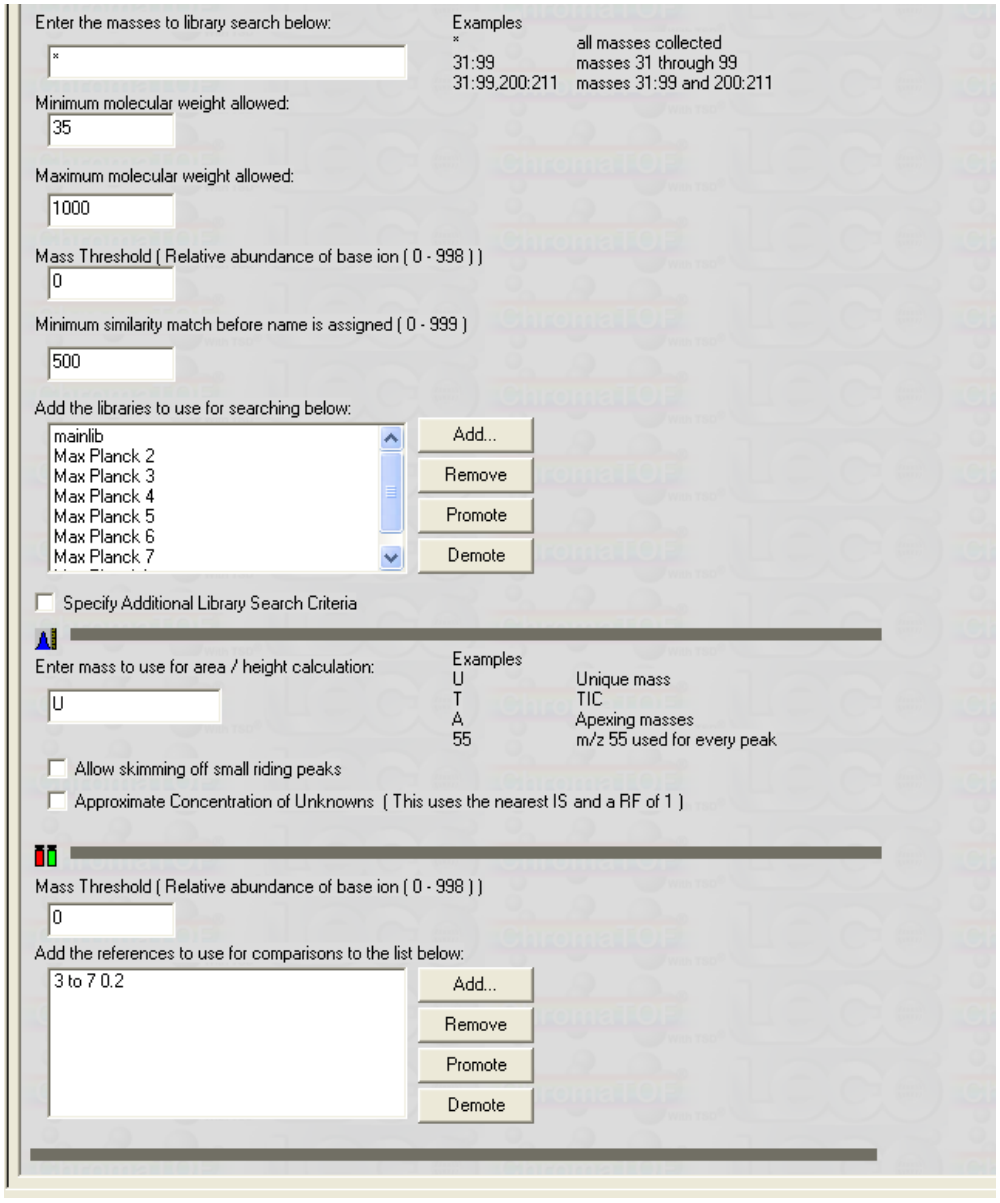

The reference "3 to 7 0.2" referred to above is a previously run chromatogram that has all of the target peaks identified with *. After processing, target analytes will also have * next to their identifications and the peak areas will all be calculated using the same m/z ratio. References must be processed using the exact same processing method (minus the reference) as the chromatogram for which they are added, therefore, there is a reference for the 0.2 second and the 0.1 second data processing methods. These can be found under

"References" on the left side of the screen when ChromaTOF is open. The references used in this work were calculated using a first dimension retention time deviation of 7 seconds (one modulation period) and a second dimension retention time deviation of 0.2 seconds.

The quant mass (or the m/z that the peak area is calculated at) of an analyte that was processed using a reference cannot be changed. Therefore, succinate and glucose are not included in the references. This way, the quant mass can be manually changed to calculate the area of both the labeled and unlabeled analyte. For more information on creating a reference see "Building a Reference" on page 5-125 of the manual.

Alanine, valine, proline, glycine, fumarate, threonine, malate, aspartate, phenylalanine, 3-phosphoglycerate, ornithine, tyrosine, ribose-5-phosphate, glucose-6-phosphate, succinate and methionine data were taken from the 0.2 second processing results. Lactate, pyruvate, leucine, isoleucine, serine, glutamate, lysine and glucose were taken from the 0.1 second data processing. The peak area, average peak areas, standard deviations, relative standard deviations and results of Q-tests can be found in the excel file "3,7,17 july" located in the "gly-tca data" folder on the desktop. All cells highlighted in dark red were deleted and if average values were not calculated, the plate was not included in the final data set. All of the files created for Chapter 2 are also included in this folder and the prism files used to complete one-way ANOVE analysis are located in the Chapter 2 subfolder.

Fisher Ratio Data

In order to calculate a Fisher Ratio, data sets must be placed into groups within the software. Because of the way the software works, once a file has been added to a

group, it cannot be added to a second group. In order to get around this, each data file was exported and then imported with a different number added to the end of the file name and then reprocessed. All files used for the Fisher Ratio analysis were only processed using the 0.2 second data processing method. The reprocessed files can be found in the "Fisher 3 to 7," "Fisher 3 to 17," "Fisher 7 to 17," and "Fisher 3 to 3" folders located under "Acquired Samples." The actual Fisher Ratio results can be located under "Statistical Compare" and are labeled as "3 to 7 (july)," "3 to 17 (july)," "7 to 17 (july)," and "3 to 3 (july)."

The gas chromatograph, mass spec and autosampler methods used to run the samples discussed in Chapter 2 follow.

Gas Chromatograph Method:

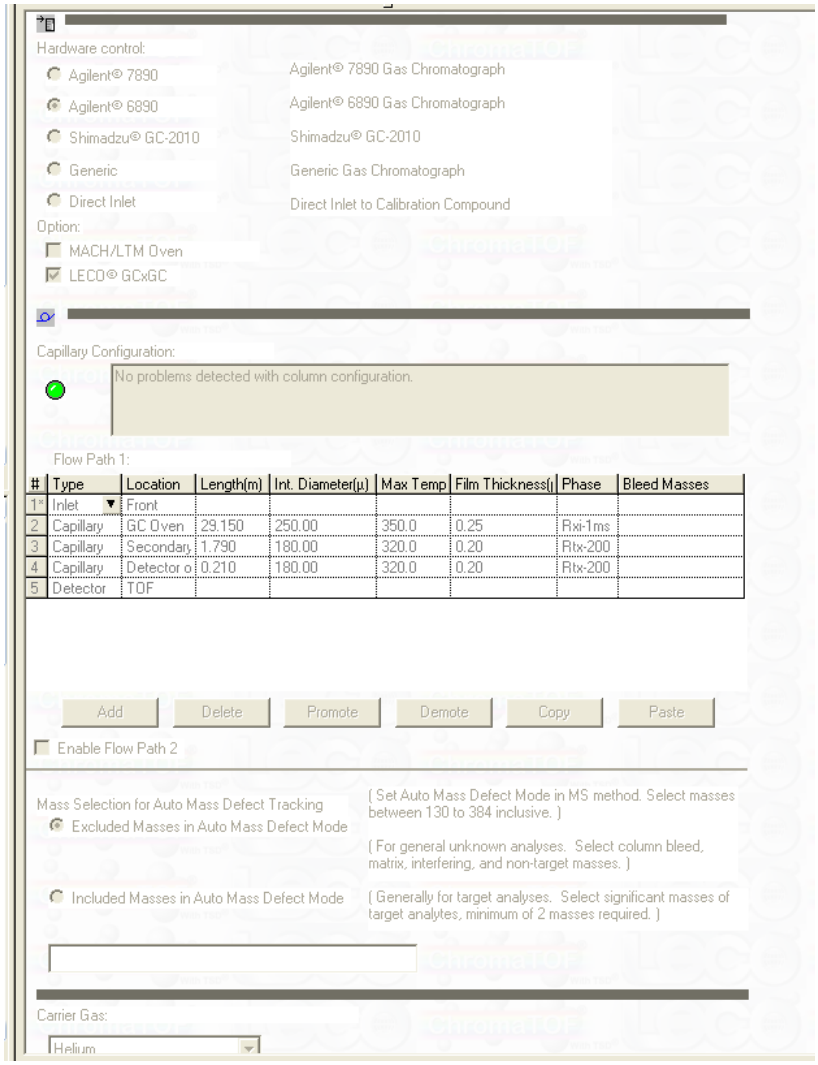

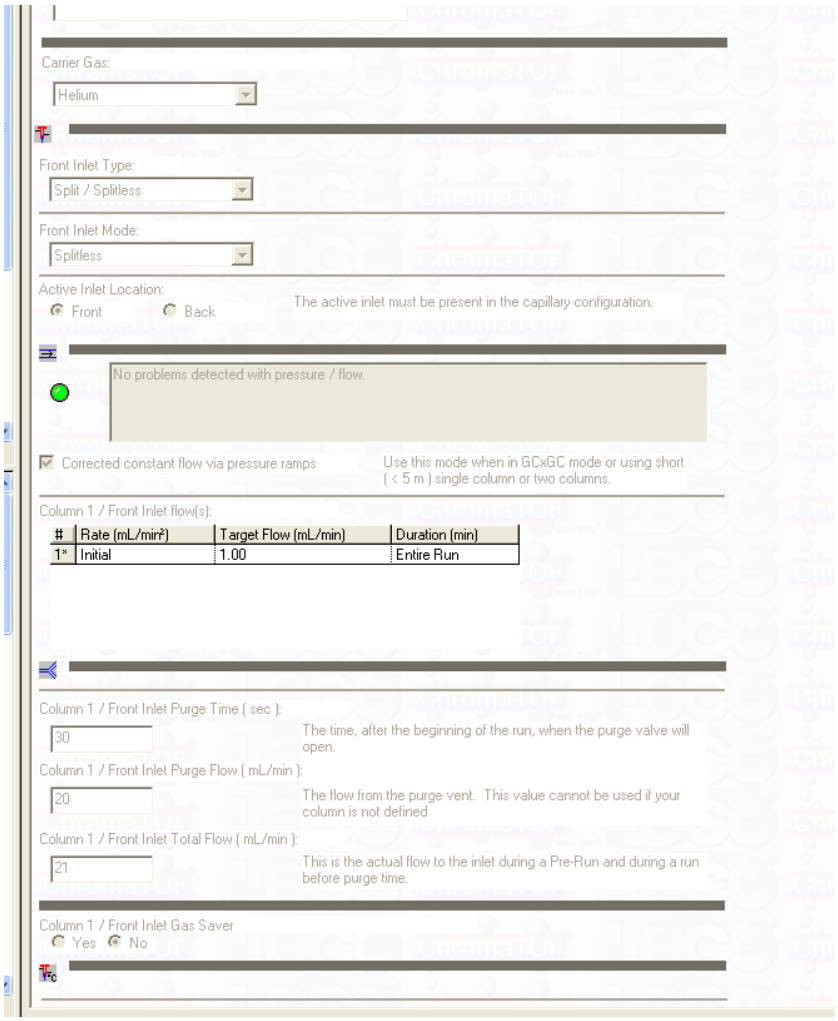
Carrier Gas:
Helium
Front Inlet Type:
Split / Splitless
Front Inlet Mode:
Splitless
Active Inlet Location:
Front
Back
The active inlet must be present in the capillary configuration.
No problems detected with pressure / flow.
Corrected constant flow via pressure ramps
Use this mode when in GCxGC mode or using short (< 5 m) single column or two columns.
Column 1 / Front Inlet flow(s):
| Rate (mL/min²) | Target Flow (mL/min) | Duration (min)
1* | Initial | 1.00 | Entire Run
Column 1 / Front Inlet Purge Time (sec):
30
The time, after the beginning of the run, when the purge valve will open.
Column 1 / Front Inlet Purge Flow (mL/min):
20
The flow from the purge vent. This value cannot be used if your column is not defined
Column 1 / Front Inlet Total Flow (mL/min):
21
This is the actual flow to the inlet during a Pre-Run and during a run before purge time.
Column 1 / Front Inlet Gas Saver
Yes
No

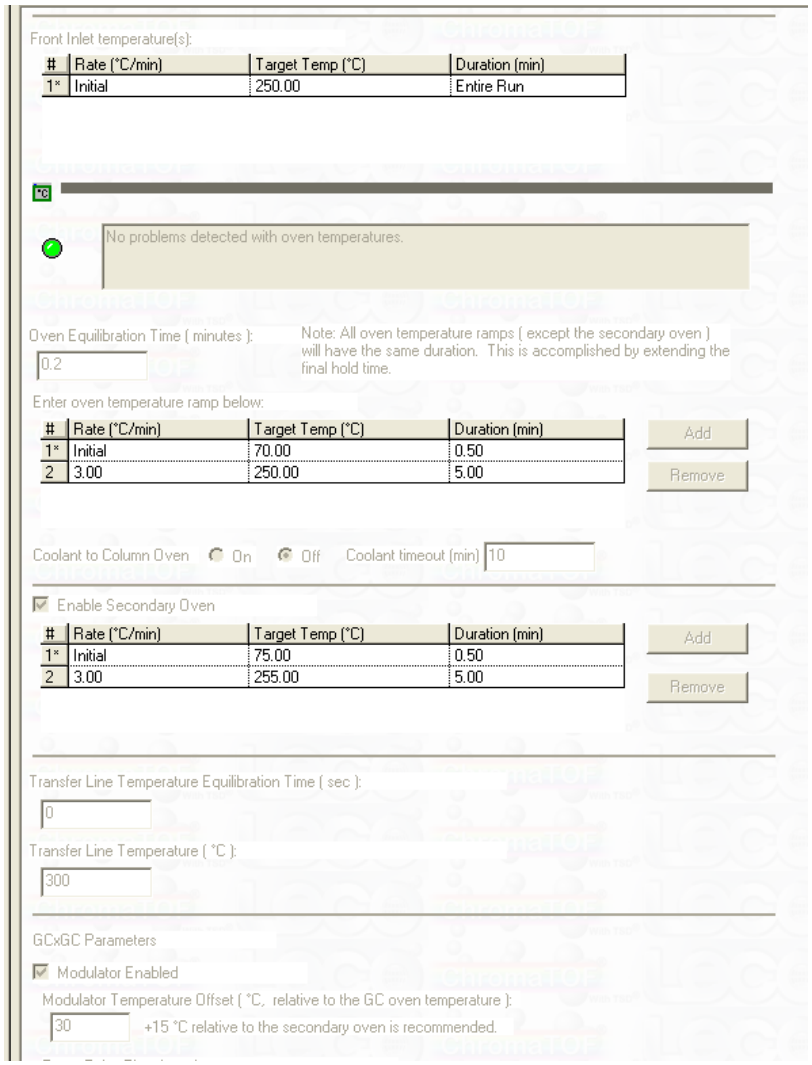
Front Inlet temperature(s):
| Rate (°C/min) | Target Temp (°C) | Duration (min)
1* | Initial | 250.00 | Entire Run
No problems detected with oven temperatures.
Oven Equilibration Time (minutes):
0.2
Note: All oven temperature ramps (except the secondary oven) will have the same duration. This is accomplished by extending the final hold time.
Enter oven temperature ramp below:
| Rate (°C/min) | Target Temp (°C) | Duration (min)
1* | Initial | 70.00 | 0.50
2 | 3.00 | 250.00 | 5.00
Add
Remove
Coolant to Column Oven On Off Coolant timeout (min) 10
Enable Secondary Oven
| Rate (°C/min) | Target Temp (°C) | Duration (min)
1* | Initial | 75.00 | 0.50
2 | 3.00 | 255.00 | 5.00
Add
Remove
Transfer Line Temperature Equilibration Time (sec):
0
Transfer Line Temperature (°C):
300
GCxGC Parameters
Modulator Enabled
Modulator Temperature Offset (°C, relative to the GC oven temperature):
30
+15 °C relative to the secondary oven is recommended.

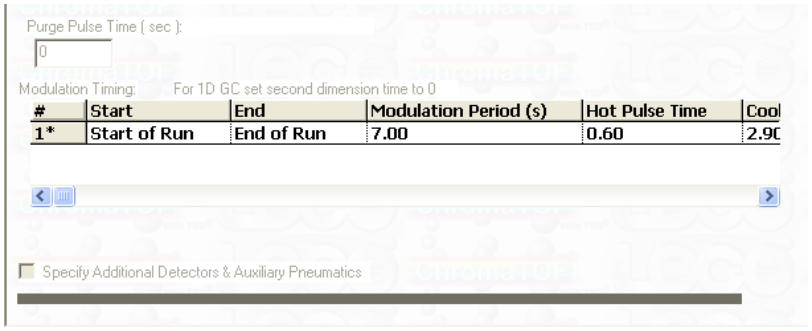
Purge Pulse Time (sec):
0
Modulation Timing: For 1D GC set second dimension time to 0
| Start | End | Modulation Period (s) | Hot Pulse Time | Cool
1* | Start of Run | End of Run | 7.00 | 0.60 | 2.90
Specify Additional Detectors & Auxiliary Pneumatics

Mass Spectral Method:

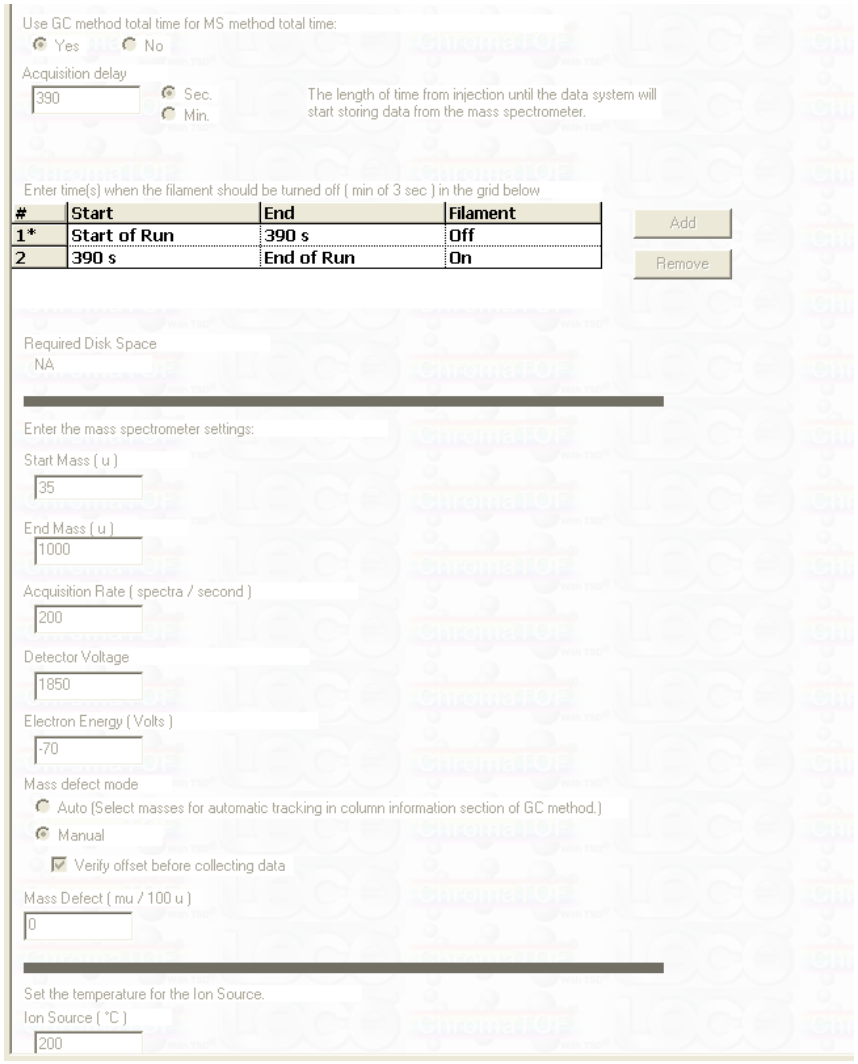

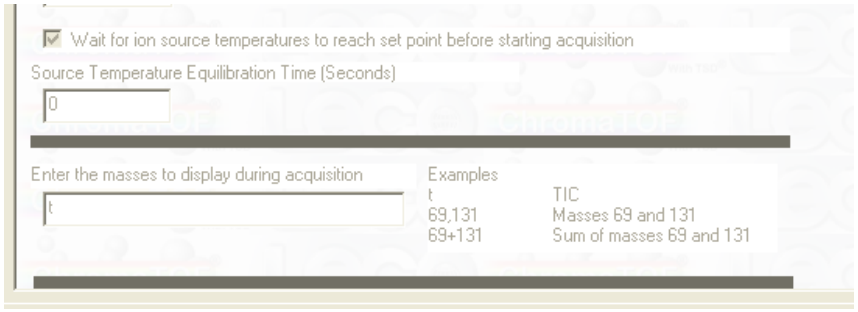

Autosampler Method:

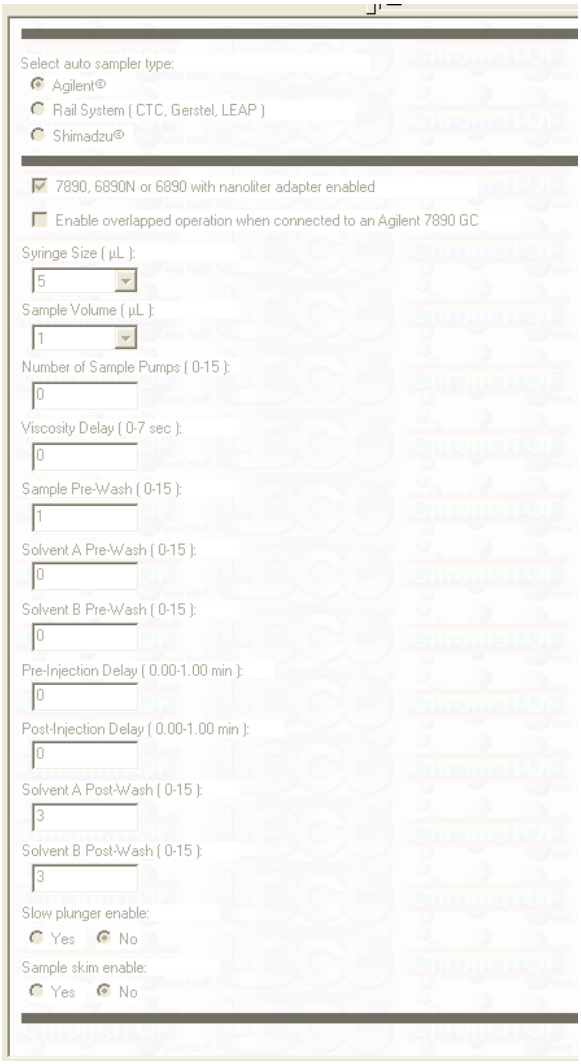

Chapter 3

Processed data files for the samples discussed in Chapter 3 can also be found on the Pegasus Workstation Computer (Drive C). The files are located in a secondary database and the software must be opened differently than previously described to access the Chapter 3 files. Double click on the gray Pegasus icon. Click change → new → ok → yes → login. Again, no password is needed. The processed chromatograms are located in the "FAMEs Paper" folder under "Acquired Samples."

The gas chromatograph, mass spec, autosampler and data processing methods used follow.

Gas Chromatograph Method:

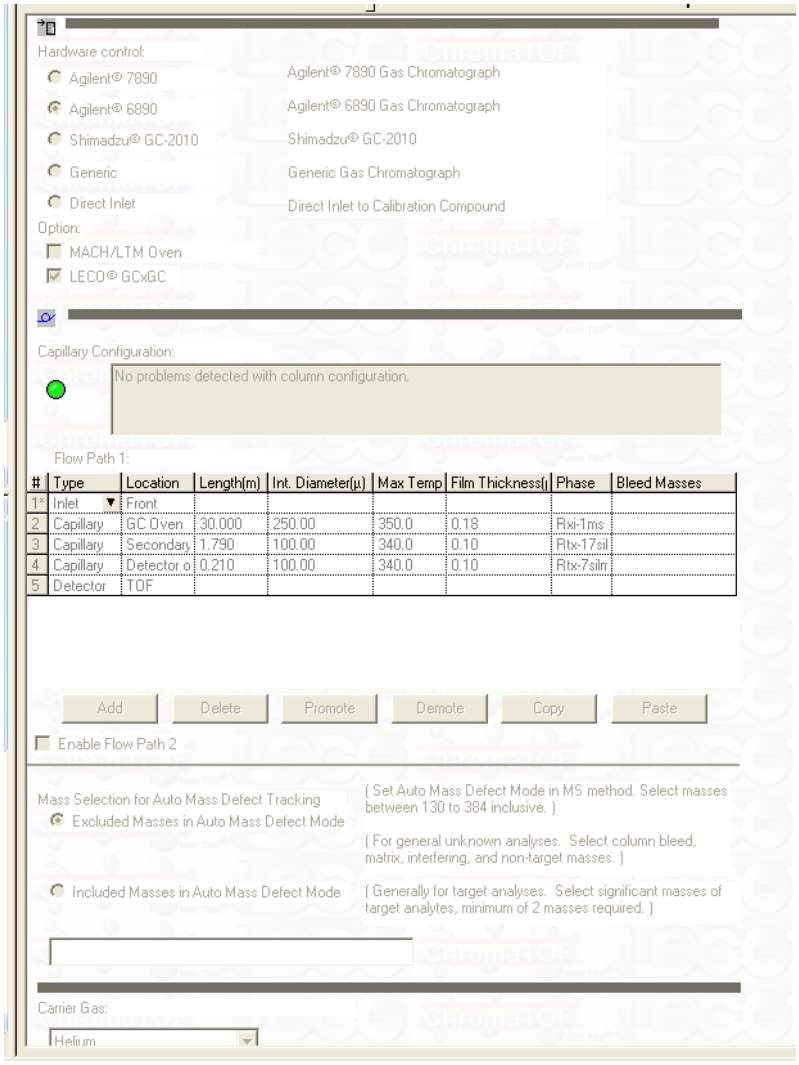

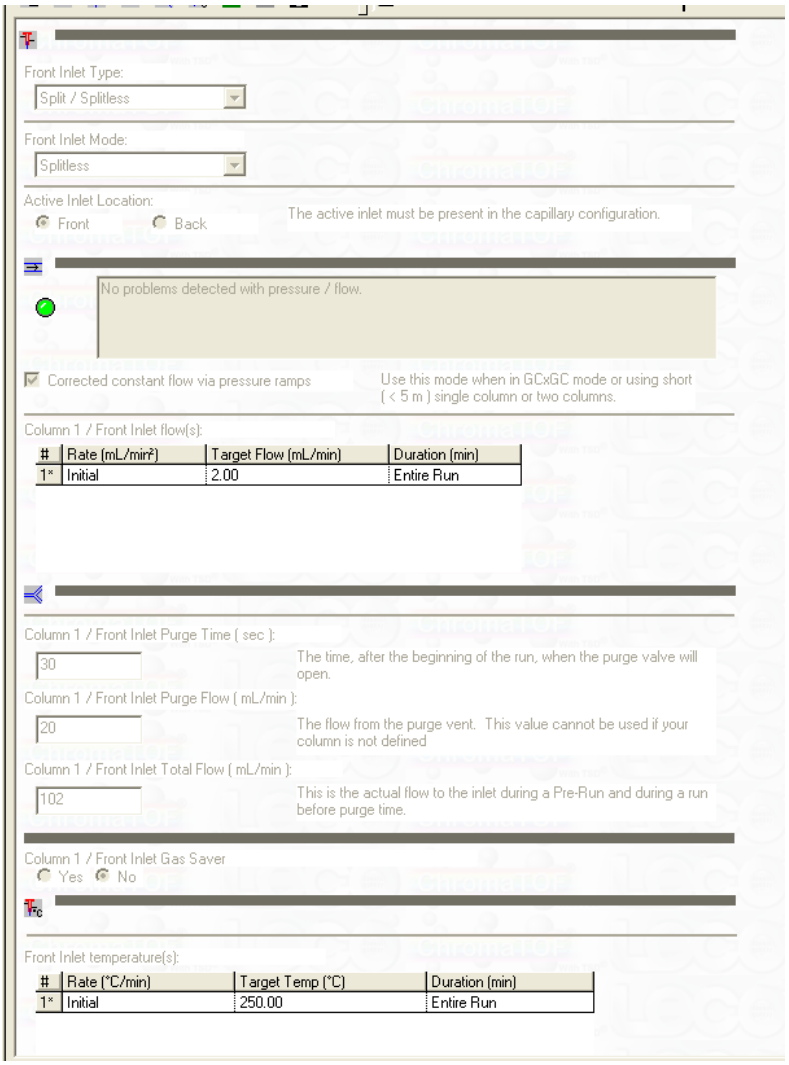
Front Inlet Type:
Split / Splitless
Front Inlet Mode:
Splitless
Active Inlet Location:
Front
Back
The active inlet must be present in the capillary configuration.
No problems detected with pressure / flow.
Corrected constant flow via pressure ramps
Use this mode when in GCxGC mode or using short (< 5 m) single column or two columns.
Column 1 / Front Inlet flow(s):
| Rate (mL/min²) | Target Flow (mL/min) | Duration (min)
1* | Initial | 2.00 | Entire Run
Column 1 / Front Inlet Purge Time (sec):
30
The time, after the beginning of the run, when the purge valve will open.
Column 1 / Front Inlet Purge Flow (mL/min):
20
The flow from the purge vent. This value cannot be used if your column is not defined
Column 1 / Front Inlet Total Flow (mL/min):
102
This is the actual flow to the inlet during a Pre-Run and during a run before purge time.
Column 1 / Front Inlet Gas Saver
Yes
No
Front Inlet temperature(s):
| Rate (°C/min) | Target Temp (°C) | Duration (min)
1* | Initial | 250.00 | Entire Run

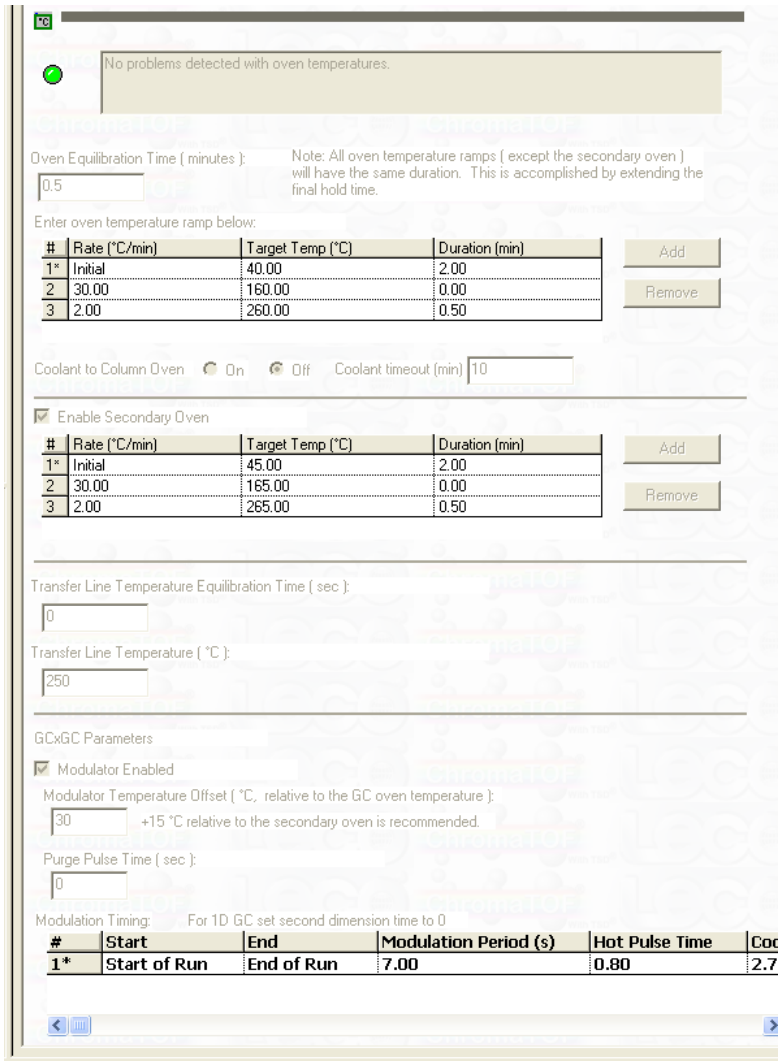
No problems detected with oven temperatures.
Oven Equilibration Time (minutes):
0.5
Note: All oven temperature ramps (except the secondary oven) will have the same duration. This is accomplished by extending the final hold time.
Enter oven temperature ramp below:
Rate (°C/min) Target Temp (°C) Duration (min)
1* Initial 40.00 2.00
2 30.00 160.00 0.00
3 2.00 260.00 0.50
Add
Remove
Coolant to Column Oven On Off Coolant timeout (min) 10
Enable Secondary Oven
Rate (°C/min) Target Temp (°C) Duration (min)
1* Initial 45.00 2.00
2 30.00 165.00 0.00
3 2.00 265.00 0.50
Add
Remove
Transfer Line Temperature Equilibration Time (sec):
0
Transfer Line Temperature (°C):
250
GCxGC Parameters
Modulator Enabled
Modulator Temperature Offset (°C, relative to the GC oven temperature):
30
+15 °C relative to the secondary oven is recommended.
Purge Pulse Time (sec):
0
Modulation Timing:
For 1D GC set second dimension time to 0
Start End Modulation Period (s) Hot Pulse Time Coo
1* Start of Run End of Run 7.00 0.80 2.7

Mass Spectral Method:

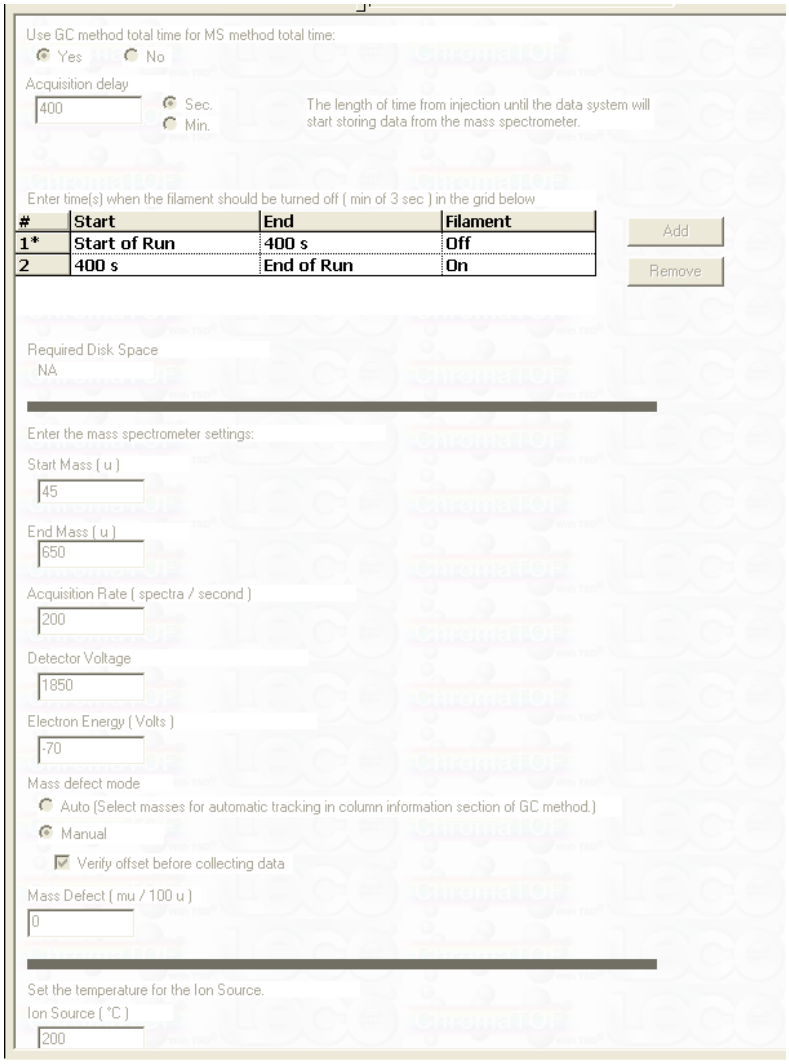

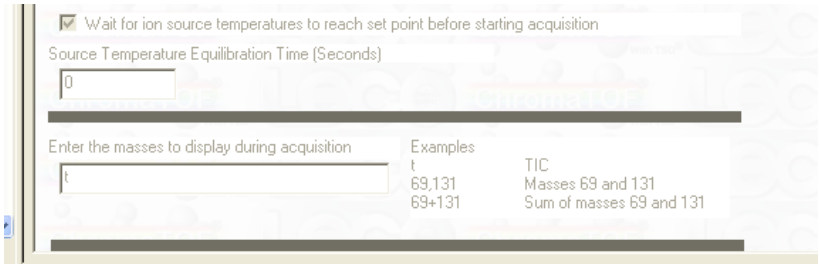

Autosampler Method:

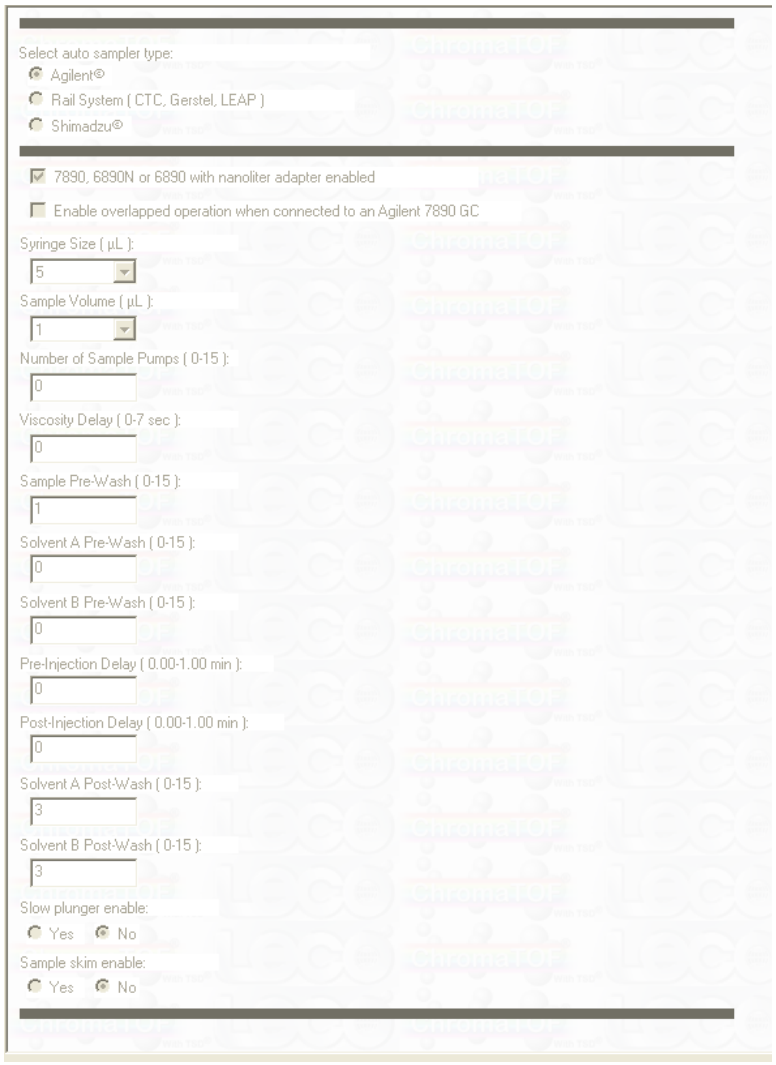

Data Processing Method:

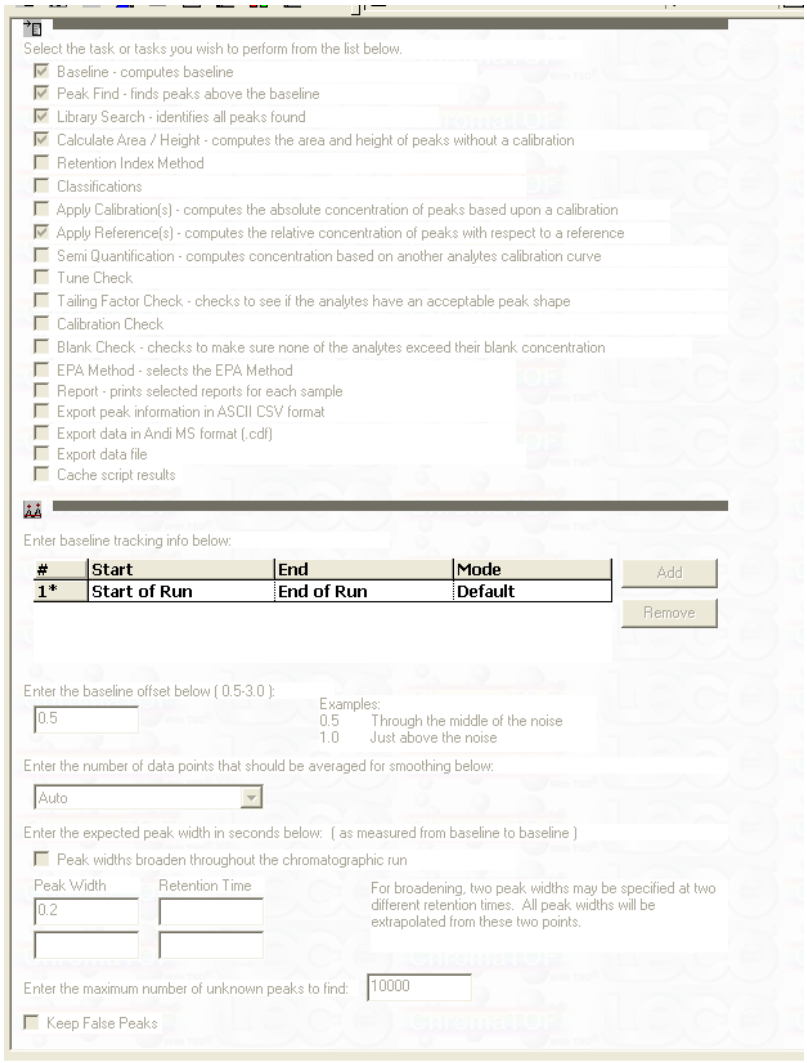

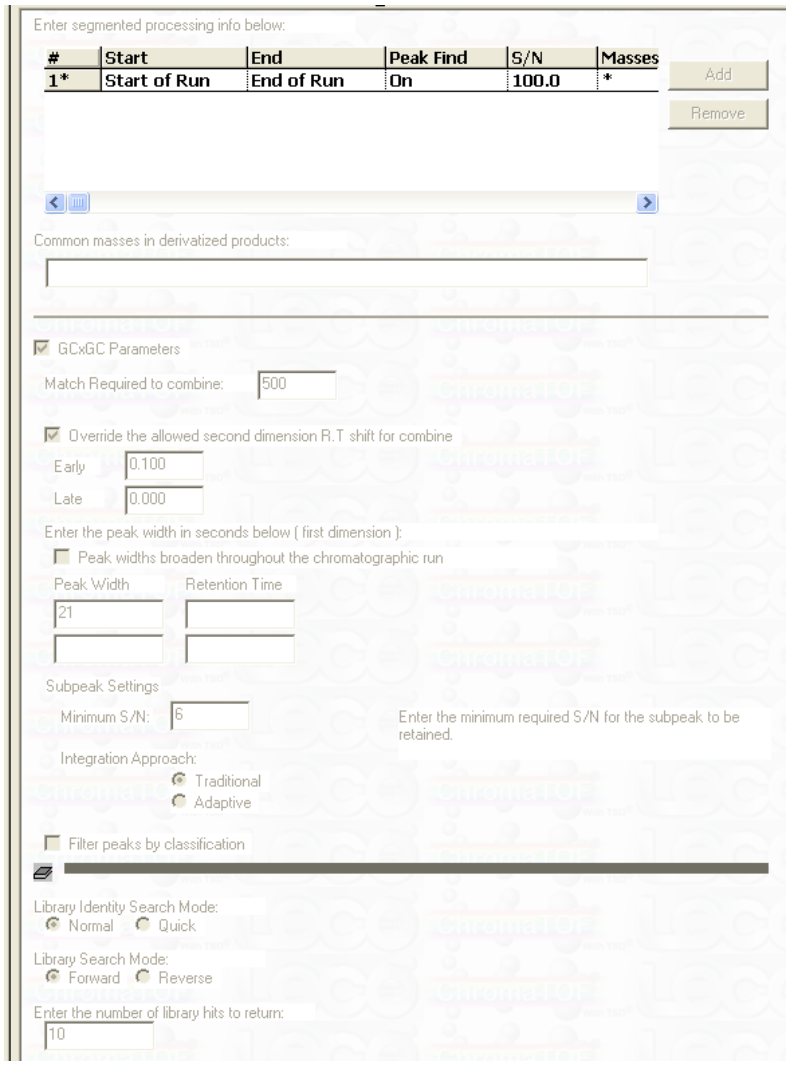
Enter segmented processing info below:
Start End Peak Find S/N Masses
1* Start of Run End of Run On 100.0 *
Add
Remove
Common masses in derivatized products:
GCxGC Parameters
Match Required to combine: 500
Override the allowed second dimension R.T shift for combine
Early 0.100
Late 0.000
Enter the peak width in seconds below (first dimension):
Peak widths broaden throughout the chromatographic run
Peak Width
Retention Time
21
Subpeak Settings
Minimum S/N: 6
Enter the minimum required S/N for the subpeak to be retained.
Integration Approach:
Traditional
Adaptive
Filter peaks by classification
Library Identity Search Mode:
Normal
Quick
Library Search Mode:
Forward
Reverse
Enter the number of library hits to return:
10

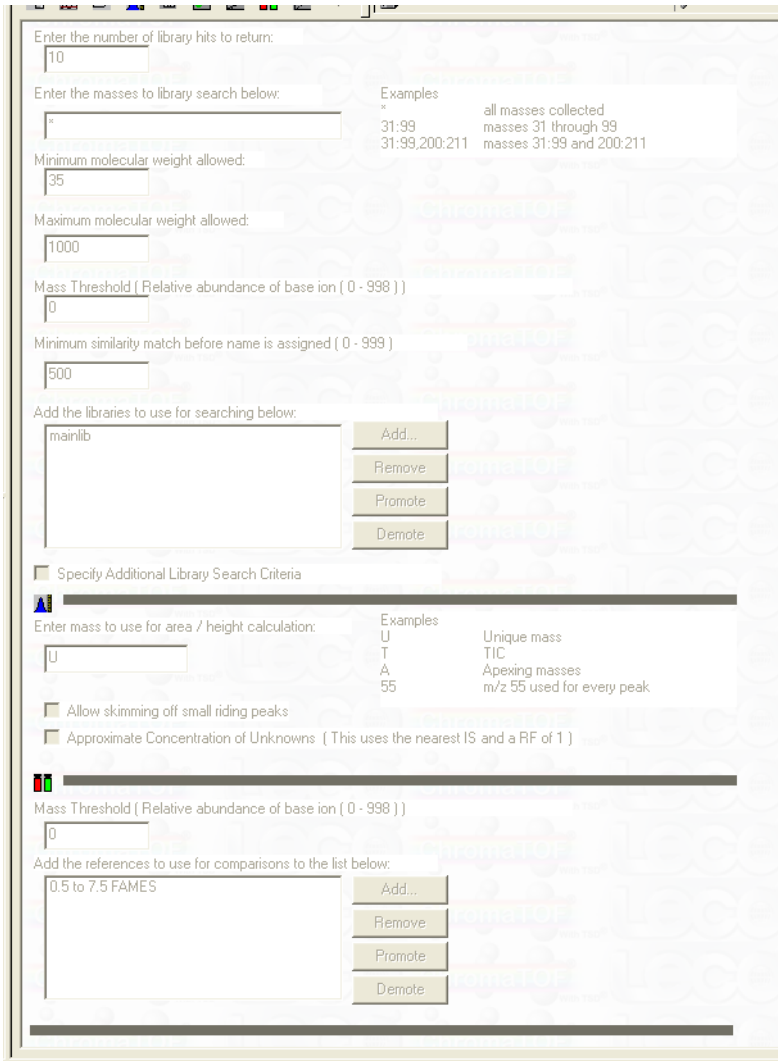
Enter the number of library hits to return:
10
Enter the masses to library search below:
*
Examples
*
all masses collected
31:99
masses 31 through 99
31:99,200:211
masses 31:99 and 200:211
Minimum molecular weight allowed:
35
Maximum molecular weight allowed:
1000
Mass Threshold (Relative abundance of base ion (0 - 998))
0
Minimum similarity match before name is assigned (0 - 999)
500
Add the libraries to use for searching below:
mainlib
Add...
Remove
Promote
Demote
Specify Additional Library Search Criteria
Enter mass to use for area / height calculation:
U
Examples
U
Unique mass
T
TIC
A
Apexing masses
55
m/z 55 used for every peak
Allow skimming off small riding peaks
Approximate Concentration of Unknowns (This uses the nearest IS and a RF of 1)
Mass Threshold (Relative abundance of base ion (0 - 998))
0
Add the references to use for comparisons to the list below:
0.5 to 7.5 FAMES
Add...
Remove
Promote
Demote